Boundary element and transfer operator methods for multi-component wave systems

Hanya A M Ben Hamdin

Thesis submitted to the University of Nottingham for the degree of Doctor of Philosophy

March 2012

Abstract

In this thesis, exact and semiclassical approaches are derived for predicting wave energy distributions in coupled cavities with variable material properties. These approaches are attractive because they can be extended to more complex built-up systems.

For the exact treatment, we describe a multi-component boundary element method. We point out that depending on the boundary conditions and the number of interfaces between sub-components, it may be advantageous to use a normal derivative method to set up the integral kernels. We describe how the arising hypersingular integral kernels can be reduced to weakly singular integral and then using the piecewise constant collocation method. The normal derivative method can be used to minimise the number of weakly-singular integrals thus leading to BEM formulations which are easier to handle.

The second component of this work concerns a novel approach for finding an exact formulation of the transfer operator. This approach is demonstrated successfully for a disc with boundary conditions changing discontinuously across the boundary. Such an operator captures the diffraction effects related to the change of boundary conditions. So it incorporates boundary effects such as diffraction and surface waves. A comparison between the exact results from the BEM against the exact transfer operator shows good agreement between both categories.

Such an exact operator converges to the semiclassical Bogomolny transfer operator in the semiclassical limit ($k \to \infty$). Having seen how the exact transfer operator behaves for a unit disc, a similar approach is adapted for the coupled-cavity configuration resulting in the semiclassical transfer operator. Our formulation for the transfer operator is applicable not only for the quantization of a system, but also to recover the Green function.

Publications

The results of Chapter 4 have been puplished in

1. G. Tanner, D.J. Chappell, H. Ben Hamdin, S. Giani, C. Seidel, F, Vogel. Acoustic energy distribution in multi-component structures-Dynamical Energy Analysis versus numerically exact results. *Proceedings of the International Conference on Noise and Vibration ISMA*, Leuven, Belgium, 2425–2436, 2010.

2. H. Ben Hamdin, G. Tanner. Multi-component BEM for the Helmholtz equation - A normal derivative method. *Accepted for publication in shock and vibration journal as special issue of the outcomes of ICEDyn 2011.*

3. H. Ben Hamdin, S. Creagh, G. Tanner. Exact formulation of the transfer operator. To be submitted to Physica A, 2012.

Dedicated to the ever living memory of my father Abdusalam and my marvellous mother Fatima. May ALLAH bestow his mercy upon them and grant them the paradise.

Acknowledgements

First and foremost, I would like to express my gratitude to GOD (ALLAH) for his precious guidance and giving me the strength, making the completion of this thesis possible, and being always with me through the difficult times and the dark hours of my research.

I am very grateful and enormously indebted to both of my supervisors Gregor Tanner and Stephen Creagh. Without their impressive depth of knowledge, skillful guidance, patience, and support over the past four years this thesis would not have been possible.

It was an honor to work with the group of MIDEA (MIDfrequency Energy Analysis) project led by Gregor Tanner. I would like to thank David Chappel for reading parts of my thesis and useful comments, Stephano Giani, Cathleen Seidel, and Dimitrii Maxsimov for useful discussion and sharing some data.

My gratitude is due to the School of Mathematical Sciences, University of Nottingham for providing an excellent research environment. I would like to thank the kind staff of my school, a special thanks is due to Dave Parkin for his immediate help and Helen Cunliff for her help and support as well as Krystyna Glowczewska, Hilary Lonsdale and Andrea Blackbourn.

Also I would like to express my thanks to the Libyan ministry of higher education for funding my studies. Throughout my PhD I was able to attend

and contribute to many conferences and workshops funded either by the school of Mathematical Sciences, University of Nottingham, MIDEA grant, and the Libyan ministry of higher education.

Finally, I would like to thank my family, especially my mother Fatima for her consistent and sincere prayers, emotional encouragement and firm believe in me. Special thanks for my siblings Salha, Fawzia, Mohammad, Hammad, Gomma, Abdusalam.

Nomenclature

1D One-Dimensional

ABCs Absorbing Boundary Conditions

BCs Boundary Conditions

BE Boundary Element

BEM Boundary Element Method

BIEM Boundary Integral Equations Method

BIEs Boundary Integral Equations

CPV Cauchy's Principle Value

DBCs Dirichlet Boundary Conditions

DDM Domain Decomposition Method

DEA Dynamical Energy Analysis

DG-FEM Discontinuous Galerkin-Finite Element Method

DGM Discontinuous Galerkin Method

DRM Dual Reciprocity Method

EBK Einstein-Brillouin Keller

FDM Finite Difference Method

FE-SEA Finite Element-Statistical Energy Analysis

FEM Finite Element Method

HFP Hadamard Finite Part

MD-DRM Dual Reciprocity Method-Multi-domain

NBCs Neumann Boundary Conditions

NRBCs Non-Reflection Boundary Conditions

PABCs Perfectly Absorbing Boundary Conditions

PML Perfectly Matched Layer

RBFs Radial Basis Functions

SEA Statistical Energy Analysis

SmEdA Statistical modal Energy distribution

SPA Stationary Phase Approximation

SSM Surface of Section Method

SVD Singular Value Decomposition

WB-SEA Wave Based-Statistical Energy Analysis

WBM Wave Based Method

WBT Wave Based Technique

WKB Einstein-Brillouin Keller

WRM Weighted Residual Method

Contents

List of Figures

Chapter 1

Introduction

Determining the wave energy distributions in complex built-up structures where material properties change from one sub-structure to the next is a common problem in mechanical engineering, acoustics, optics and quantum mechanics e.g. solving the Schrödinger equation where the potential changes discontinuously across a surface. The vibration dynamics of coupled plates with different thickness or electromagnetic waves in a homogeneous media with discontinuous changes in the dielectric constants are examples thereof.

Wave propagation through such domains is an old topic and can be traced back to Ibn Sahl in 984 [1, 2] when he considered optical media with a discontinuous change of refractive index. At the discontinuity line a ray is split into a reflected and transmitted component, such a phenomenon is referred to as ray splitting. Sahl derived a conservation law of refraction at the discontinuity interface. Such a law was later rederived by Snell in 1626, and is known as Snell's law or Snell-Descartes law [1]. In domains with abrupt changes of parameters in the wave equation (such as wave speed and absorption coefficients at the interfaces between the components), it is crucial to measure how much energy is reflected back or transmitted at the discontinuity interface. Such information is called as the reflection and transmission coefficients.

Methods of mathematical modelling can be either analytical or numeri-

cal. The most popular techniques of solving partial differential equations (PDEs) analytically were based on the use of separation of variables and series approximations. Purely analytical techniques have lost their popularity because of their limitations to simple geometries. Therefore, it is often necessary to resort to numerical techniques, as they are reliable for arbitrary geometries. These methods include the Finite Element Methods (FEMs) [3], which can be traced back to 1943 when Courant [4] considered a piecewise linear approximation over a triangular mesh. A few decades later, the Boundary Element Method (BEM) was introduced in 1963 by Jaswon [5] and Symm [6]. The BEM has advantages over other popular numerical techniques such as the FEM [7] or Finite Difference Methods (FDM) due to the reduction of the dimensionality of the problem by one, which is of particular importance from a computational point of view. Making use of the fact that the free Green function is known in each sub-domain of a complex built-up structure of different material properties, the BEM is an efficient tool to treat such problems. Furthermore, the boundary integral equations are a starting point for many asymptotic techniques in the short-wavelength (high-frequency) limit such as the Bogomolny transfer operator [8].

However, purely numerical methods become prohibitively expensive in the high-frequency limit. Thus, in this limit, asymptotic methods are often favourable. Such methods provide the connection between wave propagation and the underlying ray dynamics. Conceptually, in the limit of small wavelength ($\lambda \to 0$), the ray optics concept is sufficient to analyse the system. In this limit, a wave can be approximated as a ray that is specularly reflected at the boundary. This analogy is similar to billiard systems where a particle is elastically reflected off the walls of the billiard. The study of complex wave problems in the ray limit is often called wave or quantum chaos [9]. One semiclassical technique is the transfer operator, which is based on the short wavelength asymptotic of the free-space Green function; it was pioneered by Bogomolny in 1990 [8]. The transfer operator can be obtained from the asymptotic expression of the boundary inte-

gral kernels in the semiclassical limit [10]. Therefore, by using the semiclassical transfer operator, the free Green function is taken in the limit of large wavenumber ($k \to \infty$). The Hankel function in the free-space Green function is then approximated asymptotically by exponential functions which are easy to handle and overcome the singularity issue usually encountered in the BEM formulation. It is noteworthy to mention that both the BEM and the semiclassical transfer operator gives the quantisation condition for a system without any information about the periodic orbits, in contrast with the Gutzwiller periodic-orbits trace formula [11]. The semiclassical transfer operator enhances the applicability of the BEM in the high-frequency limit. Also it provides a method to compute the reflection and transmission coefficients explicitly.

For a continuous change of the material properties throughout the media, trajectories will undergo many changes of direction according to the change of wavenumber, thus trajectories become curves in space. This phenomenon will not be considered in this thesis. However, it can be done within the transfer operator framework. Hence, we only consider abrupt changes of material properties at certain interfaces.

Problems involving propagation of waves, ranging from quantum mechanical problems to seismic waves in elastic solids and acoustics are well described by linear wave equations. In this thesis, we will restrict our analysis to the two dimensional Helmholtz equation, although the concepts and ideas are applicable to other wave equations and for problems in higher dimensions.

Layout of the thesis

The main goal of this thesis is to introduce numerical methods to investigate the wave energy distribution in multi-component systems of different material properties in the low and high-frequency range. An important problem is to find the reflection and transmission coefficients at the interfaces between the subcomponents. The information about such coefficients are stored in an implicit

way within the BEM formulation. Thus we need to device a method to extract such information explicitly.

To put our work in perspective, in Chapter 2 an overview is presented of the existing techniques that are used to predict wave energy distributions in complex built-up structures in the low, mid and high-frequency ranges.

Preliminaries and concepts of the BEM are outlined in Chapter 3. Also some applications of the BEM, such as computing the spectrum of the Laplacian, some of the eigenfunctions and the Green function for non-convex polygonal domains in the presence or absence of absorption.

In Chapter 4 a normal derivative BEM sub-component technique is implemented to investigate the wave energy distribution in multi-component systems where the wavenumber and damping parameters change discontinuously in different parts of the system. As a starting point we explore the wave energy distribution in coupled-polygonal domains, with the aim of finding efficient methods on large scale, multi-component systems. This technique can be applied where a straightforward use of classical single-domain BEM would not be possible due to the fact that the free Green function is not known across the whole domain for multi-component structures because of the change of the wavenumber. Using the normal derivative formulation may prove useful in reducing the number of regularization procedures necessary. Then the BEM sub-components technique is demonstrated for different geometric configurations with various combinations of material parameters. We consider the absorption phenomenon which plays an important role in engineering applications and acoustics. It takes into account the loss of energy in a dissipative system due to damping of the system. We have published the results of this chapter in [12, 13]

In Chapter 5, a new formulation of the exact and the semiclassical transfer operator is presented for a disc with boundary conditions changing discontinuously across the boundary. A comparison is carried out between the exact and the semiclassical transfer operator showing the advantage of the former in

the sense that it captures diffraction effects at the discontinuity of the boundary conditions. Also, the exact transfer operator includes the evanescent contributions unlike the semiclassical Bogomolny transfer operator. Depending on the prescribed boundary conditions, the Green function or its normal derivative are calculated using both the BEM and the exact transfer operator, then a comparison is carried out showing good agreement between both approaches. Therefore it demonstrates the efficiency of using the exact transfer operator. We show that from the exact transfer operator one can retrieve the semiclassical Bogomolny transfer operator using Debye's asymptotic relations.

In Chapter 6, the ideas of Chapter 5 were adapted to the coupled-cavity configuration. There are some issues related to the non-smooth geometry of polygonal domains, such as corner and the fact that the operators involved in the formulation are not diagonal for the polygonal geometry. Therefore, we only derive the semiclassical transfer operator for coupled-cavity configuration, but we point out how the exact transfer operator for such configuration could be obtained. Then a comparison is carried out between the multi-component BEM and the semiclassical transfer operator.

Chapter 7 is dedicated to the conclusions drawn from this thesis and reiterates the main results. Some possible directions for future work are discussed.

Chapter 2

Literature review

In this chapter we will give an overview of the existing numerical methods for modelling interior/exterior/vibro-acoustic problems. For the sake of clarity, we give the classification of the problem that is considered. If the problem is enclosed by certain boundaries, and there is no interest in the outside domain, then it is referred to as an interior problem. But if one is interested in the outside part of the domain, then it is an exterior or scattering problems. A vibro-acoustic problem can be defined as a vibrating structure surrounded by a fluid, so that the vibration produces a pressure waves throughout the fluid. Most of the available numerical prediction techniques for such problems can be classified as being either deterministic (exact) or statistical techniques.

2.1 Deterministic methods for low-frequency regimes

In what follows we will present an overview of the commonly used deterministic numerical techniques. Section 2.1.1 presents the widely used Finite Element Method (FEM), and briefly mentions some optimisations of FEM such as the *hp* adaptivity and the Discontinuous Galerkin Method (DGM). §2.1.2 discusses the Wave Based Technique (WBT) and its application for modelling interior/exterior/vibro-acoustic problems. A larger discussion is dedicated to the

Boundary Element Method (BEM) in §2.1.3, discussing its various formulations, advantages and disadvantages. The last two sections, §2.1.5 and §2.1.6, concern domain decomposition techniques with direct and iterative solver, respectively. It is noteworthy to mention that the deterministic methods such as, FEM, BEM, and WBT are limited to long wavelengths of vibration (low-frequency), due to the interpolation of the solution in terms of shape functions as will be explained in the following sections.

2.1.1 Finite Element Method

The Finite Element Method (FEM) is the most popular numerical method, having being commercially developed and successful in many applications. An early text-book by Zienkiewicz and Cheung [14] in 1965 popularised the FEM. For recent references see Zienkiewicz et al. [15], also a review by Zienkiewicz and Taylor [7, 16]. For a brief history of the FEM see the reviews by Gupta and Meek [17], and Oden [18]. FEM approximates the solution over a mesh, assembled so that the continuity and equilibrium condition are met along the interfaces between their elements [19]. In FEM the domain is discretized into finite elements of triangles, quadrilateral, ...etc, then the solution is interpolated in terms of simple, polynomial shape functions. The approximate solution in terms of such shape functions does not fulfil the boundary conditions. Therefore, one needs to use a Weighted Residual Method (WRM) to minimise the residual as it will be discussed in §(2.1.4). The FEM system matrix coefficients results from simple numerical integrations, and the residual equations can be solved directly. The resultant matrix is sparsely populated with real coefficients, this allows the use of efficient storage tools for sparse matrices.

Since such shape functions are not exact solutions of the governing differential equation, a fine discretization is usually needed to maintain reasonable prediction accuracy. Therefore, the computational cost of FEM will grow in direct proportion to the frequency, leading to a prohibitively large computing

time for large structures at high frequencies. As a rule of thump, to model a wave accurately, the number of elements needed per wavelength ranges from 5 to 10, depending on the type of elements, e.g, constant, linear or quadratic, respectively. In the high-frequency limit fine discretization becomes prohibitively expensive.

Often one needs to compromise between the computational time and the accuracy by setting different treatment of the regions where the error is pronounced. Therefore FEM is optimised either by increasing the order of the shape function polynomials p or decreasing the element size h, corresponding to what is now known as the p and h adaptivity, or combining both to get the hp adaptivity [20, 21].

Furthermore the hp adaptivity can be implemented easily with the Discontinuous Galerkin method (DGM). It was first initiated by Reed and Hill in 1973 for the neutron transport linear hyperbolic equations [22]. Within the DGM the mesh refinement can be carried out independently at each element without considering continuity. So, the parameters h and p can have different values at each element. Furthermore, one could have different approximation local space at each element, because continuity at the element interfaces is not required [23, 24]. Therefore, the hp-adaptive DG-FEM methods allow more flexibility of the applicability of the FEM [25].

Although, FEM is not directly applicable to unbounded domains because it is based on the discretization of the domain, many approaches have been proposed to enforce the FEM to treat such domains. One of these approaches is the Absorbing Boundary Conditions (ABCs), also called the Non-Reflection Boundary Conditions (NRBCs) [26, 27]. The idea of such an approach is to introduce artificial boundaries with a condition that the amplitude of the reflection coefficients at such boundaries are very small, or even with vanishing reflection coefficients in what is known as Perfectly Absorbing Boundary Conditions (PABCs) [26]. Another approach is to introduce a layer of certain thickness

at R distance representing the diameter of the truncation boundary. Thus the outgoing waves will be perfectly absorbed (zero reflection) by the end of this layer. This technique is known as Perfectly Matched Layer (PML), it was first initiated by Berenger [28] in 1994 for application of electromagnetic waves with Maxwell's equation. Further, Chew and Weeden [29] proposed a PML approach that is based on the analytic continuation of the governing PDE to the complex plane. Hence, within these approaches the outgoing waves never come back to interact with the solution.

Furthermore, the unbounded domains can be modelled by infinite elements which discretize the problem domain as the finite elements do [30]. Within this approach, the shape functions are constructed as a multiplication of radial functions by another function that insures the continuity of the solution along the interface and a suitable amplitude which decays with radial distance for modelling travelling waves. To gain satisfactory accuracy, one needs to increase the radial order of the shape functions. So the domain will be divided into a close region where standard finite elements are applied, and far region where the infinite elements are applied.

2.1.2 Wave Based Technique

The Wave Based Technique (WBT) is a numerical prediction tool that was introduced by Desmet [31] in 1998. Since then it has been widely used for modelling interior/exterior/vibro-acoustics problems. It uses wave-like basis functions, which originate from Trefftz approach [32, 33]. The functions used in the Trefftz approach exactly satisfy the governing PDE, but do not necessarily fulfil the prescribed boundary conditions. Therefore, as commonly used in FEM, the WBT adopts a Galerkin weighted residual scheme [34] in which the boundary conditions are enforced by minimising the boundary residual as will be discussed in §2.1.4.

In the context of the Helmholtz equation the shape functions used for

WBT represent propagating and evanescent plane waves. Similar to the BEM and in contrast with the FEM, the WBT yields a fully populated matrix with complex entries and can not be decomposed into frequency independent matrices. It is claimed that the WBT is more efficient than FEM which employs simple polynomial shape functions that are not exact solutions for the governing PDE [31, 35]. To gain insight into this technique the reader is referred to the references [35, 36, 37] and references therein. One requirement is that the domain has to be convex, hence non-convex domains have to be decomposed into convex sub-domains. These sub-domains are recoupled again by applying continuity and equilibrium conditions at the interfaces between them.

Desmet and coworkers [38] applied the WBT for a three dimensional acoustic car-like cavity with loudspeaker excitation. Then a comparison is performed between WBT prediction and FEM prediction to experimental data, showing good agreement between the three categories. Hepberger et al. [39] also implemented such a technique to analyse the engine noise radiation in three dimensions, in which they divide the problem into bounded and unbounded regions by an artificial spherical truncation boundary. For the bounded region the exact acoustic pressure is approximated as a linear combination of wave functions that originate from Trefftz approach. While for the unbounded region, the exact pressure is interpolated in terms of radiation functions alongside with the Sommerfeld radiation condition (2.4). A comparison with BEM simulations is carried out, showing good agreement with the WBT prediction [39].

2.1.3 Boundary element method

Next we will present a historical overview of the development of the boundary element method, and discuss its different formulations. We then discuss its advantages and disadvantages.

Historical Review of BEM

In 1828 Green presented his three integral identities and theorems [40]. Though this pioneering work remained obscure during Green's life, about a century later it became the foundation for using Boundary Integral Equations (BIEs) for solving potential problems. Within the boundary integral methods the governing PDE can be transformed into an equivalent system of BIEs either directly through Green's second identity or indirectly using layer potentials with fictitious densities. During the early period of the development of boundary integral formulations, BIEs were solved analytically [41] in what is known as the Boundary Integral Equation Method (BIEM). This limited the applicability of the method to simple problems.

A major development of BIEs arose when discretization of the boundary was considered. In 1963 Jaswon [5] and Symm [6] introduced a numerical scheme to solve the BIEs and approximated the solution in terms of piecewise polynomial shape functions over boundary elements. Thus the regular integrals were computed numerically using Simpson's rule, whereas the singular integrals were integrated analytically. This is what is now known as the Boundary Element Method (BEM). In principle, whether the BIEs are solved analytically or numerically one could use the term boundary integral equations method (BIEM) [42]. However, the preferred name hereafter is the BEM, simply because is widely used.

BEM is now a very well established and well documented technique, see Cheng [42] for a historical review, Banerjee and Watson [43, 44], Brebbia [34, 45, 46, 47, 48] for an introduction. For applications in elasticity and potential theory see Jaswon [5] and Symm [6], respectively. For engineering applications see Popov et al. [49, 50], and for applications in solids and fluids see Bonnet [51]. For acoustic and electromagnetic applications see Kress [52] and Colton [53]. For a rigorous mathematical insight into BIE theories and their abstract formulation using functional analysis see Atkinson [54], Mikhlin [41], Kress [52], Dautray [55]

and Hackbusch [56].

BEM is a powerful technique for obtaining an approximate solution for PDEs that arise in scientific and engineering applications, such as elasto-dynamics, fluid dynamics, wave scattering, radiation and propagation. Before discussing the different formulations of BEM, it may be useful to introduce the possible types of boundary conditions.

Types of boundary conditions

There are a variety of boundary conditions that can be considered for a boundary value problem. They can be categorised as the following for a boundary point $x \in \partial D$, where ∂D is the boundary of the domain.
If the boundary conditions are set for $\psi(x)$, that is $\psi(x) = f(x)$, then it is called Dirichlet Boundary Conditions (DBCs). Example of this type of BCs is a membrane problem.

If the boundary conditions are set for $\frac{\partial \psi(x)}{\partial n_x}$, then it is called Neumann Boundary Conditions (NBCs). The operator $\frac{\partial}{\partial n_x}$ denotes the directional derivative along the normal vector $\vec{n}$ at the boundary element x, that is,

$$\frac{\partial}{\partial n_x} = \vec{n}_x \cdot \nabla_x,$$

where the dot denotes the scalar product, ∇_x is the gradient operator with respect to x.
An example of this type of BCs is an acoustic problem, where the acoustic potential (pressure) can not be set to zero, but the velocity can be set to zero on the boundary.

A linear combination of DBCs and NBCs is known as mixed boundary conditions, also called the Robin boundary conditions. That is,

$$A\frac{\partial \psi(x)}{\partial n_x} + B\psi(x) = f(x),$$

where A and B are constants. Example of these type of BCs occur in heat problems, where the temperature is related to the thermal flux.

Depending on the applied formulation, there are two types of BEM formulations, namely the direct BEM and indirect one as will be discussed below.

Direct BEM formulations

In this formulation, the actual physical quantities such as the displacement, traction, potential or the velocity are used to formulate the BIEs. The values of such quantities over the boundary play the role of source densities in generating the solution throughout the interior of the domain. This formulation is called the method of fundamental solution, in which such a solution is distributed regardless of the boundary. This formulation can be deduced through the Green second identity which is given as,

$$\iint_D \left(\phi\nabla^2\psi - \psi\nabla^2\phi\right) \mathrm{d}A = \int_{\partial D} \left(\phi\frac{\partial\psi}{\partial n_s} - \psi\frac{\partial\phi}{\partial n_s}\right) \mathrm{d}s, \tag{2.1}$$

where the functions ϕ and ψ are twice continuously differentiable on the domain D, and $\mathrm{d}A$ is an area element. This integral transformation allows the integral over the interior of the domain to be transformed into an integral on the boundary. This formulation is called direct, because it solves for ϕ or $\frac{\partial\phi}{\partial n_s}$ or both of them depending on the type of prescribed boundary conditions whether it is Neumann, Dirichlet or mixed boundary conditions, respectively. Using such an identity reduces the dimensionality of the problem by one, which is of particular importance from a computational point of view. This feature becomes advantageous in leading to considerably (albeit fully populated) smaller matrices. Thus, there is no need to solve large system of equations and to define complicated data structures.

An alternative direct formulation is to adopt a weighted residual method just as in FEM; this will be discussed in §2.1.4. Three publications by Jaswon [5, 57] and Symm [6] represent the birth of the direct formulation [42]. Furthermore there is a formulation which uses functions that are related to the physical quantities. Then such functions need to be integrated or differentiated to compute the actual physical quantities. Such formulation is sometimes called the

semi-direct BEM formulation [58], but can still be classified under the direct formulation.

Indirect BEM formulations

This formulation is based on using fictitious density functions to formulate the BIEs so that the solution for Neumann or Dirichlet boundary problems can be represented as a single or double-layer potential, respectively.
To obtain an integral equation for a problem with Neumann boundary conditions, one could write the unknown function ψ as a single layer potential,

$$\psi(x) = \int_{\Gamma} \sigma(s) F(s,x) ds, \tag{2.2}$$

where $F(s,x)$ is the fundamental solution of the governing PDE, which is a solution of the problem disregarding the prescribed boundary conditions. Also it is called the free-space Green function. The function $\sigma(s)$ is a fictitious, unknown density function, and Γ is the boundary of the domain.

In potential theory $\sigma(s)$ is called a monopole density function. Such a density function arises from some particular form of source distributions on the boundary [54]. The BIE (2.2) is classified as a Fredholm integral equation of the first kind [54], because the unknown function $\sigma(s)$ appears only implicitly (under the integral sign).
Similarly for Dirichlet problems, one could write the following BIE,

$$\frac{\partial \psi(x)}{\partial n_x} = c\sigma(x) + \int_{\Gamma} \sigma(s) \frac{\partial F(s,x)}{\partial n_x} ds, \tag{2.3}$$

where the integral on the right hand side of equation (2.3) is called a double layer potential, and the function $\sigma(s)$ is called a unknown dipole density function. The constant c arises from the jump relation of the double layer potential as will be discussed later in §3.3.10. The BIE (2.3) is classified as Fredholm integral equation of the second kind [54], because the unknown function $\sigma(s)$ appears both explicitly and implicitly.

These formulations are called indirect, because they are used to solve for the fictitious, unknown density function $\sigma(s)$ which has no physical relation to the problem in contrast of solving for the physical quantities directly. This formulation is preferable in combining interior/exterior problems in which the boundary does not have to be closed; it is also ideal for large scale acoustic problems with open boundaries [35].

Preliminary remarks on the BEM

The BIEs are derived for the wavefunction, its normal derivative or for both quantities, depending on whether Neumann, Dirichlet or Robin (mixed) boundary conditions are set on the boundary. The mechanism of the BEM is to discretize the boundary into a number of elements to compute the integrals numerically over such elements. The system of integral equations is converted into a linear system of algebraic equations which can be solved numerically. Direct solvers should be used if the number of unknowns is reasonably small, for example the Gaussian elimination and LU decomposition. Otherwise iterative methods should be employed if one seeks to obtain certain accuracy for the approximate solution of large number of unknowns. For iterative schemes, a suitable pre-conditioner should be used to speed up the convergence [59].

The BEM formulation depends heavily on the existence of the appropriate fundamental solutions specific to the problem being solved. This feature can be considered as a two-edged sword; on the one hand, the use of the exact fundamental solution (free solution disregarding the boundary) allows extremely accurate resolution of parameters throughout the domain. In addition it is essential, along with the Green identity, to establish the appropriate BIEs. On the other hand, since the fundamental solutions are specific to the problem being considered, there are restrictions on the applicability of BEM; for instance, for heterogeneous and non-linear problems.

In principle, the BEM is capable for solving unbounded media without

the need for artificial boundaries, since it involves neither domain discretization nor boundaries at infinity. Further, the BEM formulation inherently fulfils the Sommerfeld radiation condition [53], which is given as,

$$\lim_{R\to\infty} R\left\{\frac{\partial\phi}{\partial R} - \imath k\phi\right\} = 0, \tag{2.4}$$

where $R = |r - r_0|$ is the distance from an exterior point r to a boundary point $r_0 \in \partial D$, ϕ is the wavefunction and k is the wavenumber.
Such a condition characterises the behaviour of the solution at infinity, and eliminates the radiated plane waves and their combinations at infinity. So the BEM is unquestionably the method of choice for such categories. It finds applications in radiation, underwater acoustics, elastic wave problems in geophysics, seismology, earthquake engineering. This makes the BEM an advantageous technique over the classical domain methods for certain types of problems.

In the case of inhomogeneities and non-linearity, the BEM is not a preferable approach. In contrast, the FEM will be more suitable for such categories. However, the sub-region BEM technique as will be discussed in §2.1.5 can handle non-homogeneous problems with knowing exactly the interfaces that separate the sub-regions. Furthermore, the Dual Reciprocity Method (DRM) enlarges the applicability of BEM to non-linear categories, as will be discussed later in §2.1.7.

Non-uniqueness

A mathematical issue encountered in BEM is the non-uniqueness of the solution of an exterior problem at certain frequencies, which are the eigenfrequencies for the associated interior problem. To circumvent this disadvantage, it is reliable to use a robust approach proposed by Burton and Miller in 1971 [60]. Within this approach a linear combination between the surface Helmholtz integral equation (3.3.3) for $\mathbf{r} \in \partial D$ and its normal derivative is constructed with an arbitrary coupling parameter.

It was proved that such linear combination would yield a unique solution for all frequencies with a suitable complex-valued coupling parameter [60]. Such an approach is widely adopted in the context of three-dimensional radiation acoustic problems (Meyer [61], Terai [62], Yang [63]). However, this method suffers taking the normal derivative of the Helmholtz equation giving rise to a hypersingular integral which calls for further regularization procedures. Riddle [64] presents a treatment of the non-uniqueness problem without any need to produce another integral equation. In this thesis we are primarily interested in the interior problem so the non-uniqueness phenomenon does not play any role.

Singularity

Owing to the use of the two-point (source and receiver) singular fundamental solution, the boundary integral formulations suffer from singularities. Thus the general implementation of the BEM requires the computation of singular integrals with various types of singularities, such as weakly, strongly, and hypersingular of the order $O(\ln(|R|)$, $O(\frac{1}{R})$ and $O(\frac{1}{R^2})$, respectively, where R is the distance between the receiver and the source point. Accurate and efficient computations of such integrals have made the BEM an efficient and generally well-conditioned numerical solution procedures.

The hypersingularity arises from the need of taking the normal derivative of the Helmholtz integral equation in order to obtain a second kind Fredholm integral equation, as the first kind Fredholm integral equation may be ill-conditioned [34, 54, 60]. Furthermore, such a derivative is needed to eliminate the non-uniqueness problem as discussed in the previous section.

A great deal of research has been devoted to various ways of dealing with the hypersingularity. As we can not discuss all the cited literature, rather we mention some key references. There are several techniques to evaluate various types of singularities. The most widely used technique for regularization is the conversion of the hypersingular integral into a Cauchy principal value (CPV)

integral as will be discussed in §4.4.1.

Krisnasamy et al. [65] dealt with the hypersingularity for the acoustic wave scattering in three dimensions. Their method is free of any discretization assumption, it demands only sufficient smoothness on the density function of the hypersingular function at the singularity point for the Taylor series expansion to be applied. Then a conversion by Stokes's theorem is carried out to reduce the order of the singularity by converting the surface integrals into line integrals. They used a regularization relationship, which reduces the hypersingularity to a weak singularity.

Some approaches [66, 67] represent the hypersingular integrals in terms of the Hadamard finite-part [68]. For instance, Bose [66] regularized the hypersingular integral that arises from acoustic scattering problem in two and three dimensions by using the Hadamard finite-part representation.

In principle, there are two directions for regularization that are discussed in the literature. The first aims to remove all the non-integrable singularities analytically before any discretization is performed; such an analytic regularization is not entirely general and may be limited to certain problems. In contrast, the regularizations after discretization analyse each individual integrals by cancelling the divergent terms globally using a Galerkin or collocation formulation [69, 70]. This approach heavily requires the smoothness of the boundary [70].

Most of the techniques developed for regularization reduce the singularity to at worst weakly singular, or a complete regularization such as the singularity-free formula that is derived in [63].

A regularization formula for the hypersingular integral was first obtained by Maue [71] in 1949. It then was rederived in a simpler way by Mitzner [72] in 1966 for acoustic scattering from curved interfaces between two media of different density.

Furthermore, Kutt [73] reobtained such formula for two and three-

dimensional scattering problems by adopting the finite part of the hypersingular integral. Burton and Miller [60] used Maue'e formula for treating the resulting hypersingular integral. In the author's opinion, the Meyer's formula [61] for regularizing the hypersingular integral in three dimensions could be a rederivation of Maue's formula. However, Meyer's formula can be implemented easily with piecewise constant collocation method that is discussed in §4.7, just as has been done in [74]. In contrast, Maue's formula may be a bit complicated for numerical evaluation, so it needs a further treatment to make it ready for numerical computations.

In this thesis, we derive an integral identity for an flat interface in two dimensions, which is a special case of the formula that is derived in [60] for a curved interface.

Hornberger et al. [75] implemented the BEM for two-dimensional magnetic billiards, where they consider the interior and the exterior problem. They express the hypersingular operator as a special limit similar to the CPV integral. Then they use the asymptotic expression of the free-space Green function. Kutt [73] developed a numerical approach to evaluate one-dimensional hypersingular integrals in finite part representation using Gaussian quadrature [76]. Further, he proposed one-dimensional points and weights for Gaussian type finite quadrature for different order of the singularity, that is,

$$FP\int_0^1 \frac{f(x)}{x^k}\mathrm{d}x \approx \sum_{j=1}^{n} w_j f(x_j),$$

where x_j and w_j are a set of specially designed Gaussian points and weights, respectively, and n is the number of integration points. This method evaluates the singular integral numerically disregarding the divergent part. Such ideas can be adopted for integrations in two and three dimensions. Sladek and Sladek [69, 70] gave a survey on the treatment of all types of singularities.

A different approach of regularization is to subtract the singular part, and then evaluate the reminder (non-singular term) using Gaussian type quadra-

ture whereas the singular part is integrated using analytical integration formula. Next, we will discuss a different approach for regularization that is based on a suitable coordinate transformation whose Jacobian smoothens out the singularity.

Coordinate transformations

One of the best known coordinate transformations for treating weak singularities is attributed to Telles [77]. It is an elegant and simple way to deal with singular and nearly singular integrals. This transformation is performed in such a way that its Jacobian weakens or cancels out the singularity. Then the resulting integral can be evaluated by standard Gaussian type quadrature, such as Gauss-Legendre quadrature. Telles' transformation was originally designed to compute one-dimensional integrals with a logarithmic singularity. It uses quadratic or cubic transformations depending on whether the singular point is located at the end of an element or lying at a point within the element, respectively. This transformation will be revisited in §4.6.3 where we will present some formulae.

Another way to deal with weakly singular integrals is to use the 'tanh rule' [78], which requires dividing the integral into a sum of two integrals at the singularity point as,

$$I = \int_{\alpha}^{\beta} g(y)dy,$$

where the integrand $g(y)$ has a singularity at α or β. Then one needs to use the following variable transformation,

$$y = \left(\frac{\beta - \alpha}{2}\right)\tanh(w) + \left(\frac{\beta + \alpha}{2}\right), \qquad -\infty < w < \infty.$$

Furthermore, Hayami and Brebbia [79, 80] developed another transformation which needs to be implemented in polar coordinates.

2.1.4 Weighted Residual Methods

Mirroring the FEM, the BIEs can be solved numerically by the Weighted Residual Method (WRM) [15, 34]. To explain the procedure of the WRM, consider a differential or integral operator L as

$$L(u) = b, \qquad \text{in } \Omega. \tag{2.5}$$

where u is the exact solution of the differential or integral equation. The first step in the formulation of the WRM is to approximate the solution in terms of simple basis functions as

$$u'(x) = \sum_{i=1}^{N} c_i \phi_i(x).$$

where u' is the approximate the solution of equation (2.5). Then one needs to substitute u' into equation (2.5) to obtain

$$L(u') = a. \tag{2.6}$$

Now define the function R as

$$R = b - a. \tag{2.7}$$

where R is called the residual or error function. To make $u'(x)$ an accurate solution of equation (2.5), the constants c_i in the interpolation of $u'(x)$ need to be chosen in such a way that minimises the residual R. To minimise the error over the interior or forcing the approximate solution to obey the prescribed boundary conditions, the error function R can be distributed over the domain or the boundary respectively by multiplying it by weighted function w. Then integrate over the boundary, one obtains

$$\int_{\Omega} Rw \mathrm{d}\Omega = 0, \qquad i = 1, 2, \cdots, N \tag{2.8}$$

where

$$w = \alpha_1 \psi_1 + \ldots + \alpha_n \psi_n.$$

This weighted integral of the error R is called the WRM.

Various types of weighting functions ψ_i lead to different approximate methods such as sub-domain collocation, Galerkin or point collocation methods, all of these methods are discussed thoroughly in [34] with some illustrative examples. For instance, for the point collocation methods the weighting functions ψ_i are delta functions. The Galerkin method uses the same functions for the weighting functions as for the approximate solution, that is $\psi_i = \phi_i$. This produces a symmetric coefficient matrix which is advantageous especially for large problems [43].

Banerjee [44] discusses different types of direct and indirect BEM formulations that lead to symmetric and non-symmetric coefficients matrix. Using the WRM for the BEM formulation, it becomes easy to combine the BEM with FEM.

2.1.5 Division into sub-components

We are primarily interested in non-homogeneous media that are made up of different material properties, that is different parameters in the wave equation, such as wave velocity and absorption coefficients characterise for different regions. Therefore one can not easily apply the classical single-domain BEM discussed in Chapter 3. Thus it is crucial to develop an efficient method for such categories. Furthermore, a BEM analysis for complex shapes can be simplified by dividing the domain under consideration into simpler sub-components in what is called the multi-component or sub-region BEM. It also is known as the zoning/sub-sectioning technique [44], and is commonly used in engineering applications [44, 50, 58, 81, 82].

The core idea of this approach is to divide the non-homogeneous structure into homogeneous sub-components that can be tackled individually by the BEM, i.e. construct a BIE for each sub-component. The resulting BIEs are then combined with the continuity of the solution and the equilibrium of the energy flux across the interfaces between the sub-components. Then all the boundaries

have to be discretized, including the internal boundaries that separate the sub-components.

The subdivision into sub-components is not only employed for homogeneous media, but also for domains that suffer from irregular geometry, such as cracks, long profiles or notches to enhance the computational efficiency. The BEM sub-region technique is widely considered as an efficient tool for treating non-homogeneous domains. The subdivision approach leads to a block-banded global matrix with one block for each sub-region, and overlaps between blocks when sub-regions have an interface. This replaces the fully populated matrix by a block-banded matrix, which is computationally more convenient. One could conclude that the sub-components technique enhances the applicability of BEM.

Kita and Kamiya [81] presented a sub-region BEM approach, in which the global matrix is constructed by a superposition of the BIEs for each sub-region by implementing the continuity conditions along the interfaces. Within this approach in order to compute the global matrix, a matrix inversion for each sub-region matrix equation is required, which sometimes is not a stable operation and increase the overall computational time.

Banerjee [44] introduced an advanced multi-region assembly to deal with zoned or piecewise homogeneous bodies. In his approach, the zero-blocks never enter into the formulation, which considerably decreases the memory required to store the global matrix. On the other hand, his approach requires matrix inversion operations for the individual matrix system for each sub-region. Since the sub-component technique needs to create new boundaries (interfaces) and therefore new unknowns, this results in a large number of unknowns as we need to compute two unknowns along each interface. Therefore, for large problems, a parallel computing is often desirable as will be discussed in the next section.

The direct Gauss elimination solver is normally used to solve the linear system of equations generated by the BEM. However, for the usual feature of the

BEM matrices which are non-symmetric and dense, such solver become uneconomic. Therefor for large number of unknowns, it is wise to resort to iterative solvers to reduce the running time. Many iterative solvers have been discussed thoroughly and tested in [83] such as the conjugate and bi-conjugate gradient acceleration.

2.1.6 Domain Decomposition Method

In the analysis of large-scale models, usually some difficulties are encountered in terms of the required memory and the CPU speed. To overcome such obstacles, one needs high performance computing techniques, including parallel computing. The Domain Decomposition Method (DDM) [59] has come to reduce the computational effort involved with solving large BEM or FEM models. DDM is a tool that is artificially introduced to ease large-scale computations and in some situations, domain decomposition is natural from the physics of the problem. The domain decomposition methods offer considerable advantages for efficient computation and the ability to mix solvers. It has subsequently evolved with the development of multiprocessor computer architectures.

In principle, DDM is a perfectly convenient implementation in a parallel computing environment. Thus to be able to deal with domains of different material properties, or domains that are governed by different differential equations or boundary conditions, the domain under consideration is decomposed into sub-domains. Each sub-domain is treated separately and has its own system of equations. Then one needs to apply the continuity conditions between the neighbouring sub-domains. This approach produces a block-banded or even a sparse matrix when dealing with a large number of sub-domains in which the number of zero-blocks increases [84]. This is the most appealing feature of the DDM, because the sparse system can be solved efficiently by iterative solvers. The criterion for the choice of the suitable iterative solver relies on the PDE and the type of decomposition. For example, the Lagrange multiplier is used

for a non-overlapping decomposition, while the Schwarz formulation is used for overlapping decomposition [59].

Sugino et al. [85] showed the utility of the DDM analysis with the BEM for an interface motion of two-layer fluid. They constructed BIEs for the Laplace equation for each sub-domain in conjunction with compatibility and equilibrium conditions on the interfaces. Suitable iterative solvers are favoured with the DDM, such as Schwarz's iterative algorithms and many other types of iterative algorithms that are discussed thoroughly in [59]. Consider an interface between two media which belongs to both the left and right sub-domains, that is $\Gamma = \Gamma_l$ and Γ_r, respectively. Uzawa's method [86] was implemented as an iterative scheme for boundary conditions (BCs) along both interfaces Γ_l and Γ_r. Such a scheme sets an initial Dirichlet BCs along interfaces, and then calculating the flux at the interfaces. Successive updates of the flux on the interface between the sub-domains are carried out until the required accuracy is reached.

Furthermore, Kamiya and co-workers [86] presented a parallel implementation of the BEM with DDM, in which the boundary element analysis is performed for each sub-domain in parallel. If the continuity conditions along the interface are satisfied, then the process is terminated, if not the boundary conditions along the interface need to be modified and the process is repeated.

Three different iterative schemes are used, that is the Uzawa, Schwarz Neumann-Neumann and the Schwarz Dirichlet-Neumann methods. The Schwartz Dirichlet-Neumann method sets an initial Dirichlet and Neumann BCs along Γ_l and Γ_r, respectively. The Schwarz Neumann-Neumann method sets an initial Neumann BCs along both interfaces Γ_l and Γ_r. In Kamiya's work [86], the parameter of the iterative schemes was selected empirically, however, some effort must be dedicated to find the optimal value of such a parameter. Such a value is not only needed to speed up the convergence, but also to control the convergence of the iterative coupling methods [87]. The choice of the iterative scheme is problem dependent; specifically, it depends on the type of the BCs on the external

boundaries.

Lu and Wu [82] introduced a new sub-region BE technique based on the DDM for multi-layered elastic crack problems. This method is convenient for implementation on parallel (multiprocessor) computer architectures because the coefficient matrix for each sub-region can be calculated independently. This allows the outer boundary conditions to be changed because to do so, only the equations for the sub-region concerned need to be recalculated.

Furthermore, DDM is flexible for solving PDEs of heterogeneous character, for example, a PDE which is elliptic in one sub-region and parabolic in the other region. Due to the independent treatment of each sub-domain, the DDM lends itself conveniently to parallel computing. DDM has the advantage that no preconditioning of the matrix is needed due to the separate treatment of each sub-domain.

Within the DDM, one could have a different numerical method for different regions. For instance, if a structure is constructed of plastic and elastic regions, then the former is best analysed by FEM and the remaining infinite/semi-infinite linear elastic regions may be best analysed by BEM [87]. Another example of FE-BE coupling has been implemented to an acoustics system that contains a vibrant structure radiating sound through an opening to an exterior domain. For such a model the acoustic wave field of the interior and the exterior is analysed by FEM and BEM, respectively [88]. Finite element-boundary element method (FE-BE) coupling has been investigated intensively and implemented for a variety of applications such as fluid mechanics, fracture mechanics, electrodynamics, acoustics and mechanics [43, 44].

2.1.7 Multi-domain Dual Reciprocity Method

Attempts were made to extend the applicability of the BEM to heterogeneous and non-linear problems. In such categories, it is necessary to put the non-homogeneous or non-linear terms into a body force. Within the classical BEM for-

mulation, these terms lead to domain integrals and the BEM loses its boundary-only character.

To overcome these limitations of BEM, in 1982 Nardini and Brebbia [89] proposed a new formulation called the Dual Reciprocity Method (DRM) which depends on the use of particular solutions. A thorough introduction into the method and its applications can be found in [89, 90] and references therein. Some illustrative examples about the method are demonstrated by Brebbia [91].

To explain the core idea of this method, consider the formulation for Poisson's equation with an arbitrary source term $\chi(\mathbf{r})$ as

$$\nabla^2 u = \chi(\mathbf{r}). \tag{2.9}$$

The term $\chi(\mathbf{r})$ can represent the non-heterogeneity or the non-linearity of the problem. Within the classical BEM formulation, this term lead to domain integrals as

$$cu + \int_{\partial\Omega} \left[\frac{\partial u(x)}{\partial n_x} F - \frac{\partial F}{\partial n_x} u(x) \right] = \int_{\Omega} F \chi(\mathbf{r}) \mathrm{d}\Omega, \tag{2.10}$$

where F and Ω are respectively the fundamental solution and the domain of the problem. Thus the starting point in the DRM formulation is to express the non-homogeneous term $\chi(\mathbf{r})$ as a series of known basis functions as,

$$\chi(\mathbf{r}) = \sum_{i=1}^{N} \gamma_i f_i \tag{2.11}$$

where the functions f_i are so called the Radial Basis Functions (RBFs) [92], γ_i are unknown coefficients, and N is the number of basis functions. The functions f_i are geometry-dependent functions whose value depends only on the distance of a point x_i from the origin or any chosen centre point y, i.e,

$$f_i(x_i, y) = f_i(\mid x_i - y \mid).$$

This interpolation leads to a particular solution ψ_i of the problem,

$$\nabla^2 \psi_i = f_i. \tag{2.12}$$

These particular solutions ψ_i can be found analytically for a given basis functions f_i just by integrating equation (2.12). Substituting equations (2.11) and (2.12) into equation (2.9) leads to,

$$\nabla^2 u = \sum_{i=1}^{N} \gamma_i (\nabla^2 \psi_i). \tag{2.13}$$

Then one needs to apply the weighted residual method as addressed in §2.1.4, and Green's identity or a reciprocity principle [58, 89], which lends to the name of the method (DRM). To do so, one needs to multiply both sides of equation (2.13) by the fundamental solution F, and integrate over the domain Ω. One has

$$cu + \int_{\partial\Omega} \left[\frac{\partial u(x)}{\partial n_x} F - \frac{\partial F}{\partial n_x} u(x) \right] = \sum_{i=1}^{N} \gamma_i \int_{\Omega} F(\nabla^2 \psi_i) \mathrm{d}\Omega. \tag{2.14}$$

Each term in the RHS of equation (2.14) can be integrated by parts leading to boundary integrals.

Recently, Popov and Power [84] used the sub-regions technique that is discussed in §2.1.5 with the DRM to deal with domains of piecewise homogeneous material properties. Initially, they implemented this approach to the flow of a mixture of gases through porous media. They decomposed the structure into sub-regions, then implemented the DRM for each sub-region in what is called the Multi-Domain Dual Reciprocity Method (MD-DRM). They claimed that it is possible to treat domains with a strong variation of material properties by refining the mesh. The DRM has been widely implemented by many researchers. For instance, non-linear problems have been considered by Telles [93] and free vibration for two-dimensional structures have been considered by Samman [94].

2.2 Statistical methods for high-frequency problems

The deterministic numerical methods discussed above are usually restricted to the low-frequency range, as they become prohibitively expensive and unreliable in the mid and high-frequency range. For the high-frequency range, statistical

approaches have become popular for predicting the mean energy of the system and neglecting wave effects such as interference or diffraction. Therefore, they are often favoured only in the high-frequency range.

2.2.1 Statistical Energy Analysis

Statistical Energy Analysis (SEA) divides the system into a small number of subsystems whose response is described in terms of vibrational energy. The global SEA equations are obtained through an energy balance of each sub-system. For a detailed account about this approach, the reader is referred to a text-book by Lyon and DeJong [95]. The interaction between the subsystems is described using the balance of energy flow. This leads to a set of linear equations that can be solved for the mean wave energy stored in each sub-system.

SEA can efficiently deal with complex structures carrying wave energy over the subsystems, including a large number of reflections and scattering events. By applying this method, one can predict both the ensemble vibrational energy levels and the ensemble variance of the energy levels [96]. Despite the power of SEA, its applicability is limited to the high-frequency range.

In addition, the subsystems must be dynamically well separated and the absorption is small, as strong damping may lead to significant decay. Furthermore, the subsystems need to be sufficiently random; this condition will be fulfilled if the subsystem boundaries are sufficiently irregular. It is worth mentioning that the SEA is based on a classical ray picture and does not take into account wave phenomena.

2.2.2 Dynamical Energy Analysis

Dynamical Energy Analysis (DEA) is a thermodynamic approach in the high-frequency limit, and is based on similar ideas to SEA. This approach considers a multi reflection in terms of linear operators. Then it represents these operators in terms of basis functions resulting in SEA-type equations. A natural choice

of basis functions for problems with periodic boundary conditions is the Fourier basis, as adopted by Tanner [97]. However such a formulation encounters some difficulties, such as slow convergence and the treatment of the corners on the boundary.

These drawbacks have been avoided using Chebyshev basis functions [98]. It has been shown that DEA is an efficient technique for predicting wave energy distribution in complex built-up structures at high frequencies. Furthermore, such a tool enhances the applicability of SEA and overcomes its geometrical limitations. Consequently, DEA has more capability than SEA in the sense that it contains information about dynamical correlations between sub-systems.

This technique was implemented successfully to determine the wave energy distribution in a variety of coupled, two-cavity configurations [97]. Besides it was implemented for multi-component systems with variable material properties. A comparison is then carried out against SEA and the adaptive DG-FEM. This shows the efficiency of DEA over SEA and DG-FEM for certain regular geometries and high frequencies, respectively [12, 97, 98]. DEA removes the SEA restriction for energies to be equidistributed in subsystems, meaning it no longer matters whether a suitable SEA subdivision can be found. This makes the DEA more suitable for a big problem for many engineering applications such as interior acoustics of vehicles.

2.3 Hybrid methods for mid-frequency regimes

There are systems with large variations of local wavelength, for example a car body is constructed of different components such as bending (Panel) and stiff (frames) sub-components, in what is referred to as mid-frequency problems. To predict the wave intensity distribution in such systems, it is not reliable to use a deterministic tool as it will be prohibitively expensive.

On the other hand, using a statistical approach often loses important information about the system. Therefore, the system should be divided into sub-

systems, in which a hybrid framework should be applied. That is, the regions with long wavelengths are treated by a deterministic method and the ones with short wavelengths are treated by a statistical tool. Recently, some methods have been developed which are based on stretching the applicability of a deterministic tool; these include wave based techniques (WBTs). Other approaches are based on relaxing some of the SEA assumptions which are called the Statistical modal Energy distribution Analysis (SmEdA) [99].

An important hybrid deterministic-statistical approach has been developed by Shorter and Langley [100] for systems that exhibit a mixed character where some subsystems have a random behaviour and others have deterministic behaviour. They successfully employed a FEM for deterministic sub-systems and SEA for random subsystems to achieve a FE-SEA hybrid approach. Moreover, another hybrid FE-SEA approach has been developed in [101]. This approach involves using random diffuse field correlation functions and its relation to the Green function [102]. For example, the panels in a car body are treated by SEA whereas the frames are treated by the FEM. Furthermore, Vergote et al. [103] adopt a similar idea where they combine a Trefftz-based deterministic method with SEA to achieve a hybrid WB-SEA method. They implement this hybrid technique to a vibro-acoustic problem that is constructed of a three-dimensional deterministic acoustic cavity coupled to a two-dimensional elastic plate with random properties.

In contrast with SEA, DEA provides information about the dynamical correlations between sub-systems that play a role in systems that have elements with short and long wavelengths. Therefore, it is expected that a hybrid approach that combines a deterministic tool with DEA will be of a great importance [97].

2.4 Asymptotic methods for mid and high-frequency regimes

One of the most popular and successful tools is the semiclassical approximations, which is extensively used in quantum mechanics to provide a better understanding of the correspondence between quantum and classical mechanics. Here, we give an overview of the asymptotic methods for the high-frequency problems relating wave problems to ray dynamics. This area of research is well documented in a series of textbooks, see Haake [104], Gutzwiller [105], Brack and Bhaduri [106], Stöckmann [107], and an article review by Tanner and Søndergaard [9]. Motivated by the importance of the propagation of high-frequency waves in many fields, e.g., seismology, acoustics, optics, microwaves, and quantum mechanics, this phenomenon is a classical topic with a rich history of research and has been investigated through various approaches. For instance, Bogomolny and Huges [108] theoretically and numerically investigated the vibration of high-frequency plates by studying the Biharmonic equation in the short wavelength (high-frequency) limit.

It is known that integrable systems (constants of motion are equal to the number of degrees of freedom) such as rectangular or spherical billiards can be quantized using Einstein-Brillouin Keller (EBK) quantization condition [105]. However, for non-integrable (chaotic) systems such as stadium billiards, one can use the well known Gutzwiller periodic-orbit sum trace formula [11]. It dominated the field for a long time as the only way for quantization by summing over periodic orbits. Due to the exponential proliferation of the number of periodic orbits in chaotic system, the infinite sum or product over periodic orbits is not convergent on the real energy axis and the computed eigenvalues are not real. Gutzwiller periodic-orbit sum trace formula represents the density of states in the complex energy plane.

Some attempts were devoted to the analytic continuation of the spectral

determinant to the real energy axis. Berry and Keating [109, 110] introduced an approximation expression of the spectral determinant on the real energy axis. In 1992 Doron and Smilansky [111] presented a semiclassical quantization approach for billiards of any shape. Their approach is based on the relationship between the dynamics inside and outside the billiard.

However a new different approach for quantizing chaotic systems in the semilclassical limit was proposed by Bogomolny which will be discussed next.

2.4.1 Transfer operator method

In 1990 Bogomolny [8] pioneered a new approach for quantizing systems in the semiclassical limit; his approach is known as the Bogomolny semiclassical transfer operator. Such an operator is an appropriate way of quantizing systems without any knowledge of the periodic orbits in contrast with the Gutzwiller trace formula. Thus, this approach does not encounter any divergence problem. The stage of Bogomolny's method is a suitable Poincaré Surface of Section (PSS) which is naturally but not necessarily the boundary of the domain. The PSS is a surface drawn through the phase space of the system. Thus Bogomolny's method is known also as the Surface of Section Method (SSM) as adapted in [112, 113].

The Bogomolny semiclassical transfer operator $T(q, q'; \mathrm{E})$ at energy E is obtained by summing over all the classical trajectories on a PSS which go from the initial point q' in the same direction to the final point q with only one crossing of the PSS as,

$$T(q, q'; \mathrm{E}) = \frac{1}{\sqrt{2\pi\imath\hbar}} \sum_{\substack{cl.tr. \\ q' \to q}} A(q, q') e^{\imath\left(\frac{S(q,q';\mathrm{E})}{\hbar} - \frac{\pi\nu}{2}\right)}.$$

The function $S(q, q'; \mathrm{E}) = \int_{q'}^{q} p\mathrm{d}q$ is the action at energy E along the classical trajectory, p and q respectively refer to the momentum and position, and $\hbar$ is the Planck constant. The amplitude A provides information about the focusing of nearby trajectories [106]. The phase index ν is the Maslov index [11] counting the number of points where the semiclassical approximation breaks down.

Boasman [10, 114] obtained the transfer operator by using the asymptotic expansion of the kernels of the BIEs, then analytically and numerically he tested the accuracy of his approach for circular and chaotic billiards such as stadium and Africa billiards. He showed that the difference between both methods is of the order $O(\hbar^2)$. Also he derived a formula for the difference between the exact and the semiclassical spectra. Furthermore, he showed that both results obtained from the Bogomolny transfer operator and the semiclassical kernels of the BIEs have the same leading-order approximation, however, they are not the same when higher-order corrections are considered.

Since the Bogomolny transfer operator does not include the evanescent contribution, it can not reproduce boundary effects such as surface waves and diffraction. Therefore some thoughts have been emerged on whether one could exactly obtain such an appropriate operator. Doron and Smilansky [111] developed a scattering approach to quantization which include the leading-order corrections coming from evanescent modes. They consider the billiard interior as a scattering off the boundary of the billiard. Their approach is based on the relation between the interior and exterior of a billiard, and using the fact that the spectra of the interior problem can be computed from the scattering operator [115].

Furthermore, a work by Prosen followed in 1994 and 1995 [112, 113, 116]; he presented an abstract formulation of the exact quantum Poincaré mapping for general bound Hamiltonian system. His approach does not start from the BIEs. He showed how the exact quantum Poincaré map converges to the semiclassical Bogomolny transfer operator. Furthermore, he systematically derived the high-order corrections to the semiclassical transfer operator.

In this thesis, a novel derivation of the exact transfer operator is presented for a disc with boundary conditions change discontinuously across the boundary. Our approach is designed to accommodate multi-component systems.

2.4.2 Asymptotic methods for systems with ray-splitting

The ray-splitting phenomenon generally appears when the material properties change in a distance ϵ shorter than the wavelength ($\epsilon < \lambda$), for example, a Schrödinger equation with discontinuous step potential as discussed in [117, 118, 119]. This phenomenon also finds applications in elastic media where we have two wavenumbers corresponding to the longitudinal pressure waves and the transverse shear waves. The difference of wave speeds then leads to the occurring of ray-splitting at the discontinuity line (interface). That is an incident ray gives birth to four rays, two of them are pressure and shear rays reflected off the interface while the other two are transmitted pressure and shear waves as depicted in figure 2.1.

Ray-splitting phenomenon happens according to Snell's law, which is given as,

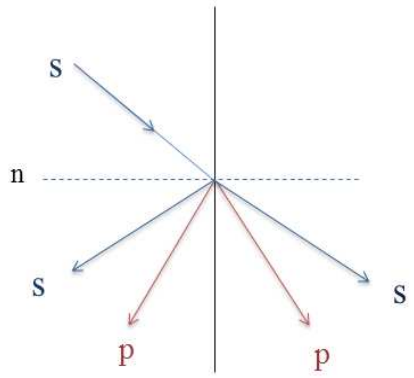

Figure 2.1: Ray splitting in elastic media, s and p stands for shear and pressure waves respectively.

$$c_1 \sin\theta_2 = c_2 \sin\theta_1, \tag{2.15}$$

where c_1 and c_2 are respectively the wave velocities for the left and right side of the interface. The angles θ_1 and θ_2 are respectively the angles of the incidence and refraction measured with respect to the normal to the interface as depicted in figure 2.2. Snell's law reflects the conservation of the tangential momentum at the ray-splitting boundary, and it is energy conserving.

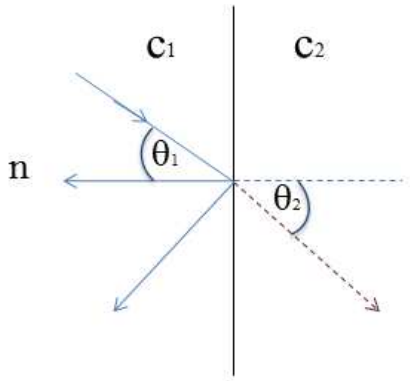

Figure 2.2: Illustrative sketch of Snell's law.

The ray-splitting phenomenon develops diffractive effects at the interface between two media. Another phenomenon is related to the ray splitting is the signature of lateral waves. Such waves behave in a different way once they hit the interface, they are travelling laterally for a distance along the interface before leaving the interface. Such waves were considered by Kohler and Blümel [120], also discussed in [117].

Asymptotic methods have been found to be powerful tools in giving information in the high-frequency limit for systems with ray-splitting. A series of papers by Blümel et al. [117, 118, 119] contributed to the development of the theory of semiclassical approximations for systems with ray splitting. Blümel et al. [117] presented a formal derivation of the semiclassical transfer operator for a two-dimensional Schrödinger equation with discontinuous step potential for a unit disc. They started from the BIEs by writing the free Green function in terms of its Fourier transform representation along infinite interface separating the two media of different material properties. Their approach is not quite handy for multi-component system, because it is not economic to have such treatment for systems with multiple interfaces.

They demonstrated that the ray splitting phenomenon makes the circular billiard chaotic. They also considered the effects of lateral waves. They carried out a comparison between the exact spectra against the semiclassical

transfer operator showing good agreement between the two categories and verifying the efficiency of the semiclassical transfer operator for systems with ray splitting.

It is worth mentioning that the semiclassical approximation for systems with ray splitting does not consider wave effects such as diffraction or tunnelling. These effects can be taken into account by considering ray dynamics in the complex plane as shown by Creagh [121].

Couchman et al [122] generalised the Gutzwiller periodic-orbit sum trace formula [11] for elastic media with ray splitting. Their trace formula sums over all closed orbits of the ray splitting problems. Such orbits are close on themselves and have specular reflection either from the external boundaries or from the interface. Such a trace formula requires the calculations of the reflection and transmission coefficients for each orbit.

It is worth mentioning that the ray splitting phenomenon in elastic media enhances the degree of chaos as discussed in [117], where rays change from pressure to shear waves. This leads to an exponential growth of the number of periodic orbits. With the absence of ray splitting Couchman's trace formula can be reduced back to the known Gutzwiller's trace formula where the closed orbits are the usual periodic orbits. Furthermore, a full derivation of the trace formula for an elastic media which support pressure and shear waves was presented by Tanner and Søndergaard [123].

Bogomolny developed a semiclassical trace formula for the high-frequency vibration of an elastic plate [108]. A powerful technique for deriving such trace formula from wave equations is to derive an asymptotic expression of the boundary integral kernels obtaining the semiclassical transfer operator.

Tanner and Søndergaard [123] adopted similar ideas of Bogomolny's work [108] to derive the short wavelength asymptotic of the boundary integral kernels of Navier-Cauchy equation for two-dimensional, homogeneous and isotropic elastic media using the asymptotic approximation from the indirect formulation

of the boundary integral equation.

Additionally, Søndergaard and Tanner derived a trace formula for an elastic, circular disc with free boundaries by writing the spectral density as the trace of the Green function [124].

Chapter 3

The boundary element method for homogeneous media

3.1 Introduction

In this chapter, we present the standard BEM which will then be used in the next chapter; to develop a multi-component BEM. we also show some of its applications. We implement the BEM for the Helmholtz equation for two-dimensional non-convex polygonal-domain with Dirichlet boundary conditions yielding the spectrum, the corresponding eigenfunctions, and the Green function. We show how to overcome the arising weak-singularity in the BIEs by deriving a further boundary integral equation. We compare the BEM treatments considering integral kernels with and without taking normal derivatives. By showing numerical example for smooth boundary (circle), we thus observe that it can be advantageous to consider normal derivative kernels.

3.2 Helmholtz equation and its fundamental solution

In this thesis, the governing wave equation is the two-dimensional scalar Helmholtz equation with constant wave velocity. Such equation arises naturally in many

physical applications related to wave propagation and vibration phenomena, such as free particle in a finite domain referred as quantum billiard problem, membrane vibrations, acoustic wave fields, electromagnetic and microwave field in cavities. For systems without potential such as billiards, the stationary (time independent) Schrödinger equation can be reduced to the Helmholtz equation with the scaling,

$$k = \left(\frac{\sqrt{2m\mathrm{E}}}{\hbar} \right)$$

where k is the wavenumber, m is the particle's mass, E is the particle's energy, and $\hbar$ is the Planck constant. We consider a polygonal-shaped domain D in the following. Such a geometry is desired in many engineering applications, such as room acoustic. The homogeneous Helmholtz equation is given as

$$(\nabla^2 + k^2)\psi(\mathbf{q}) = 0, \tag{3.2.1}$$

where ψ is the corresponding eigenfunction to the eigenvalue k, and ∇^2 is the two-dimensional Laplace operator in Cartesian coordinates.

The first step within the BEM formulations is to introduce the fundamental solution of the problem which is essential to establish the necessary BIEs. The fundamental solution of a differential equation is a solution with a unit point source equal to $\delta(\mathbf{r} - \mathbf{r}')$ applied at a given, fixed source point $\mathbf{r}'$. The following equation thus holds,

$$(\nabla^2_{\mathbf{q}} + k^2)G_0(\mathbf{q}, \mathbf{r}; k) = -\delta(\mathbf{q} - \mathbf{r}), \tag{3.2.2}$$

where the fundamental solution, also called the free-space Green function G_0 defined as,

$$G_0(\mathbf{r}, \mathbf{r}'; k) = \frac{\imath}{4} H_0^{(1)}(k|\mathbf{r} - \mathbf{r}'|). \tag{3.2.3}$$

The derivation of G_0 can be found in Appendix A. Physically, $G_0(\mathbf{r}, \mathbf{r}'; k)$ measures the response at a receiver point $\mathbf{r}$ of a source point located at $\mathbf{r}'$ propagating into the free space, disregarding the prescribed boundary conditions. The function $H_0^{(1)}(k|\mathbf{r} - \mathbf{r}'|)$ denotes the Hankel function of the first kind and zeroth order,

and

$$|\mathbf{r}-\mathbf{r}'| = \sqrt{(x-x')^2+(y-y')^2}$$

is the distance between the source $\mathbf{r}'$ and the observation point $\mathbf{r}$. Here

$$H_0^{(1)}(z) = J_0(z) + \imath\, Y_0(z),$$

where $J_0(z)$ and $Y_0(z)$ are the zeroth order Bessel functions of the first and second kind, respectively. They are given by the following power series,

$$J_0(z) = \sum_{k=0}^{\infty} \frac{(-1)^k}{(k!)^2}\left(\frac{z}{2}\right)^{2k}, \tag{3.2.4}$$

and

$$Y_0(z) = \frac{2}{\pi}\left[\ln\left(\frac{z}{2}\right)+\gamma\right] J_0(z) - \frac{2}{\pi}\sum_{k=1}^{\infty} a_k \frac{(-1)^k}{(k!)^2}\left(\frac{z}{2}\right)^{2k}, \tag{3.2.5}$$

where $a_k = \sum_{m=1}^{k} 1/m$ and

$$\gamma = \lim_{n\to\infty}\left(\sum_{m=1}^{n} 1/m - \ln n\right) = 0.57721\cdots$$

represents Euler's constant [125].

Since the free-space Green function is a function of the distance between two points, it obeys the symmetry property for $\mathbf{r}$ and $\mathbf{r}'$. A general feature of the fundamental solution is the singularity; for example, in two dimensions, one has

$$\begin{aligned} G_0(\mathbf{r},\mathbf{r}';k) &\simeq O\left(\ln|\mathbf{r}-\mathbf{r}'|\right), \\ \frac{\partial}{\partial n_{\mathbf{r}}} G_0(\mathbf{r},\mathbf{r}';k) &\simeq O\left(\frac{1}{|\mathbf{r}-\mathbf{r}'|}\right), \\ \frac{\partial^2}{\partial n_{\mathbf{r}}\partial n_{\mathbf{r}'}} G_0(\mathbf{r},\mathbf{r}';k) &\simeq O\left(\frac{1}{|\mathbf{r}-\mathbf{r}'|^2}\right). \end{aligned}$$

For the BEM formulation, one needs to utilise the free-space Green function $G_0(\mathbf{r},\mathbf{r}';k)$, which satisfies the non-homogeneous Helmholtz equation (3.2.2).

3.3 Derivation of the boundary integral equations

In this section, we show the derivation of the BIEs for the Helmholtz equation with Dirichlet boundary conditions as an eigenvalue problem. To begin one needs

to multiply equation (3.2.1) and (3.2.2) by $G_0(\mathbf{r}, \mathbf{r}'; k)$ and $\psi(\mathbf{r}')$, respectively. Then subtract the two resulting equations, and integrate over the region D with an area element $\mathrm{d}A_{\mathbf{q}}$, to obtain

$$\iint_D \left[G_0(\mathbf{q}, \mathbf{r}; k)\nabla^2_{\mathbf{q}}\psi(\mathbf{q}) - \psi(\mathbf{q})\nabla^2_{\mathbf{q}}G_0(\mathbf{q}, \mathbf{r}; k)\right] dA_{\mathbf{q}} = \iint_D \delta(\mathbf{q} - \mathbf{r})\psi(\mathbf{q})\mathrm{d}A_{\mathbf{q}}. \tag{3.3.1}$$

The integral on the right hand side (RHS) of equation (3.3.1) depends on the position of $\mathbf{r}$, and can be classified as the following,

$$\iint_D \delta(\mathbf{q} - \mathbf{r})\psi(\mathbf{q})\mathrm{d}A_{\mathbf{q}} = \begin{cases} \psi(\mathbf{r}), & \text{if } \mathbf{r} \in D; \\ \frac{1}{2}\psi(\mathbf{r}), & \text{if } \mathbf{r} \in \partial D; \\ 0, & \text{otherwise.} \end{cases} \tag{3.3.2}$$

For the left hand side (LHS) of equation(3.3.1), one needs to make use of the Green second identity (2.1) to obtain,

$$\int_{\partial D} \left[G_0(q, \mathbf{r}, ; k)\frac{\partial}{\partial n_q}\psi(q) - \psi(q)\frac{\partial}{\partial n_q}G_0(q, \mathbf{r}; k)\right] \mathrm{d}q = \begin{cases} \psi(\mathbf{r}), & \text{if } \mathbf{r} \in D; \\ \frac{1}{2}\psi(\mathbf{r}), & \text{if } \mathbf{r} \in \partial D; \\ 0, & \text{else.} \end{cases} \tag{3.3.3}$$

where $\vec{n}_q$ denotes the outward unit normal vector at the boundary point q. The operator $\frac{\partial}{\partial n_q}$ denotes the directional derivative along the normal vector $\vec{n}_q$ at the boundary element q, that is,

$$\frac{\partial}{\partial n_q}G(q, \mathbf{r}; k) = \vec{n}_q \cdot \nabla_q G(q, \mathbf{r}; k),$$

where the dot denotes the scalar product, ∇_q is the gradient operator with respect to q, and $\mathrm{d}q$ is the arc length element along the boundary D. The two-dimensional differential equation (3.2.1) is thus reduced to a one-dimensional boundary integral equation (3.3.3).

The direct substitution of DBCs, and letting $\mathbf{r} \to \beta \in \partial D$ in equation (3.3.3) leads to the following BIE

$$\int_{\partial D} G_0(q, \beta; k)\frac{\partial}{\partial n_q}\psi(q)\mathrm{d}q = 0. \tag{3.3.4}$$

This BIE is classified as Fredholm integral equation of the first kind, because the unknown $\frac{\partial}{\partial n_q}\psi(q)$ appears only implicitly, that is under the integration sign. Note that, this BIE has a logarithmically divergent kernel (weakly-singular) at $q = \beta$. Actually, we can proceed with the BIE (3.3.4) after a careful treatment of the weak-singularity of $G_0(q, \beta; k)$.

A well known trick [10, 126] to avoid this additional complication for problem with DBCs is to take the normal derivative of the BIE (3.3.3) with respect to $\mathbf{r}$ in the limit ($\mathbf{r} \to \beta \in \partial D$) transforming all G_0 terms to $\partial G_0/\partial n_\beta$ terms. Since $\mathbf{r}$ is an interior point, we may generally differentiate beneath the integral sign. That is applying the operator $(n_\beta \cdot \nabla_{\mathbf{r}})$ on (3.3.3), one obtains

$$\lim_{\mathbf{r}\to\beta} \frac{\partial}{\partial n_\beta}\psi(\mathbf{r}) = \lim_{\mathbf{r}\to\beta} \int_{\partial D} \left[\frac{\partial}{\partial n_\beta} G_0(q, \mathbf{r}; k) \frac{\partial}{\partial n_q}\psi(q) - \psi(q)\frac{\partial}{\partial n_\beta}\frac{\partial}{\partial n_q} G_0(q, \mathbf{r}; k)\right] \mathrm{d}q. \tag{3.3.5}$$

Since we aim to formulate a boundary only method, the interior field point is now positioned into the boundary $\mathbf{r} \to \beta \in \partial D$ in equation (3.3.5). This should not present any restriction or difficulties and all the integrals remain well behaved as long as the source point is located far away from β. Imposing DBCs in equation (3.3.5) leads to,

$$\lim_{\mathbf{r}\to\beta} \frac{\partial}{\partial n_\beta}\psi(\mathbf{r}) = \lim_{\mathbf{r}\to\beta} \int_{\partial D} \frac{\partial}{\partial n_\beta} G_0(q, \mathbf{r}; k) \frac{\partial}{\partial n_q}\psi(q)\mathrm{d}q. \tag{3.3.6}$$

The RHS of equation (3.3.6) known in potential theory as the double layer potential, and there is a special relation for its limit to the boundary. That is the kernel $\lim_{\mathbf{r}\to\beta} \frac{\partial}{\partial n_\beta} G_0(q, \mathbf{r}; k)$ has a jump when $\mathbf{r}$ tends to the boundary. Therefore, when formulating the BIEs, it is necessary to consider the discontinuity properties for the layer potentials as will be addressed next.

3.3.1 Classical jump relation

In this section, we present the concept of the jump conditions for the double layer potential which is defined as the following,

$$\xi(\beta) = \lim_{\mathbf{r}\to\beta} \int_{\partial D} \frac{\partial}{\partial n_\beta} G_0(q, \mathbf{r}) \frac{\partial}{\partial n_q}\psi(q)\mathrm{d}q. \tag{3.3.7}$$

Now define

$$\mu(q) = \frac{\partial}{\partial n_q}\psi(q). \tag{3.3.8}$$

Thus double layer potential ξ can be rewritten in terms of μ as

$$\xi(\beta) = \lim_{\mathbf{r}\to\beta}\int_{\partial D}\frac{\partial}{\partial n_\beta}G_0(q,\mathbf{r})\mu(q)\mathrm{d}q, \tag{3.3.9}$$

where μ is called the density of the double layer potential.

The jump condition (classical jump relation) expresses the difference between the value of the layer potential on the boundary and its value either in the interior or the exterior of the boundary ∂D as stated in the following theorem:

Classical Jump Relation

Theorem 3.3.1 *[52] The double layer potential ξ with continuous density μ can be continuously extended from an interior point in D to a boundary point $\beta \in \partial D$ with the limiting values,*

$$\xi_\pm(\beta) = \int_{\partial D}\frac{\partial G_0(q,\beta)}{\partial n_\beta}\mu(q)\mathrm{d}q \mp \frac{1}{2}\mu(\beta), \qquad \beta \in \partial D, \tag{3.3.10}$$

where

$$\xi_\pm(\beta) := \lim_{h\to+0}\xi(\beta \pm hn_\beta)$$

where n_β denotes the outward normal at β, and the indices $+$ and $-$ respectively refer to the limits obtained by approaching the boundary ∂D from outside or inside D, that is

$$\left.\begin{aligned}\xi_+(\beta) &= \lim_{\substack{z\to\beta,\\ z\in D_{ext}\xi(z)}}\xi(z)\\ \xi_-(\beta) &= \lim_{\substack{z\to\beta,\\ z\in D_{int}}}\xi(z)\end{aligned}\right\} x \in \partial D \tag{3.3.11}$$

and the integral exists as an improper integral.

In addition to the jump relation for the double layer potential, there are further classical jump relations concerning the layer potentials and their normal

derivative that are discussed thoroughly in [56].

To conclude, the interior and exterior limiting values of the double layer potential and its actual value on the boundary are related by the following relation [60]

$$[\xi]_{\partial D} = [\xi(z)]_{\text{int}} - \frac{1}{2}\mu(\beta) = [\xi(z)]_{\text{ext}} + \frac{1}{2}\mu(\beta), \tag{3.3.12}$$

where $\beta \in \partial D$ and z is either interior or exterior point.

After we introduced the jump relation for the double layer potential, we will use this concept in the BEM formulation.

Let us go back to equation (3.3.6) in the previous section and take the limit of it as ($\mathbf{r} \to \beta \in \partial D$), then applying the jump condition (3.3.10), one obtains,

$$\mu(\beta) = \int_{\partial D} \frac{\partial}{\partial n_\beta} G_0(q, \beta; k)\mu(q)\mathrm{d}q + \frac{1}{2}\mu(\beta).$$

Hence, one has

$$\mu(\beta) = 2\int_{\partial D} \mu(q)\frac{\partial}{\partial n_\beta} G_0(q, \beta; k)\mathrm{d}q. \tag{3.3.13}$$

This constitutes a Fredholm equation of the second kind as the unknown μ appears both explicitly and implicitly, that is inside and outside the integral, respectively.

The kernel of the BIE (3.3.13) is given as,

$$\frac{\partial}{\partial n_\beta} G_0(q, \beta; k) = -\frac{\imath k}{4}\cos\theta(q, \beta) H_1^{(1)}(k|q - \beta|), \tag{3.3.14}$$

and

$$\cos\theta(q, \beta) = \frac{(q - \beta).\vec{n}}{|q - \beta|}, \qquad \text{for } |q - \beta| \neq 0. \tag{3.3.15}$$

where $\theta(q, \beta)$ is the angle between the normal at the boundary point β and the chord connecting the initial boundary point q to the final boundary point β as depicted in figure 3.1.

For a very small argument of the Hankel function in the limit $q \to \beta$, one can use the following asymptotic expansion of the Hankel function as,

$$H_1^{(1)}(k|q - \beta|) \sim \frac{-2\imath}{\pi k \mid q - \beta \mid}, \qquad \text{as } \mid q - \beta \mid \to 0.$$

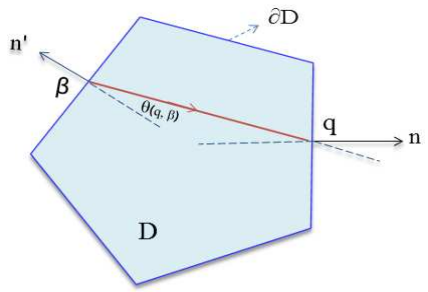

Figure 3.1: Sketch of the polygon with the boundary points q and β.

This asymptotic expansion of $H_1^{(1)}$ has a singularity of the order $O(\frac{1}{r})$, nevertheless, such singularity cancelled out by the geometric factor $\cos\theta$. For curved boundary, the term $\cos\theta(q,\beta)$ is obtained as,

$$\cos\theta(q,\beta) \sim \frac{1}{2}\kappa \mid q-\beta \mid, \qquad \text{as } q \to \beta, \tag{3.3.16}$$

where κ is the curvature of the boundary, for a circle boundary, the curvature is defined to be the reciprocal of its radius.

Thus for curved boundary, the kernel given by equation (3.3.13) becomes

$$\begin{aligned} \frac{\partial G_0(q,\beta;k)}{\partial n_\beta} &= -\frac{\imath k}{4}\cos\theta(q,\beta)H_1^{(1)}(k|q-\beta|) \\ &\sim -\frac{\kappa}{2\pi}, \qquad \text{as } q \to \beta. \end{aligned} \tag{3.3.17}$$

3.4 The secular equation for the spectrum

In this section we use the obtained boundary integral equation (3.3.13) in the previous section to obtain the eigenvalues condition. To do so, one needs to make use of the following property of the delta function,

$$\phi(y) = \int_{-\infty}^{\infty} \delta(x-y)\phi(x)\mathrm{d}x. \tag{3.4.1}$$

So,the BIE (3.3.13) can be rewritten as,

$$\int_{\partial D}\left[\delta(q-\beta) - 2\frac{\partial}{\partial n_\beta}G_0(q,\beta;k)\right]\mu(q)\mathrm{d}q = 0. \tag{3.4.2}$$

This BIE needs to be discretized on the boundary. Thus we obtain the following condition,

$$\det[I - K(q, \beta; k)] = 0. \tag{3.4.3}$$

This is called the quantization condition, also it is known as the secular equation - a equation whose real zeros are in one to one correspondence with the spectrum. The values of k which satisfy equation (3.4.3) are the eigenvalues. The notation I denotes the identity matrix and $K(q, \beta; k)$ is the boundary integral kernel defined for the boundary elements q and β as

$$K(q, \beta; k) = 2\frac{\partial}{\partial n_\beta} G_0(q, \beta; k) = -\frac{\imath k}{2} \cos\theta(q, \beta) H_1^{(1)}(k|q - \beta|). \tag{3.4.4}$$

where the boundary elements q and β will be suppressed thereafter.
In the discretization procedures, we set the size of the BEM kernel to,

$$\dim(K) \approx \frac{\text{length of the boundary (L)}}{\text{average distance between boundary elements}},$$

The average distance between boundary elements is set to $\frac{\lambda}{b}$, where $\lambda = \frac{2\pi}{k}$ is the wavelength. The constant b is the number of the boundary elements used per wavelength [10], here it has been chosen to be 5. The dimension of the BEM matrix is,

$$\dim(K) \approx \frac{Lbk}{2\pi} \tag{3.4.5}$$

with a fully populated matrix.

Note that when using numerical methods such as FEMs or FDMs to obtain the spectrum up to certain value of k, the kernel size needs to increase like,

$$\dim(K) \approx k^2, \tag{3.4.6}$$

however, with a sparsely populated matrix. Such a reduction of the scale of the problem from (3.4.6) to (3.4.5) by a factor of k is due to the distinct advantage of the BEM which only requires discretization of the boundary rather than the whole domain.

3.4.1 Singular value decomposition

In this section we compute the determinant obtained in equation (3.4.3) for a polygonal domain sketched in figure 3.2. Figure 3.3 shows the modulus of the complex-valued determinant for range of k values. For computing the determinant, it is advantageous to make use of the singular value decomposition (SVD). The calculation of the spectrum amounts to finding the zeros of the complex-valued determinant. This can be achieved by finding the minima of $|\det(I-K)|$.

The spectral points (eigenvalues) are well defined by the sharp minima of the

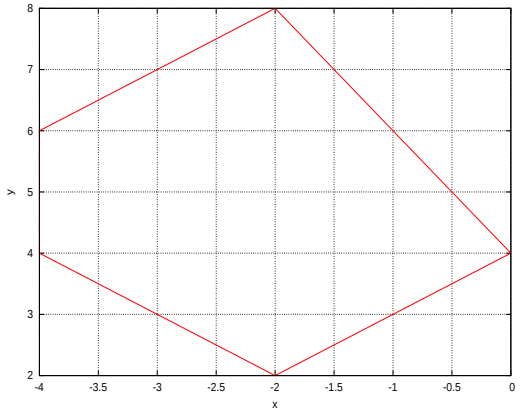

Figure 3.2: Sketch of the polygon used for computing the spectrum.

lowest singular values as a function of k. Using the SVD the determinant of the matrix $(I-K)$ can be calculated by writing,

$$(I-K) = USV^{\dagger},$$

where $V^{\dagger}$ denotes the conjugate transpose of V. The matrices U and $V^{\dagger}$ are unitary matrices of $n \times n$ dimension, and S is a diagonal matrix with real, non-negative elements $S_1 \geqslant S_2 \geqslant \ldots \geqslant S_n \geqslant 0$. The set $\{S_i\}_{i=1}^{n}$ is called the set of singular values in descending order.

Hence the determinant can be calculated as

$$|\det(I-K)| = |\det U||\det S||\det V^{\dagger}|.$$

Since the modulus of the determinant of any unitary matrix equals unity, i.e

$$|\det U| = |\det V^{\dagger}| = 1.$$

Hence, one obtains

$$|\det(I - K)| = \prod_{i=1}^{n} |S_{ii}|.$$

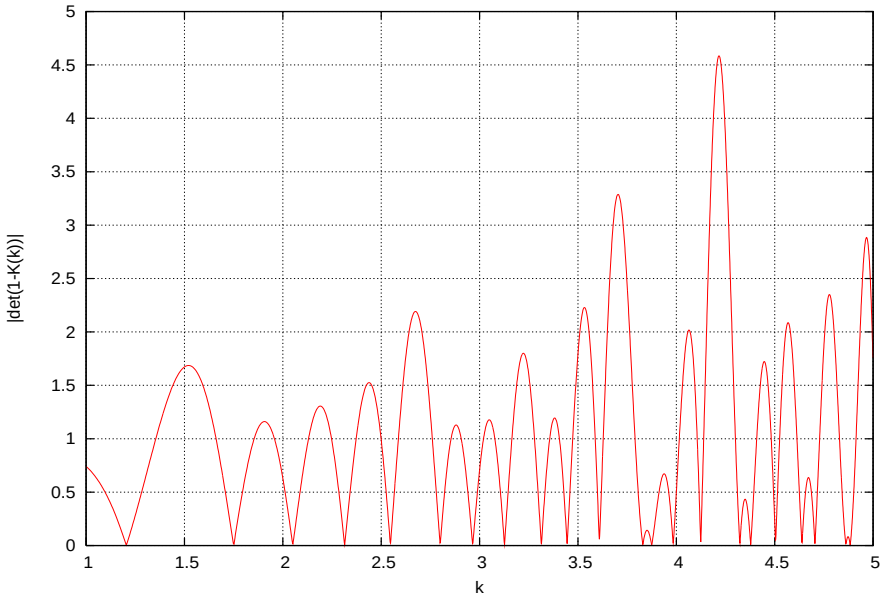

Figure 3.3: The modulus of the spectral determinant.

The reason for making use of the SVD is that wherever there is minima of the second smallest singular value, this is a sign of the existence of two nearby eigenvalues as shown in figure 3.4. In this figure one can see that between $k = 25.38$ and $k = 25.4$, there is minima of the second smallest singular value and there is two nearby eigenvalues. Usually nearby eigenvalues are easy to miss in the computations. Figure 3.5 shows that only one of two nearby eigenvalues between 62.105 and 62.11 has been captured and the other was missed. Furthermore, since the distance between successive eigenvalues decreases with increasing the wavenumber, one needs to increases the matrix size to capture nearby eigenvalues for higher range of k.

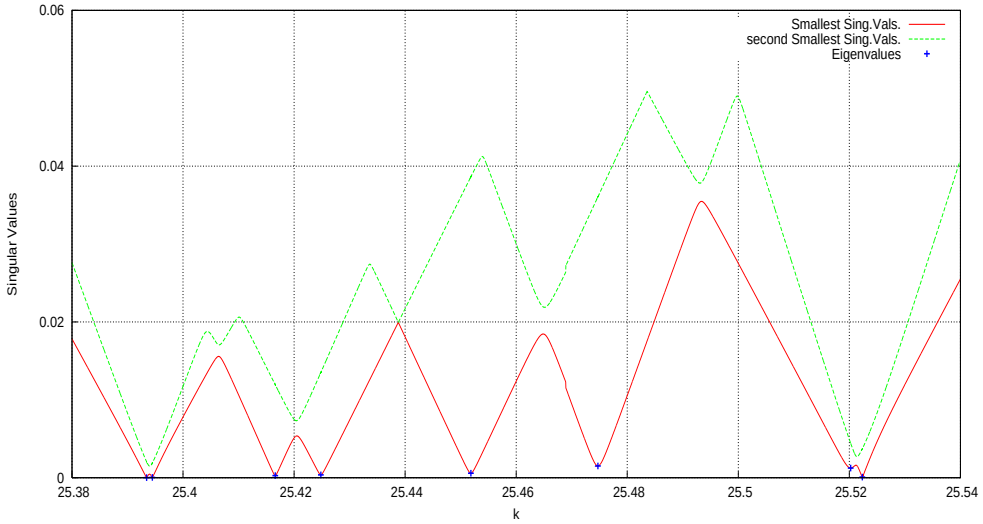

Figure 3.4: The solid and dashed lines respectively represent the smallest and second-smallest singular values, and the cross represents the eigenvalues.

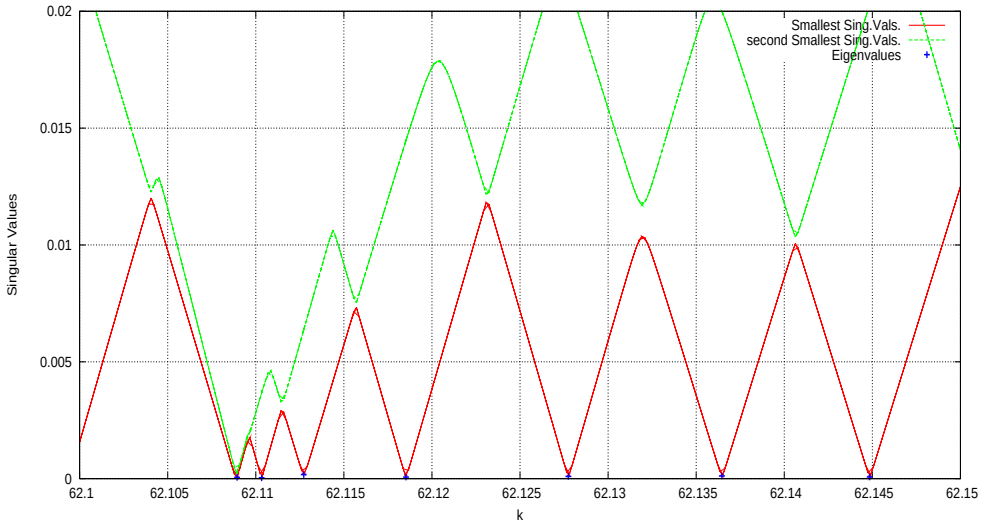

Figure 3.5: The solid and dashed lines respectively represent the smallest and second-smallest singular values, and the cross represents the eigenvalues. There is a missing eigenvalue just before $k = 62.11$

After obtaining the spectrum of about 5000 eigenvalues, still we need to check whether there were any missing eigenvalues. This check is usually can be achieved by looking into the oscillatory part of the density of state as shown next.

3.5 The density of states and the Weyl formula

We compute the spectra of about 5000 eigenvalues with $k < 62$ for a polygonal domain sketched in figure 3.2. Here we use this spectrum to compute the spectral density $N(E)$, which counts the number of energy levels below a given energy E,

$$N(E) = \{n : E_n \leq E\}.$$

It can be written in terms of the wavenumber k as a sum of the smooth part and the oscillatory (fluctuating) part [9] as,

$$N(k) = N_{\text{osc}} + N_{\text{Weyl}},$$

where $N_{\text{smooth}} = N_{\text{Weyl}}$ is the mean part of the spectral counting function $N(k)$. It also called the Weyl formula for the mode density which can for two-dimensional billiards shapes written as,

$$N_{\text{Weyl}} = \frac{1}{4\pi}\left[Ak^2 - Lk\right] + c, \tag{3.5.1}$$

which consists of the area, length and curvature terms, where A, L are the area and the perimeter of the domain, respectively. The geometric constant c denotes curvature and corners terms [9, 108]. For smooth boundaries, c is dependent on the curvature of the boundary whereas for non-smooth boundaries c is dependent upon the angle of the corners.

The area term has an interpretation that the probability for the system to be in a certain region in phase space is proportional to the volume of such a region. Figure 3.6 shows that the Weyl term N_{Weyl} goes through the histogram of the cumulative density of eigenvalues $N(k)$.

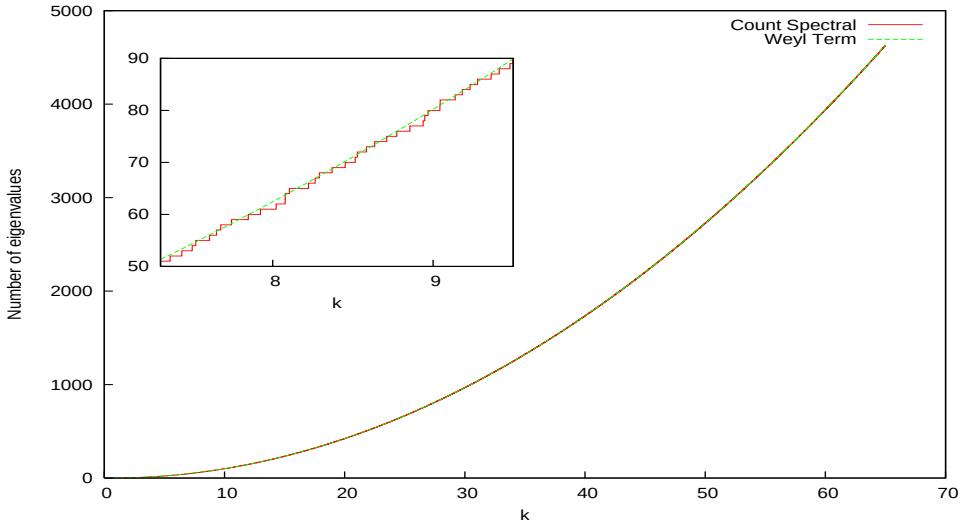

Figure 3.6: The spectral staircase counting function $N(k)$ and its average, the Weyl term N_{Weyl}, of a polygonal-shaped domain with DBCs for about 5000 eigenvalues with wavenumber $k < 62$.

3.5.1 The oscillatory part of the density of states

A quantity which sensitively indicates whether spectral points were missed or not is the fluctuating part N_{osc} of the density of states. It is the difference between the staircase function $N(k)$ counting the energy levels and the smooth part (Weyl term) N_{Weyl}, that is

$$N_{\text{osc}} = \Delta N = N(k) - N_{\text{Weyl}}.$$

Figure 3.7 shows that N_{osc} oscillates around zero, therefore it confirms that the spectrum is complete in the given range of k. A missing eigenvalue leads to an oscillatory signal as shown in figure 3.8. Therefor, the oscillatory part of the density of states offers check of obtaining the complete spectrum.

3.5.2 Computing the eigenfunctions

Once the eigenvalues are found from the quantization condition (3.4.3), one can compute the corresponding eigenfunctions by using equation (3.3.3) with $\mathbf{r}$, an interior point. Then imposing the DBCs on the LHS of equation (3.3.3), one

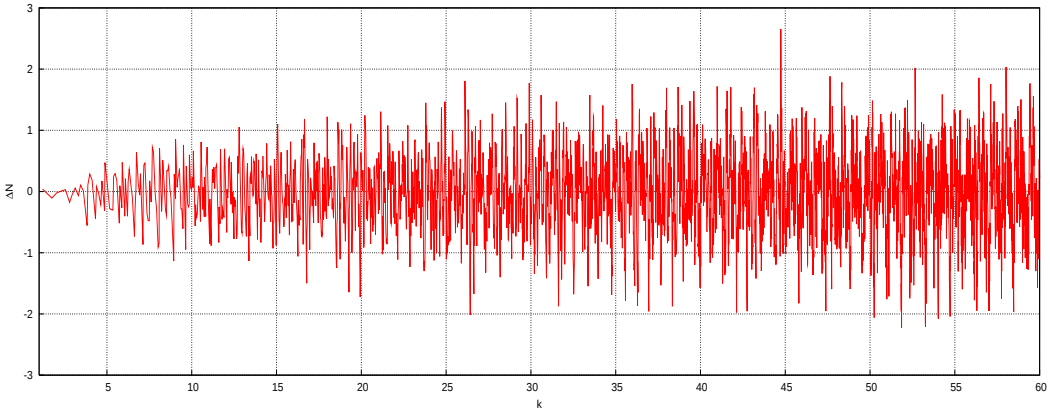

Figure 3.7: Fluctuating part of the density of states N_{osc} for about 5000 eigenvalues.

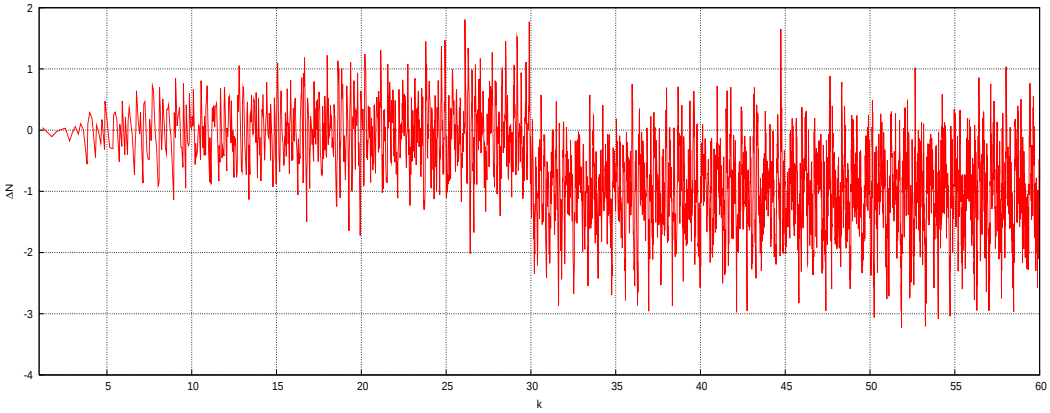

Figure 3.8: The oscillatory part of the density of states N_{osc}, with missing an eigenvalue at $k = 30.012009$

obtains,

$$\psi(\mathbf{r}) = \int_{\partial D} G_0(\mathbf{r}, q; k)\mu(q)\mathrm{d}q, \qquad \mathbf{r} \in D. \tag{3.5.2}$$

This integral is regular (non-singular) because $\mathbf{r} \in D$, thus it can be evaluated by numerical quadrature along with the computed boundary function $\mu(q)$. That is after solving the BIE (3.4.2) for the boundary function μ, one can evaluate the eigenfunction $\psi(\mathbf{r})$ at any interior point using equation (3.5.2).

3.5.3 The BEM formulation for the Green function

In this section we present the derivation of the Green function G which satisfies both the Helmholtz equation and the prescribed boundary conditions. Note that the free-space Green function G_0 is a solution of the Helmholtz equation but does not fulfil the prescribed boundary conditions. To begin with, since both G and G_0 satisfy (3.2.2), one has

$$(\nabla^2 + k^2)G(\mathbf{q}, \mathbf{r}') = -\delta(\mathbf{q} - \mathbf{r}'), \tag{3.5.3}$$

and

$$(\nabla^2 + k^2)G_0(\mathbf{q}, \mathbf{r}) = -\delta(\mathbf{q} - \mathbf{r}), \tag{3.5.4}$$

where the wavenumber k is related to the frequency as

$$k = \frac{\omega}{c} + \imath\eta, \qquad \eta > 0, \qquad \imath = \sqrt{-1},$$

where ω is the angular frequency. The constant factors c and η are respectively the wave propagation speed and the damping parameter.

Conceptually, the derivation of the Green function is similar to the derivation of the quantization condition (3.4.3). We begin by multiplying equation (3.5.3) and (3.5.4) by $G_0(q, \mathbf{r})$ and $G(q, \mathbf{r}')$, respectively, and taking the difference. Then we integrate over the domain D to obtain,

$$\begin{aligned} \iint_D \left[G_0(\mathbf{q}, \mathbf{r})\nabla^2 G(\mathbf{q}, \mathbf{r}') - G(\mathbf{q}, \mathbf{r}')\nabla^2 G_0(\mathbf{q}, \mathbf{r})\right] \mathrm{d}A_{\mathbf{q}} = \\ \iint_D \left[G(\mathbf{q}, \mathbf{r}')\delta(\mathbf{q} - \mathbf{r}) - G_0(\mathbf{q}, \mathbf{r})\delta(\mathbf{q} - \mathbf{r}')\right] \mathrm{d}A_{\mathbf{q}}. \end{aligned} \tag{3.5.5}$$

Applying the Green second identity (2.1) leads to,

$$\begin{aligned} \int_{\partial D} \left[G_0(q, \mathbf{r}; k)\frac{\partial G(q, \mathbf{r}')}{\partial n_q} - G(q, \mathbf{r}')\frac{\partial G_0(q, \mathbf{r}; k)}{\partial n_q}\right] \mathrm{d}q = \\ G(\mathbf{r}, \mathbf{r}'; k) - G_0(\mathbf{r}, \mathbf{r}'). \end{aligned} \tag{3.5.6}$$

Then applying the prescribed boundary conditions, one obtains,

$$G(\mathbf{r}, \mathbf{r}') = G_0(\mathbf{r}, \mathbf{r}') + \int_{\partial D} G_0(q, \mathbf{r})\mu(q, \mathbf{r}')\mathrm{d}q \tag{3.5.7}$$

where,

$$\mu(q, \mathbf{r}') = \frac{\partial}{\partial n_q} G(q, \mathbf{r}').$$

The Green function at any interior point $\mathbf{r}$ for a given source point $\mathbf{r}'$ can be computed using equation (3.5.7) [127].

The term $G_0(\mathbf{r}, \mathbf{r}')$ in equation (3.5.7) represents the direct contribution of rays starting at the source $\mathbf{r}'$ and reaching a receiver point $\mathbf{r}$ without any reflection from the boundary. The second term in equation (3.5.7) is called the single layer potential or the elementary potential with density $\mu(q, \mathbf{r}')$. Such a term represents the indirect contribution of rays which reach a receiver point after hitting the boundary at least once. Conceptually, it represents the correction to the free-space Green function to construct the full Green function with all reflections and propagation.

To formulate the BIE we follow the same steps in §3.3 by taking the normal derivative of equation (3.5.7) in the limit ($\mathbf{r} \to \beta \in \partial D$) , and applying the jump conditions (3.3.10). One obtains,

$$\int_{\partial D} \left[\delta(q - \beta) - K(q, \beta; k)\right] \mu(q, \mathbf{r}') \mathrm{d}q = 2 \frac{\partial}{\partial n_q} G_0(q, \mathbf{r}'; k). \tag{3.5.8}$$

This is a non-homogeneous Fredholm integral equation of the second kind. The kernel $K(q, \beta; k)$ is given by equation (3.4.4). After discretizing the boundary, equation (3.5.8) can be evaluated numerically to obtain the system of algebraic equations,

$$(I - K)\boldsymbol{\mu} = \boldsymbol{b}. \tag{3.5.9}$$

The vectors $\boldsymbol{b}$ and $\boldsymbol{\mu}$ are the source and solution vectors, respectively. Since the matrix $(I - K)$ is antisymmetric and fully populated with non-zero coefficients, direct solvers such as Gaussian elimination or the LU decomposition should be used.

The boundary function $\mu(q, \mathbf{r}')$ is periodic of its argument with the period equal to the perimeter of the boundary L, that is

$$\mu(q, \mathbf{r}')|_{q=0} = \mu(q, \mathbf{r}')|_{q=L}.$$

The BEM analysis can be performed to find all the boundary unknowns and then in a post-processing procedures, by positioning the source point $\mathbf{r}'$ at the point of interest. The Green function can be calculated at any interior point by a numerical quadrature for the non singular integrals in equation (3.5.7) using the boundary data $\mu(q, \mathbf{r}')$. Next we show some results.

3.5.4 Results for the Green function

The Green function at a specific receiver point $\mathbf{r}$ is calculated by summing over all contribution from paths starting at a fixed source point $\mathbf{r}'$ and ending at $\mathbf{r}$ including the direct ones plus paths that hit the boundary at least once before reaching $\mathbf{r}$. We observed that slight change in k leads to a completely different structure of the Green function. This means that the wave function is very sensitive to the change of the frequency resulting in different interference patterns.

We include the absorption phenomenon in terms of a complex values of the wavenumber with positive imaginary part ($\Im(k) \geq 0$) representing the damping of the system.

We consider three example domains as depicted in figure 3.9 such as weakly and strongly coupled polygonal sub-components referred to as configuration A and B, respectively, as well as a more regular configuration that is constructed of an irregular and rectangular structure denoted configuration C. The latter could correspond to a room that is coupled to a corridor. We show plots of the Green function for different parameters of the wavenumber and damping factors. Figure 3.10 shows the Green function for configurations A, B and C. It

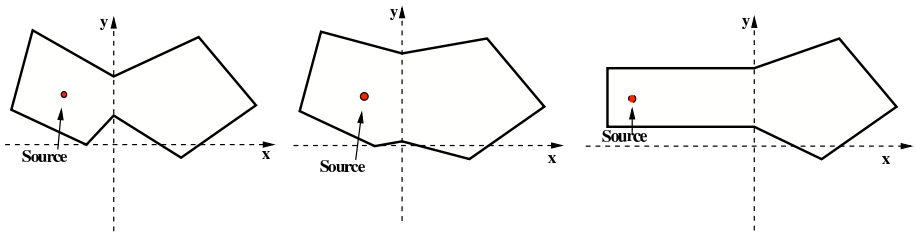

Figure 3.9: From the left to the right configurations A, B and C, respectively.

shows that for low absorption, there are still some long paths from the multi-reflection on the boundary, that are surviving and contributing to the Green function. But this is not the case with strong damping where the pattern of the Green function looks much like the direct contribution (circle waves coming out from the source point). This means the only surviving paths are the direct ones from the source to the receiver point.

In addition, we observe that at high absorption, the wave energy produced from the source is damped out before reaching the interface.

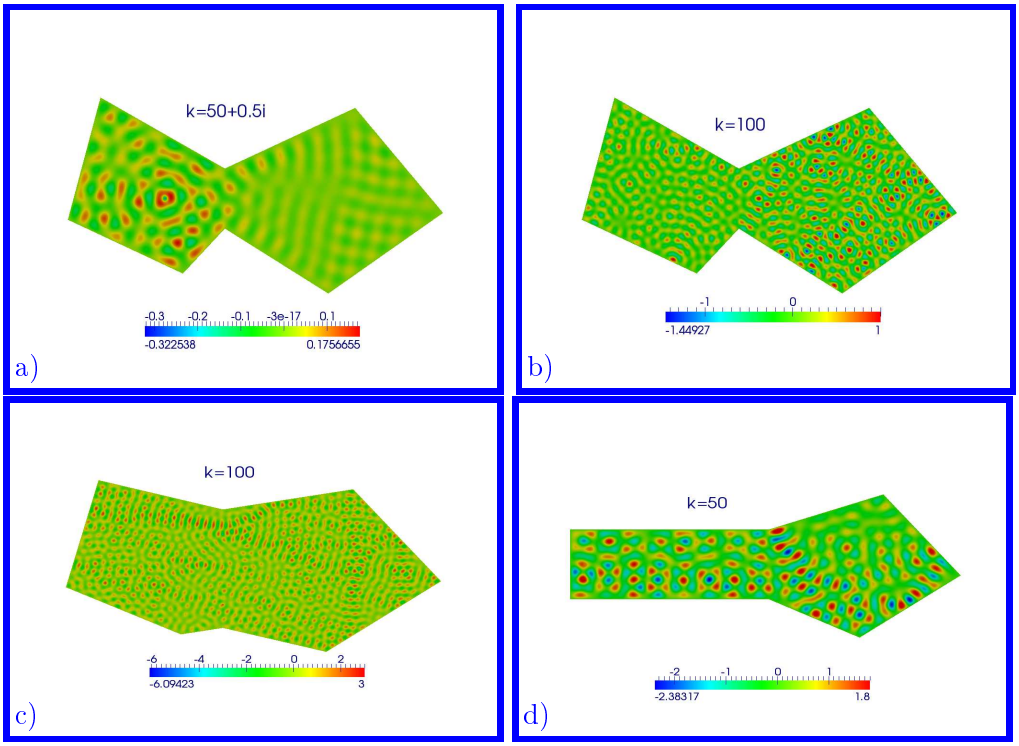

Figure 3.10: $\Re(G(\mathbf{r}, \mathbf{r}'; k))$ for configuration. A, B and C with different range of wavenumbers k with and without absorption, the imaginary part of k represents the damping of the system.

3.6 The Accuracy of the solution

In the absence of absorption, (real values of the wavenumber k), the Green function is real as it is understood from equation (3.5.3) that the Laplace operator ∇^2, and the delta function $\delta(\mathbf{r}-\mathbf{r}')$ both are real quantities. Therefore, only the real part of the Green function is contributing to the solution. The imaginary part is non-zero only when considering the absorption phenomena, that is the wavenumber k is complex-valued. This will be used in verifying our numerical computation. The $\Im G(\mathbf{r},\mathbf{r}';k)$ must be small compared to $\Re(G(\mathbf{r},\mathbf{r}';k))$ as shown in the figure 3.11 which compares the real and the imaginary parts of the solution vector μ for configuration A.

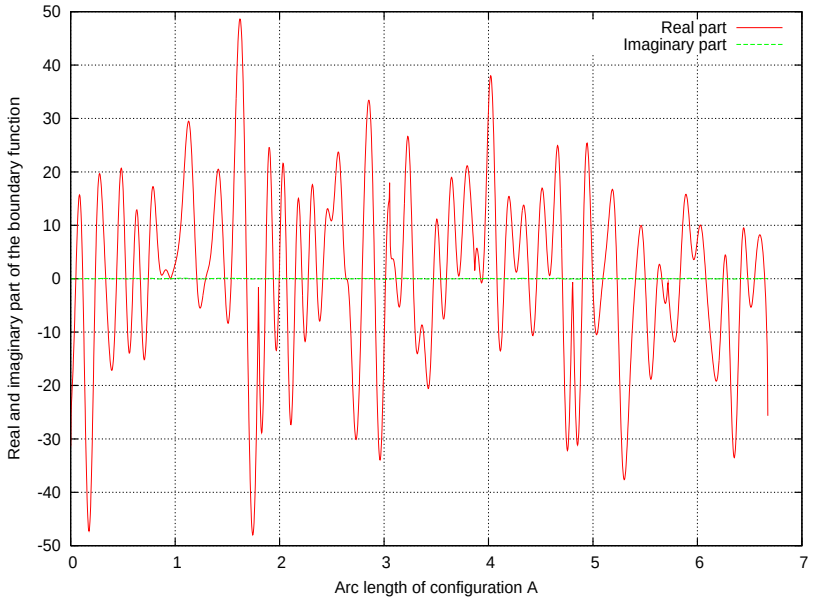

Figure 3.11: The real and imaginary par of the solution vector μ for $k = 50$ for 4500 boundary elements.

3.7 Advantages of the normal derivative equation

Here, we discuss the preference of the second kind Fredholm BIE (3.3.13) over the first kind Fredholm equation (3.3.4). Firstly, it is worth mentioning that, the Fredholm equation of the first and second kind both possess a unique solution and are well adopted for numerical calculations [34]. An ill-conditioning problem is usually associated with equations of the first kind, however this does not arise here, because the presence of the singularity of the kernel ensures diagonal dominance in the system matrix and the problem will be well-conditioned [60, 34]. We used the BIE (3.3.13) to obtain all the results shown in this chapter, because it is non-singular in contrast to the BIE (3.3.4).

On the other hand, the BIE (3.3.4) leads to a symmetric matrix, due to the symmetry property of the free space Green function, whereas the BIE (3.3.13) leads to a non-symmetric matrix due to the term $\cos\theta$. We carry out a comparison between both equations for a unit disc with Dirichlet boundary conditions. Respectively, figures 3.12 and 3.13 show plots of the real and imaginary part of the boundary function μ, calculated using the original BIE (3.3.4) and the normal derivative equation (3.3.13). As the imaginary part of μ gives the measure of the error, figure 3.13 shows that the normal derivative equation (3.3.13) is more efficient than the original BIE (3.3.4), therefore in the next chapter we will use analogous derivation to derive the BIEs.

However, the determinant condition obtained from the BIE (3.3.4) is not stable and becomes exponentially small as one increases the number of boundary elements. For instance, for 200 BEs the values of the determinant are smaller than the machine underflow threshold, thus the output of the programme is just zeros, that is, this equation is not numerically stable. Whereas equation (3.3.13) works efficiently for computing the spectrum. Table 5.1 shows the first ten of the sequence of the eigenvalues of a circle with DBCs, which coincide with the analytic eigenvalues (zeros of Bessel functions) as tabulated in [125].

In conclusion, for a smooth boundary such as a circle the normal derivative equation (3.3.13) works more efficiently than the original BIE (3.3.4). Built on this observation we argue that the second kind integral equation is more stable than using the first kind integral equation. We argue that the singularity of G_0 is responsible for the inaccuracy and the stability problem.

However, for a non-smooth geometries (edges and corners), the normal is not defined (not unique) at the corners. Hence, corner corrections need to be considered as it may affect the accuracy [34]. Therefore the normal derivative method for non-smooth geometries is spoiled by the corners problem. Next, we discuss how the corner issue is treated in the literature.

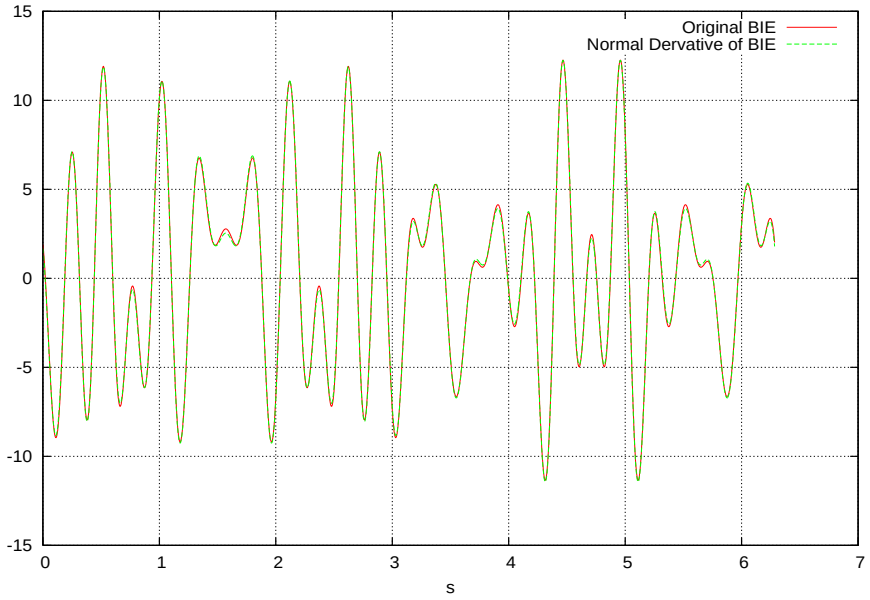

Figure 3.12: $\Re(\mu)$ for a unit circle with Dirichlet boundary conditions for $k = 50$ and 2000 boundary elements.

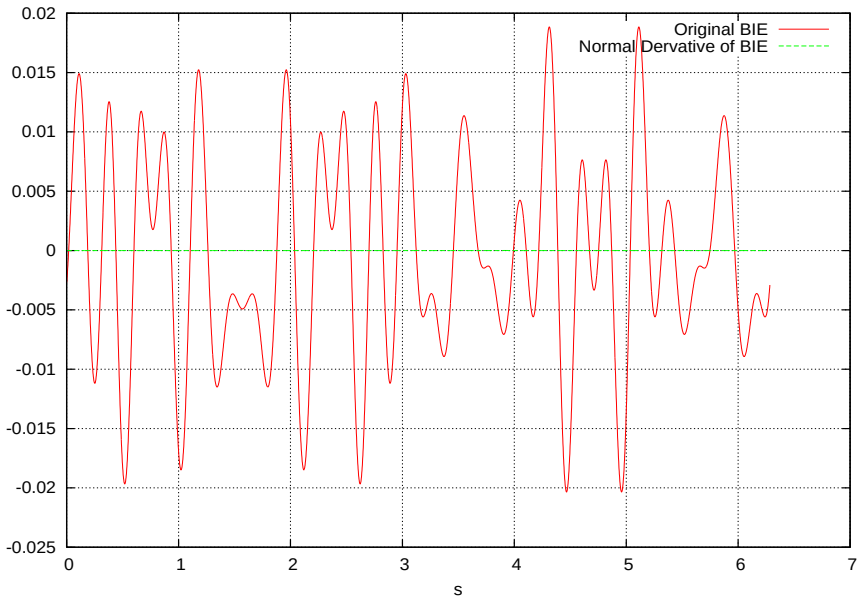

Figure 3.13: $\Im(\mu)$ for a unit circle with Dirichlet boundary conditions for $k = 50$ and 2000 boundary elements.

3.8 Corner corrections for non-smooth boundaries

A geometry with sharp corners or edges are commonly used in modelling engineering problems. The BEM formulation is based on the Green second identity (2.1) which requires that the involved functions to be twice continuously differentiable. However, for boundaries with edges and corners, we make the assumption that the boundary is piecewise twice differentiable, that is, the boundary is constructed as finite union of twice differentiable sub-intervals, nevertheless the whole boundary is not twice differentiable. Corner nodes cause problems for two reasons. Firstly, the normal vector at a corner is not well defined, and the normal derivatives $\frac{\partial\psi(q)}{\partial n}$ changes its value sharply across the corner. This leads to discontinuity of $\frac{\partial\psi(q)}{\partial n}$ across the corner. Secondly, at a corner node, the standard jump relation (3.3.10) is no longer valid and needs to be adjusted to accommodate the corners. Therefore, the treatment of corners in the BEM formulation requires great care in order to obtain an accurate numerical solution

in the presence of corners.

Here, we present some approaches to treat difficulties related to the corners. One possibility is to introduce a small curvature rounding off the corner [58]. Such a procedure provides a reasonable results close to the corner, but is not very accurate at the corner itself.

For non-smooth boundaries, the jump relation of the double layer potential given by equation (3.3.10) also needs to be modified to accommodate the corner. This modification contains an extra angle-dependent factor wherever we meet a corner. At the corner x_i, the jump relation need to be adjusted as,

$$\xi_{\pm}(x_i) = \int_{\partial D} \frac{\partial G_0(x_i, q)}{\partial n_{x_i}} \mu(q) \mathrm{d}q \mp \frac{1}{2} \delta_i^{\pm} \mu(x_i), \qquad i = 1, \cdots, N, \tag{3.8.1}$$

where,

$$\delta_i^{+} = \frac{\gamma_i}{\pi}, \qquad \delta_i^{-} = 2 - \frac{\gamma_i}{\pi}$$

and γ_i is the angle at a corner with $0 < \gamma_i < \pi$, as depicted in figure 3.14 and N is the number of corners [52]. One problem with the implementation of this formula is the difficulty in specifying a corner precisely during the discretization procedure.

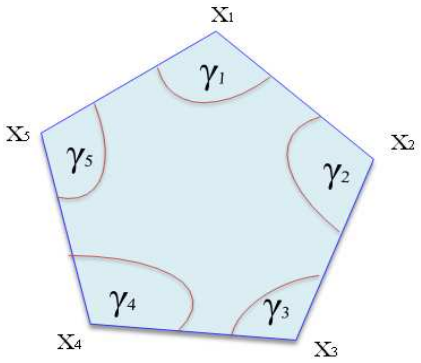

Figure 3.14: polygon with corners x_i and angles γ_i for $i = 1, \ldots, 5$.

Yan and Lin [128] present a review article of the treatment of the corner problem. Amongst other types of treatment, they presented the corner node splitting method. Within this method, the corner node x is split into two nodes

$x-\epsilon$ and $x+\epsilon$ as depicted in figure 3.15. Each of the new nodes shifts the corner node by a small distance ϵ away from both sides, this gets rid of the corner node. Therefore, one can apply the standard jump relation (3.3.10). This method is also called discontinuous, because both $\psi(q)$ and $\frac{\partial\psi(q)}{\partial n}$ have different values at the two new nodes. If one uses the weighted residual method as discussed in §2.1.4 to solve the BIE, then the shape functions used in the interpolation need to be adjusted accordingly to accommodate the two new nodes. For a more in depth discussion of this method and other methods, the reader is referred to [45, 58, 128]. The disadvantage of this approach is the increase in the number of degrees of freedom.

For the purpose of this thesis, the corner issue is not an important theme because the diffraction effects coming from the corners should decay by increasing the number of boundary elements.

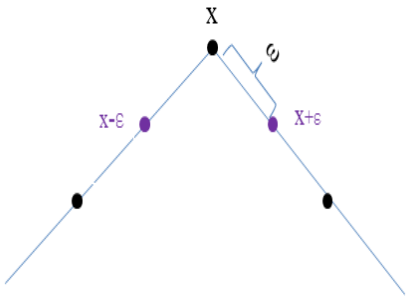

Figure 3.15: Sketch of corner node x split into two new nodes $x-\epsilon$ and $x+\epsilon$, the original nodes are in black, the new nodes in purple.

3.9 Conclusions

We give a concise account of the BEM, which is a numerical tool that gives approximate eigenvalues as the minima of the spectral determinant. We implement this method for the Helmholtz equation for two-dimensional concave polygonal domains with Dirichlet boundary conditions yielding the spectrum, the corresponding the eigenfunctions, and Green function. We numerically identify the

spectrum of about 5000 eigenvalues with wavenumber $k < 62$; the oscillatory part of the density of state confirms that there are no missing eigenvalues. Furthermore, we obtain the Green function both in the presence and the absence of absorption.

So far we assume that all the convex components that construct the concave domain have the same material properties. This means all the components have the same wavenumber. Realistically, this is not always the case, as real-life models may have discontinuous change of materials properties. For such categories, it is not possible to apply the classical single-domain BEM presented in this chapter, because the free-space Green function is not known for the whole structure. Therefore, it is crucial to develop an efficient method for such categories as will be discussed in the next chapter.

Chapter 4

Multi-component boundary element method

4.1 Introduction

For multi-component systems with material parameters changing discontinuously, such as the wave speed and absorption coefficients at the interfaces between the components, generally the free-space Green function is known only for sub-components, but not for the whole system. A BEM analysis of such categories with a complex shape can be simplified by decomposing the domain into sub-components. The BIE for each sub-component is constructed in conjunction with the compatibility and the equilibrium conditions along the interfaces. This is known as multi-component BEM treatment [44, 50, 58, 81, 82].

In this chapter we implement this decomposition technique. We analytically derive an integral identity for the arising hypersingular integrals. This facilitates the numerical evaluation of the remaining problem. Finally, we demonstrate the applicability of the method and discuss the attainable accuracy. We have published the results of this chapter in [12, 13].

4.2 Wave problem statement

As starting point, we consider a two-cavity configuration in two dimensions as elucidated in figure 4.1. Our aim is a generalisation of the method to large scale, multi-component systems. In this section, we will state all the assumptions of the model.

The considered domain $\Omega = \Omega_1 \cup \Omega_2$ is decomposed into two sub-domains with

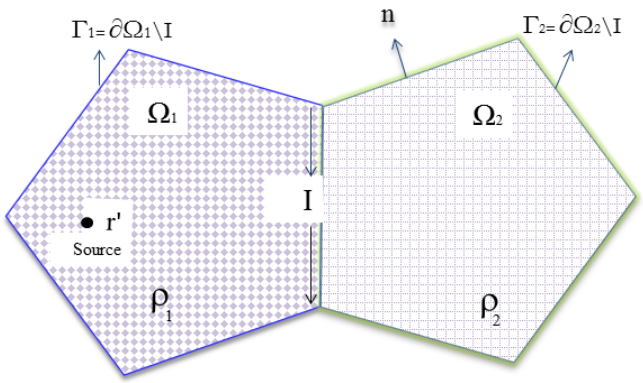

Figure 4.1: Geometric configuration of the coupled-cavity.

different material properties. That is Ω_1 and Ω_2 are separated by a change of the material densities between ρ_1 and ρ_2 at the interface, with $\rho_1 \neq \rho_2$. They are related by,

$$\frac{\rho_1}{\rho_2} = \frac{k_1^2}{k_2^2}. \tag{4.2.1}$$

Therefore, the wave speed and absorption coefficients may change discontinuously at the interface between the left sub-domain Ω_1 and the right sub-domain Ω_2. The governing differential equation is the homogeneous Helmholtz equation given as,

$$(\nabla^2 + k_j^2)u = 0, \qquad j = 1, 2 \tag{4.2.2}$$

where u is the wavefunction, and j is the index of the sub-domain. The wavenumber k_j is given as,

$$k_j = \frac{\omega}{c_j} + \imath\eta_j, \qquad \eta_j > 0, \qquad \imath = \sqrt{-1},$$

where ω is the angular frequency at which the structure is excited. The constant factors c and η are the wave propagation speed and the damping parameters, respectively.

Here, we do not restrict ourselves to a certain application. The Helmholtz equation for domains with different parameters describes many physical phenomena such as a free particle in finite domain with discontinuous step potential, an electromagnetic cavity with discontinuous refractive index, acoustic cavities of different materials for example air/solid or fluid/solid.
We shall denote the external boundary for each sub-domain by,

$$\Gamma_j = \partial\Omega_j \backslash I, \qquad I = \partial\Omega_1 \cap \partial\Omega_2,$$

where I denotes the internal boundary (interface). We aim to derive the Green function that obeys the prescribed boundary conditions and solves the following inhomogeneous Helmholtz equation,

$$(\nabla^2_{\mathbf{r}} + k^2) G(\mathbf{r}, \mathbf{r}'; k) = -\delta(\mathbf{r} - \mathbf{r}'). \tag{4.2.3}$$

The function $G(\mathbf{r}, \mathbf{r}'; k)$ describes the amplitude of the wave field throughout the interior of Ω, where $\mathbf{r}'$ and $\mathbf{r}$ are the source and the observation points respectively. The source excitation is represented by the two-dimensional $\delta-$distribution. For coupled system, we have two set of boundary conditions either on the external or the internal boundaries as described in the next section.

4.2.1 The boundary Conditions

We consider DBCs for the Green function $G(\mathbf{r}, \mathbf{r}'; k)$ along the external boundary Γ_j, that is,

$$G_j(q, \mathbf{r}'; k_j) = 0, \qquad q \in \Gamma_j. \tag{4.2.4}$$

In addition to the DBCs along Γ_j, for a coupled system one needs to impose the continuity of the Green function and the equilibrium of the energy flux across

the interface. This can be written as

$$\left.\begin{aligned} G_1(q,\mathbf{r}';k_1) &= G_2(q,\mathbf{r}';k_2) \\ \rho_2\frac{\partial G_1(q,\mathbf{r}';k_1)}{\partial n_q} &= -\rho_1\frac{\partial G_2(q,\mathbf{r}';k_2)}{\partial n_q} \end{aligned}\right\}, \qquad q \in I. \tag{4.2.5}$$

The operator $\frac{\partial}{\partial n_q}$ denotes the directional derivative along the normal vector $\vec{n}$ at the boundary element q, that is,

$$\frac{\partial}{\partial n_q} = \vec{n}_q \cdot \nabla_q,$$

where the dot denotes the scalar product, ∇ is the gradient operator with respect to q.

The functions G_1 and G_2 refer to the Green function for the left and right sub-domain, respectively. These conditions guarantee the continuity of the wavefunction and the conservation of energy flux normal to the interface. They are called the continuity conditions.

Having introduced the governing Helmholtz equation and the prescribed boundary conditions, next we formulate the boundary integral equations for the model.

4.3 Derivation of the boundary integral equations

In this section the direct BIEs for each component $j = 1, 2$ will be derived using similar methods to those discussed in §3.5.3. To begin with, since both $G_{1,2}$ and G_0 satisfy the Helmholtz equation (4.2.3), one has,

$$(\nabla^2_{\mathbf{q}} + k_j^2)G_j(\mathbf{q},\mathbf{r}';k_j) = -\delta(\mathbf{q}-\mathbf{r}'), \tag{4.3.1}$$

$$(\nabla^2_{\mathbf{q}} + k_j^2)G_0(\mathbf{q},\mathbf{r};k_j) = -\delta_{1j}\,\delta(\mathbf{q}-\mathbf{r}), \tag{4.3.2}$$

where we assume that the source is located in the left sub-component, i.e, $\mathbf{r}' \in \Omega_1$. Here, δ_{ij} is the Kronecker delta symbol defined as,

$$\delta_{ij} \equiv \begin{cases} 1, & \text{if } i = j; \\ 0, & \text{if } i \neq j. \end{cases}$$

After multiplying equation (4.3.1) and equation (4.3.2) by $G_0(\mathbf{q},\mathbf{r};k_j)$ and $-G_j(\mathbf{q},\mathbf{r}';k_j)$, respectively, adding the resulting equations and integrating over the domain Ω_j, one has

$$\begin{aligned}&\iint_{\Omega_j}[G_0(\mathbf{q},\mathbf{r};k_j)\nabla^2 G_j(\mathbf{q},\mathbf{r}';k_j)-G_j(\mathbf{q},\mathbf{r}';k_j)\nabla^2 G_0(\mathbf{q},\mathbf{r};k_j)]\mathrm{d}A_{\mathbf{q}}=\\&\iint_{\Omega_j}[G_j(\mathbf{q},\mathbf{r}';k_j)\delta(\mathbf{q}-\mathbf{r})-\delta_{1j}G_0(\mathbf{q},\mathbf{r};k_j)\delta(\mathbf{q}-\mathbf{r}')]\mathrm{d}A_{\mathbf{q}}.\end{aligned}\tag{4.3.3}$$

where $j=1,2$, and $\mathrm{d}A_{\mathbf{q}}$ is an area element. Treating this equation in a similar manner of what we did in §3.5.3, one has

$$\begin{aligned}\int_{\partial\Omega_j}\left[G_0(q,\mathbf{r};k_j)\frac{\partial G_j(q,\mathbf{r}';k_j)}{\partial n_q}-G_j(q,\mathbf{r}';k_j)\frac{\partial G_0(q,\mathbf{r};k_j)}{\partial n_q}\right]\mathrm{d}q=\\-\delta_{1j}G_0(\mathbf{r},\mathbf{r}';k_j)+G_j(\mathbf{r},\mathbf{r}';k_j),\end{aligned}\tag{4.3.4}$$

Now, one needs to partition the integral in the BIE (4.3.4) by writing the boundary of each sub-component using

$$\partial\Omega_j=\Gamma_j\cup I,\qquad j=1,2.$$

Then implementing DBCs (4.2.4) in the BIE (4.3.4) one obtains,

$$\begin{aligned}&\int_I\left[G_0(q,\mathbf{r};k_j)\frac{\partial G_j^I(q,\mathbf{r}';k_j)}{\partial n_q}-G_j^I(q,\mathbf{r}';k_j)\frac{\partial G_0(q,\mathbf{r};k_j)}{\partial n_q}\right]\mathrm{d}q\\+&\int_{\Gamma_j}G_0(q,\mathbf{r};k_j)\frac{\partial G_j(q,\mathbf{r}';k_j)}{\partial n_q}\mathrm{d}q=-\delta_{1j}G_0(\mathbf{r},\mathbf{r}';k_j)+G_j(\mathbf{r},\mathbf{r}';k_j),\end{aligned}\tag{4.3.5}$$

where G_j^I denotes the Green function along the interface I.

Note that the integrands in the BIE (4.3.5) are bounded as long as $\mathbf{r}$ is an interior point. Nevertheless, difficulties may arise in the numerical evaluation of these integrals when considering the limit $\mathbf{r}\to\beta\in\partial\Omega_j$.
In the BIE (4.3.5), for example, G_0 has a logarithmic singularity when $\beta\in I$. The weakly singular terms can be regularised using, for example, a Telles transformation [77] as discussed in §4.6.3.

Assuming the boundary is smooth in a small neighbourhood of the point β, the limit $\lim_{\mathbf{r}\to\beta}\partial G_0(q,\mathbf{r})/\partial n_q=0$ at $\beta=q$, but it has a jump when $\mathbf{r}$

tends to the boundary as follows

$$\lim_{\mathbf{r}\to\beta} \partial G_0(q,\mathbf{r})/\partial n_q = \partial G_0(q,\beta)/\partial n_q + \frac{1}{2}\delta(q-\beta) \tag{4.3.6}$$

with $\beta \in \partial\Omega$, which is known as the jump relation [56].

To avoid the treatment of the weak singularity, similar to the treatment of the single-domain cavity with Dirichlet BCs in §3.5.3, we take the normal derivative of the BIE (4.3.5) with respect to $\mathbf{r}$ or β transforming all G_0 terms to $\partial G_0/\partial n_\beta$ terms. These can in turn be handled by the jump relation, equation (4.3.6), clearly separating the regular and singular part.

We propose to extend this idea to multi-component domain with Dirichlet BC on the outer boundaries. We proceed by taking the normal derivative of the BIE (4.3.5) with respect to $\mathbf{r}$, and then let the interior point $\mathbf{r}$ approach the boundary point β. That is, we apply the operator $\vec{n}_\beta \cdot \nabla_{\mathbf{r}}$ to both sides of the BIE (4.3.5). Subsequently we position the interior point $\mathbf{r}$ onto the boundary, that is, $\mathbf{r} \to \beta \in \partial\Omega$. Here we need to classify three cases for the boundary point β in which $\beta \in \Gamma_j$ or I. Some integrals become singular (integrand is infinite at the singularity point) or even hypersingular while others remain regular as will be discussed next.

4.3.1 Cases for the boundary point β

In this section we consider different cases for boundary point β when taking the normal derivative of equation (4.3.5). If $\beta \in \Gamma_j$, then we are able to exchange the order of differentiation and integration for the first and the second integrals in the BIE (4.3.5). The double layer potential in the third term in equation (4.3.5) has a jump at $\mathbf{r} \to \beta \in \Gamma_j$, thus one can apply the classical jump relation

(3.3.10). One obtains

$$\int_I \left[\frac{\partial G_0(q,\beta);k_j}{\partial n_\beta}\mu_j^I(q,\mathbf{r}') - G_j^I(q,\mathbf{r}';k_j)\frac{\partial^2 G_0(q,\beta;k_j)}{\partial n_\beta \partial n_q}\right]\mathrm{d}q$$
$$+\int_{\Gamma_j}\frac{\partial G_0(q,\beta;k_j)}{\partial n_\beta}\mu_j(q,\mathbf{r}')\mathrm{d}q + \frac{\mu_j(\beta,\mathbf{r}')}{2} = \mu_j(\beta,\mathbf{r}') - \delta_{1j}\frac{\partial G_0(\beta,\mathbf{r}';k_j)}{\partial n_\beta}, \tag{4.3.7}$$

where the boundary function $\mu_j(\beta,\mathbf{r}')$ is calculated as

$$\mu_j(\beta,\mathbf{r}') = \lim_{\mathbf{r}\to\beta}\frac{\partial G_j(\mathbf{r},\mathbf{r}';k_j)}{\partial n_\beta}, \qquad j=1,2.$$

For the case $\beta \in I$, we are not able to interchange the order of differentiation and integration when taking the normal derivative of the second integral in equation (4.3.5), because the limiting integrand has a $1/(\beta-q)^2$ singularity (hypersingular) which is non-integrable. This integral needs to be interpreted in a limiting sense similar to Cauchy's principal value integral by excluding the infinite part that contains the singularity as addressed in the next section. Therefore, the hypersingular integral is defined by taking the limit in the following way,

$$\frac{\partial}{\partial n_\beta}\int_I \frac{\partial G_0(q,\beta;k_j)}{\partial n_q}\mathrm{d}q = \lim_{\mathbf{r}\to\beta}\int_I \frac{\partial^2 G_0(q,\mathbf{r};k_j)}{\partial n_\beta \partial n_q}\mathrm{d}q \neq \int_I \lim_{\mathbf{r}\to\beta}\frac{\partial^2 G_0(q,\mathbf{r};k_j)}{\partial n_\beta \partial n_q}\mathrm{d}q.$$

It should be noted that the 'limit of the integral $\neq$ the integral of the limit '.

To avoid the hypersingular integral above one needs to take the limits properly and then do the numerical evaluation. Later we will explain how the non-singular expression is obtained.

Assuming the integrand has been transformed into a well behaved function in this limit, one has,

$$\int_I \frac{\partial G_0(q,\beta;k_j)}{\partial n_\beta}\mu_j^I(q,\mathbf{r}')\mathrm{d}q + \frac{\mu_j^I(q,\mathbf{r}')}{2} - \frac{\partial}{\partial n_\beta}\int_I G_j^I(q,\mathbf{r}';k_j)\frac{\partial G_0(q,\beta;k_j)}{\partial n_q}\mathrm{d}q$$
$$+\int_{\Gamma_j}\frac{\partial G_0(q,\beta;k_j)}{\partial n_\beta}\mu_j(q,\mathbf{r}')\mathrm{d}q = -\delta_{1j}\frac{\partial G_0(\beta,\mathbf{r}';k_j)}{\partial n_\beta} + \mu_j^I(q,\mathbf{r}'). \tag{4.3.8}$$

The limit of the integrand of the first integral in equation (4.3.8) for $\beta \in I$ has a jump when $\mathbf{r}$ tends to the boundary.

Since the hypersingular kernels bring difficulties in terms of the numerical evaluation, efforts must be dedicated to do the regularization. Next, we present the concept of Cauchy's principle value integral followed by the regularization procedures.

4.4 Cauchy's principal value integral

Even though the integrands of the singular integrals become infinite at the singularity point, one still can evaluate such integrals by rewriting them as a special limit in what is known as the Cauchy Principal Value (CPV) integral. To give the concept of the CPV, consider the following integral,

$$\oint_a^b \frac{f(x)}{x - x_0} \mathrm{d}x, \qquad x_0 \in (a, b),$$

where $f(x)$ is assumed to be Hölderian function at x_0 as defined later in this section, and $f(x_0) \neq 0$, so that the singularity of order one. This singularity is not integrable in the usual sense (Riemann or Lebesgue integral), because the integral is singular at the point $x = x_0$. Nevertheless, this integral can be reformulated in a limiting sense using the CPV integral as

$$\oint_a^b \frac{f(x)}{x - x_0} \mathrm{d}x = \lim_{\epsilon \to 0} \left\{ \int_a^{x_0 - \epsilon} \frac{f(x)}{x - x_0} \mathrm{d}x + \int_{x_0 + \epsilon}^b \frac{f(x)}{x - x_0} \mathrm{d}x \right\}, \qquad a < x < b. \tag{4.4.1}$$

Despite the fact that the integrand is infinite at the singularity point, the integral is well behaved around the singular point. The CPV integrals can be denoted as $C.P.V \int$ or $\oint$ to indicate that it is an improper integral.

For the existence of the CPV integral, the function $f(x)$ necessarily needs to be Hölder continuous on the interval (a, b).

Definition [Hölder continuous] A function f is Hölder continuous on the interval (a, b) if,

$$\mid f(x) - f(x') \mid \leq C \mid x - x' \mid^{\beta}, \qquad \forall x, x' \in (a, b), \tag{4.4.2}$$

where $0 < \beta \leq 1$, and $C > 0$ is a constant [55].

For a higher order singularity, the CPV integral may still be singular. In this case, one needs to use the Hadamard Finite-Part (HFP) integral, which is attributed to Jacques Hadamard [68]. It can be considered as a generalisation of the CPV integral. It expresses an integral as a sum of finite and infinite parts, then considers only the finite part.

4.5 Regularization of the hypersingular integral

One needs to convert the hypersingular integral into a form which reduces the strength of the singularity to at worst weakly singular. Such a transformation procedure is called regularization. The hypersingular integral can be written as,

$$\begin{aligned}\lim_{\mathbf{r}\to\beta}\frac{\partial}{\partial n_\beta}\int_\gamma G(q,\mathbf{r}')\frac{\partial G_0(q,\mathbf{r})}{\partial n_q}\mathrm{d}q = \lim_{\mathbf{r}\to\beta}\Bigg\{\frac{\partial}{\partial n_\beta}\int_\gamma \frac{\partial G_0(q,\mathbf{r})}{\partial n_q} \\ \times\left[G(q,\mathbf{r}')-G(\mathbf{r},\mathbf{r}')\right]\mathrm{d}q + G(\mathbf{r},\mathbf{r}')\frac{\partial}{\partial n_\beta}\int_\gamma\frac{\partial G_0(q,\mathbf{r})}{\partial n_q}\mathrm{d}q\Bigg\}\end{aligned} \tag{4.5.1}$$

where γ is the arc-length that contains the singularity point and we just add and subtract the following term

$$\lim_{\mathbf{r}\to\beta} G(\mathbf{r},\mathbf{r}')\frac{\partial}{\partial n_\beta}\int_\gamma\frac{\partial G_0(q,\mathbf{r})}{\partial n_q}\mathrm{d}q.$$

Therefore, for the sake of simplicity, let us start by considering the integral,

$$\frac{\partial}{\partial n_\beta}\int_\gamma\frac{\partial G_0(q,\beta)}{\partial n_q}\mathrm{d}q = \lim_{\mathbf{r}\to\beta}\int_\gamma\frac{\partial^2 G_0(\mathbf{r},q)}{\partial n_\beta\partial n_q}\mathrm{d}q,$$

neglecting for the moment the term $[G(q,\mathbf{r}')-G(\mathbf{r},\mathbf{r}')]$ as it will be treated later in §4.7.

4.5.1 Integral identity for the hypersingular integral

A convenient expression for the hypersingular integrand is derived in Appendix C and the following relation is obtained,

$$\frac{\partial^2 G_0(\mathbf{r},q)}{\partial n_\beta\partial n_q} = -\frac{\imath}{4}\left\{\frac{\mathrm{d}}{\mathrm{d}q}\left[\frac{k\sigma}{\rho}H_1^{(1)}(k\rho)\right]+k^2H_0^{(1)}(k\rho)\right\}. \tag{4.5.2}$$

where the notations $\sigma = |q - \beta|$, $\rho = |\mathbf{r} - q|$ and $\Delta\mathbf{r} = |\mathbf{r} - \beta|$ as depicted in figure 4.2.

Hence, the integral of the second derivative of the Green function is of the form

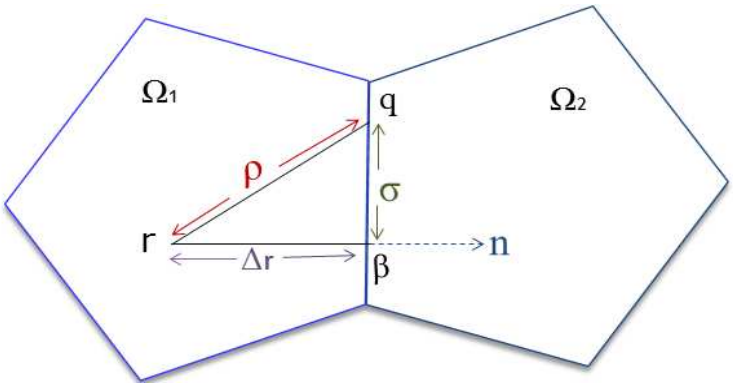

Figure 4.2: Geometrical illustration of an interior point $\mathbf{r}$ approaching a boundary point $\beta \in \partial\Omega$, $\rho = |\mathbf{r} - q|$, $\sigma = |\beta - q|$ and $\Delta\mathbf{r} = |\mathbf{r} - \beta|$.

$$\lim_{\Delta\mathbf{r}\to 0}\int_\gamma \frac{\partial^2}{\partial n_\beta \partial n_q} G_0(\beta, q)\mathrm{d}q = \frac{\imath}{4}\lim_{\Delta\mathbf{r}\to 0}\left\{k^2\int_\gamma H_0^{(1)}(k\rho)\mathrm{d}q + \int_\gamma -\frac{\mathrm{d}}{\mathrm{d}q}\left[k\frac{\sigma}{\rho}H_1^{(1)}(k\rho)\right]\mathrm{d}q\right\}, \tag{4.5.3}$$

which decomposes the hypersingular integral into a weakly singular integral and another integral which can be computed numerically.

The first integral in the RHS of equation (4.5.3) has a weak (integrable) singularity of the order $O(\ln|\rho|)$, so taking the limit commutes with performing the integration. For convenience, let us assume that $\beta = 0$, that is, $\sigma = q$. However, for the second integral one needs to do the integral first and then take the limit $\Delta\mathbf{r} \to 0$; one obtains

$$\begin{aligned}
\lim_{\Delta\mathbf{r}\to 0}\int_0^q \frac{\partial^2}{\partial n_\beta \partial n_q} G_0(\beta, q)\mathrm{d}q &= \frac{\imath}{4}\lim_{\Delta\mathbf{r}\to 0}\left\{k^2\int_0^q H_0^{(1)}(k\rho)\mathrm{d}q\right. \\
&+ \left.\int_0^q -\frac{\mathrm{d}}{\mathrm{d}q}\left[k\frac{\sigma}{\rho}H_1^{(1)}(k\rho)\right]\mathrm{d}\sigma\right\} \\
&= \frac{\imath}{4}\left\{k^2\int_0^q H_0^{(1)}(kq)\mathrm{d}q - \lim_{\Delta\mathbf{r}\to 0}\left[k\frac{\sigma}{\rho}H_1^{(1)}(k\rho)\right]_0^q\right\} \\
&= \frac{\imath}{4}\left\{k^2\int_0^q H_0^{(1)}(kq)\mathrm{d}q - kH_1^{(1)}(kq)\right\}, \qquad (4.5.4)
\end{aligned}$$

where we used $\gamma = [q, \beta]$ and $\beta = 0$.

If one takes the limit before doing the integration in the second term on the RHS of equation (4.5.4), then

$$\begin{aligned}\int_0^q \lim_{\Delta\mathbf{r}\to 0} -\frac{\mathrm{d}}{\mathrm{d}q}\left[k\frac{\sigma}{\rho}H_1^{(1)}(k\rho)\right]\mathrm{d}q &= \int_0^q -\frac{\mathrm{d}}{\mathrm{d}q}\left[k\frac{\sigma}{\sigma}H_1^{(1)}(k\sigma)\right]\mathrm{d}q \\ &= \left[kH_1^{(1)}(kq)\right]_0^q \to \infty,\end{aligned}$$

which is diverging when the argument of the Hankel function q tends to zero.

Maintaining the right order, that is, evaluating the integral first and then taking the limit leads to the following non-singular expression [60, 71, 72, 73] for the singularity point β

$$\lim_{\Delta r\to 0}\int_\beta^{\beta+\sigma}\frac{\partial^2 G_0(q,\mathbf{r})}{\partial n_\beta \partial n_q}\mathrm{d}q = k^2\int_\beta^{\beta+\sigma} G_0(q,\beta)\mathrm{d}q + \frac{\mathrm{d}}{\mathrm{d}q}G_0(\beta+\sigma,\beta). \qquad (4.5.5)$$

The limit process discussed above can be easily illustrated by sketching the hypersingular integrand in the limit ($\Delta r \to 0$). Figure 4.3 shows that when $\Delta\mathbf{r} = 0$, the real part of such an integrand blows up to infinity at the singularity point. By considering small $\Delta r > 0$, one observes that the area above the x-axis, region A_1 in Figure 4.3, is cancelled by the corresponding area below the x-axis, region A_2. Hence, the integrals remain finite and the limit $\Delta r \to 0$ exists. Clearly, changing the limit and integration leads to singular behaviour.

Having done the regularization, one can evaluate the original hypersingular integral term using equation (4.5.5) as

$$\begin{aligned}&\lim_{\Delta r\to 0}\frac{\partial}{\partial n_\beta}\int_\gamma G(q,\mathbf{r}')\frac{\partial G_0(q,\beta)}{\partial n_q}\mathrm{d}q = \lim_{\Delta r\to 0}\frac{\partial}{\partial n_\beta}\int_\gamma \frac{\partial G_0(q,\beta)}{\partial n_q} \\ &\times\left[G(q,\mathbf{r}') - G(\beta,\mathbf{r}')\right]\mathrm{d}q + G(\beta,\mathbf{r}')\left\{k^2\int_\gamma G_0(q,\beta)\mathrm{d}q + \frac{\mathrm{d}}{\mathrm{d}q}G_0(q,\beta)\Big|_\sigma\right\}.\end{aligned} \qquad (4.5.6)$$

Note that the integral containing the term $[G(q,\mathbf{r}') - G(\beta,\mathbf{r}')]$ is not regular but it can be readily integrated numerically by using a piecewise constant collocation approximation as will be shown in §4.7.

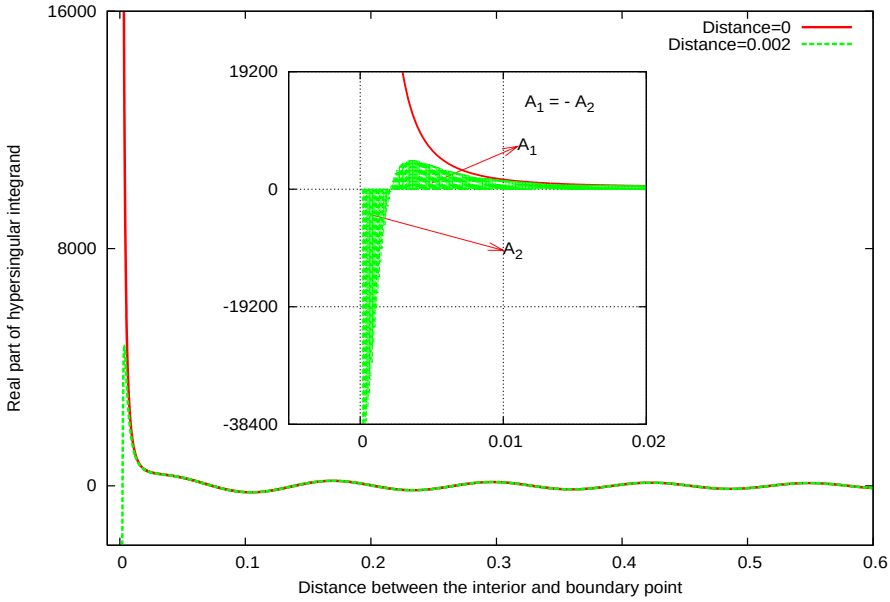

Figure 4.3: Real part of the hypersingular integrand $\Re\left(\frac{\partial^2 G_0(q,\beta)}{\partial n_q \partial n_\beta}\right)$ against the distance between the interior point $\mathbf{r}$ and the boundary point β. The solid red line for the distance $\Delta\mathbf{r} = 0$, and the dashed, green line for the distance $\Delta\mathbf{r} = 0.002$.

For a problem with DBCs, one can see that taking the normal derivative transfers the weakly singular terms containing G_0 from the outer boundaries to the interface. The logarithmic singularities requires further regularisation. This may be achieved by a suitable coordinate transformation such as a Telles transformation [77] or by expanding the Hankel function and integrating out the logarithmically divergent term explicitly as will be discussed next.

4.6 Treating the weakly singular integral

Here we will discuss some of the possible ways of treating the weakly singular integrals. These include the logarithmic Gaussian quadrature, subtraction of the singularity, and suitable variable transformations.

4.6.1 Gaussian quadrature

A simple way to numerically approximate a regular (non-singular) integral is the standard Gaussian quadrature (GQ). In one-dimension it can be implemented as,

$$\int_{-1}^{1} f(x)\mathrm{d}x \approx \sum_{i=1}^{n} f(x_i)w_i, \tag{4.6.1}$$

where x_i and w_i are the Gaussian quadrature points and the associated weighting functions, respectively, and n is the number of integration points. The integration range for the standard GQ is from -1 and 1. Thus one may need a linear transformation to accommodate general integration limits from a to b, as follows

$$\int_{a}^{b} f(x)\mathrm{d}x = \left(\frac{b-a}{2}\right)\int_{-1}^{1} f\left[\frac{b+a}{2} + \left(\frac{b-a}{2}\right)\xi\right]\mathrm{d}\xi.$$

GQ evaluates the integrand at a given number of points called the Gaussian coordinates, then the function is multiplied by a weight function and the sum is taken to approximate the integral. A large number of Gaussian points leads to a better accuracy. The standard GQ is not sufficiently accurate for weakly singular (logarithmic) integrals, even with a large number of Gaussian points. The logarithmic Gaussian quadrature is designed to treat such integrals. This evaluates the integral of a function $f(x)$ over the range from 0 and 1 numerically as,

$$\int_{0}^{1} f(x)\ln\left(\frac{1}{x}\right)\mathrm{d}x \simeq \sum_{i=1}^{n} f(x_i)w_i, \tag{4.6.2}$$

where the x_i and w_i are the Gaussian quadrature points and the associated weighting functions, respectively. It is noteworthy to mention that the integral is taken over the limits from 0 to 1. Therefore, one needs to do a linear transformation in order to accommodate general limits. We should emphasise that, for logarithmic Gaussian quadrature the Gaussian points and weighting functions are different from those for the standard Gaussian quadrature. The Gaussian quadrature points and the associated weighting functions for standard and logarithmic GQ for different values of n are tabulated in the textbook by Stroud and Secrest [129], and can also be found in [34, 58].

4.6.2 Singularity subtraction

The integral of the free-space Green function $G_0(q,\beta)$ is an integral of Bessel functions $J_0(k|q-\beta|)$ and $Y_0(k|q-\beta|)$. The latter becomes logarithmically singular when q and β are in the same boundary element. An asymptotic expansion of $G_0(q,\beta)$ is used in which the divergent term is separated as,

$$\begin{aligned}\int G_0(q,\beta;k)\mathrm{d}q &= \frac{\imath}{4}\left\{\int\left[H_0^1(k|q-\beta|)-\frac{2\imath}{\pi}\ln(k|q-\beta|)\mathrm{d}q\right]\right.\\ &+ \left.\int\frac{2\imath}{\pi}\ln(k|q-\beta|)\mathrm{d}q\right\}. \qquad (4.6.3)\end{aligned}$$

The integral on the first line of the RHS of equation (4.6.3) is continuous and can be integrated numerically using standard Gaussian quadrature. However, the integral on the second line of the RHS of equation (4.6.3) can be integrated analytically using

$$\int\ln|z|\mathrm{d}z = z[\ln|z|-1].$$

4.6.3 Telles' transformation

The Telles transformation [77] is a popular variable transformation method to treat the weakly singular integral. The Jacobian of such transformation merely weakens or cancels out the singularity. This approach uses a quadratic or cubic variable transformation, depending on whether the singular point is lying at the end of the element (integration domain) or within the element, respectively. Consider the integral

$$I=\int_{-1}^{1}f(x)\mathrm{d}x,$$

where $f(x)$ is a weakly singular function at one of the extremities of the integral. This means that the singularity point x_0 satisfies $|x_0|=1$. We can use the following quadratic transformation for the integral I,

$$I=\int_{-1}^{1}f\left[(1-\zeta^2)\frac{x_0}{2}+\zeta\right](1-\zeta x_0)\mathrm{d}\zeta, \qquad (4.6.4)$$

where ζ is the new coordinate. Since the Jacobian vanishes at x_0 then the resulting non-singular integral can be evaluated numerically by Gaussian quadrature given by equation (4.6.1).

For the case $|x_0| < 1$, one needs to partition the integral into two integrals at the singularity point and employ (4.6.4) for each integral. However, Telles introduced another cubic transformation for the case that the singularity point lies within the element, that is $|x_0| < 1$. Hence one needs to use the following non-linear transformation,

$$I = \int_{-1}^{1} f\left[\frac{(\zeta - \zeta')^3 + \zeta'(\zeta'^2 + 3)}{1 + 3\zeta'^2}\right] \frac{3(\zeta - \zeta'^2)}{1 + 3\zeta'^2} \mathrm{d}\zeta, \tag{4.6.5}$$

where ζ' is given as

$$\zeta' = \sqrt[3]{\gamma^* x_0 + |\gamma^*|} + \sqrt[3]{\gamma^* x_0 - |\gamma^*|} + x_0, \tag{4.6.6}$$

and γ^* is given as

$$\gamma^* = x_0^2 - 1.$$

To demonstrate the validity of the method, Telles [77] presented some examples that show the efficiency of his transformation. We give a simple illustrative example

$$I = \int_{-1}^{1} \ln|x| dx.$$

The singularity point $x_0 = 0$ is located within the integration range, so one needs to use the cubic transformation (4.6.5) as follows,

$\gamma^* = -1$ and $\zeta' = \sqrt[3]{0+1} + \sqrt[3]{0-|1|} = 0$,

$$I = \int_{-1}^{1} \ln|x| \mathrm{d}x = \int_{-1}^{1} \ln\left|\frac{\zeta^3 + 0}{1 + 0}\right| 3\zeta \mathrm{d}\zeta = 3\int_{-1}^{1} \zeta \ln|\zeta^3| \mathrm{d}\zeta.$$

Therefore, one can easily see that the Jacobian cancels the singularity and vanishes at the singularity point. Then the resulting integral can be computed by Gaussian quadrature. As it has been addressed in §(4.6.1), the logarithmically singular integral can be evaluated using the logarithmic Gaussian quadrature (4.6.2). Nevertheless, Telles shows that using his transformation first,

and then using the Gaussian quadrature greatly improves the accuracy and gives better results than logarithmic Gaussian quadrature.

4.7 Collocation method

In the collocation method, a function G can be expressed as a histogram, that is, approximated by piecewise constant basis functions as,

$$G(q) = \sum_{i=1}^{N} c_i \psi_i(q). \tag{4.7.1}$$

Dividing the boundary into sub-intervals s_i, we obtain

$$\partial\Omega = \bigcup_{i=1}^{N} s_i,$$

where the basis functions

$$\psi_i(q) = \begin{cases} 1, & \text{if } q \in s_i; \\ 0, & \text{otherwise.} \end{cases}$$

The point q is called the collocation point which is chosen to be the mid point of the sub-interval s_i as depicted in figure 4.4, and N is the number of collocation points.

The collocation method can be applied to the following integral

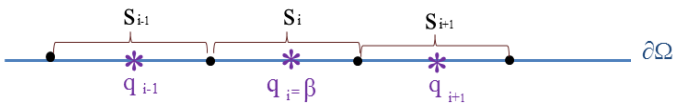

Figure 4.4: Sketch of the boundary $\partial\Omega$ divided into sub-intervals s_i, the dots are the boundary elements and the stars are the collocation points q_i (the mid point of s_i).

$$\lim_{\Delta r \to 0} \frac{\partial}{\partial n_\beta} \int_\gamma \frac{\partial G_0(q,\beta)}{\partial n_q} \left[G(q, \mathbf{r}') - G(\beta, \mathbf{r}') \right] \mathrm{d}q$$

where β is the singularity point. We denote the kernel of the integral as, $K(q,\beta;k)$, and for simplicity we suppress the source point $\mathbf{r}'$ in our notations. Using the interpolation (4.7.1) leads to

$$\begin{aligned}\int_I K(q,\beta;k)\,[G(q)-G(\beta)]\,\mathrm{d}q &\simeq \sum_{i=1}^{N} c_i \int_{s_i} \psi_i(q) K(q,\beta;k)\mathrm{d}q \\ &- c_j \int_{\gamma} K(q,\beta;k)\mathrm{d}q, \end{aligned} \tag{4.7.2}$$

where

$$I = \bigcup_{i=1}^{N} s_i$$

as depicted in figure 4.4. The function $G(\beta) = c_j$ where $s_j = \gamma$, and the singularity point β is the mid-point of the arc-length γ. If $q = \beta$ in the first integral on the RHS of equation (4.7.2), then $c_i = c_j$. Therefore the term between the square brackets $c_i - c_j$ vanishes when the collocation point β lies in the range of integration.

Hence by using the interpolation (4.7.1), the term containing the factor $[G(q,\mathbf{r}') - G(\beta,\mathbf{r}')]$ in equation (4.5.6) is vanishing on the sub-interval γ where the integral kernel becomes hypersingular.

4.8 Discretization and matrix formulations

Having treated both the hypersingular and the weakly singular integrals of the BIEs analytically, the following regularized BIEs can be solved efficiently by numerical means.

For $\beta \in \Gamma_j$, we have the following BIE

$$\begin{aligned}&\int_I \left[\frac{\partial G_0(q,\beta)}{\partial n_\beta}\mu^I(q,\mathbf{r}') - G^I(q,\mathbf{r}')\frac{\partial^2 G_0(q,\beta)}{\partial n_\beta \partial n_q}\right]\mathrm{d}q \\ &+ \int_{\Gamma_j}\left[\frac{\partial G_0(q,\beta)}{\partial n_\beta} - \frac{\delta(q-\beta)}{2}\right]\mu_j(q,\mathbf{r}')\mathrm{d}q = -\delta_{1j}\frac{\partial G_0(\beta,\mathbf{r}')}{\partial n_\beta}.\end{aligned} \tag{4.8.1}$$

For $\beta \in I$, we have the following BIE

$$\int_I \left[\frac{\partial G_0(q,\beta)}{\partial n_\beta} - \frac{\delta(q-\beta)}{2}\right]\mu^I(q,\mathbf{r}')\mathrm{d}q - \int_{I\setminus\gamma} G^I(q,\mathbf{r}')\frac{\partial^2 G_0(q,\beta)}{\partial n_\beta \partial n_q}\mathrm{d}q$$
$$+\left[\frac{\imath k_j^2}{2}\left\{\int_\gamma \left[H_0^1(k|q-\beta|) - \frac{2\imath}{\pi}\ln(k|q-\beta|)\mathrm{d}q\right] + \int_\gamma \frac{2\imath}{\pi}\ln(k|q-\beta|)\mathrm{d}q\right\}\right.$$
$$\left.-\frac{\imath k_j}{2}H_1^{(1)}\left(\frac{k_j\Delta q}{2}\right)\right]G^I(\beta,\mathbf{r}') + \int_{\Gamma_j}\frac{\partial G_0(q,\beta)}{\partial n_\beta}\mu_j(q,\mathbf{r}')\mathrm{d}q = -\delta_{1j}\frac{\partial G_0(\beta,\mathbf{r}')}{\partial n_\beta}, \tag{4.8.2}$$

with Δq the distance between the boundary points, and β being the centroid of the interval γ, that is

$$\gamma = \left[\beta - \frac{\Delta q}{2}, \beta + \frac{\Delta q}{2}\right].$$

We implemented the continuity conditions (4.2.5) implicitly as

$$\rho_2\mu_1^I = -\rho_1\mu_2^I = \mu^I, \qquad G_1^I = G_2^I = G^I.$$

Let us emphasise that the BIE (4.8.1) is regular, and the BIE (4.8.2) only contain a weakly singular integral along γ. Therefore depending on the boundary conditions and the number of interfaces between sub-components, it may be advantageous to take normal derivatives. This minimises the number of weakly singular integrals, thus leading to BEM formulations which are easier to handle.

All the boundaries have to be discretized including the internal boundaries that separate the sub-domains. Now, the boundary integral formulation can be written in matrix form as

$$\mathbf{A}\boldsymbol{\mu} = \mathbf{b}.$$

The global matrix $\mathbf{A}$ and the vector $\mathbf{b}$ can be decomposed into sub-matrices and sub-vectors as follows

$$\begin{bmatrix} \mathbf{K}_{\Gamma_1\Gamma_1} & \mathbf{F}_{\Gamma_1 I} & \mathbf{S}_{\Gamma_1 I} & \mathbf{0} \\ \mathbf{F}_{I\Gamma_1} & \mathbf{K}_{II} & \mathbf{H}_{II} & \mathbf{0} \\ \mathbf{0} & \mathbf{K}_{II} & \mathbf{H}_{II} & \mathbf{F}_{I\Gamma_2} \\ \mathbf{0} & \mathbf{F}_{\Gamma_2} & \mathbf{S}_{\Gamma_2 I} & \mathbf{K}_{\Gamma_2\Gamma_2} \end{bmatrix} \begin{Bmatrix} \boldsymbol{\mu}_1^{\Gamma_1} \\ \boldsymbol{\mu}^I \\ \mathbf{G}^I \\ \boldsymbol{\mu}_2^{\Gamma_2} \end{Bmatrix} = \begin{Bmatrix} \mathbf{b}_{\Gamma_1} \\ \mathbf{b}_I \\ \mathbf{0} \\ \mathbf{0} \end{Bmatrix}.$$

Here $\mathbf{A}$ is a $N \times N$ square matrix with dimension,

$$N = N_{\Gamma_j} + 2N_I, \qquad j = 1, 2,$$

where N_{Γ_j} and N_I are the number of boundary elements on Γ_j, and I, respectively. The sub-matrices $\mathbf{K}$, $\mathbf{F}$ and $\mathbf{S}$ are given as,

$$\begin{aligned}
\mathbf{K}_{\Gamma_j\Gamma_j}(m,i) &= \left[2\frac{\partial G_0(q_m,q_i)}{\partial n_{q_i}} - \delta_{mi}\right]\Delta q, \qquad q_m, q_i \in \Gamma_i, \\
\mathbf{F}_{\Gamma_j I}(m,i) &= 2\frac{\partial G_0(q_m,q_i)}{\partial n_{q_i}}\Delta q, \qquad q_i \in \Gamma_j, q_m \in I, \\
\mathbf{S}_{\Gamma_j I}(m,i) &= -2\frac{\partial^2 G_0(q_m,q_i)}{\partial n_{q_i}\partial n_{q_m}}\Delta q, \qquad q_i \in \Gamma_j, q_m \in I.
\end{aligned}$$

The source vector $\mathbf{b}$ is constructed as,

$$\begin{aligned}
\mathbf{b}_{\Gamma_1}(i) &= -2\frac{\partial G_0(q_i,\mathbf{r}')}{\partial n_{q_i}}, \qquad q_i \in \Gamma_1 \\
\mathbf{b}_I(i) &= -2\frac{\partial G_0(q_i,\mathbf{r}')}{\partial n_{q_i}}, \qquad q_i \in I.
\end{aligned}$$

The matrix that corresponds to the hypersingular term is given as,

$$\mathbf{H}_{II}(m,n) = \begin{cases} -2\left[k_j^2 F(\Delta q) - \frac{\imath k_j}{2} H_1^{(1)}\left(\frac{k_j \Delta q}{2}\right)\right], & \text{if } q_m = q_n; \\ \mathbf{S}_{II}(m,n), & \text{if } q_m \neq q_n, \end{cases}$$

where $F(\Delta q)$ is given by equation (4.6.3). The block $\mathbf{K}_{\Gamma_j\Gamma_j}$ expresses the rays starting and ending on the boundary Γ_j, $\mathbf{F}_{\Gamma_j I}$ and $\mathbf{S}_{\Gamma_1 I}$contains the rays starting on Γ_j and ending at the interface, $\mathbf{H}_{II}$ contains the rays starting and ending on the interface itself, and similarly for the other sub-matrices.

The sub-matrices in the third and fourth row blocks of the global matrix have the same structure as the ones on the first and the second row blocks, apart from changing the value of the wavenumber. In contrast with the classical single-domain BEM, the multi-component treatment leads to a block-banded matrix with one block for each sub-region, and overlaps between blocks when sub-regions have a common interface. As the number of sub-domains increases,

the number of zero blocks in the global matrix also grow. For a large number of sub-domains we have a banded matrix which is advantageous computationally, and allows us to exploit linear solvers for banded linear systems.
The linear system considered here has a unique solution (the number of unknowns equal to the number of equations) and can be solved using a direct solver, such as LU decomposition. The system should be solved for the four sub-vectors of unknowns,

$$\boldsymbol{\mu} = \{\boldsymbol{\mu}_1, \boldsymbol{\mu}^I, \mathbf{G}^I, \boldsymbol{\mu}_2\}^T.$$

Then after obtaining the boundary function $\boldsymbol{\mu}$, one needs to plug it into equation (4.3.5) to obtain the Green function throughout the interior of the domain.

4.9 Applications

We apply the multi-component BEM to different geometric configurations with different combinations of material parameters as considered in [12]. Three such example domains are depicted in figure 3.9. We plot the real part of the Green function as shown in figures 4.5 and 4.6 for the three configurations.

For configuration A shown in figure 4.5 a and b, the interface is relatively small compared with the arc-length of the boundary. Wave solutions are thus enhanced in the left domain in the case of damping. In contrast, for configuration B shown in figure 4.5 c and d, waves easily escape to the right sub-domain and the solution has a more uniform appearance.

For configuration C shown in figure 4.5 e, f, it is interesting to observe the bouncing ball modes in the pattern of the wave function, such modes usually live between parallel boundaries.

From the Green function, we can compute the energy density E as

$$E = |G(\mathbf{r}, \mathbf{r}')|^2.$$

So the mean energy density over the interior of the domain can be computed as,

$$E = \frac{1}{A}\int |G(\mathbf{r},\mathbf{r}')|^2 \mathrm{d}x\mathrm{d}y,$$

where A is teh area of the domain. Figure 4.7 shows a comparison between the mean energy densities in the left and the right sub-domains for configuration A with the same value of the wavenumber in each sub-domain: $\Re(k_1) = \Re(k_2) = 100$. The damping factor $\Im(k)$ takes the discrete values $0, 0.1, 0.2, ..., 1.4$. At zero damping, the mean energy density in the right sub-domain is higher than the corresponding value in the left sub-domain. However, with damping the mean energy densities in the left sub-domain are always higher than those in the right sub-domain. By increasing the damping, the mean energy density decreases in both sub-domains.

4.10 Accuracy of the results

In the absence of absorption, it should be noted from equation (4.2.2) that the Green function should be real because the Laplace operator ∇^2 and the delta function $\delta(\mathbf{r}-\mathbf{r}')$ both are real quantities, and k is considered real. We use this fact to verify our numerical computation in which the imaginary part of the Green function $\Im(G(\mathbf{r},\mathbf{r}';k))$ must be small compared to the real part $\Re(G(\mathbf{r},\mathbf{r}';k))$.

To demonstrate the accuracy of the multi-component BEM, we show a comparison of the imaginary part of $\boldsymbol{\mu}$ calculated using the multi-component BEM method for the case $k_1 = k_2$ against the single-domain BEM as shown in figure 4.8. One can observe that by dividing the domain under consideration into sub-components, we gain more accurate solution compared with the treatment of the domain as single region using the same number of boundary elements. This is attributed to the fact that in the multi-component BEM we have more degrees of freedom than the classical singe-domain BEM.

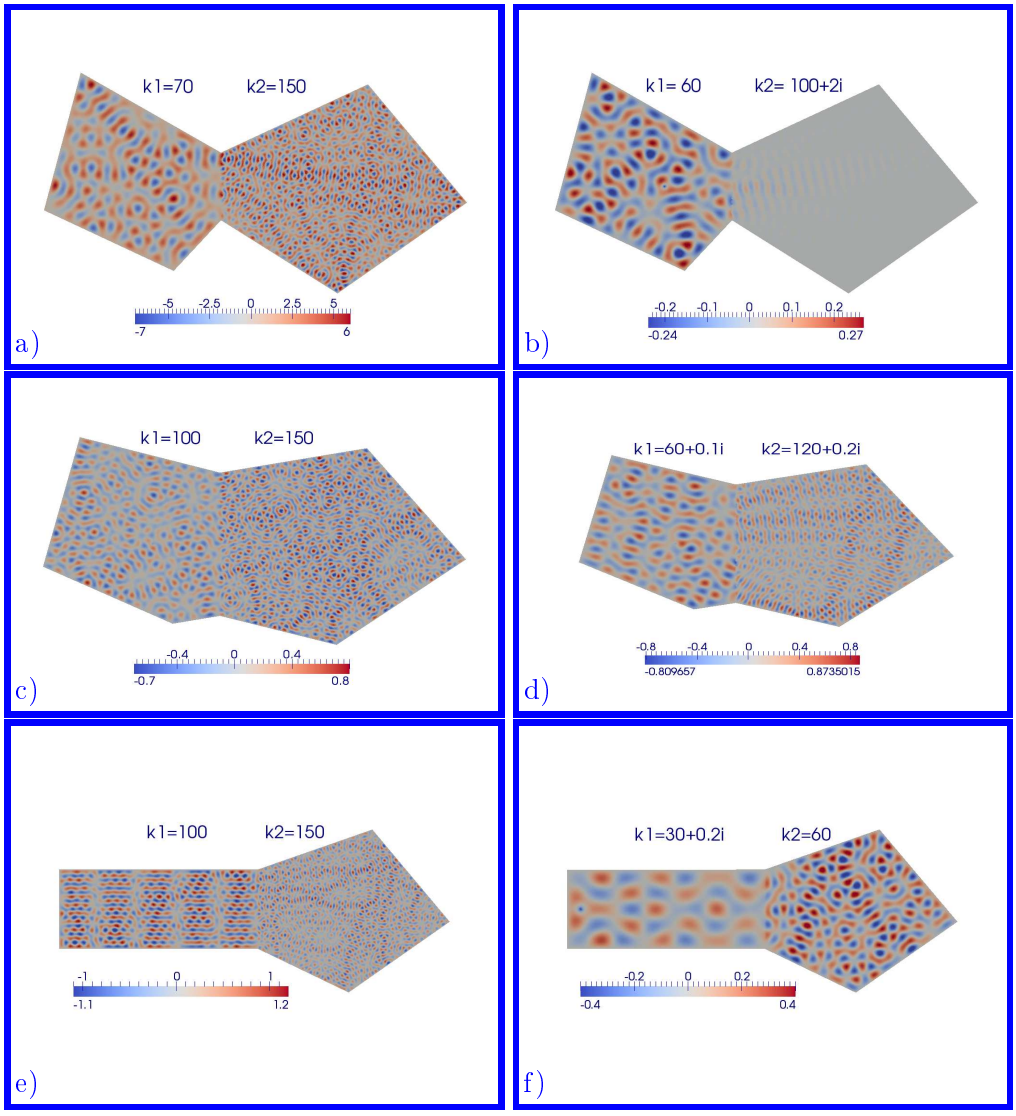

Figure 4.5: $\Re(G(\mathbf{r}, \mathbf{r}'; k))$ for configuration. A, B and C with different range of wavenumbers k, the imaginary part of k represents the damping of the system.

4.11 Conclusions

In this chapter we implemented a normal derivative multi-component technique to investigate the wave energy distribution in multi-component systems where the

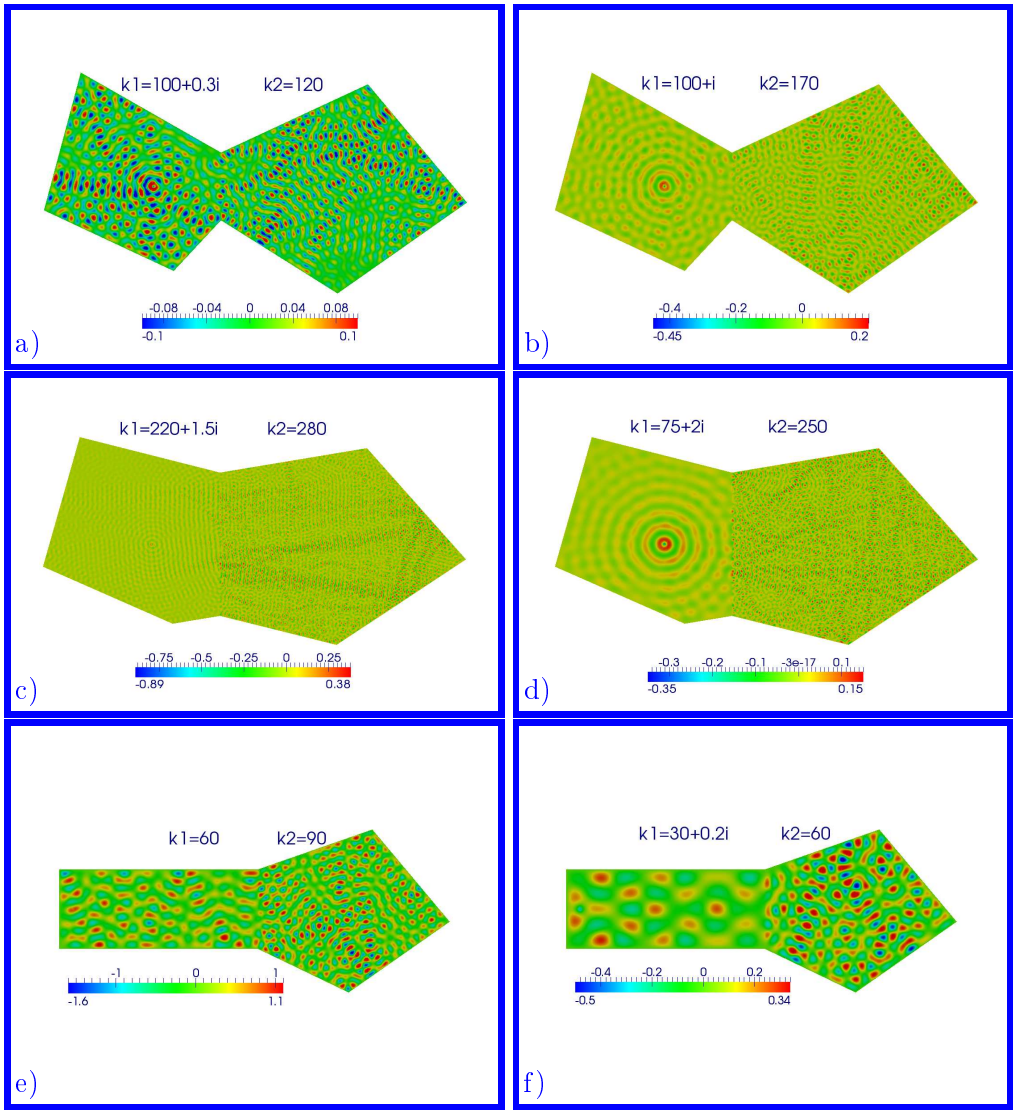

Figure 4.6: $\Re(G(\mathbf{r}, \mathbf{r}'; k))$ for configuration. A, B and C with different range of wavenumbers k, the imaginary part of k represents the damping of the system.

wavenumber and damping parameters change discontinuously in different parts of the system. This technique can be applied where a straightforward use of classical single-domain BEM would not be possible. This is due to the fact that the free Green function is only known for homogeneous problems and thus not

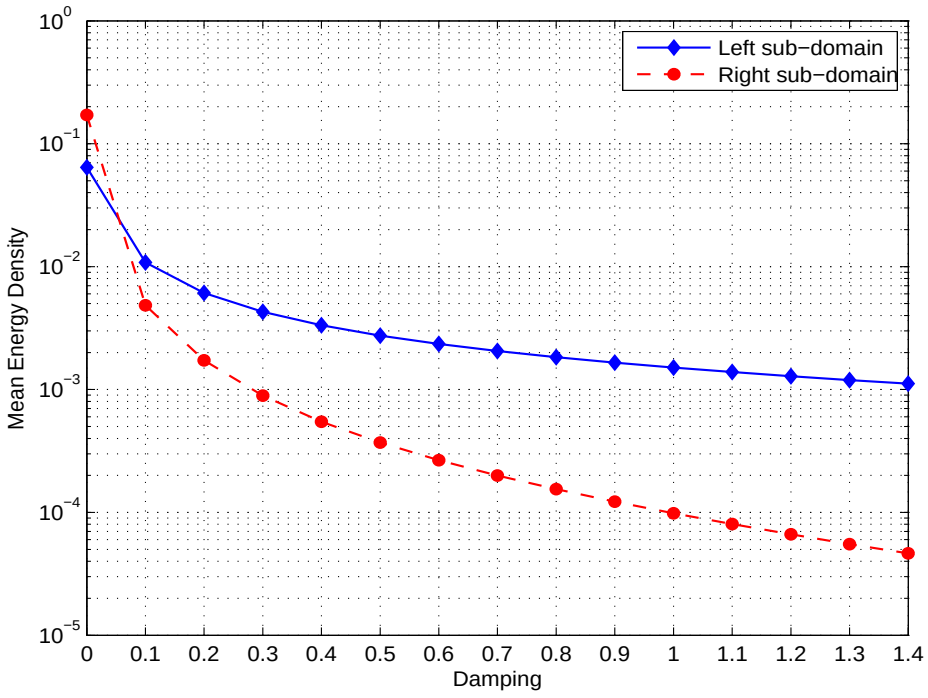

Figure 4.7: Mean energy densities in left and right sub-domain for configuration A for $\Re(k_1) = \Re(k_2) = 100$.

known for multi-component structures. Using the normal derivative formulation may prove useful in reducing the number of regularisation procedures necessary.

To treat the arising hypersingular integral, we introduced an elegant and simple way for deriving an integral identity which reduces the hypersingular integral into a weakly singular integral. A second step of evaluating the hypersingular integral is done by using a piecewise constant collocation method. Therefore, we have developed a code and have tested it against the classical single-domain BEM demonstrating the efficiency of the method.

We have applied the method to several coupled-cavity configurations. This approach can be easily implemented for complex built-up structures such as the configuration depicted in figure 4.9. However for large problems the associated linear system will grow very large and increasingly sparse. In such cases the di-

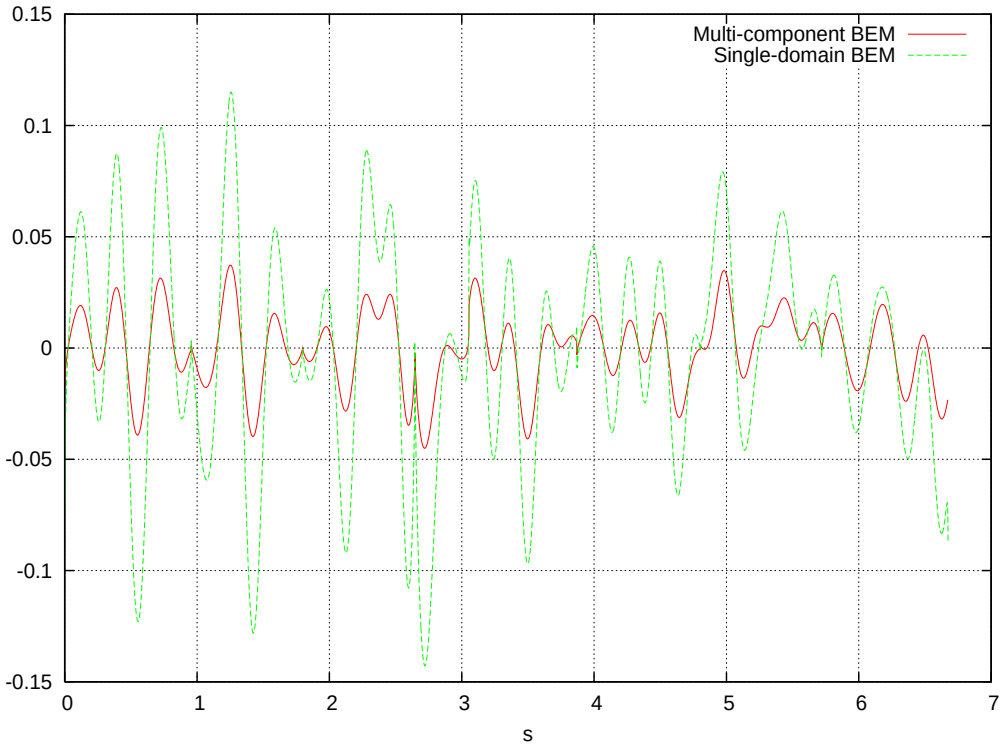

Figure 4.8: $\Im(\boldsymbol{\mu})$ for $k = 30$ with 3000 boundary elements for both methods.

rect solvers do not seem to be economic. Thus, the iterative solvers as discussed in §2.1.6 will be preferable to the direct solvers employed here.

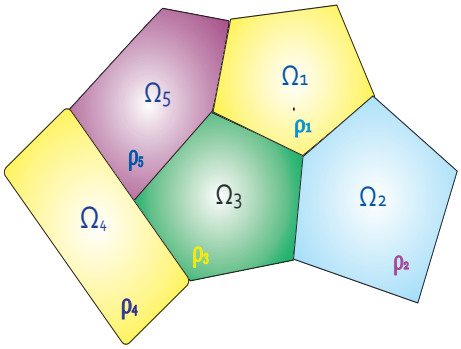

Figure 4.9: Example of a multi-component system.

Chapter 5

Transfer operator for a disc with discontinuous boundary conditions

5.1 Introduction

In the preceding chapter, we obtained the Green function of the coupled-cavity configuration with different material properties. From this quantity we can compute the mean energy throughout the configuration. However, for such domains, it is crucial to measure how much energy is reflected or transmitted at the discontinuity of the material properties. A measure of this is provided by the reflection and transmission coefficients. These coefficients provide the probability of a wave to be reflected or transmitted and they are stored in an implicit way within the BEM formulation. Therefore, it is crucial to develop an approach to obtain such coefficients explicitly. One possible way to do so is using the transfer operator pioneered by Bogomolny [8]. To form such an operator for the coupled cavities, we first consider a disc with boundary conditions changing discontinuously across the boundary, for example, Dirichlet boundary conditions along one part of the

boundary and Neumann boundary conditions along the rest of the boundary. Such a model incorporates similar features to the coupled-cavities in the sense that the discontinuity in the material properties leads to discontinuity in the boundary conditions. At a corner of a non-smooth boundary, it is expected that we have diffraction effects similar to the effect coming from the discontinuity of the boundary conditions. The goal of this chapter is to present the derivation of the transfer operator and point out where semiclassical approximations can be made at each step of the derivation.

The reason for starting with the disc problem is that, the circular geometry offers a clean test environment and many simplifications to investigate the accuracy of the obtained transfer operator. These include the fact that the circle does not include certain complications, such as corners. Also due to the rotational symmetry of the circle, the Fourier transform of any boundary operator form a diagonal matrix in momentum space, which is advantageous from a computational point of view and facilitates the formulation.

The discontinuity of the boundary conditions allows us to test how the exact transfer operator captures diffraction effects. Our formulation for the exact transfer operator starts from the BIEs with the boundary functions expressed in terms of the incoming and the outgoing plane waves. We obtain a map which relates the incoming waves to the outgoing waves. We call this map the shift operator.

It should be remarked that the discontinuity of the boundary condition does not affect the accuracy of the shift operator, because such an operator is derived from the BIEs without any reference to the boundary conditions. A second operator which we call the reflection operator relates the outgoing waves to the incoming waves. Such a map is derived only from the knowledge of the prescribed boundary conditions as shown in §5.6. Then, the transfer operator is constructed by combining the shift and the reflection operator to form the transfer operator for which the physical solution is an eigenfunction. Having

done this for a disc, similar ideas can be adapted for other geometries as will be discussed in Chapter 6.

Section §5.14 shows that the obtained exact transfer operator shows good agreement with the BEM results. The exact transfer operator incorporates boundary effects such as diffraction and surface waves unlike the semiclassical Bogomolny transfer operator. For a disc with Dirichlet boundary conditions, §5.5 shows that how the exact transfer operator can be reduced to the semiclassical Bogomolny transfer operator. The formulation for the exact transfer operator presented here based on ideas developed by Stephen Creagh.
To illustrate the basic ideas of the formulation of the transfer operator, we begin by presenting a one-dimensional problem.

5.2 Formulation of the transfer operator for a one-dimensional problem

In this section, we show how to derive the transfer operator for one-dimensional problem, for instance, a one-dimensional beam of length a as depicted in figure 5.1. We show how the actual boundary function, (either the Green function or

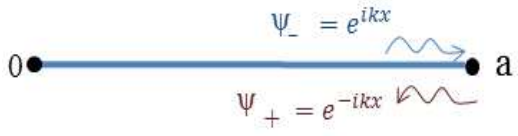

Figure 5.1: One-dimensional beam of length a.

its normal derivative depending on the prescribed boundary conditions), can be rewritten in terms of the incoming and outgoing waves and present a relation that connects both of them.

The starting point of the derivation of the transfer operator is the one-

dimensional BIEs for the Helmholtz equation given as,

$$\begin{bmatrix}\psi(0)\\ \psi(a)\end{bmatrix} = \sum_{x'\in\{0,a\}} \left[G_0(x,x';k)\mu(x') - \frac{\partial G_0(x,x';k)}{\partial n'}\psi(x')\right]_{x=0,a}, \tag{5.2.1}$$

where G_0 is the one-dimensional free-space Green function (derived in Appendix A) as

$$G_0(x,x';k) = \frac{\imath}{2k}e^{\imath k|x-x'|}. \tag{5.2.2}$$

The BIE (5.2.1) can be written using G_0 and its normal derivative as,

$$\begin{bmatrix}\psi(0)\\ \psi(a)\end{bmatrix} = \frac{\imath}{2k}\begin{bmatrix}1 & e^{\imath ka}\\ e^{\imath ka} & 1\end{bmatrix}\begin{bmatrix}\mu(0)\\ \mu(a)\end{bmatrix} + \frac{1}{2}\begin{bmatrix}1 & e^{\imath ka}\\ e^{\imath ka} & 1\end{bmatrix}\begin{bmatrix}\psi(0)\\ \psi(a)\end{bmatrix}. \tag{5.2.3}$$

Now we introduce the following operators,

$$\hat{G}_0 = \frac{\imath}{2k}\left\{\begin{bmatrix}I & 0\\ 0 & I\end{bmatrix} + \begin{bmatrix}0 & e^{\imath ka}\\ e^{\imath ka} & 0\end{bmatrix}\right\}, \tag{5.2.4}$$

where we decompose the operator $\hat{G}_0$ into a diagonal and off-diagonal part. We denote to the off-diagonal parts of $\hat{G}_0$ by $\hat{R}_0$, that is,

$$\hat{G}_0 = \frac{\imath}{2k}(\hat{I} + \hat{R}_0). \tag{5.2.5}$$

Similarly, we define,

$$\hat{G}_1 = -\frac{1}{2}(\hat{I} + \hat{R}_1), \tag{5.2.6}$$

where $\hat{I}$ is the identity operator.

The operators $\hat{R}_0$ and $\hat{R}_1$ are defined as,

$$\hat{R}_0 = \hat{R}_1 = \begin{bmatrix}0 & e^{\imath ka}\\ e^{\imath ka} & 0\end{bmatrix}. \tag{5.2.7}$$

Our notations distinguishes between $\hat{R}_0$ and $\hat{R}_1$, because their higher dimensional analogous are not equal. Hereafter, we refer to $\hat{G}_0$ and $\hat{G}_1$ as the Green operators. Thus the BIE (5.2.1) can be written in terms of these operators as,

$$\psi = \hat{G}_0\mu - \hat{G}_1\psi. \tag{5.2.8}$$

Further to the decomposition of the boundary integral kernels, we represent the solution of the Helmholtz equation as a superposition of plane waves. For instance, these waves are respectively classified as incoming waves ($e^{\imath kx}$) and outgoing waves ($e^{-\imath kx}$) to and from the vertex a as depicted in figure 5.1. One needs to consider the opposite sign for the other end of the beam. That is, the boundary functions ψ and μ can be decomposed as

$$\psi = \psi_- + \psi_+, \tag{5.2.9}$$

and

$$\mu = \frac{\partial \psi(s)}{\partial n_s} = \imath k(\psi_- - \psi_+), \tag{5.2.10}$$

where ψ_- and ψ_+ are respectively the incoming and the outgoing waves. Hereafter, ψ_- and ψ_+ are called the scattering amplitudes.

To proceed with the derivation of the transfer operator, one needs to plug equations (5.2.5), (5.2.6), (5.2.9) and (5.2.10) into the BIE (5.2.8). One has,

$$\psi_- + \psi_+ = \frac{\imath}{2k_1}(\hat{I} + \hat{R}_0)\cdot \imath k_1(\psi_- - \psi_+) + \frac{1}{2}(\hat{I} + \hat{R}_1)(\psi_- + \psi_+). \tag{5.2.11}$$

This equation is reduced to the following equation,

$$\psi_- = \left(\frac{\hat{R}_0 + \hat{R}_1}{2}\right)\psi_+, \tag{5.2.12}$$

using $\hat{R}_0 = \hat{R}_1$ as shown by equation (5.2.7), one has

$$\psi_- = \hat{R}\psi_+. \tag{5.2.13}$$

where $\hat{R} = \hat{R}_0 = \hat{R}_1$. The operator $\hat{R}$ is called the shift operator and maps the outgoing wave vector ψ_+ to the incoming wave vector ψ_-.

Since the shift operator $\hat{R}$ does not know anything about the prescribed boundary condition, one needs to construct another relation which incorporates these conditions. Such a map is derived from the knowledge of the boundary conditions. If we set Dirichlet boundary conditions at the two end points of the beam, that is,

$$\psi(0) = \psi(a) = 0, \tag{5.2.14}$$

this leads to,

$$\psi_+ = -\hat{I}\psi_-. \tag{5.2.15}$$

This relation maps the incoming wave vectors to the outgoing wave vectors. We call this map the reflection operator.

To form the transfer operator, we now combine the shift operator with the reflection operator by inserting equation (5.2.15) into equation (5.2.13). One has,

$$\psi_- = -\hat{R}\hat{I}\psi_- = \hat{T}\psi_-, \tag{5.2.16}$$

where $\hat{T}$ is called the transfer operator, it is a mapping of the incoming wave vector at a certain boundary point into the incoming wave vector after one travel along the beam. Equation (5.2.16) gives the quantization condition of the beam as,

$$\det(\hat{I} - \hat{T}) = 0.$$

In conclusion, the formulation of the transfer operator starts out by expressing the boundary integral kernels as diagonal and off-diagonal parts, then decomposing the boundary functions in terms of the scattering amplitudes. In the light of the one-dimensional approach developed here. We extend this formulation to the two-dimensional case. However, the treatment is less straightforward then.

5.3 Singular part of the Green operator $\hat{G}_0$

In this section we present the operator formulation of the shift operator for a two-dimensional disc, generalising the one-dimensional case that has been discussed in the previous section. In the one-dimensional treatment, the diagonal part of the boundary integral operators played an important role. Thus, we need to consider analogous contributions in the two-dimensional case as well.

The derivation of the shift operator starts from the BIE where the physical solution is an eigenfunction. The BIE (3.3.3) can be written in terms of

the Green operators $\hat{G}_0$ and $\hat{G}_1$ as,

$$\psi = \hat{G}_0\mu - \hat{G}_1\psi. \tag{5.3.1}$$

This is the basic BIE before applying the prescribed boundary conditions. The Green operators $\hat{G}_0$ and $\hat{G}_1$ are defined as,

$$\hat{G}_0\mu = \lim_{\mathbf{r}\to\beta}\int_{\partial\Omega} G_0(q,\mathbf{r};k)\mu(q)\mathrm{d}q, \tag{5.3.2}$$

and,

$$\hat{G}_1\psi = \lim_{\mathbf{r}\to\beta}\int_{\partial\Omega} \frac{\partial G_0(q,\mathbf{r};k)}{\partial n_q}\psi(q)\mathrm{d}q, \tag{5.3.3}$$

where $\mathbf{r}$ and β are respectively an interior and boundary point, and $\partial\Omega$ is the boundary of the unit disc.

Since the two-dimensional free-space Green function has a logarithmic singularity, the diagonal and off-diagonal part of the Green operators $\hat{G}_0$ and $\hat{G}_1$ will be called the singular and regular parts, respectively. That is,

$$\hat{G}_0 = \hat{G}_0^{\mathrm{reg}} + \hat{G}_0^{\mathrm{sing}},$$

where $\hat{G}_0^{\mathrm{reg}}$ carries the contribution from the boundary. The goal of this section is to derive the singular part of the Green operator $\hat{G}_0$, and in the following section we derive its regular part.

To proceed with the derivation of $\hat{G}_0^{\mathrm{sing}}$, let us assume that the boundary can be approximated by a straight line. We then express $\hat{G}_0^{\mathrm{sing}}$ in the following limit,

$$\begin{aligned} G_0^{\mathrm{sing}}(s,s';k) &= \frac{\imath}{4}\lim_{\epsilon\to 0} H_0^{(1)}(k\rho(s,s')) \\ &= \frac{\imath}{4}\lim_{\epsilon\to 0} H_0^{(1)}(k\sqrt{|s-s'|^2+\epsilon^2}), \end{aligned} \tag{5.3.4}$$

where s and s' are boundary points, and ϵ being a small distance from the boundary as depicted in figure 5.2; the singularity shows up when $\epsilon \to 0$. For simplicity, we set $s' = 0$.

It should be mentioned that for a straight line boundary that is, $\rho(s,s') = \sqrt{|s-s'|^2+\epsilon^2}$, we have $\hat{G}_0^{\mathrm{sing}} = \hat{G}_0$, this means there is no contribution from the

boundary.

However this is not the case for curved boundary because

$$\rho(s,s') \sim \sqrt{|s-s'|^2+\epsilon^2},$$

that is, it neglects the curvature of the boundary. This is a good approximation of the boundary for uncritically reflected waves from the boundary (not tangentially incident on the boundary).

It is convenient for our formulation to express $\hat{G}_0^{\text{sing}}$ in momentum space. To do

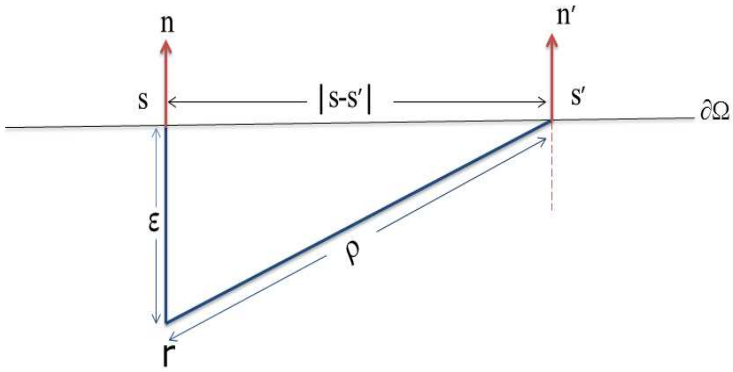

Figure 5.2: Straight line boundary with boundary points s and s' and $\mathbf{r}$ is an interior point.

so, one takes the Fourier transform of equation (5.3.4), that is,

$$\begin{aligned}\tilde{G}_0^{\text{sing}} &= \frac{\imath}{4}\lim_{\epsilon\to 0}\int_{-\infty}^{\infty} e^{-\imath ksp}H_0^{(1)}(k\sqrt{s^2+\epsilon^2})\mathrm{d}s \\ &= \frac{\imath}{4}\lim_{\epsilon\to 0}\begin{cases}\frac{2}{k\sqrt{1-p^2}}e^{\imath k\epsilon\sqrt{1-p^2}}, & \text{if } p^2<1,\\ \frac{-2\imath}{k\sqrt{p^2-1}}e^{-k\epsilon\sqrt{p^2-1}}, & \text{if } p^2>1.\end{cases}\end{aligned} \tag{5.3.5}$$

This is not a unique definition of $\hat{G}_0^{\text{sing}}$, but it captures the logarithmically singular part of G_0 and is found later to give a decomposition of the boundary integral equations which has the expected semiclassical limits. We believe that an alternative definition of $\hat{G}_0^{\text{sing}}$ which takes the curvature of the boundary into account may lead to better-converging decompositions of the boundary integral equations but we do not pursue these in this thesis. Alternative definitions

of the singular part should in any case have the same leading-order semiclassical limit.

For clarity of notations, we shall use the notation 'tilde' for the Fourier transform. For the second line of equation (5.3.5), we borrow the result for the integral from Gradshteyn et al. [130].

Now let us introduce the operator $\hat{p}_n$ which is defined formally as,

$$\hat{p}_n = \sqrt{1-\hat{p}^2}, \tag{5.3.6}$$

where the operator $\hat{p}$ generally is defined in position space as,

$$\hat{p} = \frac{1}{\imath k}\frac{\partial}{\partial s},$$

where s is the arc-length coordinate.

The operator $\hat{p}_n$ acts on a function $\psi(s)$ as,

$$\hat{p}_n\psi(s) \quad = \quad \sqrt{\frac{k}{2\pi}}\int_{-\infty}^{\infty} \mathrm{d}p\sqrt{1-p^2}\tilde{\psi}(p)e^{\imath spk}.$$

where $\tilde{\psi}(p)$ is the Fourier transform of $\psi(s)$ defined as,

$$\tilde{\psi}(p) = \sqrt{\frac{k}{2\pi}}\int_{-\infty}^{\infty} e^{-\imath kps}\psi(s)\mathrm{d}s. \tag{5.3.7}$$

Equation (5.3.7) shows how the operator $\hat{p}_n$ acts on the wavefunction ψ. When $p^2 < 1$, ψ will be a propagating wavefunction, but if $p^2 > 1$, then $\psi(s)$ corresponds to an evanescent wavefunction which decays in a direction normal to the boundary.

Performing the limit ($\epsilon \to 0$) in equation (5.3.5) and using (5.3.6), one has

$$\hat{G}_0^{\text{sing}} = \begin{cases} \frac{\imath}{2k\hat{p}_n} & \text{if } p^2 < 1, \\ \frac{1}{2k\hat{p}_n} & \text{if } p^2 > 1. \end{cases} \tag{5.3.8}$$

It is worth mentioning that, equation (5.3.8) gives the singular part of $\hat{G}_0$ for any smooth boundary and therefore does not consider the treatment of the corners for non-smooth boundaries. Next we show how to obtain the regular part of $\hat{G}_0$.

5.3.1 The regular part of the Green operator $\hat{G}_0$

In the preceding section, we generally obtained the singular part of $\hat{G}_0$ which is valid for any smooth boundary. However, here we show how to obtain its regular part specifically for a unit disc. Similarly to the derivation of the singular part of $\hat{G}_0$, we start from the free-space Green function for a boundary point a and an exterior point $\mathbf{r}$ of a distance ϵ from the boundary, that is $r = a+\epsilon$, as illustrated in figure 5.3. Then later we will let $r \to a$. One has,

$$G_0(a, \mathbf{r}; k) = \frac{\imath}{4} H_0^{(1)}(k\rho(a, \mathbf{r})). \tag{5.3.9}$$

The length of the trajectory connecting the boundary point a and the exterior

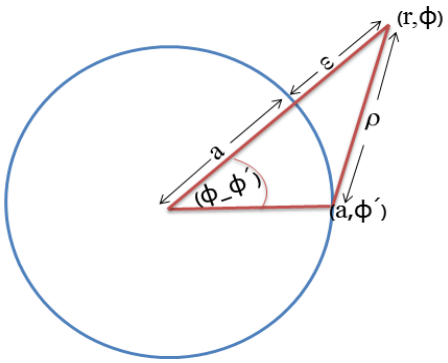

Figure 5.3: Sketch of the exterior point $\mathbf{r} = (r, \phi)$ and the boundary point $\mathbf{a} = (a, \phi')$.

point $\mathbf{r}$ can be parametrised in terms of the angles ϕ and ϕ' by using the law of cosines. Then we use the addition theorem given by equation (9.1.79) in [125], one obtains,

$$\begin{aligned} G_0(a, \mathbf{r}; k) &= \frac{\imath}{4} H_0^{(1)}(k\sqrt{a^2 + r^2 - 2ar\cos(\phi - \phi')}) \\ &= \frac{\imath}{4} \sum_{n=-\infty}^{\infty} H_n^{(1)}(kr) J_n(ka) e^{\imath n(\phi - \phi')} \end{aligned} \tag{5.3.10}$$

We now would like to see how the operator $\hat{G}_0$ acts on a boundary function μ. Since for a closed boundary, any boundary function must be periodic,

the continuous boundary function μ can be written in Fourier basis as,

$$\mu(\phi) = \sum_{m=-\infty}^{\infty} \mu_m e^{\imath m\phi}, \tag{5.3.11}$$

Using equation (5.3.10) and equation (5.3.11), one has,

$$\begin{aligned} \hat{G}_0\mu &= \frac{\imath}{4}\sum_n\sum_m H_n^{(1)}(kr)J_n(ka)\mu_m \oint a e^{\imath[n\phi+(m-n)\phi']}\mathrm{d}\phi' \\ &= \frac{\imath\pi a}{2}\sum_m H_m^{(1)}(kr)J_m(ka)e^{\imath m\phi}\mu_m, \end{aligned}$$

where we have used the orthogonality property of the exponential functions. Therefore, the Green operator $\hat{G}_0$ forms a diagonal matrix in momentum representations, with diagonal elements equal to,

$$(G_0)_{mm} = \frac{\imath\pi a}{2}H_m^{(1)}(kr)J_m(ka). \tag{5.3.12}$$

It should be noted that by considering $\mathbf{r}$ as an interior point, one obtains

$$(G_0)_{mm} = \frac{\imath\pi a}{2}H_m^{(1)}(ka)J_m(kr). \tag{5.3.13}$$

We now take either equation (5.3.12) or equation (5.3.13) in the limit $(r \to a)$. One has

$$(G_0)_{mm} = \frac{\imath\pi a}{2}H_m^{(1)}(ka)J_m(ka). \tag{5.3.14}$$

The one-dimensional case that is presented in the previous section offers guidance as how to formulate the corresponding Green operators for the two-dimensional case. Therefore, in a similar fashion to the one-dimensional case, $\hat{G}_0$ can be written as,

$$\hat{G}_0 = \frac{\imath}{2k}\frac{1}{\sqrt{\hat{p}_n}}(\hat{I} + \hat{R}_0)\frac{1}{\sqrt{\hat{p}_n}}, \tag{5.3.15}$$

where the regular part is problem-dependent, and it will be derived for a unit disc next.

By obtaining the regular and the singular parts of the operators $\hat{G}_0$, we can work out the explicit expression of $\hat{R}_0$ from equation (5.3.15) as,

$$\begin{aligned} \hat{R}_0 &= \frac{2k}{\imath}\sqrt{\hat{p}_n}\hat{G}_0\sqrt{\hat{p}_n} - \hat{I} \\ &= \frac{2k}{\imath}\hat{p}_n\hat{G}_0 - \hat{I}, \end{aligned}$$

where we may commute the diagonal operators $\hat{G}_0$ and $\sqrt{\hat{p}_n}$ in the special case of the disc.

The operator $\hat{p}_n$ is obtained for a disc as,

$$\hat{p}e^{\imath m\phi} = \frac{1}{\imath ka}\frac{\partial e^{\imath m\phi}}{\partial \phi},$$

thus,

$$(\hat{p})_m = \frac{m}{ka}. \tag{5.3.16}$$

Inserting $\hat{G}_0$ and $\hat{p}_n$ obtained respectively by equation (5.3.14) and (5.3.16) in equation (5.3.16), one obtains $\hat{R}_0$ as,

$$\begin{aligned}(R_0)_{mm'} &= \left(\frac{2k}{\imath}\left(\hat{p}_n\hat{G}_0\right)_{mm'} - 1\right)\delta_{mm'} \\ &= \left(\pi ka\sqrt{1-\left(\frac{m}{ka}\right)^2}H_m^{(1)}(ka)J_m(ka) - 1\right)\delta_{mm'} \\ &= \left(\pi\sqrt{(ka)^2-m^2}H_m^{(1)}(ka)J_m(ka) - 1\right)\delta_{mm'}. \end{aligned} \tag{5.3.17}$$

To conclude, we obtained the regular and singular parts of the Green operator $\hat{G}_0$, next we show how to obtain the analogous expression of the operator $\hat{G}_1$.

5.3.2 The regular and singular parts of the Green operator $\hat{G}_1$

As we have established in 3.3.1, the normal derivative of G_0 has a jump when taking the limit of an interior point to the boundary. The object of this section is to obtain the regular and singular parts of the operator $\hat{G}_1$.

The idea of the evaluation of $\hat{G}_1$ on the boundary is based on the relation (3.3.12) which relates the evaluation of $\frac{\partial G_0(q,\mathbf{r})}{\partial n'}$ in the interior, exterior and the boundary. Thus using the relation (3.3.12) we extract the regular part of $\hat{G}_1$. That is taking the average of the limiting values of $\frac{\partial G_0(q,\mathbf{r})}{\partial n'}$ approaching the boundary along the normal from inside and outside the domain. By doing so, the singular part is cancelled out.

From equation (5.3.12), the operator $\hat{G}_0$ can be evaluated at an exterior point $r > a$ as,

$$(G_0^{\text{ext}})_{mm'} = \frac{\imath\pi a}{2}H_m^{(1)}(kr)J_m(ka)\delta_{mm'}, \tag{5.3.18}$$

and $\hat{G}_0$ evaluated at an interior point $r < a$ as,

$$(G_0^{\text{int}})_{mm'} = \frac{\imath\pi a}{2} H_m^{(1)}(ka) J_m(kr)\delta_{mm'}. \tag{5.3.19}$$

Since, for a disc, the radius is normal to the boundary, one has

$$\frac{\partial G_0}{\partial n'} = \frac{\partial G_0}{\partial a}.$$

Thus using equations (5.3.18) and (5.3.19) the normal derivative of $\hat{G}_0$ with respect to the exterior point $\mathbf{r}$, one has

$$\begin{aligned} \lim_{\substack{\mathbf{r}\to a,\\ r>a}} (G_1^{\text{ext}})_{mm'} &= \lim_{\substack{\mathbf{r}\to a,\\ r>a}} \frac{\imath\pi ka}{2} H_m^{(1)}(kr) J'_m(ka)\delta_{mm'} \\ &= \left(\frac{1}{2} + \frac{\imath\pi ka}{2} H_m^{(1)}(ka) J'_m(ka)\right)\delta_{mm'}, \end{aligned} \tag{5.3.20}$$

and $\hat{G}_1$ evaluated at an interior point $r < a$ as

$$\begin{aligned} \lim_{\substack{\mathbf{r}\to a,\\ r<a}} (G_1^{\text{int}})_{mm'} &= \lim_{\substack{\mathbf{r}\to a,\\ r<a}} \frac{\imath\pi ka}{2} (H_m^{(1)}(ka))' J_m(kr)\delta_{mm'} \\ &= \left(-\frac{1}{2} + \frac{\imath\pi ka}{2} (H_m^{(1)}(ka))' J_m(ka)\right)\delta_{mm'}. \end{aligned} \tag{5.3.21}$$

The arising terms $\pm\frac{1}{2}$ in equations (5.3.20) and (5.3.21) come from the jump relation of $\hat{G}_1$ given by equation (3.3.12).

The average of the exterior and interior values given by equations (5.3.20) and (5.3.21), respectively, evaluates $\hat{G}_1$ on the boundary, so

$$(G_1^{\text{bou}})_{mm'} = \frac{\imath\pi ka}{4} \left(H_m^{(1)}(ka) J_m(ka)\right)' \delta_{mm'}. \tag{5.3.22}$$

Hereafter we set $z = ka$.

The Wronskian of $H_m^{(1)}(z)$ and $J_m(z)$ [125] is given as,

$$W(J_m(z), H_m^{(1)}(z)) = J_m(z)(H_m^{(1)}(ka))' - J'_m(z)H_m(z) = \frac{2\imath}{\pi z}. \tag{5.3.23}$$

If we invoke the Wronskian (5.3.23) into equation (5.3.22), then we reobtain equation (5.3.20) and equation (5.3.21).

The singular part of the Green operator $\hat{G}_1$ can be obtained by taking the difference between the exterior and interior values given by equation (5.3.20) and equation (5.3.21), respectively as,

$$\begin{aligned}(G_1^{\text{sing}})_{mm} &= (G_1^{\text{ext}})_{mm} - (G_1^{\text{int}})_{mm} \\ &= \frac{\imath\pi z}{2} W(J_m, H_m^{(1)}) \\ &= 1, \end{aligned} \tag{5.3.24}$$

where we have plugged the Wronskian (5.3.23) on the second line of equation (5.3.24).

In a similar fashion of writing the one-dimensional $\hat{G}_1$ as shown in §5.2, one has

$$\hat{G}_1^{\text{int}} = -\frac{1}{2}\frac{1}{\sqrt{\hat{p}_n}}\left(\hat{I} + \hat{R}_1\right)\sqrt{\hat{p}_n}, \tag{5.3.25}$$

and

$$\hat{G}_1^{\text{ext}} = -\frac{1}{2}\frac{1}{\sqrt{\hat{p}_n}}\left(-\hat{I} + \hat{R}_1\right)\sqrt{\hat{p}_n}. \tag{5.3.26}$$

The average of equations (5.3.25) and (5.3.26) evaluate $\hat{G}_1$ on the boundary, one has

$$\hat{G}_1^{\text{bou}} = -\frac{1}{2}\frac{1}{\sqrt{\hat{p}_n}}\hat{R}_1\sqrt{\hat{p}_n} \tag{5.3.27}$$

To evaluate the boundary operator $\hat{R}_1$, one needs to use $\hat{G}_1^{\text{bou}}$ given by equation (5.3.27), one has

$$\hat{R}_1 = -2\sqrt{\hat{p}_n}\hat{G}_1^{\text{bou}}\frac{1}{\sqrt{\hat{p}_n}}. \tag{5.3.28}$$

Since for a disc, the operators $\hat{G}_1^{\text{bou}}$, $\sqrt{\hat{p}_n}$ and $\frac{1}{\sqrt{\hat{p}_n}}$ are diagonal, so we are allowed to commute them, one has

$$(R_1)_{mm'} = \frac{-\imath\pi ka}{2}\left(H_m^{(1)}(ka)J_m(ka)\right)'\delta_{mm'}. \tag{5.3.29}$$

After obtaining the regular and singular parts of the Green operators $\hat{G}_0$ and $\hat{G}_1$, we can proceed to the derivation of the shift operator as shown next.

5.3.3 The exact and the semiclassical shift operator

To summarise, in the previous sections we introduced the decomposition of the Green operators $\hat{G}_0$ and $\hat{G}_1$ into regular and singular parts. In a similar fashion to the one-dimensional case we now decompose the boundary functions ψ and μ in terms of the incoming and outgoing waves ψ_- and ψ_+ as

$$\psi = \frac{1}{\sqrt{\hat{p}_n}}(\psi_- + \psi_+), \tag{5.3.30}$$

and

$$\mu = \imath k\sqrt{\hat{p}_n}(\psi_- - \psi_+), \tag{5.3.31}$$

where ψ_- and ψ_+ are the incoming and the outgoing wave vectors. In the one-dimensional case, the incoming and outgoing waves are only travelling to the left or to the right. However, in two dimensions they are propagating in all direction. Therefore, one needs to incorporate their direction using the operator $\sqrt{\hat{p}_n}$.

In this section, we incorporate the Green operators $\hat{G}_0$ and $\hat{G}_1$ obtained by equations (5.3.15), (5.3.25) into the BIE (5.3.1) with the decomposition relations (5.3.30) and (5.3.31) as,

$$\begin{aligned}\frac{1}{\sqrt{\hat{p}_n}}(\psi_- + \psi_+) = \frac{\imath}{2k}\frac{1}{\sqrt{\hat{p}_n}}(\hat{I} + \hat{R}_0)\frac{1}{\sqrt{\hat{p}_n}}\cdot \imath k\sqrt{\hat{p}_n}(\psi_- - \psi_+) \\ +\frac{1}{2}\frac{1}{\sqrt{\hat{p}_n}}(\hat{I} + \hat{R}_1)\sqrt{\hat{p}_n}\frac{1}{\sqrt{\hat{p}_n}}(\psi_- + \psi_+).\end{aligned} \tag{5.3.32}$$

Multiplying equation (5.3.32) by the operator $2\sqrt{\hat{p}_n}$ from the left, one arrives at the following expression,

$$\begin{aligned}\psi_- &= \left[(\hat{I} + \hat{R}_0) + (\hat{I} - \hat{R}_1\right]^{-1}(\hat{R}_0 + \hat{R}_1)\psi_+ \\ &= \hat{R}\psi_+.\end{aligned} \tag{5.3.33}$$

The operator $\hat{R}$ is called the exact shift operator for any type of smooth geometry. Since the operators $\hat{R}_0$ and $\hat{R}_1$ are diagonal for a disc, the inverse of the operator $\left[(\hat{I} + \hat{R}_0) + (\hat{I} - \hat{R}_1\right]$ is easy to calculate, however for other geometry it may be more difficult to evaluate.

To obtain the semiclassical shift operator, one can semiclassically assume that

$$\hat{R}_0 \simeq \hat{R}_1 \simeq \hat{R},$$

that is the semiclassical shift operator can be defined as,
$\hat{R}_{\text{sem}} = \hat{R}_0$ or $\hat{R}_{\text{sem}} = \hat{R}_1$.

To obtain the explicit expression of the shift operator $\hat{R}$ for the disc, one needs to substitute $\hat{R}_0$ and $\hat{R}_1$ given by equations (5.3.17) and (5.3.29), respectively, into equations (5.3.33). Using the fact that $\hat{R}_0$ and $\hat{R}_1$ commute in the special case of the disc. One has

$$\begin{aligned}
(R)_{mm} &= \frac{\pi z\sqrt{1-\left(\frac{m}{z}\right)^2}H_m^{(1)}J_m - \imath\pi z H_m^{(1)}J'_m}{\pi z\sqrt{1-\left(\frac{m}{z}\right)^2}H_m^{(1)}J_m + \imath\pi z H_m^{(1)}J'_m} \\
&= \frac{\sqrt{1-\left(\frac{m}{z}\right)^2}J_m - \imath J'_m}{\sqrt{1-\left(\frac{m}{z}\right)^2}J_m + \imath J'_m} \\
&= \frac{\sqrt{1-\left(\frac{m}{z}\right)^2} - \imath J'_m/J_m}{\sqrt{1-\left(\frac{m}{z}\right)^2} + \imath J'_m/J_m}.
\end{aligned} \tag{5.3.34}$$

These are the diagonal elements of the exact shift operator.

To investigate the difference between the operators $\hat{R}_0$, $\hat{R}_1$ and $\hat{R}$, we plot their diagonal elements for the value of the wavenumber $k = 50$ and Fourier bases from $m = -100$ to $m = 100$. For computational reasons, we need to compute the operators $\hat{R}_0$, $\hat{R}_1$ and $\hat{R}$ in a finite dimensional subspace using discrete bases. Figures 5.4 and 5.5 respectively show the real part and the modulus of the diagonal elements of the operators $\hat{R}_0$, $\hat{R}_1$ and $\hat{R}$. Both figures clearly distinguish two regions, the propagating region for $|m| < k$ and the non-propagating region for $|m| > k$. Figure 5.4 shows that the real part of the diagonal elements of all the operators have similar oscillation for $|m| < k$. However deviation starts to appear near the threshold $|m| \approx k$. In the propagating region, figure 5.5 shows that the modulus of the exact shift operator $|\hat{R}|$ obeys the unitarity property

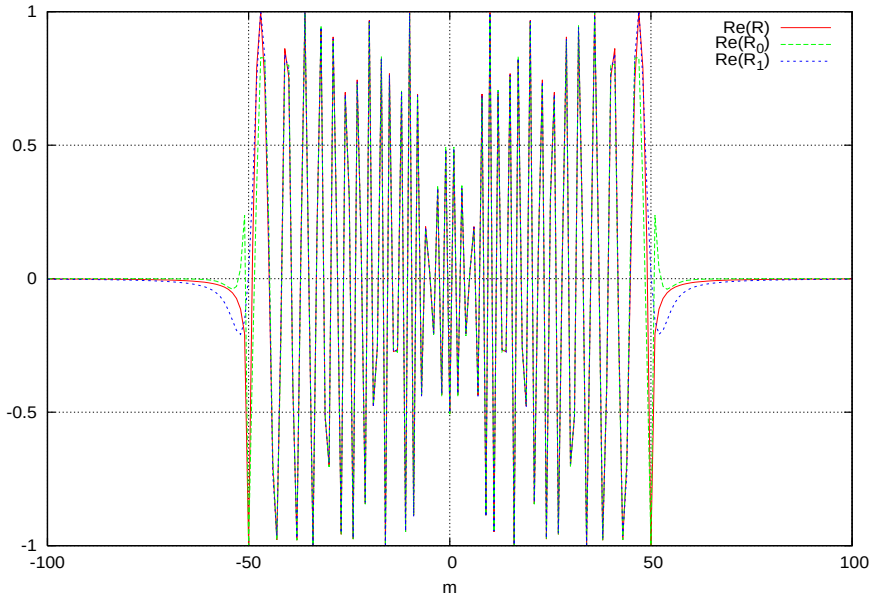

Figure 5.4: Real part of the diagonal elements of the operators $\hat{R}_0$, $\hat{R}_1$ and $\hat{R}$.

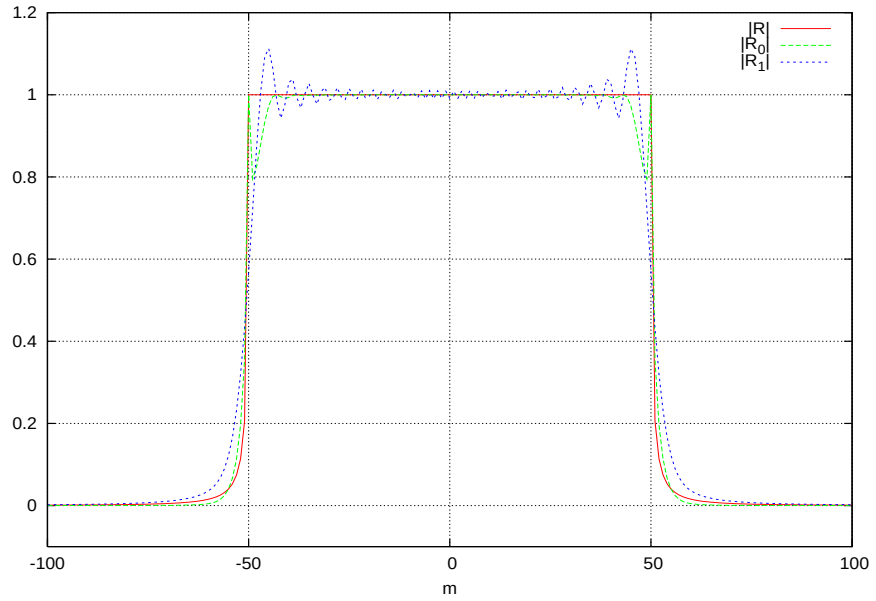

Figure 5.5: Modulus of the diagonal elements of the operators $\hat{R}_0$, $\hat{R}_1$ and $\hat{R}$.

defined as,

$$|R_{mm}|^2 = R_{mm}R^*_{mm} = 1, \qquad \text{for } |m| \leq k, \tag{5.3.35}$$

where R^*_{mm} is the complex conjugate of R_{mm}. Conversely, both $|(R_0)_{mm}|$ and $|(R_1)_{mm}|$ exhibit small oscillations around this value, that is,

$$|(R_{0,1})_{mm}| = 1 + \text{oscillations}, \qquad \text{for } m \leq k. \tag{5.3.36}$$

The unitarity property (5.3.35) is violated for $|m| > k$. At the threshold $|m| = k$ the propagating waves become decaying waves. Also, one can see that all the diagonal elements of the operators $\hat{R}_0$, $\hat{R}_1$ and $\hat{R}$ decay in the tail region $|m| \gg k$. Next we show asymptotically how the exact shift operator $\hat{R}$ decays for $|m| \gg k$.

5.3.4 Asymptotic expression of the shift operator for $|m| \gg z$

Here we investigate how the diagonal elements of the shift operator $\hat{R}$ decay in the tail region, that is, in the limit ($|m| \gg z$). In such a limit, Bessel functions can be written in their asymptotic expansion for large order m using Debye's asymptotic expansion [125]. This expansion approximates the Bessel functions as an exponential function with slowly varying amplitude similar to the Wentzel-Kramers-Brillouin (WKB) approximation connecting the oscillatory and evanescent region of the solution at either side of turning points. Debye's asymptotic expansion [125] of Bessel functions in the limit $|m| \gg z$ is given as,

$$J_m(m\text{sech}(\alpha)) = \frac{e^{m(\tanh(\alpha)-\alpha)}}{\sqrt{2m\pi\tanh(\alpha)}}\left(1 + \sum_{k=1}^{\infty}\frac{u_k(t)}{m^k}\right), \tag{5.3.37}$$

and

$$J'_m(m\text{sech}(\alpha)) = \sqrt{\frac{\sinh(2\alpha)}{4\pi m}}e^{m(\tanh(\alpha)-\alpha)}\left(1 + \sum_{k=1}^{\infty}\frac{v_k(t)}{m^k}\right). \tag{5.3.38}$$

These relations has the following transformation,

$$z = m\text{sech}(\alpha). \tag{5.3.39}$$

where α is fixed and positive, m is large and positive. The series $u_k(t)$ and $v_k(t)$ are given by equations (9.3.9) and (9.3.12) in [125], where t is defined as,

$$t = \coth(\alpha). \tag{5.3.40}$$

Inserting the transformation (5.3.39) into (5.3.40), leads to,

$$t = \frac{m/z}{\sqrt{\left(\frac{m}{z}\right)^2 - 1}}. \tag{5.3.41}$$

Using the approximation (5.3.37) and (5.3.38) for the ratio J'_m/J_m that is involved in the expression of the exact shift operator given by equation (5.3.34), one has

$$J'_m/J_m \quad = \quad \sqrt{\sinh(\alpha)\cosh(\alpha)\tanh(\alpha)} \left(\frac{1 + \sum_{k=1}^{\infty} \frac{v_k(t)}{m^k}}{1 + \sum_{k=1}^{\infty} \frac{u_k(t)}{m^k}} \right). \tag{5.3.42}$$

By considering the leading-order terms of the series u_k and v_k, one has

$$\begin{aligned} \left(\frac{1 + \sum_{k=1}^{\infty} \frac{v_k(t)}{m^k}}{1 + \sum_{k=1}^{\infty} \frac{u_k(t)}{m^k}} \right) &= 1 + \sum_{k=1}^{\infty} \frac{w^k}{m^k} \\ &\simeq 1 + v_1 - u_1 \\ &= 1 + \frac{-9t + 7t^3}{24} - \frac{3t - 5t^3}{24} \\ &= 1 + \frac{1}{2}(-t + t^3). \end{aligned} \tag{5.3.43}$$

Using equation (5.3.41), one has

$$t^2 - 1 = \frac{1}{\left[\left(\frac{m}{z}\right)^2 - 1\right]},$$

and

$$1 + \frac{1}{2}(-t + t^3) = 1 + \frac{1}{2} \frac{m/z}{\left[\left(\frac{m}{z}\right)^2 - 1\right]^{\frac{3}{2}}}. \tag{5.3.44}$$

Inserting equation (5.3.44) into equation (5.3.43), then substituting the resulting equation into (5.3.42) and finally in equation (5.3.34), one has

$$\begin{aligned} (R)_{mm} &\simeq \frac{-1}{4z\left[\left(\frac{m}{z}\right)^2 - 1\right]^{\frac{3}{2}}}, \qquad |m| \gg z, \\ &= (R_{\text{asy}})_{mm}\,. \end{aligned}$$

where $\hat{R}_{\text{asy}}$ is called the asymptotic expansion of the exact shift operator $\hat{R}$ in the limit $|m| \gg z$.

It should be noted that the asymptotic shift operator decays algebraically as $\hat{R}_{\text{asy}} \sim \frac{1}{m^3}$ rather than exponentially. This is due to the definition of $\hat{p}_n$ and the set-up of the decomposition relations for the boundary functions given by equations (5.3.30) and (5.3.31), therefore the exponentially decaying waves are hidden into the formulation.

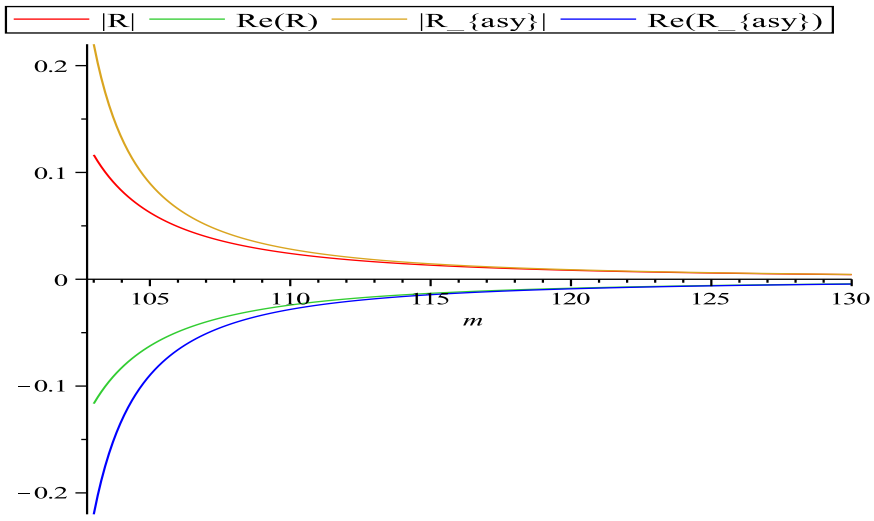

Figure 5.6: The modulus and the real parts of the diagonal elements of the exact shift operator $\hat{R}$ compared to its asymptotic $\hat{R}_{\text{asy}}$.

Figure 5.6 compares the modulus and the real part of the diagonal elements of $\hat{R}_{\text{asy}}$ against the corresponding quantity of the exact shift operator $\hat{R}$ for the value of the wavenumber $k = 100.5$ and the size of Fourier basis from $m = 103$ to $m = 130$. This range of m allows us to see the difference between the operators $\hat{R}$ and its asymptotic $\hat{R}_{\text{asy}}$ for $|m| \approx z$. It shows that the asymptotic $\hat{R}_{\text{asy}}$ has prominent deviation from the exact $\hat{R}$ near the threshold $|m| = z$, where the Debye asymptotic breaks down for $|m| \approx z$. Conversely, figure 5.7 shows that Debye's approximation works quite well for $|m| \gg z$.

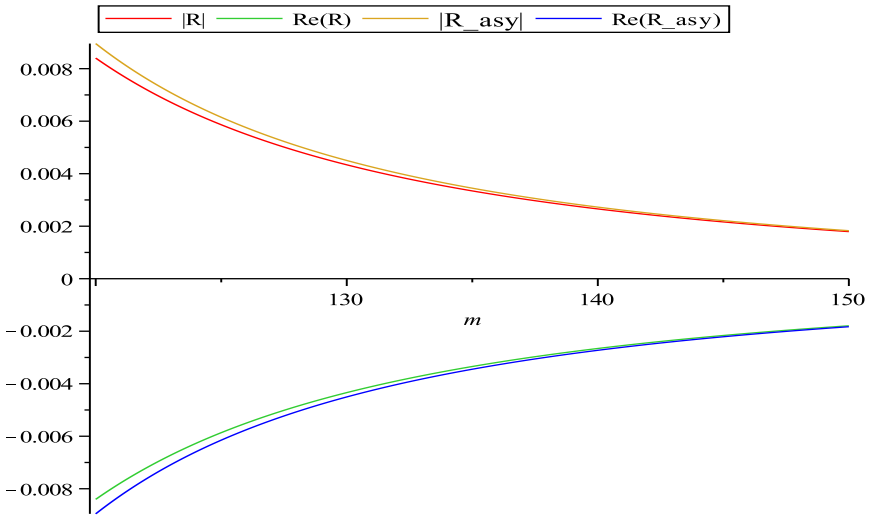

Figure 5.7: The modulus and the real parts of the diagonal elements of the exact shift operator $\hat{R}$ compared to its asymptotic $\hat{R}_{\text{asy}}$. in the tail region.

5.4 The transfer operator for a disc with DBCs

As an illustration of the transfer operator approach, here we show how the transfer operator for the unit disc with DBCs can be obtained in position space. The DBCs is defined as,

$$\psi(s) = 0, \qquad s \in \partial\Omega,$$

where $\partial\Omega$ is the boundary of the disc.

In §5.3.3, we have obtained the shift operator in momentum space, that is,

$$\begin{aligned} \psi_- &= R_{mm}\psi_+ \\ &= \mathcal{F}(R_{mm} * \psi_+) \end{aligned} \tag{5.4.1}$$

where we used the convolution theorem. Now take the inverse Fourier transform of equation (5.4.1), one has,

$$\psi_-(s) = \sum_{s'} R(s - s')\psi_+(s'), \tag{5.4.2}$$

and $R(s-s')$ is obtained by,

$$R(s-s') = \sum_m R_{mm} e^{\imath m(s-s')}. \tag{5.4.3}$$

which forms a non-diagonal matrix. Thus, the shift operator in position space depends on the difference $(s-s')$, whereas it is a diagonal in momentum space. Therefore the transfer operator for a disc with DBCs in position and momentum space is obtained respectively as,

$$T(s,s') = -\sum_m \left[\frac{\sqrt{1-\left(\frac{m}{z}\right)^2} J_m - \imath J'_m}{\sqrt{1-\left(\frac{m}{z}\right)^2} J_m + \imath J'_m} \right] e^{\frac{2\pi\imath m(s-s')}{L}}, \tag{5.4.4}$$

where L is the length of the boundary and,

$$T_{mm'} = -\delta_{mm'} R_{mm} = -\left[\frac{\sqrt{1-\left(\frac{m}{z}\right)^2} J_m - \imath J'_m}{\sqrt{1-\left(\frac{m}{z}\right)^2} J_m + \imath J'_m} \right]. \tag{5.4.5}$$

where the minus sign is due to the Dirichlet boundary conditions.
By using the transfer operator in momentum space, we can construct the following quantization condition as,

$$\det(I - T_{mm}) = \prod_{m=-\infty}^{\infty} \left(\frac{-2\sqrt{1-\left(\frac{m}{z}\right)^2} J_m}{\sqrt{1-\left(\frac{m}{z}\right)^2} J_m + \imath J'_m} \right), \qquad |m| \neq z. \tag{5.4.6}$$

Thus the zeros (eigenspectrum) of the determinant of the matrix $(I - T_{mm})$ are just the zeros of Bessel functions as can be seen from equation (5.4.6). Respectively figures 5.8 and 5.9 show the modulus of the spectral determinant computed using the transfer operator and the BEM. Both determinants have minima at the same positions as shown in figure 5.10 which plots the SVD of the determinant as presented in §3.4.1. Table 5.1 shows the obtained eigenvalues from both methods which agree exactly with the zeros of Bessel functions that are listed in [125]. So we demonstrate that equation (5.4.6) give the same spectrum as that obtained from the corresponding secular equation of the BEM, even though each equation uses a different basis. However, the scale of the BEM determinant is different

from the corresponding scale of the transfer operator. Figure 5.10 shows that the minima of the smallest singular values of the BEM determinant at the eigenvalue $k = 50.8438$ is higher than the corresponding minima of the transfer operator. This behaviour of the BEM determinant can be attributed to the different basis of each method and the large scale of the BEM determinant. We defer the discussion of the difference of the scale of the spectral determinant obtained from both methods to §5.9.

To conclude, we have obtained the transfer operator for a disc with DBCs. Such an operator can be reduced to the semiclassical Bogomolny transfer operator in the semiclassical limit as shown next.

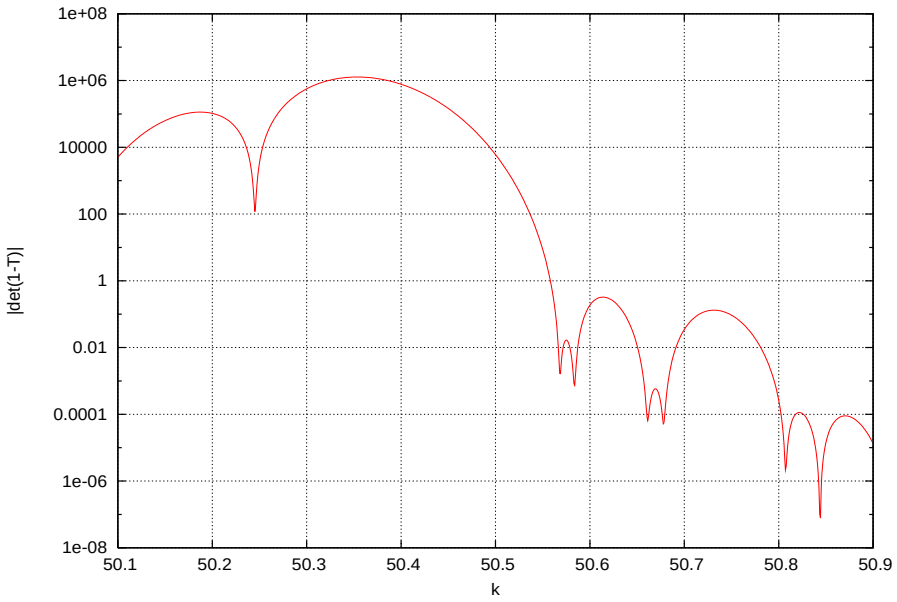

Figure 5.8: Semi-Log plot of the modulus of the determinant $|\det(I - T)|$ calculated by the transfer operator.

5.5 Bogomolny transfer operator for a disc with DBCs

In the previous section, we obtained the exact transfer operator for a disc with DBCs given by equation (5.4.4). In this section, we show how to reduce it to the

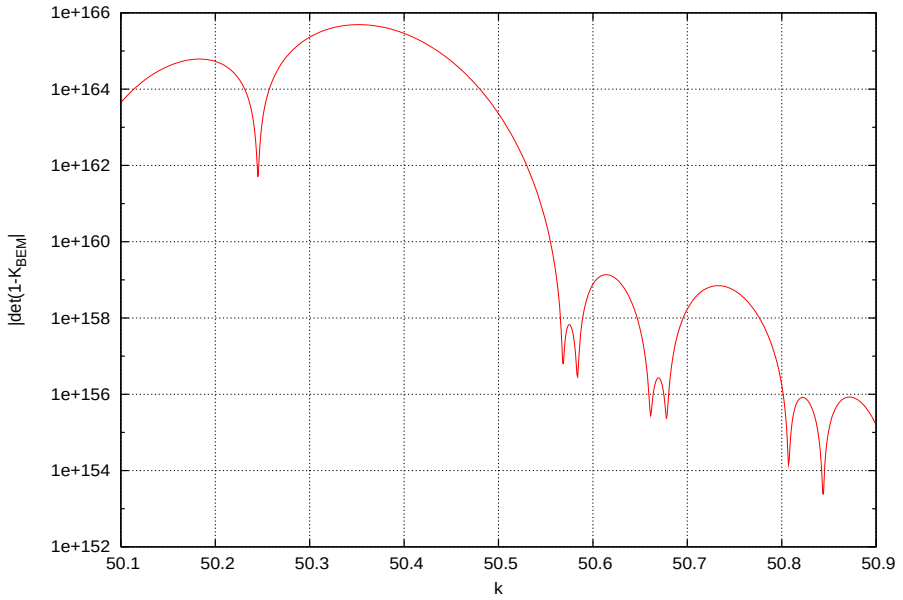

Figure 5.9: Semi-Log plot of the modulus of the determinant $|\det(I-K_{\mathrm{BEM}})|$ calculated by the BEM.

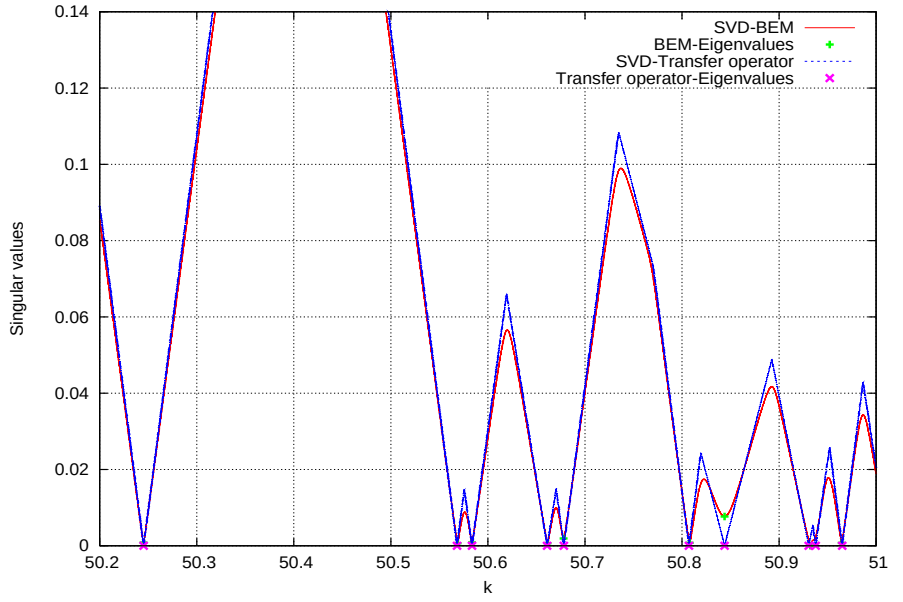

Figure 5.10: The smallest singular values and the eigenvalues computed using the BEM and the exact transfer operator.

Table 5.1: The eigenvalues of the unit disc with DBCs within the k range $[50.1, 51]$.

i	Eigenvalues(k)
1	50.2453
2	50.5681
3	50.5836
4	50.6610
5	50.6782
6	50.8071
7	50.8438
8	50.9306
9	50.9377
10	50.9650

semiclassical Bogomolny transfer operator. The first level of approximation is to approximate the exact shift operator $\hat{R}$ by $\hat{R}_0$. One has

$$T(s,s';k) = -\frac{1}{2\pi}\sum_{m=-\infty}^{\infty}[\pi\sqrt{z^2-m^2}H_m^{(1)}(z)J_m(z)-1]e^{\imath m(s-s')}. \qquad (5.5.1)$$

where s' and s are respectively the initial and final boundary points of the trajectory. Equation (5.5.1) can be simplified using the Poisson summation formula which relates a function f to its Fourier transform as,

$$\sum_{m=-\infty}^{\infty} f(m) = \sum_{n=-\infty}^{\infty}\int_{-\infty}^{\infty}\mathrm{d}x e^{2\pi\imath xn} f(x).$$

Thus,

$$T(s,s';k) = -\frac{1}{2\pi}\sum_{n=-\infty}^{\infty}\int_{-\infty}^{\infty}[\pi\sqrt{z^2-x^2}H_x(z)J_x(z)-1]e^{\imath x(s-s')}e^{2\pi\imath xn}\mathrm{d}x. \qquad (5.5.2)$$

The second level of approximation is to use Debye's asymptotic expansion of Bessel functions for large $|m|$ and $z > |m|$. The leading-order term of the Bessel

functions [125] are given as,

$$J_x(x\sec\beta) = \sqrt{\frac{2}{\pi x\tan\beta}}\cos\Psi, \tag{5.5.3}$$

$$Y_x(x\sec\beta) = \sqrt{\frac{2}{\pi x\tan\beta}}\sin\Psi, \tag{5.5.4}$$

where $0 < \beta < \frac{\pi}{2}$, $\Psi = x(\tan\beta - \beta) - \frac{\pi}{4}$.

This approximation uses the following transformation $z = x\sec\beta$.

Using these approximations, the Hankel function can be approximated as,

$$H_x^{(1)}(x\sec\beta) = \sqrt{\frac{2}{\pi x\tan\beta}}e^{\imath\Psi}. \tag{5.5.5}$$

If we substitute equations (5.5.5), (5.5.3) into (5.5.2), then we obtain,

$$T(s,s';k) = \frac{1}{2\pi}\sum_{n=-\infty}^{\infty}\int_0^{\frac{\pi}{2}}\mathrm{d}\beta z\sin\beta\left[\pi z\sqrt{1-\cos^2\beta}\left(\frac{2}{\pi x\tan\beta}\right)e^{\imath\Psi}\cos\Psi - 1\right]e^{\imath x[(s-s')+2\pi n]} \tag{5.5.6}$$

where $x = \frac{z}{\sec\beta}$.

Using $\cos\Psi = \left(\frac{e^{\imath\Psi}+e^{-\imath\Psi}}{2}\right)$, equation (5.5.6) can be reduced to,

$$T(s,s';k) = \frac{e^{-\imath\frac{\pi}{2}}}{2\pi}\sum_{n=-\infty}^{\infty}\int_0^{\frac{\pi}{2}} z\sin\beta e^{\imath zf(\beta)}\mathrm{d}\beta, \tag{5.5.7}$$

where

$$f(\beta) = \cos\beta[2(\tan\beta - \beta) + (s-s') + 2\pi n].$$

This oscillatory integral can be done by the stationary phase approximation (SPA). The stationary phase condition is

$$f'(\beta) = [2\beta - (s-s') - 2\pi n]\sin\beta = 0.$$

The solution of this equation is,

$$\beta_0 = \left[\frac{(s-s')+2\pi n}{2}\right].$$

We can set $n = 0$ which corresponds to taking the first term in the Poisson summation formula, because for other values of n, the obtained stationary points

lie outside the range $0 < \beta < \frac{\pi}{2}$. Therefore the only stationary point which lies within the given range is,

$$\beta_0 = \frac{(s - s')}{2}.$$

To complete the SPA, we need to compute,

$$f''(\beta) = 2\sin\beta - 2\beta\cos\beta - (s - s')\cos\beta,$$

which implies,

$$f''(\beta_0) = 2\sin\left|\frac{s - s'}{2}\right|.$$

Thus, evaluating the integral (5.5.7) at the stationary points β_0 leads to,

$$T(s, s'; k) = \frac{e^{-\imath\frac{\pi}{2}}\sqrt{2\imath\pi}}{2\pi}\sin\left|\frac{s - s'}{2}\right|\sqrt{\frac{z}{2\left|\sin\left|\frac{s-s'}{2}\right|\right|}}e^{2\imath z\sin\left|\frac{s-s'}{2}\right| - \frac{\imath\pi\nu}{2}}, \qquad (5.5.8)$$

where the phase $\nu = 0$ because $f''(\beta_0) > 0$.

For a unit disc ($a = 1$), we have $z = k$, and the length of any chord connecting the two boundary points s and s' is given as,

$$\rho(s, s') = 2\sin\left|\frac{s - s'}{2}\right|,$$

as depicted in figure 5.11. Also, the angle between the chord connecting s' to s

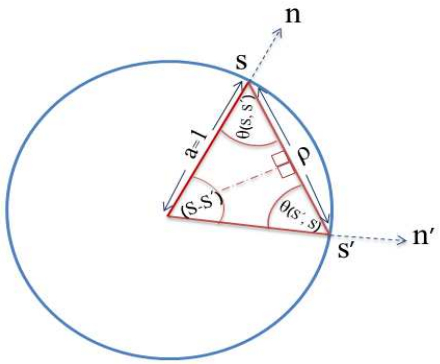

Figure 5.11: Sketch of the unit disc.

and the normal at the boundary point s', is equal to the corresponding angle at s, that is

$$\cos\theta(s, s') = \cos\theta(s', s).$$

Also, for a circle we have,

$$\cos\theta(s,s') = \sin\left|\frac{s-s'}{2}\right|.$$

Thus one obtains the semiclassical Bogomolny transfer operator for a unit disc as,

$$T(s,s';k) = \frac{1}{\sqrt{2\pi\imath}}\sqrt{\frac{k}{\rho(s,s')}}\sqrt{\cos\theta(s,s')\cos\theta(s',s)}e^{\imath k\rho(s,s')}. \tag{5.5.9}$$

This is consistent with known results [10].

5.6 The reflection operator

In §5.3.3, we derived the shift operator which does not know anything about the prescribed boundary conditions. Thus, we need to devise another operator which carries the information about the boundary conditions. Such an operator is called the reflection operator, because it tells us how an incoming wave is reflected once it hits the boundary.

In this section we consider a disc with boundary conditions changing discontinuously across the boundary. That is, we set Dirichlet boundary conditions along one part of the boundary and we set Neumann boundary conditions along the rest, as depicted in figure 5.12. These conditions can be formulated as,

$$\left.\begin{aligned} \psi(s) &= 0, \qquad s\in\Gamma_D,\\ \mu(s) = \frac{\partial\psi(s)}{\partial n_s} &= 0, \qquad s\in\Gamma_N, \end{aligned}\right\}, \qquad \text{Mixed BCs} \tag{5.6.1}$$

where Γ_D and Γ_N refer to the Dirichlet and Neumann parts, respectively. The goal of this section is to present the derivation of the reflection operator exactly and semiclassically, and then show a comparison between them. For convenience we proceed to a derivation in momentum space.

5.6.1 The exact reflection operator

We now show how to obtain the exact reflection operator. We start out by formulating the mixed boundary conditions described by equation (5.6.1) in terms

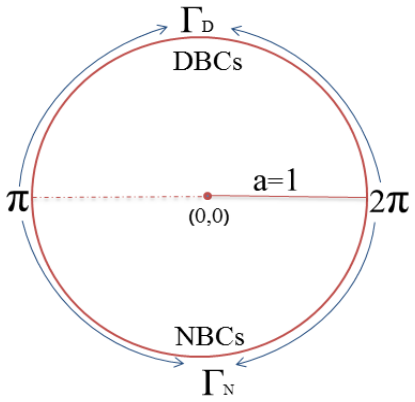

Figure 5.12: Sketch of the unit disc with mixed boundary conditions.

of the characteristic function χ as,

$$\chi_D \psi(s) = 0, \qquad s \in \Gamma_D, \tag{5.6.2}$$

and,

$$\chi_N \mu(s) = 0, \qquad s \in \Gamma_N. \tag{5.6.3}$$

The characteristic function χ_N is defined by,

$$\chi_D(s) = \begin{cases} 1, & \text{if } s \in \Gamma_D, \\ 0, & \text{otherwise}, \end{cases} \tag{5.6.4}$$

and similarly for $\chi_N(s)$. Now one needs to insert equations (5.3.30) and (5.3.31) into the boundary conditions (5.6.2) and (5.6.3), respectively,

$$\chi_D \psi = \chi_D \frac{1}{\sqrt{\hat{p}_n}}(\psi_- + \psi_+) = 0, \tag{5.6.5}$$

and,

$$\frac{1}{\imath k}\chi_N \mu = \chi_N \sqrt{\hat{p}_n}(\psi_- - \psi_+) = 0. \tag{5.6.6}$$

Note that the characteristic function does not in general commute with the operators $\sqrt{\hat{p}_n}$ and $\frac{1}{\sqrt{\hat{p}_n}}$. We multiply equation (5.6.5) by $\hat{p}_n$, then subtract the resulting equation from equation (5.6.6), one has

$$\hat{p}_n \chi_D \frac{1}{\sqrt{\hat{p}_n}}(\psi_- + \psi_+) - \chi_N \sqrt{\hat{p}_n}(\psi_- - \psi_+) = 0. \tag{5.6.7}$$

Multiplying equation (5.6.7) by $\frac{1}{\sqrt{\hat{p}_n}}$, and rearranging leads to,

$$\left(\sqrt{\hat{p}_n}\chi_D\frac{1}{\sqrt{\hat{p}_n}}+\frac{1}{\sqrt{\hat{p}_n}}\chi_N\sqrt{\hat{p}_n}\right)\psi_+=\left(\frac{1}{\sqrt{\hat{p}_n}}\chi_N\sqrt{\hat{p}_n}-\sqrt{\hat{p}_n}\chi_D\frac{1}{\sqrt{\hat{p}_n}}\right)\psi_-. \tag{5.6.8}$$

Therefore, the exact reflection operator $\hat{S}_{\rm ex}$ in momentum space is obtained as,

$$\hat{S}_{\rm ex}=\left(\sqrt{\hat{p}_n}\chi_D\frac{1}{\sqrt{\hat{p}_n}}+\frac{1}{\sqrt{\hat{p}_n}}\chi_N\sqrt{\hat{p}_n}\right)^{-1}\left(\frac{1}{\sqrt{\hat{p}_n}}\chi_N\sqrt{\hat{p}_n}-\sqrt{\hat{p}_n}\chi_D\frac{1}{\sqrt{\hat{p}_n}}\right). \tag{5.6.9}$$

Equation (5.6.8) can be written as,

$$\psi_+=\hat{S}_{\rm ex}\psi_-. \tag{5.6.10}$$

In Appendix E, we show that the following commutators,

$$\left[\chi_{(D,N)},\frac{1}{\sqrt{\hat{p}_n}}\right]=\chi_{(D,N)}\frac{1}{\sqrt{\hat{p}_n}}-\frac{1}{\sqrt{\hat{p}_n}}\chi_{(D,N)}, \tag{5.6.11}$$

and

$$[\chi_{(D,N)},\sqrt{\hat{p}_n}]=\chi_{(D,N)}\sqrt{\hat{p}_n}-\sqrt{\hat{p}_n}\chi_{(D,N)}, \tag{5.6.12}$$

both have localised effects at the discontinuity of the boundary condition. The function $\chi_{(D,N)}$ refers to the characteristic functions calculated either along Dirichlet or Neumann parts. However, semiclassically we can approximate the reflection operator by neglecting the contribution from the commutators as shown next.

5.6.2 The semiclassical reflection operator

We now present the semiclassical reflection operator. From the exact reflection operator derived in the previous section, we can obtain the semiclassical reflection operator by assuming that the characteristic functions $\chi_{(D,N)}$ commute with the operators $\sqrt{\hat{p}_n}$ and $\frac{1}{\sqrt{\hat{p}_n}}$ in equation (5.6.9), then one has,

$$\hat{S}_{\rm sem}=\left(\chi_D+\chi_N\right)^{-1}\left(\chi_N-\chi_D\right) \tag{5.6.13}$$

where,

$$\chi_D+\chi_N=\hat{I},$$

and

$$\chi_N - \chi_D = \hat{S}_{\text{sem}}.$$

This shows that by neglecting the contribution from the commutators (5.6.11), the exact reflection operator $\hat{S}_{\text{ex}}$ is reduced to the semiclassical reflection operator $\hat{S}_{\text{sem}}$.

Now we proceed to the derivation of the semiclassical reflection operator by writing the mixed boundary conditions (5.6.1) in terms of the characteristic function χ as,

$$S_{\text{sem}}\psi_+(s) = [\chi_N(s) - \chi_D(s)]\psi_-(s). \tag{5.6.14}$$

we prefer to obtain this equation in momentum space by taking its Fourier transform of equation (5.6.14), one has

$$\begin{aligned} S_{\text{sem}}\tilde{\psi}_+ &= (\tilde{\chi}_N - \tilde{\chi}_D)_m * \tilde{\psi}_- \\ &= \sum_{m'} (\tilde{\chi}_N - \tilde{\chi}_D)_{m-m'} (\tilde{\psi}_-)_{m'}, \end{aligned}$$

where we have applied the convolution theorem given as

$$\tilde{f} * \tilde{g} = \sum_{m'} f_{(m-m')} g_{m'}.$$

The Fourier transform of $\chi_D(s)$ is,

$$\begin{aligned} \mathcal{F}(\chi_D(s)) = (\tilde{\chi}_D)_m &= \frac{1}{L}\int_0^L e^{\frac{-2\pi\imath ms}{L}}\chi_D(s)\mathrm{d}s \\ &= \frac{d}{L}e^{\frac{-2\pi\imath m}{L}}\operatorname{sinc}\left(\frac{dm}{L}\right), \end{aligned}$$

where d is the length of the Dirichlet part, and L is the length of the whole boundary; (for a unit disc $L = 2\pi$). The function sinc is called the sin cardinal function and is defined by,

$$\operatorname{sinc}\left(\frac{dm}{L}\right) = \frac{L}{dm\pi}\sin\left(\frac{dm\pi}{L}\right).$$

In a similar manner, we obtain the Fourier transform of $\chi_N(s)$ as

$$(\tilde{\chi}_N)_m = \frac{b}{L}e^{\frac{\imath m\pi(\frac{b}{L}-2)}{L}}\operatorname{sinc}\left(\frac{bm}{L}\right), \tag{5.6.15}$$

where $b = 2\pi - d$ is the length of the Neumann part.

Thus the semiclassical reflection operator in momentum space is obtained as,

$$(S_{\text{sem}})_{mm'} = (\tilde{\chi}_N - \tilde{\chi}_D)_{m-m'} \,. \tag{5.6.16}$$

It should be noted that the reflection operator in momentum space given by (5.6.16) forms a full matrix, whereas in position space given by equation (5.6.14) it forms a diagonal matrix with diagonal elements -1 and 1 along the Dirichlet and the Neumann parts, respectively. The reflection operator retains the behaviour of the $\text{sinc}(x)$ function, that is, S_{sem} is diagonally dominant whereas the off-diagonal elements becomes small as they go away from the diagonal.

5.6.3 Comparison between the exact and the semiclassical reflection operator

In this section, we demonstrate a brief comparison between the exact reflection operator $\hat{S}_{\text{ex}}$ and the semiclassical reflection operator $\hat{S}_{\text{sem}}$ for a unit disc.

Figure 5.13 shows a contour plot of the modulus of the diagonal elements of the exact and the semiclassical reflection matrix. The x and y axes of the contour plot represent the indices (i, j) of the matrix. This comparison is carried out for the wavenumber value $k = 15.1$, and Fourier basis size from $m = -30$ to $m = 30$, where m is the index of Fourier basis. We set the length of Dirichlet and Neumann parts equal to π. Figure 5.13 shows that the reflection operator forms a diagonally dominant matrix, and the difference between the elements of S_{ex} and S_{sem} is pronounced at the diagonal elements with indices equal to $i = 15$ and $i = 45$.

For a close look at the difference which appears at these diagonal elements, we compute the percentage relative error between the diagonal elements of S_{ex} and S_{sem} for the same parameters mentioned above as

$$|\text{ Error }|\ \% = \left| \frac{(S_{\text{ex}})_{mm} - (S_{\text{sem}})_{mm}}{(S_{\text{ex}})_{mm}} \right| \times 100.$$

Figure 5.14 shows the percentage relative error between the exact and semiclassical results. It shows that the error is pronounced around the Fourier indices $m = -15, m = 15$. Here because we used positive indices for the diagonal elements for the reflection matrix from $i = 1$ and $i = 2N + 1$, where N is the size of Fourier basis, this is equivalent to $i = -N$ and $i = N$. That is the matrix indices $i = 15$ and $i = 45$ correspond to the Fourier basis indices $m = -15, m = 15$. The spike at the diagonal elements of the exact reflection operator with indices $i = 15$ and $i = 45$ is attributed to a mathematical issue in the definition of the operator involved in the formulation of the exact reflection operator. This issue is related to the singularity of the operator $\frac{1}{\sqrt{\hat{p}_n}}$ at $|m| = k$ in momentum space. The semiclassical reflection operator does not have such operator, so its diagonal elements do not show any spike.

After obtaining the shift and reflection operators exactly and the semiclassically, we combine both operators to construct the exact and the semiclassical transfer operator for the unit disc as shown next.

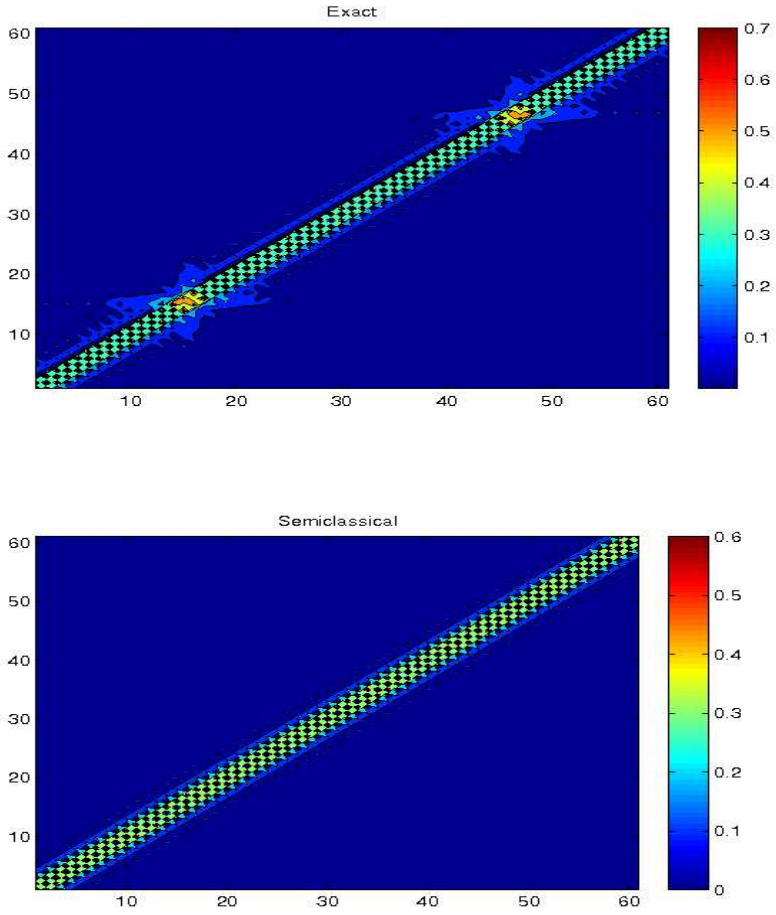

Figure 5.13: The modulus of the elements of the exact and the semiclassical reflection matrix. The x and y axes of the contour plot represents the indices i and j of the matrix.

5.7 The transfer operator

To summarise the previous sections, for a disc with mixed boundary conditions we have derived the exact shift operator (5.3.34) and the exact reflection operator (5.6.9), both computed in momentum space. In this section, we construct the exact and the semiclassical transfer operator. To form the exact transfer operator

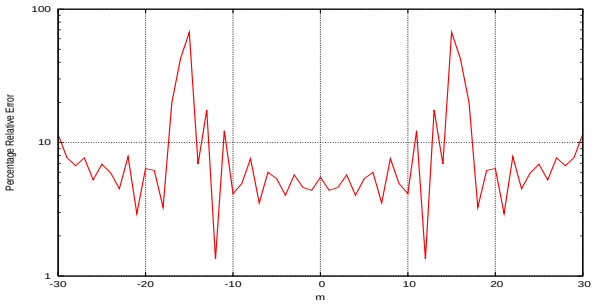

Figure 5.14: The percentage relative error between the modulus of the diagonal elements of the exact and semiclassical reflection matrix.

one needs to plug equation (5.6.10) into equation (5.3.33). One has,

$$\psi_- = \hat{R}\hat{S}_{\text{ex}}\psi_-, \tag{5.7.1}$$

$$(\hat{I} - \hat{T}_{\text{ex}})\psi_- = 0 \tag{5.7.2}$$

where $\hat{T}_{\text{ex}}$ is the exact transfer operator.

Regarding the semiclassical transfer operator, we construct two versions. The first denoted as $\hat{T}^{(1)}_{\text{sem}}$ is construed by combining the exact shift operator $\hat{R}$ and the semiclassical reflection operator as

$$\psi_- = \hat{R}\hat{S}_{\text{sem}}\psi_- = \hat{T}^{(1)}_{\text{sem}}\psi_-. \tag{5.7.3}$$

The second version $\hat{T}^{(2)}_{\text{sem}}$ is construed by combining the semiclassical shift operator $\hat{R}_0$ and the semiclassical transfer operator,

$$\psi_- = \hat{R}_0\hat{S}_{\text{sem}}\psi_- = \hat{T}^{(2)}_{\text{sem}}\psi_-. \tag{5.7.4}$$

We need to investigate the accuracy of the exact transfer operator $\hat{T}_{\text{ex}}$ against $\hat{T}^{(1)}_{\text{sem}}$ and $\hat{T}^{(2)}_{\text{ex}}$. Figure 5.15 shows the spectral determinant of the transfer operator method obtained exactly or semiclassically. It shows that the semiclassical transfer operator $\hat{T}^{(1)}_{\text{ex}}$ gives reasonably good results compared to $\hat{T}_{\text{ex}}$. However, by using $\hat{T}^{(2)}_{\text{ex}}$, the minima of the spectral determinant exhibit a shift from those of $\hat{T}_{\text{ex}}$ as shown in figure 5.15.

Ideally, we want to compare the results with BEM, next we present the BEM formulation for the disc.

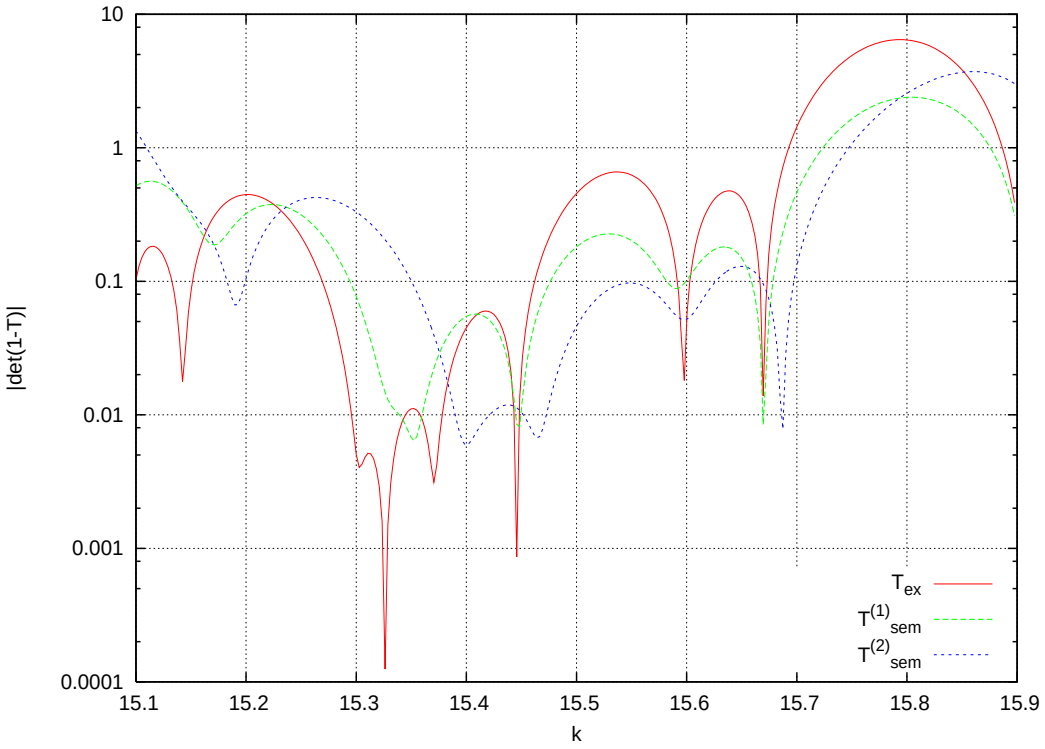

Figure 5.15: Semi-Log plot of the modulus of the spectral determinant $|\det(I-T)|$ calculated by the exact transfer operator and two versions of the semiclassical transfer operator $\hat{T}^{(1)}_{\rm sem}$ and $\hat{T}^{(2)}_{\rm sem}$.

5.8 BEM formulation for a disc with mixed boundary conditions

The object of this section is to present the BEM formulation for a disc with mixed boundary conditions described by equation (5.6.1). Similar to the derivation of the BIEs in §3.5.3, we obtain the following BIEs for a disc. That is,

$$\begin{aligned}&\int_{\Gamma_D}\left[G_0(q,\mathbf{r})\mu_D(q,\mathbf{r}')-\frac{\partial G_0(q,\mathbf{r})}{\partial n_q}\psi_N(q,\mathbf{r}')\right]\mathrm{d}q+\\&\int_{\Gamma_N}\left[G_0(q,\mathbf{r})\mu_D(q,\mathbf{r}')-\frac{\partial G_0(q,\mathbf{r})}{\partial n_q}\psi_N(q,\mathbf{r}')\right]\mathrm{d}q=-G_0(\mathbf{r},\mathbf{r}')+G(\mathbf{r},\mathbf{r}').\end{aligned}\tag{5.8.1}$$

where $\mathbf{r}$ and $\mathbf{r}'$ are respectively the interior and source points, and Γ_D and Γ_N refer to the Dirichlet and Neumann parts, respectively. The boundary functions

ψ and μ are the Green function and its normal derivative along the Dirichlet and Neumann parts, respectively. Applying the mixed boundary conditions described by equation (5.8.1) leads to,

$$\int_{\Gamma_D} G_0(q,\mathbf{r})\mu_D(q,\mathbf{r}')\mathrm{d}q - \int_{\Gamma_N} \frac{\partial G_0(q,\mathbf{r})}{\partial n_q}\psi_N(q,\mathbf{r}')\mathrm{d}q = -G_0(\mathbf{r},\mathbf{r}') + G(\mathbf{r},\mathbf{r}'). \tag{5.8.2}$$

We now need to take the interior point $\mathbf{r}$ to the boundary, therefore, we consider two cases.

Firstly, letting $\mathbf{r} \to \beta \in \Gamma_D$ in equation (5.8.2), leads to the following BIE,

$$\int_{\Gamma_D} G_0(q,\beta)\mu_D(q,\mathbf{r}')\mathrm{d}q - \int_{\Gamma_N} \frac{\partial G_0(q,\beta)}{\partial n_q}\psi_N(q,\mathbf{r}')\mathrm{d}q = -G_0(\beta,\mathbf{r}'), \tag{5.8.3}$$

Secondly, letting $\mathbf{r} \to \beta \in \Gamma_N$ in equation (5.8.2), leads to

$$\int_{\Gamma_D} G_0(q,\beta)\mu_D(q,\mathbf{r}')\mathrm{d}q - \int_{\Gamma_N} \left[\frac{\partial G_0(q,\beta)}{\partial n_q} - \frac{\delta(q-\beta)}{2}\right]\psi_N(q,\mathbf{r}')\mathrm{d}q = -G_0(\beta,\mathbf{r}'), \tag{5.8.4}$$

where the delta function $\delta(q-\beta)$ comes from applying the jump relation (3.8.1) for $\lim_{\mathbf{r}\to\beta} \frac{\partial G_0(q,\mathbf{r})}{\partial n_q}$.

Thus from the BIEs (5.8.3) and (5.8.4), we can construct the following system of equations,

$$\begin{bmatrix} G_0(q,\beta;k) & -\frac{\partial G_0(q,\beta;k)}{\partial n_q} \\ G_0(q,\beta;k) & -\left[\frac{\partial G_0(q,\beta;k)}{\partial n_q} - \frac{\delta(q-\beta)}{2}\right] \end{bmatrix} \begin{bmatrix} \mu_D \\ \psi_N \end{bmatrix} = \begin{bmatrix} -G_0(\beta,\mathbf{r}';k), & \beta \in \Gamma_D \\ -G_0(\beta,\mathbf{r}';k), & \beta \in \Gamma_N \end{bmatrix}. \tag{5.8.5}$$

This system can be written as,

$$K_{\mathrm{BEM}}\,\Phi = b$$

where K_{BEM} is the BEM kernel, $\Phi = \{\mu_D, \psi_N\}$ is the solution vector, and b is the source vector.

The kernels $G_0(q,\beta;k)$ and $\frac{\partial G_0(q,\beta;k)}{\partial n_q}$ are obtained for a disc as,

$$\begin{aligned} G_0(q,\beta;k) &= \frac{\imath k}{4} H_0^{(1)}(k\rho(q,\beta)) \\ &= \frac{\imath k}{4} H_0^{(1)}\left(2k\sin\left|\frac{q-\beta}{2}\right|\right), \end{aligned} \tag{5.8.6}$$

and,

$$\begin{aligned}\frac{\partial G_0(q,\beta;k)}{\partial n_q} &= \frac{-\imath k}{4}\cos\theta(q,\beta)H_1^{(1)}(k\rho(q,\beta)) \\ &= \frac{-\imath k}{4}\sin\left|\frac{q-\beta}{2}\right| H_1^{(1)}\left(2k\sin\left|\frac{q-\beta}{2}\right|\right), \qquad (5.8.7)\end{aligned}$$

where $\rho(q,\beta)$ and $\cos\theta(q,\beta)$ are calculated as depicted in figure 5.11.

After taking care of the weak singularity for the kernel in the first block of K_{BEM} matrix, the system (5.8.5) can be solved for the boundary functions μ and ψ along the Dirichlet and Neumann parts, respectively.

In §5.10, we will compare the spectral determinant obtained from the BEM against the transfer operator method. Before doing this, we examine the connection between the two methods next .

5.9 Connection between the BEM and the transfer operator methods

Prior to carrying out the comparison between the BEM and the transfer operator method, it is interesting to investigate the basis change from the BEM to the transfer operator formulation. A possible way to do so is to insert the Green operator formulations into the matrix K_{BEM}. Since the Green operators given by equations (5.3.15), (5.3.25) clearly separate the regular and singular parts, we need to rewrite the BIE (5.8.4) as,

$$\begin{aligned}\int_{\Gamma_D} G_0(q,\beta)\mu_D(q,\mathbf{r}')\mathrm{d}q - \int_{\Gamma_N}\left[\frac{\partial G_0(q,\beta)}{\partial n_q}+\frac{\delta(q-\beta)}{2}\right]\psi_N(q,\mathbf{r}')\mathrm{d}q = \\ \psi_N(\beta,\mathbf{r}') - G_0(\beta,\mathbf{r}'), \qquad \beta\in\Gamma_N,\end{aligned} \qquad (5.9.1)$$

where we separate the term coming from the jump conditions. Now the term between the square brackets in equation (5.9.1) can be replaced by,

$$\int_{\Gamma_N}\left[\frac{\partial G_0(q,\beta)}{\partial n_q}+\frac{\delta(q-\beta)}{2}\right]\psi_N(q,\mathbf{r}')\mathrm{d}q \to -\frac{1}{2}\frac{1}{\sqrt{\hat{p}_n}}\left(\hat{I}+\hat{R}_1\right)\sqrt{\hat{p}_n}\psi_N. \qquad (5.9.2)$$

The first integrand in the BIE (5.9.1) is not singular because $q \in \Gamma_D$, and $\beta \in \Gamma_N$, so we do not consider the singular part of $\hat{G}_0$, that is

$$\lim_{\mathbf{r}\to\beta} \int_{\Gamma_D} G_0(q,\mathbf{r})\mu_D(q,\mathbf{r}')\mathrm{d}q \to \frac{\imath}{2k}\frac{1}{\sqrt{\hat{p}_n}}\hat{R}_0\frac{1}{\sqrt{\hat{p}_n}}\mu_D. \tag{5.9.3}$$

Now let us analyse the BIE (5.8.3) in terms of the singularity. The first integrand in the BIE (5.8.3) has a weak singularity at $q = \beta \in \Gamma_D$, thus we need to consider the singular part of $\hat{G}_0$, that is

$$\lim_{\mathbf{r}\to\beta} \int_{\Gamma_D} G_0(q,\mathbf{r})\mu_D(q,\mathbf{r}')\mathrm{d}q \to \frac{\imath}{2k}\frac{1}{\sqrt{\hat{p}_n}}(\hat{I}+\hat{R}_0)\frac{1}{\sqrt{\hat{p}_n}}\mu_D. \tag{5.9.4}$$

The second integrand in the BIE (5.8.3) is not singular because $q \in \Gamma_D$, and $\beta \in \Gamma_N$, so we do not consider the singular part of $\hat{G}_1$, that is

$$\lim_{\mathbf{r}\to\beta} \int_{\Gamma_N} \frac{\partial G_0(q,\mathbf{r})}{\partial n_q}\mu_D(q,\mathbf{r}')\mathrm{d}q \to \frac{1}{2}\frac{1}{\sqrt{\hat{p}_n}}\hat{R}_1\sqrt{\hat{p}_n}\mu_D. \tag{5.9.5}$$

Therefore, using the relations (5.9.2), (5.9.3), (5.9.4) and (5.9.5), the BEM matrix K_{BEM} given by equation (5.8.5) can be transformed to the new basis as,

$$K_{\mathrm{BEM}} = \begin{bmatrix} \frac{\imath}{2k}\frac{1}{\sqrt{\hat{p}_n}}(\hat{I}+\hat{R}_0)\frac{1}{\sqrt{\hat{p}_n}} & \frac{1}{2}\frac{1}{\sqrt{\hat{p}_n}}\hat{R}_1\sqrt{\hat{p}_n} \\ \frac{\imath}{2k}\frac{1}{\sqrt{\hat{p}_n}}\hat{R}_0\frac{1}{\sqrt{\hat{p}_n}} & \frac{1}{2}\frac{1}{\sqrt{\hat{p}_n}}\left(\hat{I}+\hat{R}_1\right)\sqrt{\hat{p}_n} - \hat{I} \end{bmatrix}. \tag{5.9.6}$$

where we only consider the singular parts of the operators $\hat{G}_0$ and $\hat{G}_1$ on the diagonal blocks.

By doing some manipulations, the matrix (5.9.6) can be rearranged as,

$$K_{\mathrm{BEM}} = \left(\frac{1}{2}\right)\left(\frac{\imath}{2k}\right)\begin{bmatrix} \frac{1}{\sqrt{\hat{p}_n}} & 0 \\ 0 & -\frac{1}{\sqrt{\hat{p}_n}} \end{bmatrix}\begin{bmatrix} (\hat{I}+\hat{R}_0) & \hat{R}_1 \\ -\hat{R}_0 & (\hat{I}-\hat{R}_1) \end{bmatrix}\begin{bmatrix} \frac{1}{\sqrt{\hat{p}_n}} & 0 \\ 0 & \sqrt{\hat{p}_n} \end{bmatrix}$$

We now can compute the spectral determinant of K_{BEM} by doing the dicretization of the boundary. Thus, one obtains,

$$\begin{aligned} \det(K_{\mathrm{BEM}}) &= \left(\frac{1}{2}\right)^N\left(\frac{\imath}{2k}\right)^N \det\begin{bmatrix} \frac{1}{\sqrt{\hat{p}_n}} & 0 \\ 0 & -\frac{1}{\sqrt{\hat{p}_n}} \end{bmatrix} \\ &\times \det\left\{\begin{bmatrix} \hat{I} & 0 \\ 0 & \hat{I} \end{bmatrix} - \begin{bmatrix} -\hat{R}_0 & -\hat{R}_1 \\ \hat{R}_0 & \hat{R}_1 \end{bmatrix}\right\}\det\begin{bmatrix} \frac{1}{\sqrt{\hat{p}_n}} & 0 \\ 0 & \sqrt{\hat{p}_n} \end{bmatrix}, \end{aligned}$$

where N is the number of boundary points, the power of N comes from doing the discretization. The minus sign in front of the blocks on the first row of the matrix of $\hat{R}$ is attributed to DBCs, whereas the plus sign in front of the blocks on the second row corresponds to NBCs. This means that the prescribed boundary condition are incorporated, we can form the transfer operator from such matrix as,

$$\det(K_{\text{BEM}}) = \left(\frac{1}{2}\right)^N \left(\frac{\imath}{2k}\right)^N \det\left(\frac{-1}{\hat{p}_n}\right) \det \begin{bmatrix} (\hat{I}+\hat{T}_{DD}) & \hat{T}_{DN} \\ -\hat{T}_{ND} & (\hat{I}-\hat{T}_{NN}) \end{bmatrix}.$$

where $\hat{T}_{DD} = -\hat{R}_0$, $\hat{T}_{DN} = -\hat{R}_1$, $\hat{T}_{NN} = \hat{R}_1$ and $\hat{T}_{ND} = \hat{R}_0$, where the subscripts D and N refers to the Dirichlet and Newmann boundary conditions, respectively. Therefore, we obtain a relation between the secular equation obtained from the BEM and the transfer operator as,

$$\det(K_{\text{BEM}}) = f(k,N)\det(I-T) \tag{5.9.7}$$

where $f(k,N)$ is a function of number of boundary points and the wavenumber k, the operator $\sqrt{\hat{p}_n}$ depends on such quantities as well.

Equation (5.9.7) shows that the scale of the BEM determinant should be different from the scale of the determinant obtained by the transfer operator method. Also $\det(K_{\text{BEM}})$ should increase by increasing the number of the boundary points. However, this change of basis should not affect the spectrum as shown next.

5.10 Comparison of the spectral determinant of the transfer operator and the BEM

In this section we carry out a comparison of the spectral determinant obtained from the exact transfer operator and the BEM methods.

The lower plot of figure 5.16 shows the spectral determinant of the BEM, whereas the upper plot in figure 5.16 shows the spectral determinant of the exact transfer

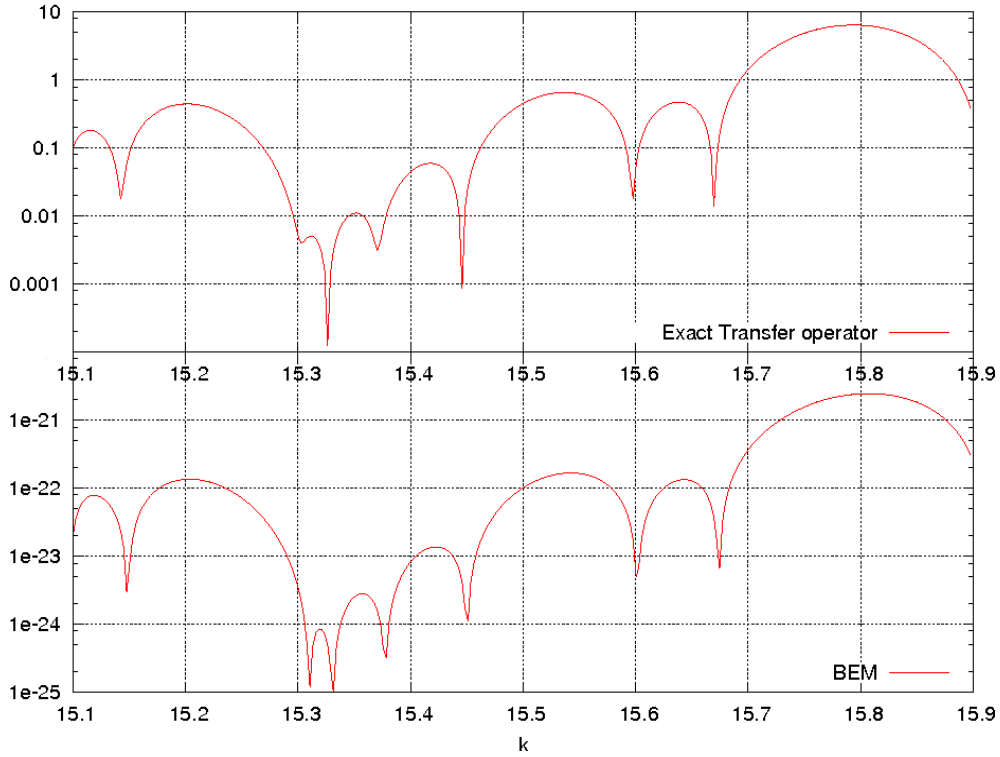

Figure 5.16: Semi-Log plot of the modulus of the determinants $|\det(I-T)|$ calculated by the exact and semiclassical transfer operator and the BEM $\det(K_{\mathrm{BEM}})$.

operator methods. The exact transfer operator shows sharp minima same as the BEM at similar positions, however the minima of the spectral determinant computed using the exact transfer operator is worse than the corresponding minima of the BEM around $k = 15.3$ as shown in figure 5.16. This behaviour of the transfer operator can be attributed to the fact that the transfer operator is not fully convergent due to the singularity of the operator $\frac{1}{\sqrt{p_n}}$ in momentum space.

Another thing to observe is that the spectral determinant of the BEM and the transfer operator have different scale. This is attributed to the different basis of each methods as it has been addressed by equation (5.9.7) in the previous section.

So far we have formulated the transfer operator for an eigenvalue problem ob-

taining the spectral determinant. Next we will consider the formulation for the transfer operator where the physical solution is the Green function.

5.11 Transfer operator formulation for the Green function

In §5.3 we have formulated the transfer operator for an eigenvalue problem where the physical solution is the eigenfunction. To be able to recover the Green function we need to consider the source term G^{free} in the BIE (3.5.6) given as,

$$\psi - G^{\text{free}} = \hat{G}_0\mu - \hat{G}_1\psi. \tag{5.11.1}$$

The free-space Green function G^{free} forms a vector for fixed source point and the other argument being a boundary point, whereas the Green operator $\hat{G}_0$ obtained by equation (5.3.15) forms a matrix where both of its arguments are boundary points. By including the source in equation (5.11.1), ψ will be the Green function of the system on the boundary.

Therefore in this section we consider the formulation of the transfer operator where the physical solution is the Green function or its normal derivative depending on the type of the boundary conditions. To do so, we incorporate the Green operators $\hat{G}_0$ and $\hat{G}_1$ obtained by equations (5.3.15), (5.3.25) into the BIE (5.11.1) along with the decomposition relations (5.3.30) and (5.3.31) as,

$$\begin{aligned}\frac{1}{\sqrt{\hat{p}_n}}(\psi_- + \psi_+) - G^{\text{free}} = \frac{\imath}{2k}\frac{1}{\sqrt{\hat{p}_n}}(\hat{I} + \hat{R}_0)\frac{1}{\sqrt{\hat{p}_n}}\cdot \imath k\sqrt{\hat{p}_n}(\psi_- - \psi_+) \\ +\frac{1}{2}\frac{1}{\sqrt{\hat{p}_n}}(\hat{I} + \hat{R}_1)\sqrt{\hat{p}_n}\frac{1}{\sqrt{\hat{p}_n}}(\psi_- + \psi_+).\end{aligned} \tag{5.11.2}$$

Doing some manipulation, then multiplying equation (5.11.2) from the left by the operator $\sqrt{\hat{p}_n}$, one has

$$\left[(\hat{I} + \hat{R}_0) + (\hat{I} - \hat{R}_1)\right]\psi_- = (\hat{R}_0 + \hat{R}_1)\psi_+ + 2\sqrt{\hat{p}_n}G^{\text{free}}. \tag{5.11.3}$$

We now need to multiply equation (5.11.3) from the left by the following operator

$$\left[(\hat{I} + \hat{R}_0) + (\hat{I} - \hat{R}_1)\right]^{-1}.$$

One arrives at the following equation,

$$\begin{aligned}\psi_- &= \left[(\hat{I}+\hat{R}_0)+(\hat{I}-\hat{R}_1)\right]^{-1}(\hat{R}_0+\hat{R}_1)\psi_+ \\ &+ 2\left[(\hat{I}+\hat{R}_0)+(\hat{I}-\hat{R}_1)\right]^{-1}\sqrt{\hat{p}_n}G^{\text{free}} \\ &= \hat{R}\psi_+ + 2\left[(\hat{I}+\hat{R}_0)+(\hat{I}-\hat{R}_1)\right]^{-1}\sqrt{\hat{p}_n}G^{\text{free}}, \qquad (5.11.4)\end{aligned}$$

where $\hat{R}$ is the exact shift operator is obtained as

$$\hat{R} = \left[(\hat{I}+\hat{R}_0)+(\hat{I}-\hat{R}_1)\right]^{-1}(\hat{R}_0+\hat{R}_1) \qquad (5.11.5)$$

Now, we combine the shift and the reflection operator to form the transfer operator by inserting equation (5.6.10) into equation (5.11.4). One has

$$\psi_- = \hat{R}\hat{S}\psi_- + 2\left[(\hat{I}+\hat{R}_0)+(\hat{I}-\hat{R}_1)\right]^{-1}\sqrt{\hat{p}_n}G^{\text{free}}. \qquad (5.11.6)$$

This equation can be written as,

$$(\hat{I}-\hat{T})\psi_- = 2\left[(\hat{I}+\hat{R}_0)+(\hat{I}-\hat{R}_1)\right]^{-1}\sqrt{\hat{p}_n}G^{\text{free}}, \qquad (5.11.7)$$

where $\hat{T}$ is the transfer operator.

The free-space Green function G^{free} is given in momentum space as,

$$(\tilde{G})_m^{\text{free}} = \frac{\imath}{4}H_m^{(1)}(kr)J_m(kr')e^{\imath m\phi'}. \qquad (5.11.8)$$

where (r',ϕ') are the polar coordinates of the source point $\mathbf{r}'$, and r is the radius of the disc.

To carry out a comparison between the exact and the semiclassical transfer operator, we compute the scattering amplitudes ψ_- and ψ_+ by using both approaches. To do so, one needs to solve equation (5.11.7) for ψ_-, then plug ψ_- into the following equation to obtain ψ_+ as,

$$\psi_+ = \hat{S}\psi_-,$$

where $\hat{S}$ is the reflection operator either calculated exactly or semiclassically. Next we present a discussion of the obtained results.

5.12 Results and discussion

In this section, we show a comparison between the results obtained from the exact and the semiclassical transfer operator. The exact transfer operator $\hat{T}_{\text{ex}}$ is obtained using the exact reflection operator given by (5.6.9) and the exact shift operator $\hat{R}$, whereas the semiclassical transfer operator $\hat{T}_{\text{sem}}$ is obtained using the semiclassical reflection operator given by equation (5.6.16) and the semiclassical shift operator $\hat{R}_0$.

We carry out the comparison for the scattering amplitudes ψ_- and ψ_+ obtained either by using the exact or the semiclassical transfer operator. Using the fact that for real values of the wavenumber, the boundary functions ψ and μ are real functions as has been established in §3.6. So, the accuracy of the scattering amplitudes can be checked using the decomposition relations (5.3.30) and (5.3.31) which relate the scattering amplitudes to the boundary functions. Also, to check the behaviour of the exact and the semiclassical scattering amplitudes at the discontinuity of the boundary conditions. We extract the contribution coming from the commutators (5.6.11) by considering the quantities $(\psi_+ + \psi_-)$ and $(\psi_+ - \psi_-)$ along the Dirichlet and Neumann parts, respectively, using the exact and the semiclassical transfer operator.

For all the calculations in this section, we set the length of the Dirichlet and Neumann parts both equal to π as depicted in figure 5.12. Thus, in our discussion below we will refer to the points $(s = 0, \pi)$ as the discontinuity points. The source point is located at the symmetry line $y = 0$, $r' = (0, -0.5)$. Arbitrarily, we chose the value of the wavenumber to be $k = 50.1$. For the computations of the discrete Fourier transform, we truncate the series to a finite sum, that is, the Fourier basis runs from $m = -N$ to $m = N$, where we set $N = 380$.

At first let us discuss the scale of the real and imaginary parts of the scattering amplitudes ψ_- and ψ_+ shown respectively in figures 5.17 and 5.18. These scattering amplitudes are obtained by both the exact and the semiclassical

transfer operator. In essence, the fact that the boundary functions ψ and μ are real functions should be built into the scattering amplitudes ψ_- and ψ_+ through the decomposition relations (5.3.30) and (5.3.31). It is understood from the decomposition relation (5.3.30) for ψ that ψ_- and ψ_+ should be dominantly real along the Neumann part as shown in figure 5.17. Since we have the complex number $\imath$ in front of the RHS of equation (5.3.31), thus ψ_- and ψ_+ should be dominantly imaginary along the Dirichlet part as shown in figure 5.18.

Another thing to check is the boundary conditions described by equation (5.6.1). As we have already mentioned in the previous paragraph, the real parts of the scattering amplitudes $\Re(\psi_-)$ and $\Re(\psi_+)$ is the measure of the error along the Dirichlet part, whereas their imaginary part $\Im(\psi_-)$ and $\Im(\psi_+)$ is the measure of the error along the Neumann part. We observe that by using the exact transfer operator $\Re(\psi_-)$ and $\Re(\psi_+)$ along Dirichlet part for $s \in (0, \pi]$ are smaller than those of the semiclassical transfer operator as shown in figure 5.17. By using the exact transfer operator $\Im(\psi_-)$ and $\Im(\psi_+)$ along Neumann part for $s \in (\pi, 2\pi]$ are smaller than those of the semiclassical transfer operator as shown in figure 5.18. These results verifies that the exact transfer operator gives more accurate results than the semiclassical transfer operator.

Another feature to observe is that by looking at figure 5.18, one can see that the real and imaginary part of ψ_- is always smooth along the whole boundary including the discontinuity points either by using the exact or the semiclassical transfer operator. However this is not the case with ψ_+. By using the exact transfer operator, ψ_+ has spike at the discontinuity points as shown in the lower plot of figure 5.18, whereas it looks quite smooth when using the semiclassical transfer operator. This gives an indication that the exact transfer operator incorporates diffraction effects coming from the discontinuity of boundary conditions, whereas the semiclassical one neglects them.

The reason for the different behaviours of ψ_+ and ψ_- is that the outgoing wave ψ_+ incorporates any effects coming from the boundary such as the

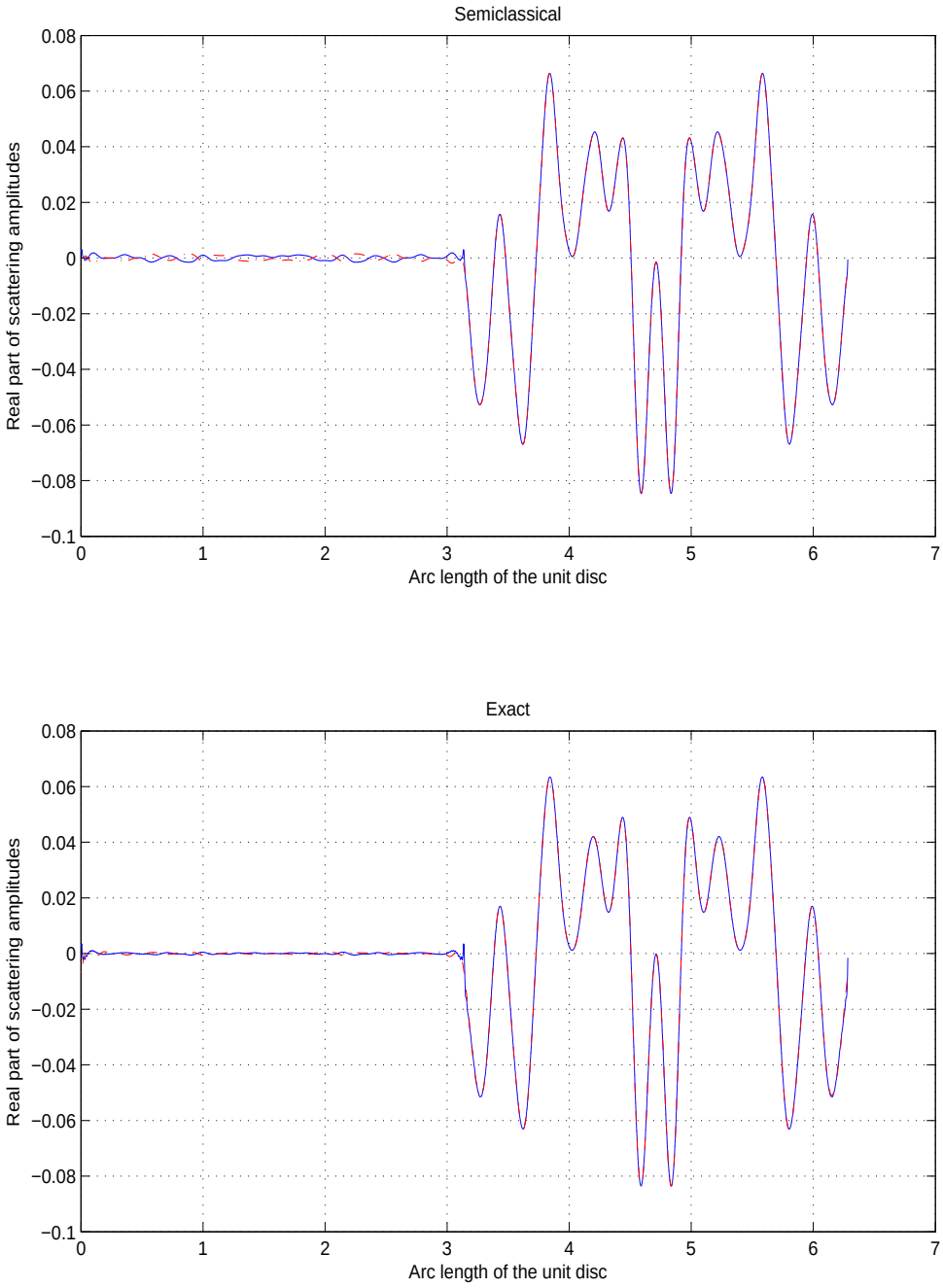

Figure 5.17: The blue and the red line respectively represent the real part of ψ_+ and ψ_- calculated from the semiclassical and the exact transfer operator.

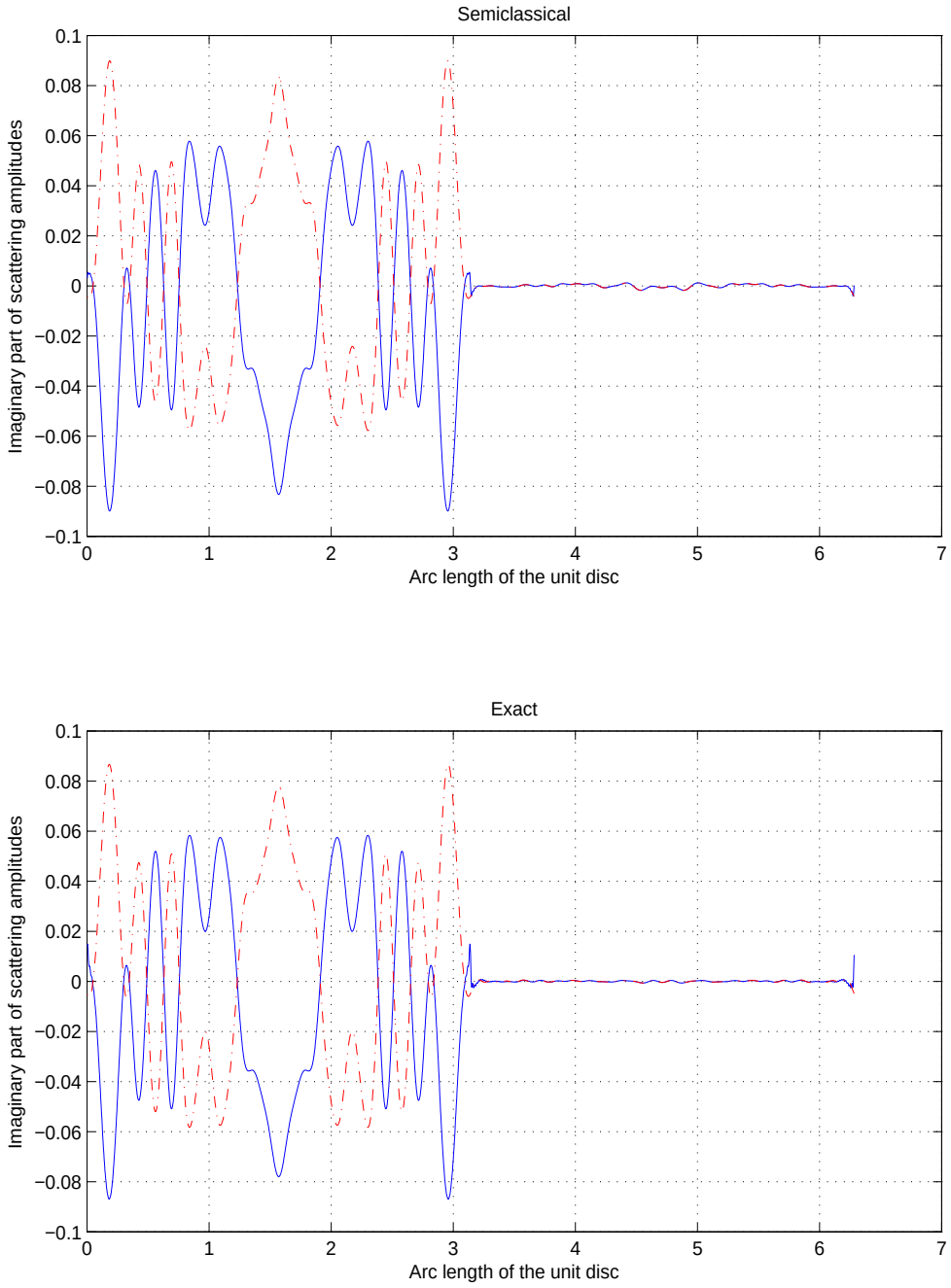

Figure 5.18: The solid and the dashed line respectively represent the imaginary part of ψ_+ and ψ_- calculated from the semiclassical and the exact transfer operator.

discontinuity of the boundary conditions. The sharpness of ψ_+ at the discontinuity points is attributed to the resulting diffraction effects at the discontinuity points. Physically, once an initial incoming wave hits the boundary at the discontinuity points, the emerging diffractive wave appears as a point like distributional source in ψ_+.

In Appendix E, we show that the commutators have localised diffraction effects at the discontinuity points and an oscillatory contribution around such points. To compare the semiclassical transfer operator against the exact in terms of incorporating boundary effects. We extract the commutators contribution to ψ_+ by considering the following quantities

$$[\psi_+(s) + \psi_-(s)], \qquad s \in \Gamma_D \tag{5.12.1}$$

and

$$[\psi_+(s) - \psi_-(s)], \qquad s \in \Gamma_N, \tag{5.12.2}$$

where Γ_D and Γ_N refer to the Dirichlet and Neumann parts, respectively. Using the exact and the semiclassical transfer operator. Figure 5.19 shows the imaginary part of these quantities (5.12.1) and (5.12.2), it can be seen at the discontinuity points, the commutators have localised contribution which looks like sinc function as zoomed in the little window in figure 5.19 which is the Fourier transform of a delta function in a finite basis. This could give an indication of the existence of distributional terms in diffraction effects. Such effects decay away from the discontinuity points. We argue that truncating the Fourier basis to a finite size is responsible for the ringing behaviour at the discontinuity points. However the semiclassical approximation does not show this behaviour, because it neglects the commutator contributions.

To conclude, it was shown that the exact transfer operator gives more accurate results than the semiclassical in terms of incorporating the boundary conditions and diffraction effects at the discontinuity of boundary conditions. After we check the accuracy of the scattering amplitudes ψ_+ and ψ_-, and verify

our expectation of their behaviour, we will use them to recover the boundary function ψ and μ as shown next.

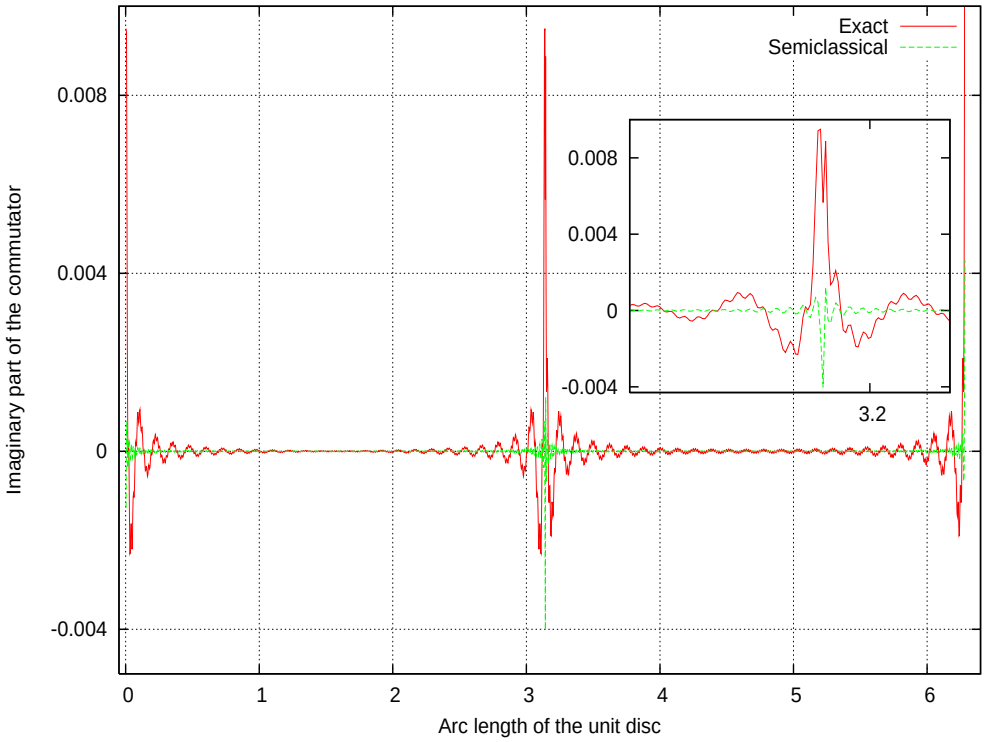

Figure 5.19: The imaginary part of the quantities $(\psi_+ + \psi_-)$ and $(\psi_+ - \psi_-)$ along the Dirichlet-part $(0, \pi]$ or Neumann-part $(\pi, 2\pi]$, respectively.

5.13 Recovering the Green function from the transfer operator

In this section we recover the Green function ψ or its normal derivative μ along the Neumann or Dirichlet part, respectively, from the transfer operator method. To obtain these boundary functions, one needs to plug the scattering amplitudes ψ_- and ψ_+ in the decomposition relations (5.3.30) and (5.3.31), respectively. The scattering amplitudes ψ_+, and ψ_- are obtained in momentum space, and so

are the boundary functions ψ and μ. We then need to take their inverse Fourier transform to get them in position space by using equation (5.3.11). We compute the boundary function μ using the exact and the semiclassical transfer operator, then we compare the attainable accuracy of each operator. Figure 5.20 shows that the boundary functions μ has spike at the discontinuity points whereas ψ looks smooth at the discontinuity points as shown in figure 5.22. This indicates the fact that the exact transfer operator captures the diffraction effects, whereas the semiclassical one neglects them.

Since for real values of k, the boundary functions ψ and μ should be real, so the imaginary part is the measure of the error of the boundary functions ψ and μ as has been addressed in §3.6. According to this measure of error figures 5.21 and 5.23 show that the exact transfer operator gives more accurate results than the semiclassical transfer operator. The symmetry in the plots of the boundary functions μ at $\frac{\pi}{2}$, and ψ at $\frac{3\pi}{2}$ is due to the fact that the source point is located at the symmetry line $y = 0$, $r' = (0, -0.5)$.
For a rigorous check of our results, we will compare our results with the BEM as shown next.

5.14 Comparison between the exact transfer operator and the BEM

In this section, we carry out a comparison between the exact transfer operator and the BEM in terms of the accuracy of the Green function or its normal derivative μ along the Neumann and Dirichlet parts, respectively. The results shown here are for the value of the wavenumber $k = 50.1$, and the length of Dirichlet and Neumann part both equal to π. Thus, in our discussion below we will refer to the points $(s = 0, \pi)$ as the discontinuity points. For the BEM computations we used 761 boundary elements and for the transfer operator the size of Fourier basis from $m = -380$ to $m = 380$, where m is the index of Fourier basis. That

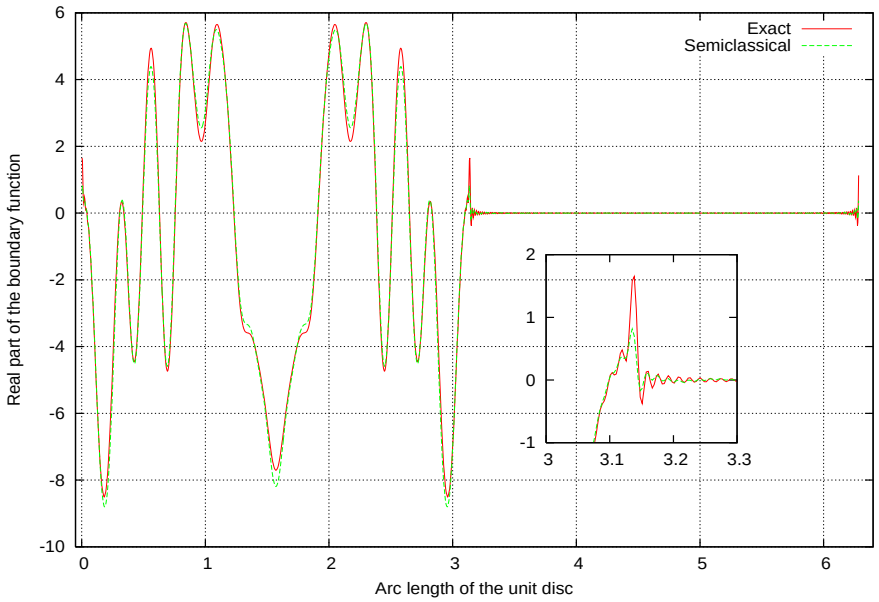

Figure 5.20: $\Re(\mu)$ recovered from ψ_+, and ψ_- using the exact and semiclassical transfer operator.

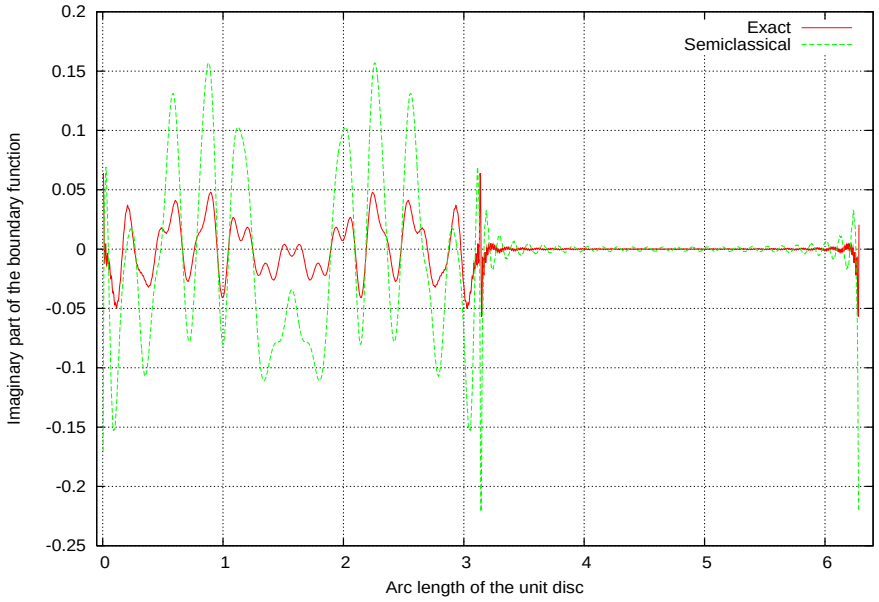

Figure 5.21: $\Im(\mu)$ recovered from ψ_+, and ψ_- using the exact and semiclassical transfer operator.

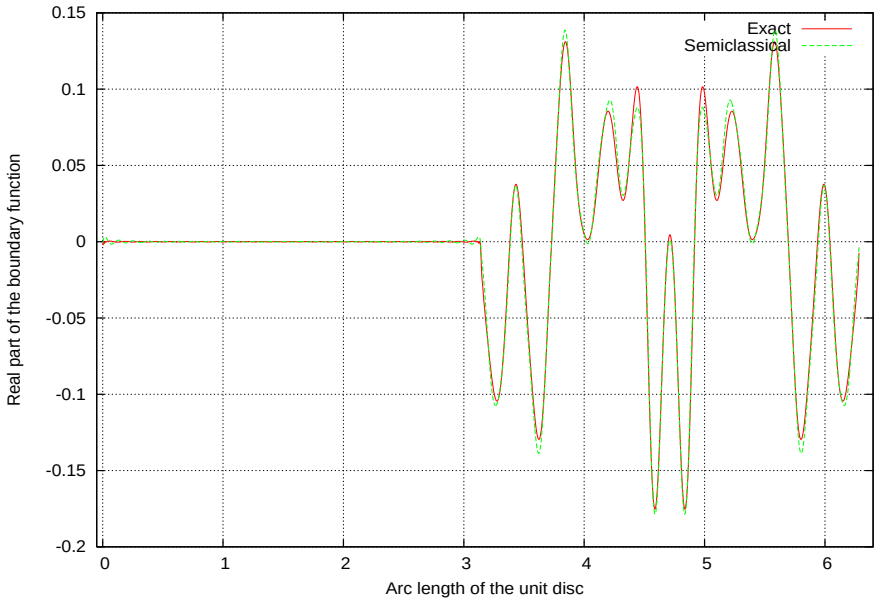

Figure 5.22: $\Re(\psi)$ recovered from ψ_+, and ψ_- using the exact and semiclassical transfer operator.

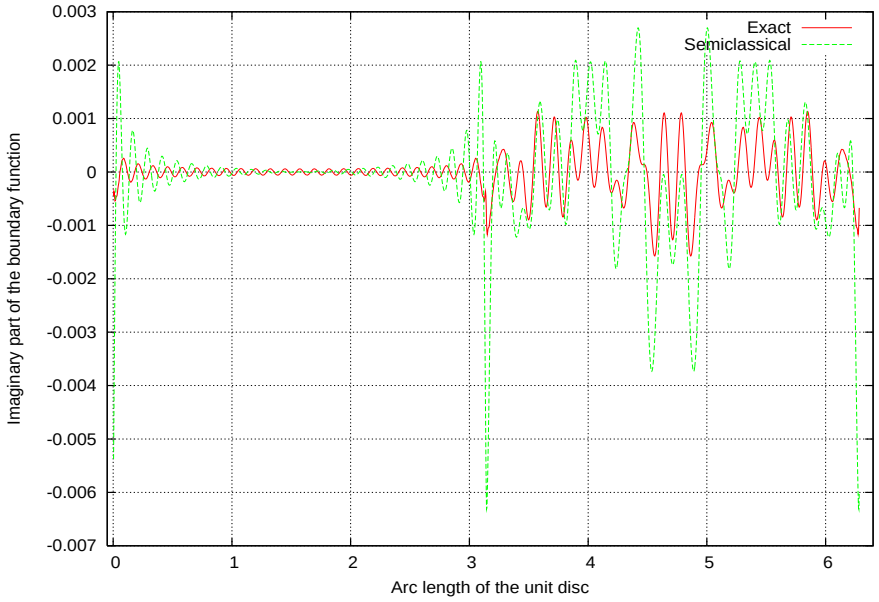

Figure 5.23: $\Im(\psi)$ recovered from ψ_+, and ψ_- using the exact and semiclassical transfer operator.

is, we have used the same matrix size for both methods.

Since the scale of the Green function along the Newmann part is relatively smaller than the scale of its normal derivative μ along the Dirichlet part, we plot each quantity separately. Figure 5.24 shows the real part of μ along Dirichlet part computed by the BEM and the exact transfer operator using the same matrix size. We observe that both approaches behave exactly the same at the discontinuity points ($s = 0, \pi$). However, overall there is a small deviation between the two results. This is due to the use of finite basis, and the different basis representations of each method as has been discussed in §5.9.

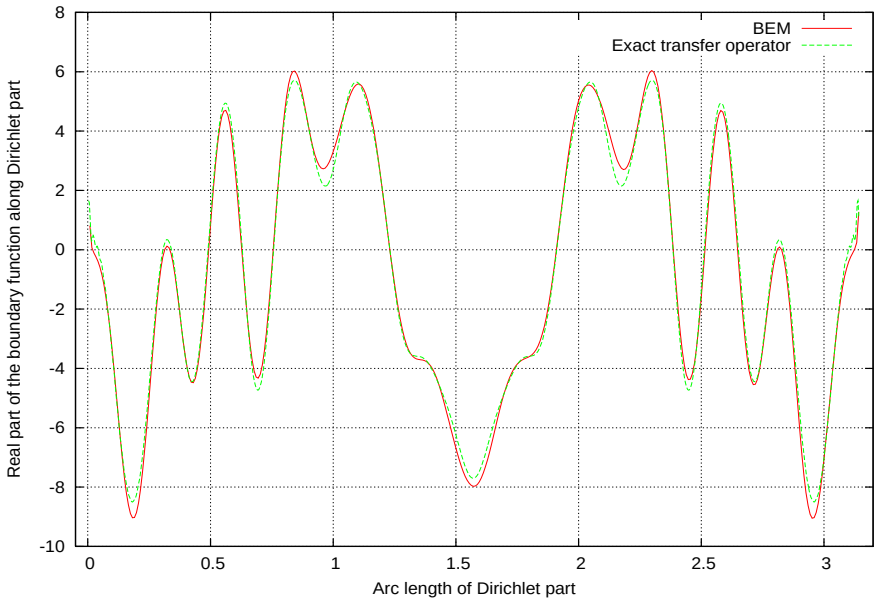

Figure 5.24: $\Re(\mu)$ computed from the BEM and the exact transfer operator.

To compare the attainable accuracy of both methods, we look at the imaginary part of the boundary functions which is the measure of the error as has been established in §3.6. Figure 5.25 shows that both methods have comparable measure of error.

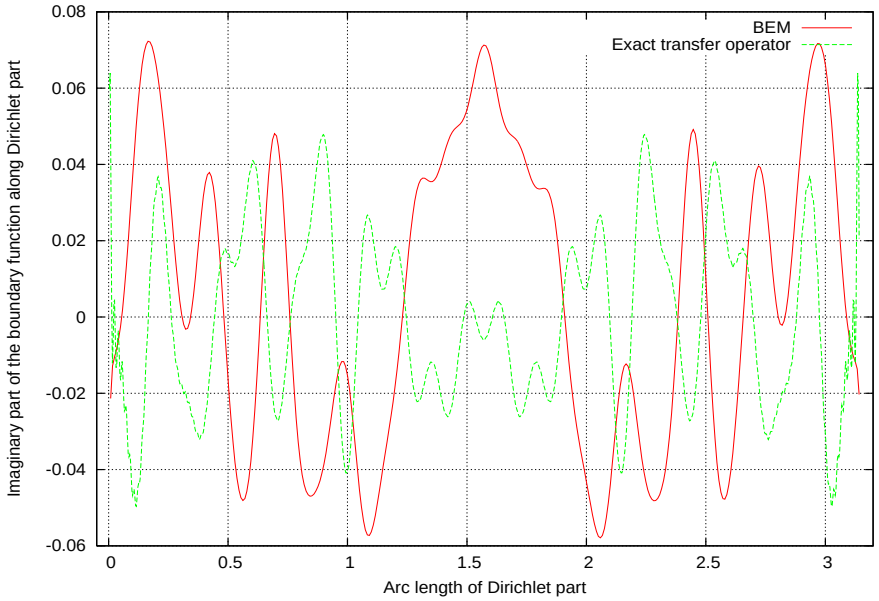

Figure 5.25: $\Im(\mu)$ computed from the BEM and the exact transfer operator.

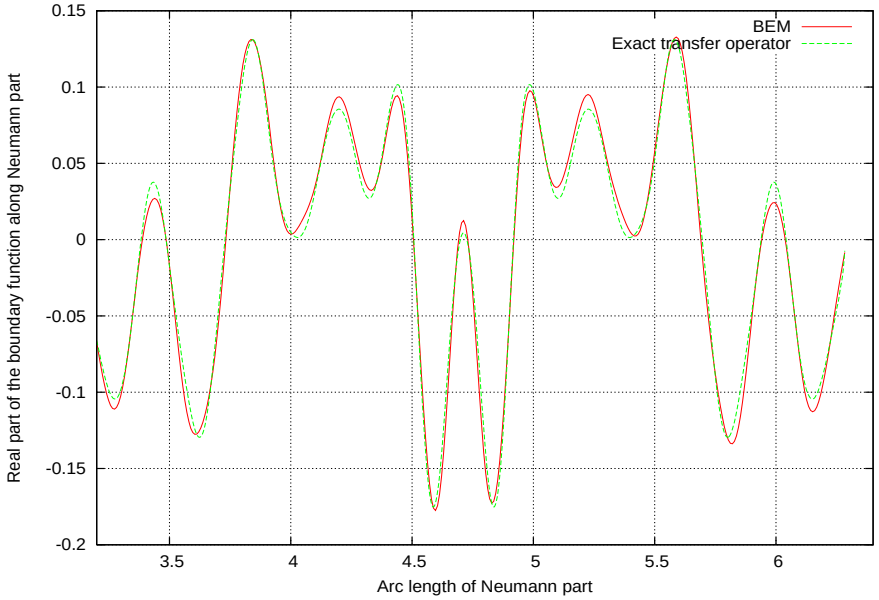

Figure 5.26: $\Re(\psi)$ computed from the BEM and the exact transfer operator.

5.15 Conclusions

In this chapter we have introduced a new formulation of the exact transfer operator where the physical solution is the eigenfunctions or the Green function. We point out any possible semiclassical approximations can be made at each step of the derivation. We demonstrated this technique for a cavity of circular geometry with boundary conditions changing discontinuously across the boundary. We found that the obtained transfer operator incorporates diffraction effects at the discontinuity of the boundary conditions. From the exact approach we show how the semiclassical transfer operator can be obtained, then we demonstrate a comparison between the exact and the semiclassical results. For a rigorous check, we carry out a comparison with the BEM showing good agreement between both approaches.

Chapter 6

Transfer operator for coupled cavities

6.1 Introduction

Based on the ideas that have been developed in the previous chapter for the transfer operator of a single cavity of circular shape with discontinuous boundary conditions, we derive an analogous approach for coupled cavities of different material properties. The disc problem has similar features to the coupled-cavity configuration in the sense that the discontinuity in the material properties at finite interfaces leads to discontinuities in the boundary conditions. We set up the coupled cavities as two coupled polygons with an interface of finite length along the common segment between both polygons. Hence the end points of the interface will be corners. The behaviour of the solution at the discontinuity in the boundary conditions of a disc is analogous to the behaviour of the solution at the end points for the interfaces between the coupled cavities. Both types of discontinuities appear in a distance smaller than the wavelength, thus they develop diffraction effects. As in Chapter 5, the transfer operator is derived by combining two operators, the first one is obtained from the relevant BIEs and is

called the shift operator. The second operator is obtained from the prescribed boundary conditions and is called the scattering operator.

The derivation of the shift operator involves two levels of approximations, the first one is that the derivation of the singular part of the Green operator $\hat{G}_0$ presented in §5.3 is built on the assumption that the boundary is locally flat, thus it does not account for the corners of irregular geometries. The second level of approximation is using the asymptotic expansion of the boundary kernels.

For the coupled cavities following the same steps of deriving the scattering operator as in §5.6.1 leads to a complicated expression for the reflection and transmission coefficients. Thus to facilitate the derivation, we proceed semiclassically by neglecting the contributions from the commutators (5.6.11).
Having obtained both the shift and the scattering operators semiclassically, we combine them to form the semiclassical transfer operator.

Our formulation of the transfer operator is done in such a way that it can in principle be made exact, and it is clear where the semiclassical approximations are made at each stage of the derivation. This makes our approach is different from the approach considered by Blümel et al. [117], and Prange et al. [118]. They present the semiclassical transfer operator for the Schrödinger equation in two dimensions with discontinuous step potential. They consider a half-plane interface separating two media of different material properties. That is, they ignore the contribution coming from the boundary and consider only an infinite interface at $x = 0$. Since they consider the problem in free space (disregarding the boundary of the domain), they approximate the Green function of the system by the free-space Green function on infinite interface. Then they take its Fourier transform in the y-direction and do the resulting integral by the stationary phase approximations yielding the reflection and transmission coefficients. Our approach is more suitable to accommodate complex built-up structure with multiple interfaces.
To approach the treatment of the coupled cavities, first we present a one-dimensional

problem which has a discontinuous change of material properties.

6.2 Formulation of the transfer operator for a one-dimensional problem

The objective for this section is to develop some ideas in one dimension that will be generalised for the treatment of the coupled cavities in two dimensions. We present the formulation of the transfer operator for a one-dimensional beam which has an abrupt change of material properties at the discontinuity point $x = 0$. First we proceed with the derivation of the shift operator. We decompose the beam at the point $x = 0$ into a left part $[-a, 0]$ and right part $[0, b]$ as depicted in figure 6.1. For the left and right part of the beam we have the wavenumber values k_1 and k_2, respectively.

Following the same steps of the one-dimensional problem as presented in §5.2,

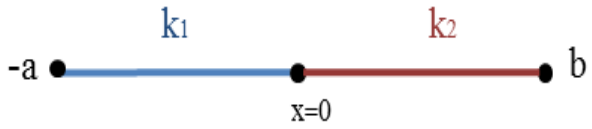

Figure 6.1: One-dimensional beam of length $a + b$ with discontinuity of material properties at $x = 0$.

one obtains the shift operator for the left-part of the beam as,

$$\psi_- = \hat{R}^L \psi_+, \tag{6.2.1}$$

where $\hat{R}^L$ is called the shift operator, and ψ_- and ψ_+ are respectively the incoming and the outgoing waves for the left part of the beam. Hereafter, they are called the scattering amplitudes. Similarly, we derive the shift operator for the right part of the beam as,

$$\phi_- = \hat{R}^R \phi_+. \tag{6.2.2}$$

where ϕ_- and ϕ_+ are respectively the incoming and the outgoing waves for the right part of the beam.

Now we can combine equation (6.2.1) with equation (6.2.2), to obtains

$$\begin{bmatrix} \psi_- \\ \phi_- \end{bmatrix} = \begin{bmatrix} \hat{R}^L & 0 \\ 0 & \hat{R}^R \end{bmatrix} \begin{bmatrix} \psi_+ \\ \phi_+ \end{bmatrix}. \tag{6.2.3}$$

Using the partition of the boundary $\partial\Omega = \{a, 0, b\}$, equation (6.2.3) can be written as,

$$\begin{bmatrix} \psi_-^{(a)} \\ \psi_-^{(0)} \\ \phi_-^{(0)} \\ \phi_-^{(b)} \end{bmatrix} = \begin{bmatrix} \hat{R}^L_{aa} & \hat{R}^L_{a0} & 0 & 0 \\ \hat{R}^L_{0a} & \hat{R}^L_{00} & 0 & 0 \\ 0 & 0 & \hat{R}^R_{00} & \hat{R}^R_{0b} \\ 0 & 0 & \hat{R}^R_{b0} & \hat{R}^R_{bb} \end{bmatrix} \begin{bmatrix} \psi_+^{(a)} \\ \psi_+^{(0)} \\ \phi_+^{(0)} \\ \phi_+^{(b)} \end{bmatrix}, \tag{6.2.4}$$

where $\psi_-^{(a)}$ and $\psi_+^{(a)}$ respectively denotes the incoming and outgoing waves at the end point a, and similarly $\phi_-^{(b)}$ and $\phi_+^{(b)}$ at the end point b. The notations $\psi_-^{(0)}$ and $\psi_+^{(0)}$ respectively denotes the incoming and outgoing waves at the left side of the discontinuity point $x = 0$, and similarly $\phi_-^{(0)}$ and $\phi_+^{(0)}$ at the right side of the discontinuity point $x = 0$.

This equation can be written in a compact form as,

$$\Psi_- = \hat{R}\Psi_+, \tag{6.2.5}$$

where $\hat{R}$ is the shift operator for the whole beam, and $\Psi_- = \{\psi_-^{(a)}, \psi_-^{(0)}, \phi_-^{(0)}, \phi_-^{(b)}\}$, and similarly for the outgoing wave vector Ψ_+.

Since the shift operator $\hat{R}$ does not know anything about the prescribed boundary conditions, one needs to construct another operator which incorporates such conditions. Such a map can be derived from the knowledge of the boundary conditions.

Similarly to the treatment in §5.1, one needs to decompose the wave-functions in terms of plane waves as,

$$\psi = A(\psi_- + \psi_+), \tag{6.2.6}$$

$$\phi = B(\phi_- + \phi_+). \tag{6.2.7}$$

The constants $A = \sqrt{\frac{\rho_1}{k_1}}$ and $B = \sqrt{\frac{\rho_2}{k_2}}$ are chosen to guarantee the conservation of the energy flux across the discontinuity point, that is, the obtained operator will be unitary. The constants ρ_1 and ρ_2 are respectively the material densities in the left and the right side of the beam and they are related by equation (4.2.1). We begin by incorporating the boundary condition at the end points a, b. We set Dirichlet boundary conditions at these points, that is,

$$\psi(a) = \phi(b) = 0. \tag{6.2.8}$$

Inserting the boundary conditions (6.2.8) into equation (6.2.6) and equation (6.2.7), leads to

$$\psi_+^{(a)} = -\psi_-^{(a)}, \tag{6.2.9}$$

and

$$\phi_+^{(b)} = -\phi_-^{(b)}, \tag{6.2.10}$$

For domains with discontinuous changes of material properties, one also needs to incorporate the following continuity and equilibrium conditions across the discontinuity point $x = 0$ given as

$$\psi^{(0)}(x) = \phi^{(0)}(x), \qquad \rho_2 \frac{\partial \psi^{(0)}(x)}{\partial n} = -\rho_1 \frac{\partial \phi^{(0)}(x)}{\partial n}. \tag{6.2.11}$$

Inserting equations (6.2.6) and (6.2.7) into (6.2.11), and using the fact that the incoming wave are just $(e^{\imath kx})$ and outgoing waves are $(e^{-\imath kx})$ to and from the vertex b, respectively. One needs to consider the opposite sign for the right end of the beam. After some lines of algebra, the following relation between the incoming and outgoing waves from both sides of the discontinuity point is obtained,

$$\begin{bmatrix} \psi_+^{(0)} \\ \phi_+^{(0)} \end{bmatrix} = \begin{bmatrix} \left(\frac{\alpha-\beta}{\alpha+\beta}\right) & \frac{2B\beta}{A(\alpha+\beta)} \\ \frac{2A\alpha}{B(\alpha+\beta)} & -\left(\frac{\alpha-\beta}{\alpha+\beta}\right) \end{bmatrix} \begin{bmatrix} \psi_-^{(0)} \\ \phi_-^{(0)} \end{bmatrix}, \tag{6.2.12}$$

where we used the notations $\alpha = \rho_2 k_1$, $\beta = \rho_1 k_2$.

Combining the relations obtained from the external and internal boundary con-

ditions given by equations (6.2.9), (6.2.10) and (6.2.12), one obtains

$$\begin{bmatrix} \psi_+^{(a)} \\ \psi_+^{(0)} \\ \phi_+^{(0)} \\ \phi_+^{(b)} \end{bmatrix} = \begin{bmatrix} -1 & 0 & 0 & 0 \\ 0 & r & t & 0 \\ 0 & t & -r & 0 \\ 0 & 0 & 0 & -1 \end{bmatrix} \begin{bmatrix} \psi_-^{(a)} \\ \psi_-^{(0)} \\ \phi_-^{(0)} \\ \phi_-^{(b)} \end{bmatrix}. \tag{6.2.13}$$

This equation can be written in a compact form as,

$$\Psi_+ = \hat{S}\Psi_-, \tag{6.2.14}$$

where $\Psi_+ = \{\psi_+^{(a)}, \psi_+^{(0)}, \phi_+^{(0)}, \phi_+^{(b)}\}$, and similarly for the incoming wave vector Ψ_-.

The map $\hat{S}$ is called the scattering operator. It forms a unitary matrix with diagonal elements correspond to the reflection coefficients r obtained as

$$r = \left(\frac{\rho_2 k_1 - \rho_1 k_2}{\rho_2 k_1 + \rho_1 k_2}\right). \tag{6.2.15}$$

The off-diagonal elements of S correspond to the transmission coefficients t obtained as

$$t = \left(\frac{2\sqrt{\rho_1 \rho_2 k_1 k_2}}{\rho_2 k_1 + \rho_1 k_2}\right). \tag{6.2.16}$$

The equations (6.2.15) and (6.2.18) can be simplified using the relation (4.2.1) between ρ's and k's, so one reobtains the reflection and transmission coefficients in terms of k's as

$$r = \left(\frac{1 - k_1 k_2}{1 + k_1 k_2}\right), \tag{6.2.17}$$

$$t = \left(\frac{2\sqrt{k_1 k_2}}{k_1 + k_2}\right). \tag{6.2.18}$$

The probability of a ray to be reflected or transmitted is obtained as $|r|^2$ or $|t|^2$, respectively.

To formulate the transfer operator, we now combine the shift and the scattering operator by inserting equation (6.2.14) into equation (6.2.5) to form the transfer operator as

$$\psi_- = \hat{R}\hat{S}\psi_- = \hat{T}\psi_-, \tag{6.2.19}$$

where $\hat{T}$ is called the transfer operator. This equation gives the quantization condition of the beam as,

$$\det(\hat{I} - \hat{T}) = 0.$$

In conclusion, the formulation of the transfer operator starts out by expressing the boundary integral kernels as diagonal and off-diagonal parts, and also decomposing the boundary functions in terms of the scattering amplitudes. In the light of the one-dimensional approach developed here, next we extend this formulation to coupled cavities in two dimensions. However, such treatment is less straightforward because the scattering amplitudes are propagating in all directions not only to the left or to the right as for the one-dimensional case.

6.3 The shift operator

In this section we present the formulation of the shift operator for the coupled cavities where the physical solution is an eigenfunction. The coupled-cavity configuration consists of the left sub-domain Ω_1 and right sub-domain Ω_2 as depicted in figure 6.2.

The formulation of the transfer operator starts from the BIE without any reference to the boundary conditions. The shift operator will be derived

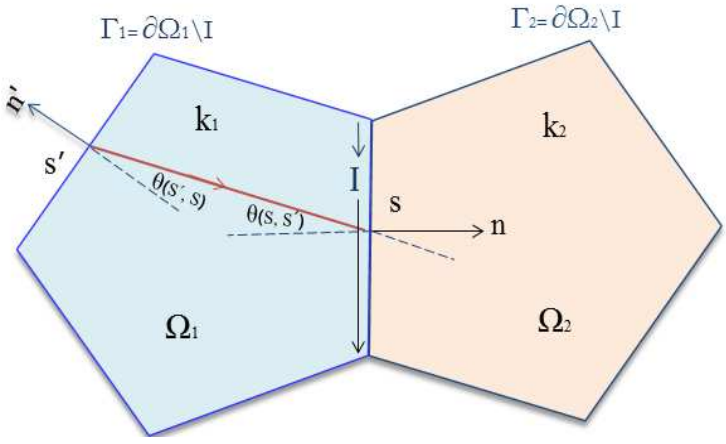

Figure 6.2: Sketch of the coupled-cavity configuration.

separately for each sub-domain similar to the analogy of the multi-component BEM introduced in Chapter 4. The BIE (3.5.6) for the left sub-domain can be rewritten in the following way

$$\psi = \hat{G}_0\mu - \hat{G}_1\psi, \tag{6.3.1}$$

where the Green operators $\hat{G}_0$ and $\hat{G}_1$ are defined as,

$$\hat{G}_0\mu = \lim_{\mathbf{r}\to\beta}\int_{\partial\Omega_1} G_0(q,\mathbf{r};k_1)\mu(q)\mathrm{d}q, \tag{6.3.2}$$

and,

$$\hat{G}_1\psi = \lim_{\mathbf{r}\to\beta}\int_{\partial\Omega_1} \frac{\partial G_0(q,\mathbf{r};k_1)}{\partial n_q}\psi(q)\mathrm{d}q, \tag{6.3.3}$$

where $\partial\Omega_1$ is the whole boundary of the left sub-domain including the interface, and k_1 is the wavenumber in the left sub-domain.

It should be noted that, here we work out the shift operator from the original BIE whereas the formulation of the multi-component BEM in Chapter 4 considers the normal derivative of the BIE. However, if one prefers to proceed with the normal derivative of the BIE, then the corresponding Green operators can be derived in a similar fashion.

Similarly to the disc problem presented in the previous chapter, we decompose the wavefunctions in the left and right sub-domain in terms of incoming and outgoing waves as,

$$\psi = \frac{A}{\sqrt{\hat{p}_n}}(\psi_- + \psi_+), \tag{6.3.4}$$

and

$$\phi = \frac{B}{\sqrt{\hat{q}_n}}(\phi_- + \phi_+). \tag{6.3.5}$$

where A and B are constants, ψ_- and ψ_+ are respectively the incoming and the outgoing waves vectors for the left sub-domain. Similarly ϕ_- and ϕ_+ for the right sub-domain. The decomposition of the boundary functions in one dimension shown in §6.2 was simpler than equations (6.3.4) and (6.3.5), in the sense that in one dimension the incoming and the outgoing waves are only travelling to the left or to the right, whereas in two dimensions these waves are propagating in all

directions. The information of their direction is stored in the operators $\sqrt{\hat{p}_n}$ and $\sqrt{\hat{q}_n}$. The operator $\sqrt{\hat{p}_n}$ is a global operator which acts on the whole boundary of the left sub-domain, including the interface, and similarly $\sqrt{\hat{q}_n}$ for the right sub-domain.

The operator $\sqrt{\hat{p}_n}$ is different than $\sqrt{\hat{q}_n}$ only by the value of the wavenumber. These operators incorporate the angle between incoming or outgoing wave and the normal at the boundary as it will be shown semiclassically in §6.6.
For the normal derivative of the wave functions, one has

$$\mu = \frac{\partial \psi}{\partial n} = \imath k_1 \sqrt{\hat{p}_n}(\psi_- - \psi_+), \tag{6.3.6}$$

and

$$\varphi = \frac{\partial \phi}{\partial n} = \imath k_2 \sqrt{\hat{q}_n}(\phi_- - \phi_+). \tag{6.3.7}$$

where the boundary functions μ and φ are respectively the normal derivative of the Green function in the left and right sub-domain.

We derive the shift operator for each sub-domain in a similar manner to the derivation of the shift operator for a disc in §5.3.3. For the left sub-domain, one needs to insert the Green operators $\hat{G}_0$ and $\hat{G}_1$ given by equations (5.3.15) and (5.3.25) and the decomposition relations (6.3.4) and (6.3.6) into the BIE (6.3.1), one has,

$$\begin{aligned}\frac{1}{\sqrt{\hat{p}_n}}(\psi_- + \psi_+) = \frac{\imath}{2k_1}\frac{1}{\sqrt{\hat{p}_n}}(\hat{I} + \hat{R}_0)\frac{1}{\sqrt{\hat{p}_n}}\cdot \imath k_1 \sqrt{\hat{p}_n}(\psi_- - \psi_+) \\ + \frac{1}{2}\frac{1}{\sqrt{\hat{p}_n}}(\hat{I} + \hat{R}_1)\sqrt{\hat{p}_n}\frac{1}{\sqrt{\hat{p}_n}}(\psi_- + \psi_+).\end{aligned} \tag{6.3.8}$$

Multiplying equation (6.3.8) by $2\sqrt{\hat{p}_n}$ from the left and rearranging, one has

$$(2\hat{I} + \hat{R}_0 - \hat{R}_1)\psi_- = (\hat{R}_0 + \hat{R}_1)\psi_+. \tag{6.3.9}$$

We now multiply equation (6.3.9s) from the left by the operator $(2\hat{I}+\hat{R}_0-\hat{R}_1)^{-1}$, one has

$$\begin{aligned}\psi_- &= (2\hat{I} + \hat{R}_0 - \hat{R}_1)^{-1}(\hat{R}_0 + \hat{R}_1)\psi_+ \\ &= \hat{R}\psi_+\end{aligned} \tag{6.3.10}$$

where $\hat{R}$ is the exact shift operator.

Since the operators $\hat{R}_0$ and $\hat{R}_1$ are not diagonal for polygonal geometries, the inverse of the operator $(2\hat{I}-\hat{R}_0-\hat{R}_1)$ may be difficult to evaluate. Thus to facilitate the computations, we semiclassically assume that $\hat{R}_0 \simeq \hat{R}_1 \simeq \hat{R}$. Thus equation (6.3.10) can be reduced to the following,

$$\psi_- = \hat{R}_{\partial\Omega_1}\psi_+. \tag{6.3.11}$$

where the subscript $\partial\Omega_1$ denotes the boundary of the left sub-domain.
In a similar fashion, we obtain the shift operator for the right sub-domain as

$$\phi_- = \hat{R}_{\partial\Omega_2}\phi_+. \tag{6.3.12}$$

where $\partial\Omega_2$ is the whole boundary of the right sub-domain including the interface. We now collect equations (6.3.11) and (6.3.12) to form the shift operator for the coupled-cavity configuration as,

$$\begin{bmatrix}\psi_-\\ \phi_-\end{bmatrix} = \begin{bmatrix}\hat{R}_{\partial\Omega_1} & \mathbf{0}\\ \mathbf{0} & \hat{R}_{\partial\Omega_2}\end{bmatrix}\begin{bmatrix}\psi_+\\ \phi_+\end{bmatrix}. \tag{6.3.13}$$

Now one needs to partition the boundary of each sub-domain using,

$$\partial\Omega_j = \Gamma_j \cup I, \qquad j = 1, 2.$$

We denote to the external boundary for each sub-domain by,

$$\Gamma_j = \partial\Omega_j \backslash I, \qquad I = \partial\Omega_1 \cap \partial\Omega_2$$

where I denotes the internal boundary (interface) as depicted in figure 6.2. Thus by using this partition, equation (6.3.13) can be written in terms of the characteristic function as,

$$\begin{bmatrix}\chi_{\Gamma_1}\psi_-\\ \chi_I\psi_-\\ \chi_I\phi_-\\ \chi_{\Gamma_2}\phi_-\end{bmatrix} = \begin{bmatrix}\hat{R}_{\Gamma_1\Gamma_1} & \hat{R}_{\Gamma_1 I} & \mathbf{0} & \mathbf{0}\\ \hat{R}_{I\Gamma_1} & \hat{R}_{II} & \mathbf{0} & \mathbf{0}\\ \mathbf{0} & \mathbf{0} & \hat{R}_{II} & \hat{R}_{I\Gamma_2}\\ \mathbf{0} & \mathbf{0} & \hat{R}_{\Gamma_2 I} & \hat{R}_{\Gamma_2\Gamma_2}\end{bmatrix}\begin{bmatrix}\chi_{\Gamma_1}\psi_+\\ \chi_I\psi_+\\ \chi_I\phi_+\\ \chi_{\Gamma_2}\phi_+\end{bmatrix} \tag{6.3.14}$$

where the characteristic functions χ_{Γ_1}, χ_I and χ_{Γ_2} are defined by equation (5.6.4). This equation can be written in a compact form as,

$$\Psi_- = \hat{R}\Psi_+, \tag{6.3.15}$$

where $\hat{R}$ is the shift operator for the coupled-cavity configuration. Hereafter, we use the following notation for the outgoing wave vector,

$$\Psi_+ = \{\chi_{\Gamma_1}\psi_+, \chi_I\psi_+, \chi_I\phi_+, \chi_{\Gamma_2}\phi_+\} = \{\psi_+^L, \psi_+^I, \phi_-^I, \phi_+^R\}, \tag{6.3.16}$$

and similarly for the incoming wave vector Ψ_-.

The functions ψ_-^L and ψ_-^I are respectively the incoming wave sub-vector along the outer boundary of the left sub-domain and the interface, and similarly for ϕ_-^R and ϕ_-^I for the right sub-domain.

The obtained shift operator $\hat{R}$ is semiclassical for two reason, first we do not consider the treatment of corners in the derivation of the singular part of the Green operator $\hat{G}_0$ in §5.3, and the second reason is the fact that $\hat{R}_0 \simeq \hat{R}_1 \simeq \hat{R}$ has been used.

For the disc case presented in the previous chapter, we present the regular part of $\hat{G}_0$ and $\hat{G}_1$ in momentum space to take the advantage that they are diagonal in this space. This advantage does not hold for the polygonal geometry, so we present them in position space.

From equation (5.3.15) we can have $\hat{R}_0$ as,

$$\hat{R}_0 = \frac{2k}{\imath}\sqrt{\hat{p}_n}\hat{G}_0\sqrt{\hat{p}_n} - \hat{I}. \tag{6.3.17}$$

Now $\hat{R}_0$ can be obtained asymptotically for $k|s-s'| \gg 1$ by using the asymptotic expansion of the Hankel functions $H_0^{(1)}$ for large arguments $k|s-s'| \to \infty$ and fixed ν [125] given as,

$$H_\nu^{(1)}(k|s-s'|) \simeq \sqrt{\frac{2}{\pi k|s-s'|}}e^{\imath\left(k|s-s'|-\frac{\nu\pi}{2}-\frac{\pi}{4}\right)}. \tag{6.3.18}$$

where $|s-s'|$ is the length of the chord connecting the boundary point s to s'. Also the operator $\sqrt{\hat{p}_n}$ will be obtained semiclassically in §6.4 as

$$(\hat{p}_n)_{ss'} \simeq \cos\theta(s,s'), \tag{6.3.19}$$

where $\theta(s,s')$ is the angle between the normal at the boundary point s and the chord connecting the initial boundary point s' to the final boundary point s. Similarly $\theta(s',s)$ is the corresponding angle at the boundary point s' as illustrated in figure 6.2.

Using the asymptotic approximations (6.3.18) (6.3.19), one obtains the semiclassical shift operator as,

$$R_{sc}(s,s';k) = \frac{1}{\sqrt{2\pi\imath}}\sqrt{\frac{k}{L(s,s')}}\sqrt{\cos\theta(s,s')\cos\theta(s',s)}e^{\imath kL(s,s')}, \qquad (6.3.20)$$

where we used $(\imath)^{\pm\frac{1}{2}} = e^{\pm\imath\frac{\pi}{4}}$.

To conclude, we obtained the semiclassical shift operator for the coupled cavities. We still need to derive another operator which incorporates the boundary conditions as shown next.

6.4 The scattering operator

In this section, we present a derivation of the operator which carries the information about the boundary conditions for the coupled-cavity configuration of different material properties. Such an operator tells us how an incoming wave is scattered off the boundary once it hits any part of the boundary of the coupled cavities. Thus, it will be called the scattering operator, and it will be derived locally at each part of the boundary.

First let us introduce the prescribed boundary conditions for the coupled-cavity configuration. We set Dirichlet boundary conditions along the external boundary (excluding the interface) of the coupled cavity as elucidated in figure 6.2, that is,

$$\left.\begin{aligned} \chi_{\Gamma_1}\psi(s) = 0, \qquad s\in\Gamma_1. \\ \chi_{\Gamma_2}\phi(s) = 0, \qquad s\in\Gamma_2, \end{aligned}\right\}, \qquad \text{Dirichlet BCs.} \qquad (6.4.1)$$

The function χ_{Γ_1} denotes the characteristic function defined by equation (5.6.4).

Further to the Dirichlet boundary conditions along the external boundary Γ_j, one needs to impose the continuity conditions of the wavefunction and the

equilibrium of the energy flux normal to the interface as given by the following equations,

$$\left.\begin{aligned} \chi_I\psi(s) &= \chi_I\phi(s) \\ \rho_2\chi_I\frac{\partial\psi(s)}{\partial n_s} &= \rho_1\chi_I\frac{\partial\phi(s)}{\partial n_s} \end{aligned}\right\}, \qquad s\in I. \tag{6.4.2}$$

The constants ρ_1 and ρ_2 are the material densities of the left and the right subdomain, respectively; they are related by equation (4.2.1).

To proceed with the derivation of the scattering operator, let us insert the DBCs (6.4.1) into the decomposition relations given by equations (6.3.4) and (6.3.5). One obtains the following relations,

$$\chi_{\Gamma_1}\psi_+ = -\chi_{\Gamma_1}\psi_-, \tag{6.4.3}$$

and

$$\chi_{\Gamma_2}\phi_+ = -\chi_{\Gamma_2}\phi_-, \tag{6.4.4}$$

where we assumed that χ_I commute with the operators $\frac{1}{\sqrt{\hat{p}_n}}$ and $\frac{1}{\sqrt{\hat{q}_n}}$. This semiclassical procedure neglects the contribution from the following commutator,

$$C = \left[\chi_I, \frac{1}{\sqrt{\hat{p}_n}}\right]. \tag{6.4.5}$$

In Appendix E, we show that the contributions of the commutator (6.4.5) decays in the semiclassical limit $k\to\infty$.

Also we need to incorporate the continuity conditions along the interface, so we need to plug the decomposition relations given by equations (6.3.4) and (6.3.5) into the first line of the conditions described by equation (6.4.2). One has

$$\chi_I\frac{A}{\sqrt{\hat{p}_n}}(\psi_- + \psi_+) = \chi_I\frac{B}{\sqrt{\hat{q}_n}}(\phi_- + \phi_+). \tag{6.4.6}$$

The constants $A=\sqrt{\frac{\rho_1}{k_1}}$ and $B=\sqrt{\frac{\rho_2}{k_2}}$ are chosen to guarantee the conservation of the energy flux across the discontinuity point, that is, the obtained scattering operator will be unitary.

Keeping the order of the characteristic function χ_I with the operators $\sqrt{\hat{p}_n}$ and $\sqrt{\hat{q}_n}$ will complicate the calculations and leads to a complicated expres-

sion of the reflection and transmission coefficients. Thus, to facilitate the calculations we proceed by commuting χ_I with the operators $\frac{1}{\sqrt{\hat{p}_n}}$ and $\frac{1}{\sqrt{\hat{q}_n}}$. However, as we have already mentioned, this procedure neglects the contributions from the commutator (6.4.5). One has

$$\chi_I\psi_+ = \frac{B\sqrt{\hat{p}_n}}{A\sqrt{\hat{q}_n}}\chi_I(\phi_- + \phi_+) - \chi_I\psi_-. \tag{6.4.7}$$

Also, inserting the decomposition relations given by equations (6.3.4) and (6.3.5) into the second line of the conditions described by equation (6.4.2) leads to

$$A\frac{\imath k_1}{\rho_1}\chi_I\sqrt{\hat{p}_n}(\psi_- - \psi_+) = -B\frac{\imath k_2}{\rho_2}\chi_I\sqrt{\hat{q}_n}(\phi_- - \phi_+). \tag{6.4.8}$$

For simplicity, define $\sigma = \frac{k_1}{\rho_1}$ and $\gamma = \frac{k_2}{\rho_2}$. Assuming that we can commute the characteristic function χ_I with the operators $\sqrt{\hat{q}_n}$ and $\sqrt{\hat{p}_n}$, equation (6.4.8) can be reduced to,

$$\chi_I\phi_+ = \frac{\sigma A}{\gamma B}\frac{\sqrt{\hat{p}_n}}{\sqrt{\hat{q}_n}}\chi_I(\psi_- - \psi_+) + \chi_I\phi_-. \tag{6.4.9}$$

Now, one needs to plug equation (6.4.9) into equation (6.4.7), one arrives at the following relation,

$$\chi_I\psi_+ = \left(\frac{\sigma\hat{p}_n - \gamma\hat{q}_n}{\sigma\hat{p}_n + \gamma\hat{q}_n}\right)\chi_I\psi_- + \frac{2B}{A}\left(\frac{\gamma\sqrt{\hat{p}_n\hat{q}_n}}{\sigma\hat{p}_n + \gamma\hat{q}_n}\right)\chi_I\phi_-. \tag{6.4.10}$$

where we also commute the operators $\sqrt{\hat{p}_n}$ with $\sqrt{\hat{q}_n}$.

This equation can be abbreviated as,

$$\chi_I\psi_+ = \hat{r}\chi_I\psi_- + \hat{t}\chi_I\phi_-, \tag{6.4.11}$$

where $\hat{r}$ and $\hat{t}$ are the reflection and transmission coefficients obtained as,

$$\hat{r} = \left(\frac{\sigma\hat{p}_n - \gamma\hat{q}_n}{\sigma\hat{p}_n + \gamma\hat{q}_n}\right), \tag{6.4.12}$$

and

$$\hat{t} = \frac{2B}{A}\left(\frac{\gamma\sqrt{\hat{p}_n\hat{q}_n}}{\sigma\hat{p}_n + \gamma\hat{q}_n}\right). \tag{6.4.13}$$

Similarly, one can construct the following relation,

$$\chi_I\phi_+ = -\hat{r}\chi_I\phi_- + \hat{t}\chi_I\psi_-. \tag{6.4.14}$$

Equation (6.4.11) can be interpreted as saying that part of the outgoing wave ψ_+ is reflected back with a reflection coefficient r, and the other part is transmitted to the right sub-domain with a transmission coefficient t.

We now combine equations (6.4.3), (6.4.4), (6.4.11), and (6.4.14) to form the scattering operator as the following,

$$\begin{bmatrix} \chi_{\Gamma_1}\psi_+ \\ \chi_I\psi_+ \\ \chi_I\phi_+ \\ \chi_{\Gamma_2}\phi_+ \end{bmatrix} = \begin{bmatrix} -\hat{I} & \mathbf{0} & \mathbf{0} & \mathbf{0} \\ \mathbf{0} & \hat{r} & \hat{t} & \mathbf{0} \\ \mathbf{0} & \hat{t} & -\hat{r} & \mathbf{0} \\ \mathbf{0} & \mathbf{0} & \mathbf{0} & -\hat{I} \end{bmatrix} \begin{bmatrix} \chi_{\Gamma_1}\psi_- \\ \chi_I\psi_- \\ \chi_I\phi_- \\ \chi_{\Gamma_2}\phi_-. \end{bmatrix}. \tag{6.4.15}$$

This equation can be written in a compact form as,

$$\Psi_+ = \hat{S}\Psi_-. \tag{6.4.16}$$

Using equation (6.3.16) the outgoing wave vector can be written as

$$\Psi_+ = \{\psi_+^L, \psi_+^I, \phi_+^I, \phi_+^R\},$$

and similarly for the incoming wave vector Ψ_-.

The map $\hat{S}$ is called the scattering operator with diagonal elements correspond to the reflection coefficients r, whereas the off-diagonal elements correspond to the transmission coefficients t. It incorporates all the information about the boundary conditions, therefore it tells us what happens to an incoming wave ψ_- once it hits either the external boundaries Γ_1 and Γ_2 or the internal boundary I.

6.5 The semiclassical transfer operator

To summarise, in the previous sections we obtained both the shift and the scattering operator semiclassically. We now combine them to construct the semiclassical transfer operator $\hat{T}$. Inserting the outgoing vector given by equation (6.4.15) into

equation (6.3.14) with using (6.3.16), leads to

$$\begin{bmatrix} \psi_-^L \\ \psi_-^I \\ \phi_-^I \\ \phi_-^R \end{bmatrix} = \begin{bmatrix} \hat{R}_{\Gamma_1\Gamma_1} & \hat{R}_{\Gamma_1 I} & \mathbf{0} & \mathbf{0} \\ \hat{R}_{I\Gamma_1} & \hat{R}_{II} & \mathbf{0} & \mathbf{0} \\ \mathbf{0} & \mathbf{0} & \hat{R}_{II} & \hat{R}_{I\Gamma_2} \\ \mathbf{0} & \mathbf{0} & \hat{R}_{\Gamma_2 I} & \hat{R}_{\Gamma_2\Gamma_2} \end{bmatrix} \begin{bmatrix} -\hat{I} & \mathbf{0} & \mathbf{0} & \mathbf{0} \\ \mathbf{0} & \hat{r} & \hat{t} & \mathbf{0} \\ \mathbf{0} & \hat{t} & -\hat{r} & \mathbf{0} \\ \mathbf{0} & \mathbf{0} & \mathbf{0} & -\hat{I} \end{bmatrix} \begin{bmatrix} \psi_-^L \\ \psi_-^I \\ \phi_-^I \\ \phi_-^R \end{bmatrix}.$$

This equation can be rearranged as the following,

$$\begin{bmatrix} \psi_-^L \\ \psi_-^I \\ \phi_-^I \\ \phi_-^R \end{bmatrix} = \begin{bmatrix} \hat{T}^d_{\Gamma_1\Gamma_1} & \hat{T}^d_{\Gamma_1 I} & \mathbf{0} & \mathbf{0} \\ \hat{T}^r_{I\Gamma_1} & \hat{T}^r_{II} & \hat{T}^t_{II} & \hat{T}^t_{I\Gamma_2} \\ \hat{T}^t_{I\Gamma_1} & \hat{T}^t_{II} & -\hat{T}^r_{II} & \hat{T}^r_{I\Gamma_2} \\ \mathbf{0} & \mathbf{0} & \hat{T}^d_{\Gamma_2 I} & \hat{T}^d_{\Gamma_2\Gamma_2} \end{bmatrix} \begin{bmatrix} \psi_-^L \\ \psi_-^I \\ \phi_-^I \\ \phi_-^R, \end{bmatrix} \tag{6.5.1}$$

where the superscripts d, r and t denotes the direct, reflection and transmission contributions to the transfer operator. They are obtained as,

$$\hat{T}^d_{\Gamma_1\Gamma_1} = (-1)\hat{R}_{\Gamma_1\Gamma_1},$$

$$\hat{T}^r_{I\Gamma_1} = \hat{R}_{I\Gamma_1}\hat{r},$$

and

$$\hat{T}^t_{I\Gamma_1} = \hat{R}_{I\Gamma_1}\hat{t}.$$

Using the semiclassical shift operator given by equation (6.3.20), one obtains the different contributions $\hat{T}^d$, $\hat{T}^r$, and $\hat{T}^t$ as,

$$T^d(s,s';k) = \frac{1}{\sqrt{2\pi\imath}}\sqrt{\frac{k}{L(s,s')}}\sqrt{\cos\theta(s,s')\cos\theta(s',s)}e^{\imath kL(s,s')-\imath\pi}. \tag{6.5.2}$$

This includes contributions from rays away from the interface and the phase $e^{-\imath\pi}$ is due to the Dirichlet boundary conditions on the external boundary. Furthermore,

$$T^r(s,s';k) = \frac{1}{\sqrt{2\pi\imath}}\sqrt{\frac{k}{L(s,s')}}\sqrt{\cos\theta(s,s')\cos\theta(s',s)}e^{\imath kL(s,s')}r(s,s'), \tag{6.5.3}$$

$$T^t(s,s';k) = \frac{1}{\sqrt{2\pi\imath}}\sqrt{\frac{k}{L(s,s')}}\sqrt{\cos\theta(s,s')\cos\theta(s',s)}e^{\imath kL(q,q')}t(s,s'), \quad (6.5.4)$$

where the functions $r(s,s')$ and $t(s,s')$ are respectively the reflection and transmission coefficients.

Since we have a straight line interface, the blocks $\hat{T}^r_{II}$ and $\hat{T}^t_{II}$ vanish because the term $\cos\theta(s,s')$ vanishes for boundary elements lying on the same edge. Therefore, the system (6.5.1) can be reduced to the following set of equations,

$$\begin{bmatrix} \psi^L_- \\ \psi^I_- \\ \phi^I_- \\ \phi^R_- \end{bmatrix} = \begin{bmatrix} \hat{T}^d_{\Gamma_1\Gamma_1} & \hat{T}^d_{\Gamma_1 I} & \mathbf{0} & \mathbf{0} \\ \hat{T}^r_{I\Gamma_1} & \mathbf{0} & \mathbf{0} & \hat{T}^t_{I\Gamma_2} \\ \hat{T}^t_{I\Gamma_1} & \mathbf{0} & \mathbf{0} & \hat{T}^r_{I\Gamma_2} \\ \mathbf{0} & \mathbf{0} & \hat{T}^d_{\Gamma_2 I} & \hat{T}^d_{\Gamma_2\Gamma_2} \end{bmatrix} \begin{bmatrix} \psi^L_- \\ \psi^I_- \\ \phi^I_- \\ \phi^R_- \end{bmatrix}. \quad (6.5.5)$$

The sub-block $\hat{T}^d_{\Gamma_1\Gamma_1}$ expresses the rays starting and ending on the external boundary Γ_1, $\hat{T}^r_{I\Gamma_1}$ contains the rays that are reflected from the interface I back to the right sub-domain Γ_1. The sub-block $\hat{T}^t_{I\Gamma_2}$ contains the rays that are transmitted from the interface I to the right sub-domain Γ_2, and similarly for the other sub-blocks.

It should be noted that further reductions can be made to equation (6.5.5) as shown below. From this equation, one has the following equations,

$$\psi^L_- = \hat{T}^d_{\Gamma_1\Gamma_1}\psi^L_- + \hat{T}^d_{\Gamma_1 I}\psi^I_-, \quad (6.5.6)$$

$$\psi^I_- = \hat{T}^r_{I\Gamma_1}\psi^L_- + \hat{T}^t_{I\Gamma_2}\phi^R_-, \quad (6.5.7)$$

$$\phi^I_- = \hat{T}^t_{I\Gamma_1}\psi^L_- + \hat{T}^r_{I\Gamma_2}\phi^R_-, \quad (6.5.8)$$

$$\phi^R_- = \hat{T}^d_{\Gamma_2\Gamma_2}\phi^R_- + \hat{T}^d_{\Gamma_2 I}\phi^I_-. \quad (6.5.9)$$

Substitute equation (6.5.7) into equation (6.5.6), leads to

$$\psi^L_- = \hat{T}^d_{\Gamma_1\Gamma_1}\psi^L_- + \hat{T}^d_{\Gamma_1 I}[\hat{T}^r_{I\Gamma_1}\psi^L_- + \hat{T}^t_{I\Gamma_2}\phi^R_-]. \quad (6.5.10)$$

And substituting equation (6.5.8) into equation (6.5.9), leads to

$$\phi^R_- = \hat{T}^d_{\Gamma_2\Gamma_2}\psi^L_- + \hat{T}^d_{\Gamma_2 I}[\hat{T}^t_{I\Gamma_1}\psi^L_- + \hat{T}^r_{I\Gamma_2}\phi^R_-]. \quad (6.5.11)$$

Therefore, equations (6.5.10) and (6.5.11) eliminate the unknowns ψ_-^I and ϕ_-^I along the interface and they only have the scattering amplitudes along the external boundaries ψ_-^L and ϕ_-^R. These equations form the following system,

$$\begin{bmatrix} \psi_-^L \\ \phi_-^R \end{bmatrix} = \begin{bmatrix} \hat{T}^d_{\Gamma_1\Gamma_1} + \hat{T}^d_{\Gamma_1 I}\hat{T}^r_{I\Gamma_1} & \hat{T}^d_{\Gamma_1 I}\hat{T}^t_{I\Gamma_2} \\ \hat{T}^d_{\Gamma_2\Gamma_2} + \hat{T}^d_{\Gamma_2 I}\hat{T}^t_{I\Gamma_1} & \hat{T}^d_{\Gamma_2 I}\hat{T}^r_{I\Gamma_2} \end{bmatrix} \begin{bmatrix} \psi_-^L \\ \phi_-^R \end{bmatrix}. \tag{6.5.12}$$

The term $\hat{T}^d_{\Gamma_1 I}\hat{T}^r_{I\Gamma_1}$ means that a ray directly goes from Γ_1 to the interface I, then it is reflected from I back to Γ_1. Similarly, the term $\hat{T}^d_{\Gamma_1 I}\hat{T}^t_{I\Gamma_2}$ means that a ray directly goes from Γ_1 to the interface I, then it is transmitted to Γ_2.
Equation (6.5.5) can be written in a compact form as,

$$\Psi_- = \hat{T}\Psi_-, \tag{6.5.13}$$

where $\hat{T}$ is the semiclassical transfer operator and $\Psi_- = \{\psi_-^L, \psi_-^I, \phi_-^I, \phi_-^R\}$.
The secular equation is obtained as,

$$\det(\hat{I} - \hat{T}) = 0, \tag{6.5.14}$$

This equation gives an approximation of the quantization condition of the system. The zeros of this equation corresponds one by one to the semiclassical eigenvalues. To be able to proceed with equation (6.5.14), we still need to work out the reflection and transmission coefficients explicitly as shown next.

6.6 Reflection and transmission coefficients

For a system with ray splitting, the reflection and transmission coefficients can be derived asymptotically by considering plane waves incident on infinite interface located along the line $x = 0$. The abrupt changes of material properties occurs at such infinite interface as shown in Appendix F. This analogy considers the problem of all space and treats the ray-splitting interface as an infinite line, hence it neglects diffraction effects coming from the two end points of the interface. This

idea is similar to the asymptotic derivation of the reflection and transmission coefficients presented by Blümel [117].

Here we aim to derive the reflection and transmission coefficients $\hat{r}$ and $\hat{t}$ from the transfer operator formulation. To do so, one needs to work out the inverse Fourier transform of $\hat{R}\hat{r}$ given as

$$\left(\hat{R}\hat{r}\right)(s,s') = \int \mathrm{d}p \int \mathrm{d}p' \left(\hat{R}\hat{r}\right)(p,p') e^{\imath kps} e^{-\imath kps}, \tag{6.6.1}$$

where $\hat{R}$ and $\hat{r}$ are respectively the shift and the reflection operators. The multiplication of these operators can be expressed as the following

$$\left(\hat{R}\hat{r}\right)(p,p') = \int \mathrm{d}p'' R(p,p'') r(p'',p'). \tag{6.6.2}$$

Inserting equation (6.6.2) into equation (6.6.1) leads to,

$$\left(\hat{R}\hat{r}\right)(s,s') = \int \mathrm{d}p \int \mathrm{d}p' \int \mathrm{d}p'' R(p,p'') r(p'',p') e^{\imath kps} e^{-\imath kp's'}. \tag{6.6.3}$$

Next we use the fact that the reflection operator $\hat{r}$ is diagonal in momentum space, that is,

$$r(p'',p') = \delta(p'',p') r(p').$$

So, equation (6.6.3) can be reduced to,

$$\left(\hat{R}\hat{r}\right)(s,s') = \int \mathrm{d}p \int \mathrm{d}p' R(p,p') r(p') e^{\imath kps} e^{-\imath kp's'}. \tag{6.6.4}$$

After using the WKB approximation of $\hat{R}$ (approximating $\hat{R}$ as an exponential function with some amplitude), the resulting integral can be done by stationary phase approximation, where $r(p')$ is a slowly varying function, that is, it does not affect the positions of the stationary points.

So for the two-dimensional integral (6.6.4), it can be shown that [8] the stationary phase condition is satisfied at, $p = \cos\theta_L$ and $p' = \cos\theta_R$, thus

$$\left(\hat{R}\hat{r}\right)(s,s') = R(s,s') r(\theta_L(s,s'), \theta_R(s,s')). \tag{6.6.5}$$

The dependence of θ_L and θ_R on s and s' will be suppressed hereafter. The angles θ_L and θ_R are the incident and refracted angles measured with respect to

the normal to the interface as depicted in figure 6.3. They are related by Snell's law ($k_1 \sin\theta_R = k_2 \sin\theta_L$).

Evaluating the reflection coefficient $r(p)$ at the stationary points leads to,

$$r(\theta_L, \theta_R) = \left(\frac{\rho_2 k_1 \cos\theta_L - \rho_1 k_2 \cos\theta_R}{\rho_2 k_1 \cos\theta_L + \rho_1 k_2 \cos\theta_R} \right). \tag{6.6.6}$$

By similar manner, we work out the operator $\hat{R}\hat{t}$ to obtain the transmission coefficients as,

$$t(\theta_L, \theta_R) = \left(\frac{2\sqrt{\rho_1 k_2 \rho_2 k_1 \cos\theta_L \cos\theta_R}}{\rho_2 k_L \cos\theta_L + \rho_1 k_2 \cos\theta_R} \right). \tag{6.6.7}$$

The equations (6.6.6) and (6.6.7) can be simplified using the relation (4.2.1)

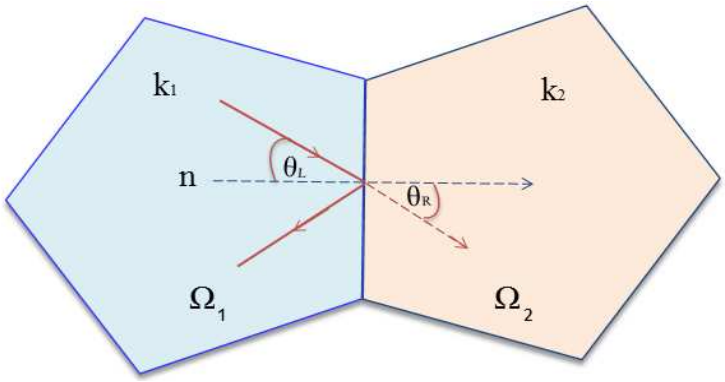

Figure 6.3: Sketch shows the ray splitting at the interface of the coupled-cavity configuration.

between ρ's and k's, one reobtain respectively the reflection and transmission coefficients as

$$r = \left(\frac{\cos\theta_L - k_1 k_2 \cos\theta_R}{\cos\theta_L + k_1 k_2 \cos\theta_R} \right), \tag{6.6.8}$$

$$t = \left(\frac{2\sqrt{k_1 k_2 \cos\theta_L \cos\theta_R}}{k_1 \cos\theta_L + k_2 \cos\theta_R} \right). \tag{6.6.9}$$

Having obtained reflection and transmission coefficients, we can evaluate the spectral determinant using equation (6.5.14) as shown next.

6.7 Comparison between the semiclassical transfer operator and the BEM

In this section we compare the spectral determinant of the coupled-cavity configuration using the quantization condition obtained by (6.5.14). We then carry out a comparison of the spectral determinant obtained from the multi-component BEM and the semiclassical transfer operator.

The efficiency of the semiclassical tools for quantisation is an old topic and can be traced back to the early nineties. For instance Sieber [131] and Tanner [132] investigated the accuracy of different semiclassical tools for quantization. Szeredi et al. [133] demonstrated that a finite approximation to the Bogomolny transfer operator for certain type of billiard produces approximate eigenvalues which are in good agreement with the exact eigenvalues. Here we are not motivated by investigating the accuracy of the semiclassical transfer operator. Rather we only want to demonstrate that the semiclassical transfer operator is a good starting point for further semiclassical analysis.

We carried out the comparison for configuration A depicted in figure 3.9 where the wave velocity c changes at the interface, that is using different value of the wavenumber in each sub-domain. For both methods we compute the spectral determinant for the frequency range ω from 1 to 20 and we set the wave velocity in the left sub-domain to 1 whereas in the right sub-domain it is 2. That is, from the relation $k = \frac{\omega}{c}$ the value of the wavenumber in the right sub-domain is always half the value of the wavenumber in the left sub-domain. Respectively, figures 6.4 and 6.5 on normal and log scales, show that the minima of the modulus of the determinant obtained from the semiclassical transfer operator and the BEM. It can be observed that the minima of the determinant obtained from the semiclassical transfer operator are not as sharp as those of the BEM. Also, the semiclassical transfer operator does not resolve nearby eigenvalues.

The non-sharpness of the minima of the semiclassical determinant is

attributed to the lack of the unitarity of the semiclassical transfer operator where the eigenvalues are not real. The larger the imaginary part of such eigenvalues (deviation from the real axis), the less sharp the minima are at the position of such eigenvalues. However, the semiclassical determinant has quite similar patterns to that of the exact determinant.

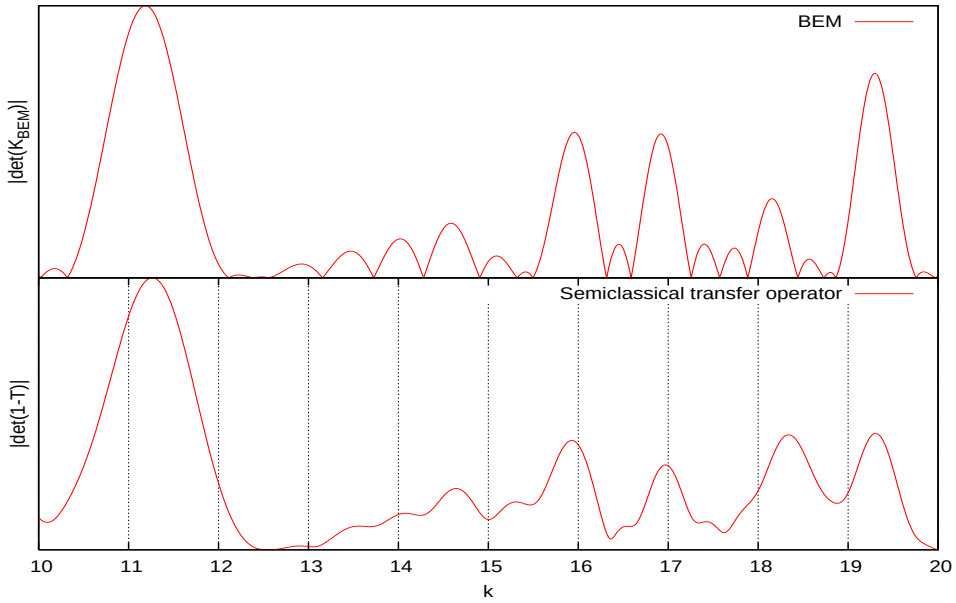

Figure 6.4: The modulus of the spectral determinant using the BEM and the semiclassical transfer operator for configuration A.

6.8 Conclusions

In this chapter we semiclassically formulated the transfer operator for coupled cavities. We point out the semiclassical approximations which have been made at each stage of the derivation. In this chapter, the semiclassical transfer operator was derived where the physical solution is an eigenfunction. However an analogous formulation for the Green function can be done in a similar manner to the disc problem presented in the previous chapter.

The reflection and transmission coefficients at the discontinuity line

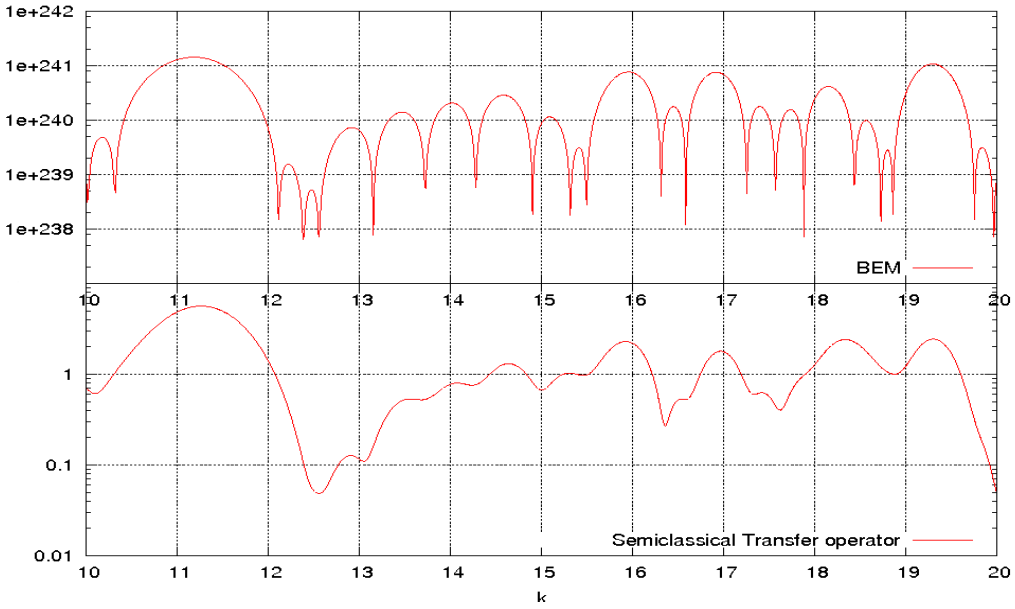

Figure 6.5: Semi-Log scale of the modulus of the spectral determinant using the BEM and the transfer operator for configuration A.

of the material properties were obtained explicitly. The semiclassical transfer operator for coupled cavities showed reasonably good results when comparing with the multi-component BEM. These results can be improved by considering the treatment of corners, that is, including the corners diffraction effects. Also it can be improved by considering the commutator contribution (6.4.5) in the derivation of the scattering operator.

Chapter 7

Conclusions and future work

In this thesis a new formulation for the exact transfer operator was proposed where the physical solution is either an eigenfunction or the Green function. Our approach is based on introducing the Green operators and decomposing the boundary functions into incoming and outgoing plane waves.

7.1 Conclusions

We consider modelling domains with abrupt changes of different material properties using the multi-component BEM and the transfer operator method. The latter is formulated semiclassically in the high frequency limit.

In Chapter 3, it was demonstrated that taking the normal derivative of the BIE for a single cavity gave more accurate and stable results than using the original BIE. This argument was supported by showing a numerical example of a disc with Dirichlet boundary conditions. Building upon this observation, in Chapter 4 this idea was extended to the BEM formulation for coupled cavities.

The problematic hypersingular integrals arising when taking the normal derivative of the BIEs were reduced to weakly singular integrals by deriving an integral identity. This integral identity was obtained by decomposing the hypersingular integrand into a weakly singular integrand and another integrand

which can be integrated numerically by using the piecewise constant collocation method. Such an integral identity was derived for a straight line boundary in two dimensions. Thus it is a special case of the identity introduced first by Maue [71] and then by many other researchers [60, 71, 72, 73]. After treating the weak singularity, the obtained BIEs were solved numerically to obtain the boundary functions.

It was observed that by decomposing the structure into sub-components, more accurate results for the boundary functions were obtained compared to the classical single-domain BEM. This is due to the fact that by considering the interface we have more degrees of freedom in the multi-component BEM. In a post-processing procedure, the Green function was computed throughout the interior of the domain. Knowing the Green function throughout the domain, the mean energy density could be computed. Some applications of the method for different geometric configurations and various combinations of the wavenumber were presented in Chapter 4.

For systems with ray splitting such as coupled cavities, it is informative to explicitly work out the reflection and transmission coefficients at the ray-splitting interface (discontinuity line of material properties). To achieve this objective, the transfer operator method was adopted. To approach the treatment of coupled cavities, a simple model was considered where an exact transfer operator was derived.

In Chapter 5, a new formulation for the exact transfer operator was introduced and demonstrated successfully for a disc with discontinuous changes in boundary conditions. Also, it was shown how the semiclassical transfer operator is obtained. Then a comparison between the exact and the semiclassical results was carried out. There was an indication that the exact transfer operator incorporated diffraction effects coming from the discontinuity of the boundary conditions, whereas the semiclassical neglects such effects.

The exact and the semiclassical transfer operator were used to compute

the spectral determinant for the unit disc with discontinuous changes of boundary conditions. For careful analysis of the performance of the semiclassical transfer operator, the semiclassical transfer operator was constructed by two ways. The first one was constructed by combining the semiclassical reflection operator and the exact shift operator denoted as $\hat{T}^{(1)}_{\rm sem}$. The second $\hat{T}^{(2)}_{\rm sem}$ was constructed by combining the semiclassical reflection operator and the semiclassical shift operator. It was found that the performance of $\hat{T}^{(2)}_{\rm sem}$ was less satisfactory than $\hat{T}^{(1)}_{\rm sem}$ in the sense that the minima of its spectral determinant exhibited a shift from those of the exact transfer operator.

Using Debye's asymptotic expansion for the Bessel functions involved in the shift operator, it was shown that the exact transfer operator for a unit disc with Dirichlet boundary conditions can be reduced to the semiclassical Bogomolny transfer operator obtained by equation (5.5.9).

To investigate the effect of a basis change of the BEM and the transfer operator, we replaced the boundary integral kernels by the Green operators obtained by equations (5.3.15) and (5.3.25). We obtained a relation between the quantization condition of both methods. This relation explained the difference of the scale of the spectral determinant obtained from each method.

Based on the conclusions drawn from Chapter 5, we had a clear picture of the performance of the semiclassical transfer operator. Due to the less straightforward treatment of coupled-cavity configurations compared to the disc problem, only a semiclassical transfer operator was derived for this configuration, however it was pointed out how it can improved to obtain the exact transfer operator .The transfer operator was formulated for an eigenvalue problem obtaining the spectral determinant. The reflection and transmission coefficients were obtained explicitly. The semiclassical transfer operator for coupled cavities showed reasonably good results when comparing with the multi-component BEM.

It worth emphasising that it was not the aim of this thesis to obtain the best possible accuracy of the semiclassical transfer operator. Rather we wanted

to demonstrate that the semiclassical transfer operator is good starting point for further semiclassical analysis. Next we highlight some ideas that were inspired by this thesis.

7.2 Future work

In this section we suggest some possible directions for future work. We point out some mathematical issues which are worth investigating, and some applications which are worth considering. As demonstrated in Chapter 5, the transfer operator approach looks promising, especially when it is formulated exactly. It would be interesting to look into the local corner diffraction effects for non-smooth boundaries. This can be done by careful treatment of the corners in the formulation of the transfer operator.

The derivation presented in §5.3 for the singular part of the Green operator, $\hat{G}_0$ was built on the assumption that the boundary is locally flat. It does not take into account the treatment of corners. That is it neglects the corner diffraction effects. So this approach can be improved by considering the treatment of corners for non-smooth boundaries.

Another mathematical issue worth investigating is that within the current formulation of the transfer operator, the singular part of the Green operator $\hat{G}_0$ is singular in momentum space as well as position space. Such singularity may have a negative effect on the convergence of the transfer operator method. Ideally it would be more suitable if the current formulation can be improved by not having such singularity in momentum space. Also in the current formulation of the exact transfer operator we observe that the evanescent contribution is hidden implicitly into the set-up of the Green operators and the wavefunctions.

In this thesis, we consider abrupt changes of material properties, but real-life applications may have continuous change of material properties. So it would be advantageous to consider these categories within the transfer operator framework.

Appendix A

Free-Space Green function

There are various methods to determine the unbounded (free)-space Green function $G_0(\mathbf{r}, \mathbf{r}'; k_0)$, which represents the solution of the corresponding differential equation disregarding the boundary. Here we shall use the Fourier integral representation of the scalar Helmholtz equation. Then do the resulting integrals by residues Cauchy theorem.

Let us start by considering the inhomogeneous Helmholtz equation in n-dimension. To avoid confusion with the Fourier variable k, we shall write the Helmholtz equation as

$$(\nabla^2_{\mathbf{r}} + k_0^2) G_0(\mathbf{r}, \mathbf{r}'; k_0) = -\delta(\mathbf{r} - \mathbf{r}'). \tag{A.1}$$

If we take the Fourier transform of (A.1) relative to $\mathbf{r}$, then we obtain

$$\tilde{G}_0(k) = \frac{e^{\imath \mathbf{k}(\mathbf{r}-\mathbf{r}')}}{(2\pi)^n (k^2 - k_0^2)}. \tag{A.2}$$

Taking the inverse Fourier transform of (A.2), one obtains,

$$G_0(\mathbf{r}, \mathbf{r}'; k_0) = \frac{1}{(2\pi)^n} \int_{\mathbb{R}^n} \frac{e^{\imath \mathbf{k}(\mathbf{r}-\mathbf{r}')}}{(k^2 - k_0^2)} \mathrm{d}^n k. \tag{A.3}$$

Note that the integral in (A.3) is ill defined if k is real. Thus we need to modify it slightly by letting $k_0 \to (k_0 + \imath\epsilon)$ where k_0, and ϵ are both real and positive. Now let $\epsilon \to 0$ to obtain

$$G_0(\mathbf{r}, \mathbf{r}'; k_0) = \frac{1}{(2\pi)^n} \lim_{\epsilon \to 0} \int_{\mathbb{R}^n} \frac{e^{\imath \mathbf{k}(\mathbf{r}-\mathbf{r}')}}{[k^2 - (k_0 + \imath\epsilon)^2]} \mathrm{d}^n k. \tag{A.4}$$

We shall deal with equation (A.4) in one, two and three dimensions to obtain the Green function in each space [3, 134]. At first let us start with the one-dimensional case,

$$G_0(x,x';k_0)=\frac{1}{2\pi}\lim_{\epsilon\to 0}\int_{-\infty}^{\infty}\mathrm{d}k\frac{e^{\imath k(x-x')}}{[k+(k_0+\imath\epsilon)][k-(k_0+\imath\epsilon)]} \tag{A.5}$$

The integrand has poles at $k=\pm(k_0+\imath\epsilon)$, therefore, the contour must be closed in the upper (lower) half complex plane for $(x-x')\geqslant 0\,((x-x')\leqslant 0)$ respectively. By using the theory of residues, one obtains,

$$G_0(x,x';k_0)=\frac{1}{2\pi}\left[(2\pi\imath)\frac{e^{\imath k_0(x-x')}}{2k_0}\theta(x-x')+(-2\pi\imath)\frac{e^{-\imath k_0(x-x')}}{-2k_0}\theta(x'-x)\right]. \tag{A.6}$$

where $\theta(x-x')$ is the unit step-function, also it is called the Heaviside function, and defined as

$$\theta(x-x')=\begin{cases}1, & \text{if } x>x';\\ 0, & \text{if } x<x'.\end{cases}$$

It can be denoted as $H(x-x')$.

The minus sign in the second term in equation (A.6) refers to the negative direction of the contour in the lower half-plane, thus

$$G_0(x,x';k_0)=\frac{\imath}{2k_0}e^{\imath k_0|x-x'|}. \tag{A.7}$$

This is the free-space Green function of the scalar Helmholtz equation in one dimension.

Secondly, we will deal with equation (A.3) in two dimensions, that is

$$G_0(\mathbf{r},\mathbf{r}';k_0)=\frac{1}{(2\pi)^2}\lim_{\epsilon\to 0}\int_{\mathbb{R}^2}\mathrm{d}^2k\frac{e^{\imath\mathbf{k}(\mathbf{r}-\mathbf{r}')}}{[k^2-(k_0+\imath\epsilon)^2]}. \tag{A.8}$$

It is convenient to turn to the polar coordinates, one has

$$G_0(\mathbf{r},\mathbf{r}';k_0)=\frac{1}{(2\pi)^2}\lim_{\epsilon\to 0}\int_0^{\infty}\mathrm{d}k\int_0^{2\pi}\mathrm{d}\theta\frac{ke^{\imath k|\mathbf{r}-\mathbf{r}'|(\cos\theta\cos\phi+\sin\theta\sin\phi)}}{[k^2-(k_0+\imath\epsilon)^2]} \tag{A.9}$$

where $\mathbf{k}=(k\cos\theta,k\sin\theta)$, and

$$(\mathbf{r}-\mathbf{r}')=(|\mathbf{r}-\mathbf{r}'|\cos\phi,|\mathbf{r}-\mathbf{r}'|\sin\phi),$$

and

$$|\mathbf{r}-\mathbf{r}'| = \sqrt{(x-x')^2+(y-y')^2}$$

is the distance between the source $\mathbf{r}'$ and the observation point $\mathbf{r}$, with $\mathbf{r} \neq \mathbf{r}'$. The Jacobian of the transformation is $|J| = k$.

Equation (A.9) needs to be rearranged using a convenient trigonometric relation, that is,

$$G_0(\mathbf{r},\mathbf{r}';k_0) = \frac{1}{(2\pi)^2}\lim_{\epsilon\to 0}\int_0^\infty \mathrm{d}k \int_0^{2\pi} \mathrm{d}\theta \frac{k e^{\imath k|\mathbf{r}-\mathbf{r}'|\cos(\theta-\phi)}}{[k^2-(k_0+\imath\epsilon)^2]} d\theta dk. \tag{A.10}$$

Recall the following integral representation of the zeroth-order Bessel function of $J_0(z)$ [125],

$$J_0(z) = \frac{1}{(2\pi)}\lim_{\epsilon\to 0}\int_0^{2\pi} e^{\imath kz\cos(\theta-\phi)}\mathrm{d}\theta \tag{A.11}$$

where ϕ is a constant. Plugging equation (A.11) into equation (A.10), one has

$$G_0(\mathbf{r},\mathbf{r}';k_0) = \frac{1}{2\pi}\int_0^\infty \frac{kJ_0(k|\mathbf{r}-\mathbf{r}'|)}{[k^2-(k_0+\imath\epsilon)^2]}\mathrm{d}k. \tag{A.12}$$

For the RHS of this equation, one needs to use the integral representation of the Hankel function [125] as,

$$G_0(\mathbf{r},\mathbf{r}';k_0) = \frac{\imath}{4}H_0^{(1)}(k_0|\mathbf{r}-\mathbf{r}'|), \tag{A.13}$$

where $H_0^{(1)}(k_0|\mathbf{r}-\mathbf{r}'|)$ denotes the zeroth-order Hankel function of the first kind. Equation (A.13) is the free-space Green function for the Helmholtz equation in two-dimensions.

Finally, we shall deal with equation (A.3) in three dimensions ,

$$G_0(\mathbf{r},\mathbf{r}';k_0) = \frac{1}{(2\pi)^3}\lim_{\epsilon\to 0}\int_{\mathbb{R}^3} \mathrm{d}^3k \frac{e^{\imath\mathbf{k}(\mathbf{r}-\mathbf{r}')}}{[k^2-(k_0+\imath\epsilon)^2]}. \tag{A.14}$$

In three dimensions, it is convenient to turn to spherical polar coordinates (k,ϕ,θ). The Jacobian of the transformation is,

$$|\ J| = k^2\sin\theta,$$

and one has

$$\begin{aligned} G_0(\mathbf{r},\mathbf{r}';k_0) &= \frac{1}{(2\pi)^3}\lim_{\epsilon\to 0}\int_0^\infty \frac{k^2\mathrm{d}k}{[k^2-(k_0+\imath\epsilon)^2]}\int_0^{2\pi}\mathrm{d}\phi\int_{-1}^{1}\mathrm{d}(\cos\theta)e^{\imath k|\mathbf{r}-\mathbf{r}'|\cos\theta} \\ &= \frac{1}{(2\pi)^3}\lim_{\epsilon\to 0}\int_0^\infty \frac{k^2\mathrm{d}k}{[k^2-(k_0+\imath\epsilon)^2]}2\pi\frac{\left[e^{\imath k|\mathbf{r}-\mathbf{r}'|}-e^{-\imath k|\mathbf{r}-\mathbf{r}'|}\right]}{\imath k\mid\mathbf{r}-\mathbf{r}'\mid}. \end{aligned}$$

Since the integrand is an even function in k, one has,

$$G_0(\mathbf{r},\mathbf{r}';k_0)=\frac{1}{2}\frac{2\pi}{\mid\mathbf{r}-\mathbf{r}'\mid(2\pi)^3}\lim_{\epsilon\to 0}\int_{-\infty}^{\infty}\mathrm{d}k\frac{k\left[e^{\imath k|\mathbf{r}-\mathbf{r}'|}-e^{-\imath k|\mathbf{r}-\mathbf{r}'|}\right]}{\imath[k^2-(k_0+\imath\epsilon)^2]}.$$

This integrand has poles at the values $k=\pm(k_0+\imath\epsilon)$, therefore, $e^{\pm\imath k|\mathbf{r}-\mathbf{r}'|}$ gives a contribution in the upper (lower) half complex plane, respectively.
Finally, one needs to employ Cauchy residues theory,

$$G_0(\mathbf{r},\mathbf{r}';k_0)=\frac{1}{2}\frac{2\pi}{(2\pi)^3}\frac{1}{\imath\mid\mathbf{r}-\mathbf{r}'\mid}\left[(2\pi\imath)\frac{e^{\imath k_0|\mathbf{r}-\mathbf{r}'|}}{2}\theta(\mathbf{r}-\mathbf{r}')-(-2\pi\imath)\frac{e^{\imath k_0|\mathbf{r}-\mathbf{r}'|}}{2}\theta(\mathbf{r}-\mathbf{r}')\right].$$

The minus sign in the second term refers to the negative direction of the contour in the lower half-plane. Therefore, we obtain the free-space Green function of Helmholtz equation in three dimensions as

$$G_0(\mathbf{r},\mathbf{r}';k_0)=\frac{e^{\imath k_0|\mathbf{r}-\mathbf{r}'|}}{4\pi\mid\mathbf{r}-\mathbf{r}'\mid}. \tag{A.15}$$

Appendix B

The Green function of a bounded system

The Green function is a solution of a differential equation, which is homogeneous everywhere except at one point. If this point lies on the boundary, the Green function is said to satisfy inhomogeneous boundary conditions, and vice versa. The Green function, corresponding to a linear, Hermitian operator $L(\mathbf{r})$ is defined as a solution of the equation

$$LG(\mathbf{r}, \mathbf{r}') = \delta(\mathbf{r} - \mathbf{r}'),$$

where $\mathbf{r}$ and $\mathbf{r}'$ are the source and the receiver points, respectively, and $\delta(\mathbf{r} - \mathbf{r}')$ is the Dirac delta distribution.

The Green function of a bounded system can be constructed from the eigenfunctions ϕ_n of a Hermitian operator L. Let us begin with the eigenvalue value problem,

$$L\phi_n(\mathbf{r}) = \lambda_n \phi_n(\mathbf{r}). \tag{B.1}$$

where $\{\phi_n\}$ is a complete set of eigenfunctions $\phi_n(\mathbf{r})$, and λ_n are the eigenvalues. The functions $\{\phi_n\}$ form an orthonormal set, that is,

$$\int \phi_n(\mathbf{r}) \phi_m^*(\mathbf{r}) \mathrm{d}\mathbf{r} = \delta_{nm}. \tag{B.2}$$

Here, δ_{nm} is the Kronecker delta symbol defined as

$$\delta_{nm} \equiv \begin{cases} 1, & \text{if } n = m; \\ 0, & \text{if } n \neq m. \end{cases}$$

Furthermore, these functions $\{\phi_n\}$ form a complete basis set in such a manner that

$$\sum_{n=0}^{\infty} \phi_n(\mathbf{r})\phi_n^*(\mathbf{r}') = \delta(\mathbf{r} - \mathbf{r}'). \tag{B.3}$$

This property is known as the closure property. Each eigenvalue λ_n has a number of corresponding linearly independent eigenfunctions $\{\phi_n\}$. This number is called the multiplicity of the eigenvalue. It is possible to form a linear combination of the eigenfunctions $\{\phi_n\}$, which are mutually orthogonal. Let us construct the Green function from the eigenfunctions of the Helmholtz equation given as,

$$\Delta\phi_n = -k_n^2\phi_n \tag{B.4}$$

where $\Delta = \text{div(grad)}$ is the Laplace operator. The corresponding Green function satisfies the equation,

$$(\Delta_{\mathbf{r}} + k^2)G(\mathbf{r}, \mathbf{r}') = -\delta(\mathbf{r} - \mathbf{r}'). \tag{B.5}$$

Now one needs to employ the fact that $\{\phi_n\}$ is a complete set, hence we can represent $G(\mathbf{r}, \mathbf{r}')$ as a function of $\mathbf{r}$ in the following form

$$G(\mathbf{r}, \mathbf{r}') = \sum_{m=0}^{\infty} A_m(\mathbf{r}')\phi_m(\mathbf{r}). \tag{B.6}$$

This representation still obeys the boundary conditions, since the set $\{\phi_n\}$ do. Plugging (B.6) and (B.4) into (B.5), one has

$$\sum_{m=0}^{\infty} (k^2 - k_m^2)A_m(\mathbf{r}')\phi_m(\mathbf{r}) = -\delta(\mathbf{r} - \mathbf{r}'). \tag{B.7}$$

Now one needs to multiply both sides of equation (B.7) by $\phi_n^*(\mathbf{r})$, then integrate over the domain, one has,

$$\sum_{m=0}^{\infty} (k^2 - k_m^2)A_m(\mathbf{r}') \int_{-\infty}^{\infty} \phi_m(\mathbf{r})\phi_n^*(\mathbf{r})d\mathbf{r} = -\int_{-\infty}^{\infty} \phi_n^*(\mathbf{r})\delta(\mathbf{r} - \mathbf{r}')d\mathbf{r} \tag{B.8}$$

Then, one needs to call the orthonormality property (B.2) for the LHS of equation (B.7), whereas for the RHS, one needs to use the following property of the delta function,

$$\int_{-\infty}^{\infty} f(\mathbf{r})\delta(\mathbf{r}-a)d\mathbf{r} = f(a).$$

Hence,

$$A_n(\mathbf{r}') = \frac{-\phi_n^*(\mathbf{r}')}{(k^2-k_n^2)}.$$

Thus, $G(\mathbf{r},\mathbf{r}')$ can be written as,

$$G(\mathbf{r},\mathbf{r}';k) = -\sum_{n=0}^{\infty} \frac{\phi_n(\mathbf{r})\phi_n^*(\mathbf{r}')}{(k^2-k_n^2)}. \tag{B.9}$$

The Green function $G(\mathbf{r},\mathbf{r}';k)$ exhibits simple poles at the values $k \to \pm k_n$. This singularity happen when a non-dissipative vibrating system is driven at one of its resonant frequencies thus giving an infinite response [135].

Appendix C

Expression for the hypersingular integrand

In this appendix, an expression of the second derivative of the free Green function (hypersingular integrand) is derived. Such an expression decomposes the hypersingular integrand into a weakly singular and regular parts.

Here we do not perform the limit of $\frac{\partial^2 G_0(\mathbf{r},q)}{\partial n_\beta \partial n_q}$ as the interior point $\mathbf{r}$ approaching a boundary point β, so we adopt the notations where β and q stand for both the parametrisation of the boundary and the vector representing the point in 2D on the boundary.

The notations $\mathbf{r}(q)$ and $\mathbf{r}(\beta)$ are the position vectors at the boundary points q and β, respectively. We differentiate with respect to β for fixed distance $|\mathbf{r}(\beta) - \mathbf{r}(q)|$ and vary the distance $|\mathbf{r} - \mathbf{r}(\beta)|$. In the derivation below, we frequently use the following relation,

$$|\mathbf{r} - \mathbf{r}(q)|^2 = |\mathbf{r} - \mathbf{r}(\beta)|^2 + |\mathbf{r}(\beta) - \mathbf{r}(q)|^2 . \tag{C.1}$$

which can be abbreviated as,

$$\rho^2 = \Delta^2 \mathbf{r} + \sigma^2, \tag{C.2}$$

where ρ is the distance between the interior point $\mathbf{r}$ and the boundary point q, σ

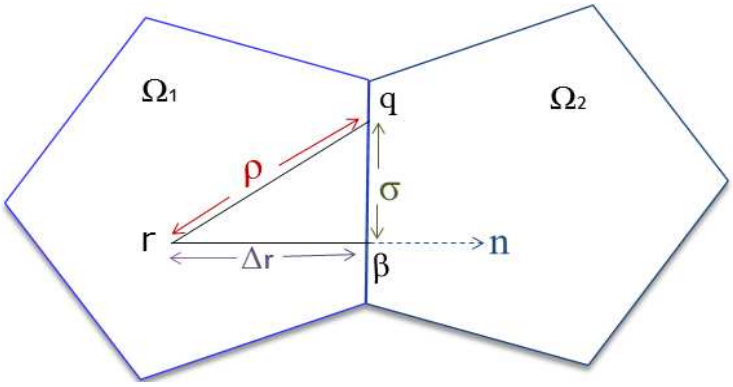

Figure C.1: Geometrical illustration of an interior point $\mathbf{r}$ approaching a boundary point $\beta \in \partial\Omega$, $\rho = |\mathbf{r} - \mathbf{r}(q)|$, $\sigma = |\mathbf{r}(\beta) - \mathbf{r}(q)|$ and $\Delta\mathbf{r} = |\mathbf{r} - \mathbf{r}(\beta)|$.

is the distance between the boundary point q and the boundary point β, and $\Delta\mathbf{r}$ is the distance between the interior point $\mathbf{r}$ and the boundary point β as depicted in figure C.1.

The second derivative of the free Green function is obtained as,

$$\begin{aligned}\frac{\partial^2 G_0}{\partial n_\beta \partial n_q} &= \frac{\partial}{\partial n_\beta}\left[G_0' \frac{\partial}{\partial n_q}\left(k\sqrt{[\mathbf{r}-\mathbf{r}(q)]^2}\right)\right] \\ &= G_0'' \frac{\partial}{\partial n_q}\left(k\sqrt{[\mathbf{r}-\mathbf{r}(q)]^2}\right) \\ &+ G_0' \frac{\partial^2}{\partial n_\beta \partial n_q}\left(k\sqrt{[\mathbf{r}-\mathbf{r}(q)]^2}\right). \end{aligned} \tag{C.3}$$

The derivative of the argument of G_0 obtained as

$$\begin{aligned}\frac{\partial}{\partial n_\beta}\left(k\sqrt{[\mathbf{r}-\mathbf{r}(q)]^2}\right) &= \frac{-2k\,|\mathbf{r}-\mathbf{r}(\beta)|}{2\sqrt{[\mathbf{r}-\mathbf{r}(q)]^2}} \\ &= -k\frac{|\mathbf{r}-\mathbf{r}(\beta)|}{|\mathbf{r}-\mathbf{r}(q)|} \\ &= -k\frac{\Delta\mathbf{r}}{\rho}, \end{aligned} \tag{C.4}$$

and similarly one has

$$\frac{\partial}{\partial n_q}\left(k\sqrt{[\mathbf{r}-\mathbf{r}(q)]^2}\right) = k\frac{\Delta\mathbf{r}}{\rho}. \tag{C.5}$$

For the second derivative of the argument of G_0, we have

$$\begin{aligned}
\frac{\partial^2}{\partial n_\beta \partial n_q}\left(k\sqrt{[\mathbf{r}-\mathbf{r}(q)]^2}\right) &= k\frac{\partial}{\partial n_\beta}\left[\frac{|\mathbf{r}-\mathbf{r}(\beta)|}{|\mathbf{r}-\mathbf{r}(q)|}\right] \\
&= k\left[\frac{\sqrt{[\mathbf{r}-\mathbf{r}(q)]^2}\cdot\frac{1}{2}\left([\mathbf{r}-\mathbf{r}(\beta)]^2\right)^{-\frac{1}{2}}\cdot -2\,|\mathbf{r}-\mathbf{r}(\beta)|}{[\mathbf{r}-\mathbf{r}(q)]^2}\right. \\
&\quad \left. -\frac{\sqrt{[\mathbf{r}-\mathbf{r}(\beta)]^2}\cdot\frac{1}{2}\left([\mathbf{r}-\mathbf{r}(q)]^2\right)^{-\frac{1}{2}}\cdot -2\,|\mathbf{r}-\mathbf{r}(\beta)|}{[\mathbf{r}-\mathbf{r}(q)]^2}\right] \\
&= k\left[\frac{-\sqrt{[\mathbf{r}-\mathbf{r}(q)]^2}+|\mathbf{r}-\mathbf{r}(\beta)|^2\left([\mathbf{r}-\mathbf{r}(q)]^2\right)^{-\frac{1}{2}}}{[\mathbf{r}-\mathbf{r}(q)]^2}\right] \\
&= -k\frac{|\mathbf{r}(\beta)-\mathbf{r}(q)|^2}{|\mathbf{r}-\mathbf{r}(q)|^3} \\
&= -\frac{k\sigma^2}{\rho^3}.
\end{aligned} \tag{C.6}$$

Substituting (C.6), (C.4) and (C.5) into (D.1), leads to

$$\begin{aligned}
\frac{\partial^2 G_0}{\partial n_\beta \partial n_q} &= \frac{\imath}{4}\left\{\left[-H_0^{(1)}(k\rho)+\frac{H_1^{(1)}(k\rho)}{k\rho}\right]\cdot\left(-k^2\frac{\Delta^2\mathbf{r}}{\rho^2}\right)-H_1^{(1)}(k\rho)\cdot\left(-k\frac{\sigma^2}{\rho^3}\right)\right\} \\
&= \frac{\imath}{4}\left\{k^2H_0^{(1)}(k\rho)\frac{\Delta^2\mathbf{r}}{\rho^2}+kH_1^{(1)}(k\rho)\left[-\frac{\Delta^2\mathbf{r}}{\rho^3}+\frac{\sigma^2}{\rho^3}\right]\right\},
\end{aligned} \tag{C.7}$$

where we used

$$G_0'' = \left[-H_0^{(1)}(k\rho)+\frac{1}{k\rho}H_1^{(1)}(k\rho)\right]\frac{\partial}{\partial q}(k\rho).$$

Using the relation (C.2), equation (C.7) can be rearranged as,

$$\begin{aligned}
\frac{\partial^2 G_0(\beta,q)}{\partial n_\beta \partial n_q} &= \frac{\imath}{4}\left\{\frac{k}{\rho}\left(1-2\frac{\Delta^2\mathbf{r}}{\rho^2}\right)H_1^{(1)}(k\rho)+k^2\frac{\Delta^2\mathbf{r}}{\rho^2}H_0^{(1)}(k\rho)\right. \\
&= \frac{\imath}{4}\left\{\frac{k}{\rho}\left(1-2\frac{\Delta^2\mathbf{r}}{\rho^2}\right)H_1^{(1)}(k\rho)-k^2\frac{\sigma^2}{\rho^2}H_0^{(1)}(k\rho)\right\} \\
&+ \frac{\imath k^2}{4}H_0^{(1)}(k\rho).
\end{aligned} \tag{C.8}$$

For simplicity, we set $\beta = 0$, that is, the distance $\sigma = q$, now consider

$$\begin{aligned} -\frac{\mathrm{d}}{\mathrm{d}q}\left[\frac{k\sigma}{\rho}H_1^{(1)}(k\rho)\right] &= \frac{-k}{\rho}H_1^{(1)}(k\rho) + k\frac{\sigma^2}{\rho^3}H_1^{(1)}(k\rho) - \frac{k\sigma}{\rho}\frac{\mathrm{d}}{\mathrm{d}q}H_1^{(1)}(k\rho) \\ &= \frac{-k}{\rho}H_1^{(1)}(k\rho) + \frac{k\sigma^2}{\rho^3}H_1^{(1)}(k\rho) + \frac{k^2\sigma^2}{\rho^2}[-H_0^{(1)}(k\rho) + \frac{1}{k\rho}H_1^{(1)}(k\rho)] \\ &= -\frac{k}{\rho}\left[1 - 2\frac{(\rho^2 - \Delta^2\mathbf{r})}{\rho^2}\right]H_1^{(1)}(k\rho) - k^2\frac{\sigma^2}{\rho^2}H_0^{(1)}(k\rho) \\ &= \frac{k}{\rho}\left[1 - 2\frac{\Delta^2\mathbf{r}}{\sigma^2}\right]H_1^{(1)}(k\rho) - k^2\frac{\sigma^2}{\rho^2}H_0^{(1)}(k\rho), \end{aligned} \tag{C.9}$$

Comparing equation (C.8) with equation (C.9), one has,

$$\frac{\partial^2 G_0}{\partial n_\beta \partial n_q} = -\frac{\imath}{4}\left\{\frac{\mathrm{d}}{\mathrm{d}q}\left[\frac{k\sigma}{\rho}H_1^{(1)}(k\rho)\right] + k^2 H_0^{(1)}(k\rho)\right\}. \tag{C.10}$$

Thus the hypersingular integrand is decomposed into a convenient form which is handy for numerical implementation.

Appendix D

The second derivative of G_0

In §4.8 we obtained the BIEs (4.8.1) and (4.8.2) which contain the second derivative of the free Green function $G_0(q,\beta;k)$ where the boundary points $q \neq \beta$. In this appendix, we obtain the second derivative of $G_0(k\rho)$ for $\rho = |q-\beta| \neq 0$. We begin with the second derivative of $H_0^{(1)}(k\rho)$ as

$$\begin{aligned}
\frac{\partial^2 H_0^{(1)}(k\rho)}{\partial n_\beta \partial n_q} &= k^2 \frac{\partial \rho}{\partial n_\beta}\frac{\partial \rho}{\partial n_q}\left(H_0^{(1)}\right)''(k\rho) + k\frac{\partial^2 \rho}{\partial n_\beta \partial n_q}\left(H_0^{(1)}\right)'(k\rho) \\
&= k^2\left[\frac{1}{k\rho}H_1^{(1)}(k\rho) - H_0^{(1)}(k\rho)\right]\frac{\partial \rho}{\partial n_\beta}\frac{\partial \rho}{\partial n_q} - k\frac{\partial^2 \rho}{\partial n_\beta \partial n_q}H_1^{(1)}(k\rho) \\
&= -k^2\frac{\partial \rho}{\partial n_\beta}\frac{\partial \rho}{\partial n_q}H_0^{(1)} + k\left[\frac{1}{\rho}\frac{\partial \rho}{\partial n_\beta}\frac{\partial \rho}{\partial n_q} - \frac{\partial^2 \rho}{\partial n_\beta \partial n_q}\right]H_1^{(1)}. \qquad \text{(D.1)}
\end{aligned}$$

The derivative of the argument ρ is obtained as,

$$\frac{\partial \rho}{\partial n_q} = \vec{n}_q \cdot \nabla \boldsymbol{\rho} = \cos\theta_q, \qquad \text{(D.2)}$$

and

$$\frac{\partial \rho}{\partial n_\beta} = \vec{n}_\beta \cdot \nabla \boldsymbol{\rho} = -\cos\theta_\beta, \qquad \text{(D.3)}$$

where $\vec{n}_q$, and $\vec{n}_\beta$ are the normal at the boundary points q and β as illustrated in figure D.1.

We now need to insert equations (D.2) and (D.3) into equation (D.1), one has

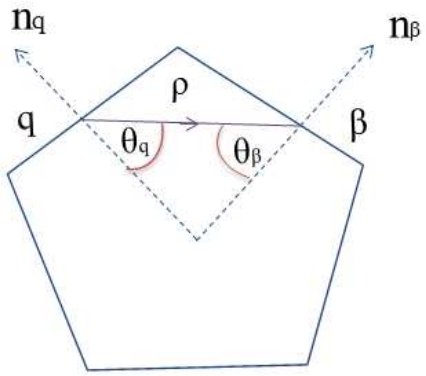

Figure D.1: Sketch of the boundary points q and β.

$$\begin{aligned}
\frac{\partial^2 G_0(k\rho)}{\partial n_\beta \partial n_q} &= \frac{\imath}{4}\left\{k^2(\hat{n}_\beta\cdot\hat{\rho})(\hat{n}_q\cdot\hat{\rho})H_0^{(1)}(k\rho)\right. \\
&+ \left.\frac{k}{\rho}\left[(\hat{n}_q\cdot\hat{n}_\beta)-2(\hat{n}_\beta\cdot\hat{\rho})(\hat{n}_q\cdot\hat{\rho})\right]H_1^{(1)}(k\rho)\right\} \\
&= \frac{\imath}{4}\left\{-k^2\cos\theta_q\cos\theta_\beta H_0^{(1)}(k\rho)\right. \\
&+ \left.\frac{k}{\rho}\left[\cos\theta_\beta\cos\theta_q+\sin\theta_\beta\sin\theta_q\right]H_1^{(1)}(k\rho)\right\} \\
&= \frac{\imath}{4}\left\{-k^2\cos\theta_\beta\cos\theta_q H_0^{(1)}(k\rho)+\frac{k}{\rho}\cos(\theta_q-\theta_\beta)H_1^{(1)}(k\rho)\right\},
\end{aligned}$$

where θ_β is the angle between the chord connecting q to β and the normal at the boundary point β, and similarly for θ_q as depicted in figure D.1.

Appendix E

Commutators acting on a wavefunction

For the derivation of the reflection operator for the unit disc presented in Chapter 5, we consider the commutator contributions in the derivation of the exact reflection operator in §5.6.1, whereas we neglect such contributions in the derivation of the semiclassical reflection operator in §5.6.2. Here in this Appendix, we will work out this contribution from the commutators of a function $F(p)$ with the characteristic function χ. The derivation presented in this section is borrowed from private notes written by Gregor Tanner. The commutator is defined as,

$$[F(p), \chi] \mid \psi >= (F\chi) \mid \psi > -(\chi F) \mid \psi > . \tag{E.1}$$

The characteristic function χ is defined as

$$(\chi\phi)(s) = H(s)\phi(s)$$

where H is the Heaviside step function defined as

$$H(s)\phi(s) = \begin{cases} \phi(s), & \text{if } s > 0, \\ \frac{1}{2}\phi(0), & \text{if } s = 0, \\ 0, & \text{s<0.} \end{cases} \tag{E.2}$$

The commutator (E.1) as a function of s is given as

$$\begin{aligned} < s \mid [F,\chi] \mid \psi > &= < s \mid F\chi \mid \psi > - < s \mid \chi F \mid \psi > \\ &= \int F(s',s'')\mathrm{d}s' \int \chi_(s',s'')\psi(s'')\mathrm{d}s'' \\ &- \int \chi_(s,s')\mathrm{d}s' \int F(s',s'')\psi(s'')\mathrm{d}s'' \\ &= \int F(s,s')H(s')\psi(s')\mathrm{d}s' - H(s)\int F(s,s')\psi(s')\mathrm{d}s'. \end{aligned}$$

Define,

$$G(s) = \int F(s,s')\psi(s')\mathrm{d}s'. \tag{E.3}$$

Thus,

$$< s \mid \chi F \mid \psi >= H(s)G(s). \tag{E.4}$$

For $< s \mid F\chi \mid \psi >$, we have,

$$< s \mid \chi \mid \psi >= H(s)\psi(s),$$

this can be written in momentum space as,

$$\begin{aligned} < p \mid \chi \mid \psi > &= < p \mid \tilde{H}\tilde{\psi} > \\ &= \frac{k}{2\pi}(\tilde{H} * \tilde{\psi})(p) \\ &= \frac{k}{2\pi}\int_{-\infty}^{\infty} \tilde{H}(p-q)\tilde{\psi}(q)\mathrm{d}q. \end{aligned} \tag{E.5}$$

where we assumed that $F(p)$ is diagonal in momentum space, and we used the convolution theorem. The functions $\tilde{H}$ and $\tilde{\psi}$ are respectively the Fourier transform of the functions H and ψ. The Fourier transform of the Heaviside step function H is given as [125],

$$\tilde{H}(p) = \frac{1}{\imath kp} + \frac{\pi}{k}\delta(p). \tag{E.6}$$

Substituting equation (E.6) into equation (E.5) leads to,

$$< p \mid \chi \mid \psi >= \frac{1}{2}\tilde{\psi}(p) + \frac{1}{2\pi\imath}\int_{-\infty}^{\infty} \frac{\tilde{\psi}(q)}{p-q}\mathrm{d}q. \tag{E.7}$$

So, one has,

$$\begin{aligned} < p \mid F\chi \mid \psi > &= \int \mathrm{d}p' < p \mid F\chi \mid \psi > \\ &= \int \mathrm{d}p' < p \mid F \mid p' >< p' \mid \chi \mid \psi > \\ &= \int \mathrm{d}p' F(p,p') < p' \mid \chi \mid \psi >, \end{aligned} \tag{E.8}$$

where we used $\mid p' >< p' \mid = I$. Now substitute equation (E.7) into equation (E.8) to obtain,

$$< p \mid F\chi \mid \psi >= \frac{1}{2}F(p)\tilde{\psi}(p) + \frac{1}{2\pi\imath}\int_{-\infty}^{\infty}\frac{F(p)\tilde{\psi}(q)}{p-q}\mathrm{d}q. \tag{E.9}$$

Taking the inverse Fourier transform of equation (E.9), leads to,

$$\begin{aligned} < s \mid F\chi \mid \psi > &= \frac{1}{2}\frac{k}{2\pi}\int_{-\infty}^{\infty}F(p)\tilde{\psi}(p)e^{\imath ksp}\mathrm{d}p \\ &+ \frac{k}{2\pi}\frac{1}{2\pi\imath}\int_{-\infty}^{\infty}\int_{-\infty}^{\infty}\frac{F(p)\tilde{\psi}(q)}{p-q}e^{\imath ksp}\mathrm{d}p\mathrm{d}q = \frac{G(s)}{2} \\ &+ \frac{k}{2\pi}\frac{1}{2\pi\imath}\int_{-\infty}^{\infty}\int_{-\infty}^{\infty}\frac{F(p)\tilde{\psi}(q)}{p-q}e^{\imath ksp}\mathrm{d}p\mathrm{d}q. \end{aligned} \tag{E.10}$$

Hence, adding equation (E.4) to equation (E.10), one obtains the commutator in position representation as,

$$< s \mid [F,\chi] \mid \psi >= \left(\frac{1}{2} - H(s)\right)G(s) + \frac{k}{2\pi}\frac{1}{2\pi\imath}\int_{-\infty}^{\infty}\int_{-\infty}^{\infty}\frac{F(p)\tilde{\psi}(q)}{p-q}e^{\imath ksp}\mathrm{d}p\mathrm{d}q. \tag{E.11}$$

For convenience, let us introduce the following notation

$$C(s) = \frac{k}{2\pi}\frac{1}{2\pi\imath}\int_{-\infty}^{\infty}\tilde{\psi}(q)\mathrm{d}q\int_{-\infty}^{\infty}\frac{F(p)}{p-q}e^{\imath ksp}\mathrm{d}p. \tag{E.12}$$

Equation E.11 express the commutator for any function $F(p)$ with the characteristic function.

First we assume that $F(p)$ is an analytic function, so the integral with respect to p can be done by the residues Cauchy theorem. Then using equation

(E.2) one obtains,

$$C(s) = \begin{cases} \frac{1}{2}G(s), & \text{if } s > 0, \\ -\frac{1}{2}G(s), & \text{if } s < 0, \\ \frac{k}{2\pi}\frac{1}{2\pi\imath}\int_{-\infty}^{\infty}\tilde{\psi}(q)\mathrm{d}q\int_{-\infty}^{\infty}\frac{F(p)}{p-q}\mathrm{d}p, & \text{s=0.} \end{cases} \tag{E.13}$$

Thus, if $F(p)$ analytic, we have

$$< s \mid [F,\chi] \mid \psi >= \left(\frac{1}{2} - H(s)\right)G(s) + C(s) = \begin{cases} 0, & \text{if } s \neq 0; \\ C(0), & \text{if } s = 0; \end{cases} \tag{E.14}$$

this means that the commutator $< s \mid [F,\chi] \mid \psi >$ has a localised contribution at $s = 0$.

We now consider the case where $F(p)$ is not analytic, therefore one needs to consider the contribution from poles and branch cuts. For instance, choose $F(p)$ as,

$$F(p) = (1-p^2)^{\frac{1}{4}} = (1-p)^{\frac{1}{4}}\cdot(1+p)^{\frac{1}{4}}.$$

This multivalued function has two branch points at $p = 1, -1$.

To make $F(p)$ a single-valued function, a branch cut must be made along $p = 1, -1$. For $s > 0 (s < 0)$, the integration contour will be in the upper (lower) half-plane, with a pole at $p = q$.

Here we consider the case $s > 0$, so we take the contribution from the branch cut at the branch point $p = 1$ and neglect the branch point at -1 which lies outside the integration contour. The branch cut at $p = 1$ runs along the y-axis from ∞ to 0 with $z = y^{\frac{1}{4}}e^{\imath\frac{3\pi}{8}}$ circling below the branch point $p = 1$, then runs from 0 to ∞ with $z = y^{\frac{1}{4}}e^{-\imath\frac{\pi}{8}}$ as depicted in figure E.1. For the case $s < 0$, the integration contour will be downward. One has

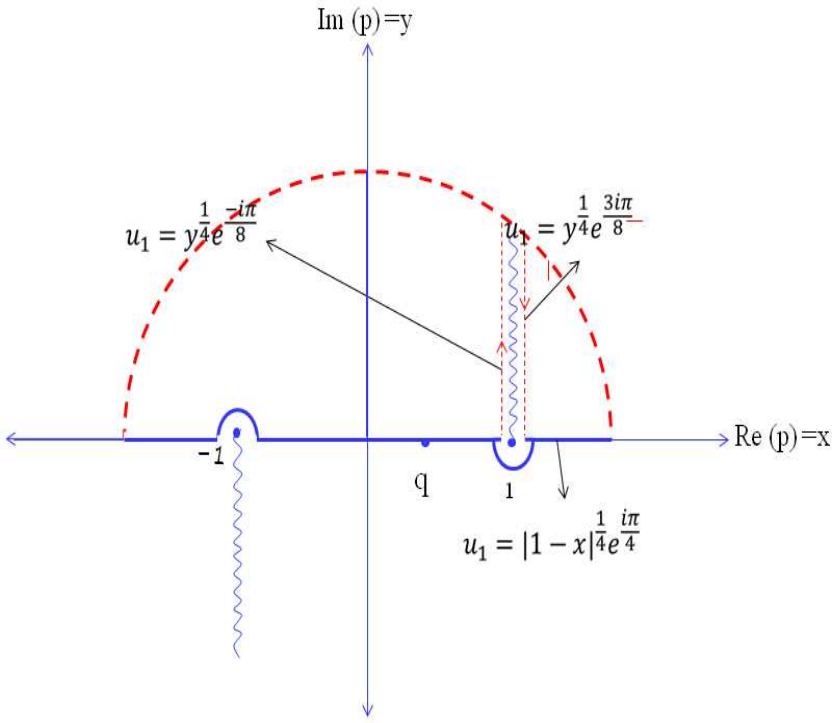

Figure E.1: The contour of the integral $\int_{-\infty}^{\infty} \frac{(1-p^2)^{\frac{1}{4}}}{p-q} e^{\imath ksp} \mathrm{d}p$.

$$
\begin{aligned}
\oint_{-\infty}^{\infty} F(p) \frac{e^{\imath ksp}}{p-q} \mathrm{d}p &= \oint_{-\infty}^{\infty} (1-p^2)^{\frac{1}{4}} \frac{e^{\imath ksp}}{p-q} \mathrm{d}p \\
&= \int_{-\infty}^{\infty} (1-p^2)^{\frac{1}{4}} \frac{e^{\imath ksp}}{p-q} \mathrm{d}p \\
&+ \imath e^{\imath \frac{3\pi}{8}} \int_{\infty}^{0} (y(2+\imath y))^{\frac{1}{4}} \frac{e^{\imath ks} e^{-ksy}}{(1+\imath y-q)} \mathrm{d}y \\
&+ \imath e^{-\imath \frac{\pi}{8}} \int_{0}^{\infty} (y(2+\imath y))^{\frac{1}{4}} \\
&\times \frac{e^{\imath ks} e^{-ksy}}{(1+\imath y-q)} \mathrm{d}y.
\end{aligned}
$$

The first term in the RHS of this equation can be computed from the residues

Cauchy theorem, one has,

$$\begin{aligned}\int_{-\infty}^{\infty}\frac{(1-p^2)^{\frac{1}{4}}}{p-q}e^{\imath ksp}\mathrm{d}p &= \imath\pi(1-q^2)^{\frac{1}{4}}e^{\imath ksq}\\ &- \imath e^{-\imath\frac{\pi}{8}}(\imath-e^{\imath\frac{\pi}{2}})e^{\imath ks}\\ &\times \int_0^{\infty}(y(2+\imath y))^{\frac{1}{4}}\frac{e^{-ksy}}{(1+\imath y-q)}\mathrm{d}y. \qquad \text{(E.15)}\end{aligned}$$

The first term of equation (E.15) represent the regular part, whereas the second term carries the contribution from the branch cuts. Plugging equation (E.15) into equation (E.12) will give the non-localised contribution, that is, for $s \neq 0$. Then plug the resulting expression into equation (E.14), one obtains,

$$\begin{aligned}< s \mid [(1-p^2)^{\frac{1}{4}}\chi] \mid \psi > &= \begin{cases}0, & \text{if } s\neq 0;\\ C(0), & \text{if } s=0;\end{cases} - \frac{k}{2\pi}\frac{(1-e^{\imath\frac{\pi}{2}})}{2\pi}e^{-\imath\frac{\pi}{8}}e^{\imath k|s|}\\ &\times \int_{-\infty}^{\infty}\tilde{\psi}(q)\mathrm{d}q\int_0^{\infty}(y(2+\imath y))^{\frac{1}{4}}\frac{e^{-k|s|y}}{(1+\imath y-q)}\mathrm{d}y\end{aligned}$$

In conclusion, it should be noted that the regular part is localised at $s=0$, where the contribution from branch cuts represent the non-localised contribution which is oscillatory around $s=0$.

Now let us estimate the order of the non-local contribution,

$$\begin{aligned}\int_0^{\infty}(y(2+\imath y))^{\frac{1}{4}}e^{-k|s|y}\mathrm{d}y\int_{-\infty}^{\infty}\frac{\tilde{\psi}(q)\mathrm{d}q}{(1+\imath y-q)} &= 2\pi\imath\int_0^{\infty}(y(2+\imath y))^{\frac{1}{4}}\tilde{\psi}(1+\imath y)e^{-k|s|y}\mathrm{d}y\\ &= 2\pi\imath\sum_{n=0}^{\infty}c_n\int_0^{\infty}y^{n+\frac{1}{4}}e^{-k|s|y}\mathrm{d}y\\ &= \frac{2\pi\imath}{k|s|}\Gamma\left(n+\frac{5}{4}\right)\sum_{n=0}^{\infty}c_n(k|s|)^{-\frac{1}{4}-n}\\ &\sim \frac{1}{k|s|}\frac{1}{(k|s|)^{\frac{1}{4}}} \qquad \text{(E.16)}\end{aligned}$$

where we assumed that,

$$(2+\imath y)^{\frac{1}{4}}\tilde{\psi}(1+\imath y)=\sum_n c_n y^n.$$

The resulting integral is Gamma function, we consider the first term of the summation $n=0$.

After inserting equation (E.16) into equation (E.12), the factor $\frac{1}{k}$ in equation (E.16) will be cancelled out by the prefactor of the integral in equation (E.12).

Therefore the order of the non-localised contribution of the commutators is estimated as $\frac{1}{k^{\frac{1}{4}}}$ which decays in the semiclassical limit $k \to \infty$.

We shall demonstrate an illustrative example for the commutator of the function $F(p) = \frac{1}{2\pi\imath}$ as,

$$[F(p), \chi](s, s') = \frac{k}{2\pi} \int \mathrm{d}p \mathrm{d}p' e^{\imath k p s} \left(\frac{1}{2\pi\imath} \right) e^{-\imath k p' s'} = \frac{1}{\imath k} \delta(s) \delta(s'). \tag{E.17}$$

This simple example demonstrates that the localised contribution of the commutators at the points $s = 0$ or $s' = 0$ has a delta function.

Appendix F

Asymptotic derivation of the reflection and transmission coefficients for coupled cavities

Here we present an asymptotic derivation of the reflection and transmission coefficients for coupled cavities of different material properties. Here, we asymptotically consider the interface where we have the discontinuous change of material properties as infinite line at $x = 0$. For the left and the right sides of the interface, we have the value of the wavenumber k and q, respectively, as depicted in figure F.1. The wavenumber in two dimensions has two components as,

$$\vec{k} = (k_x, k_y) = (k\cos\theta, k\sin\theta)$$

where

$$k = \sqrt{k_x^2 + k_y^2}.$$

We treat k_x dependent on k_y with k_y is the variable of the inverse Fourier transform.

The wave field in the left and right side of the infinite interface $u_1(k_x, x)$ and $u_2(q_x, x)$ respectively, can be decomposed as a superposition of all possible

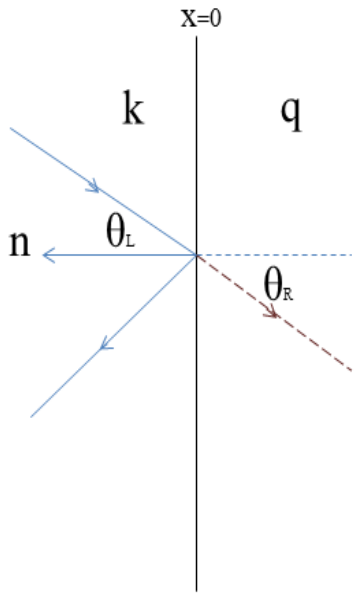

Figure F.1: Sketch of the discontinuity line at $x = 0$ separating two regions of different wavenumbers k and q.

plane waves incident on both sides of an infinite interface using the inverse Fourier transform as follows,

$$u_1(k_x, x) = A \int_{-\infty}^{\infty} [\psi_-(k_y) e^{\imath \sqrt{k^2 - k_y^2} x} + \psi_+(k_y) e^{-\imath \sqrt{k^2 - k_y^2} x}] e^{\imath k_y} \mathrm{d}k_y, \qquad x < 0, \tag{F.1}$$

where ψ_- and ψ_+ are the incoming and outgoing waves on the left side of the interface.

For the right side of the interface, one has

$$u_2(q_x, x) = A \int_{-\infty}^{\infty} [\phi_-(q_y) e^{\imath \sqrt{q^2 - q_y^2} x} + \phi_+(q_y) e^{-\imath \sqrt{q^2 - q_y^2} x}] e^{\imath q_y} \mathrm{d}q_y, \qquad x > 0, \tag{F.2}$$

where ϕ_- and ϕ_+ are the incoming and outgoing waves on the right side of the interface. Finally the constants A and B are there to guarantee the conversation of energy flux across the interface and so the obtained scattering matrix is unitary. They are chosen as

$$A = \sqrt{\frac{\rho_1}{k_x}}, \qquad B = \sqrt{\frac{\rho_2}{q_x}}.$$

The constants ρ_1 and ρ_2 are respectively the material densities in the left and the right side of the interface and related by equation (4.2.1). The infinite limits of the integral should not be a problem, because the wavefunction becomes evanescent at the limits ($k_y, q_y \to \pm\infty$), i.e, waves that are damped exponentially in the direction normal to the boundary. Semiclassically, there are no rays corresponding to the evanescent waves and they do not carry energy flux.

The plane wave representation of the wave field given in equation (F.1) is the basic foundation of Fourier optics, because when $x = 0$ the wavefunction simply becomes the Fourier transform. Along the interface, we have $k_y = q_y$, but $k_x \neq q_x$ simply because $k \neq q$. Equation (F.1) represents propagating or evanescent waves depending on whether ($k^2 > k_y^2$) or ($k^2 < k_y^2$), respectively.
Since $k_y = q_y$ along the interface, so the dependence of ψ_-, ψ_+, ϕ_-, and ϕ_+ on k_y will be suppressed hereafter.
Now we need to use the continuity conditions along the infinite interface at $x = 0$ given as

$$u_1(0) = u_2(0), \qquad \rho_2 \frac{\partial u_1}{\partial n_x}\bigg|_{x=0} = \rho_1 \frac{\partial u_2}{\partial n_x}\bigg|_{x=0}. \tag{F.3}$$

Applying the conditions (F.3) leads to the following two equations,

$$A\int_{-\infty}^{\infty}(\psi_- + \psi_+)e^{\imath k_y} = B\int_{-\infty}^{\infty}(\phi_- + \phi_+)e^{\imath q_y}, \tag{F.4}$$

and

$$\imath k_x \rho_2 A\int_{-\infty}^{\infty}(\psi_- + \psi_+)e^{\imath k_y} = \imath q_x \rho_1 B\int_{-\infty}^{\infty}(\phi_- + \phi_+)e^{\imath q_y}. \tag{F.5}$$

After some algebra, using equations (F.4) and (F.5) one obtains the following relation which maps the outgoing wavevector to the incoming wavevector,

$$\begin{bmatrix}\psi_+ \\ \psi_+\end{bmatrix} = \begin{bmatrix}\left(\frac{\alpha-\beta}{\alpha+\beta}\right) & \frac{2B\beta}{A(\alpha+\beta)} \\ \frac{2A\alpha}{B(\alpha+\beta)} & -\left(\frac{\alpha-\beta}{\alpha+\beta}\right)\end{bmatrix}\begin{bmatrix}\phi_- \\ \phi_-\end{bmatrix}, \tag{F.6}$$

where we used the notations $\alpha = \rho_2 k_x$, $\beta = \rho_1 q_x$.
This is called the scattering matrix with diagonal elements correspond to the reflection coefficients r obtained as,

$$r = \left(\frac{\alpha-\beta}{\alpha+\beta}\right) = \left(\frac{\rho_2 k\cos\theta_L - \rho_1 q\cos\theta_R}{\rho_2 k\cos\theta_L + \rho_1 q\cos\theta_R}\right). \tag{F.7}$$

The off-diagonal elements correspond to the transmission coefficients t obtained as,

$$t = \frac{2A\alpha}{B(\alpha+\beta)} = \left(\frac{2\sqrt{\rho_1 q \rho_2 k \cos\theta_L \cos\theta_R}}{\rho_2 k \cos\theta_L + \rho_1 q \cos\theta_R}\right). \tag{F.8}$$

where we substitute the x-component of k and q into the above relations. The angles θ_L and θ_R are the incident and refracted angles measured with respect to the normal to the discontinuity line and related by Snell's law ($k\sin\theta_R = q\sin\theta_L$) as depicted in figure F.1.

It should be noted that if we set $k = q$, that is $\rho_1 = \rho_2$ and $\cos\theta_L = \cos\theta_R$ in equations (F.7) and (F.8), then $r = 0$ and $t = 1$. This means that the ray will go straight as long as there is no change of material properties. The ray only bends once it encounters an abrupt change of material properties.

The matrix given in equation (F.6) is unitary. Also it has complex eigenvalues of module one. It should be pointed out that this derivation is asymptotic, because it treats the interface as infinite line, so it neglects diffraction effects coming from the end points of the interface. However, in the semiclassical limit such effects can be neglected.

References

[1] K.B. Wolf and G. Krotzsch. Geometry and dynamics in refracting systems. *Eur. J. Phy.*, **16**:14–20, 1995.

[2] R. Roshdi. A pioneer in anaclastics: Ibn sahl on burning mirrors and lenses. *Published by: The university of Chicago press on behalf of the history of science society*, **81**(3):464–491, 1990.

[3] E. Zauderer. *Partial differentail equations of applied mathematics.* John Wiley and Sons Inc, Canada, third edition, 2006.

[4] R. Courant. Variational methods for the solution of problems of equilibrium and vibration. *Bull. Am. Math. Soc.*, **49**:1–23, 1943.

[5] M.A. Jaswon. Integral equation methods in potential theory- I. *Proceedings of the Royal Society of London*, **A275**:23–32, 1963.

[6] G.T. Symm. Integral equation methods in potential theory- II. *Proceedings of the Royal Society of London*, **A275**:33–46, 1963.

[7] O.C. Zienkiewicz and R.L. Taylor. *The finite element method, volume I: Basic formulation and linear problems.* McGraw-Hill, New York, fourth edition, 1987.

[8] E.B. Bogomolny. Semiclassical quantization of multidimensional systems. *Nonlinearity*, **5**:805–866, 1992.

[9] G. Tanner and N. Søndergaard. Wave chaos in acoustics and elasticity. *Journal of Physics A: Mathematical and General*, **40**:R443–R509, 2007.

[10] P.A. Boasman. *Semiclassical accuracy for billiards*. PhD thesis, University of Bristol, 1992.

[11] M.C. Gutzwiller. Periodic orbits and classical quantization conditions. *J. Math. Phys.*, **12**:343–358, 1971.

[12] G. Tanner, D.J. Chappell, H. Ben Hamdin, S. Giani, C. Seidel, and F. Vogel. Acoustic energy distribution in multi-component structures-dynamical energy analysis versus numerically exact results. In *Proceedings of the International Conference on Noise and Vibration ISMA*, pages 2425–2436, Leuven, Belgium, 2010.

[13] H. Ben Hamdin and G. Tanner. Multi-component BEM for the Helmholtz equation - A normal derivative method. Accepted for publication in shock and vibration journal as special issue of the outcomes of ICEDyn 2011.

[14] O.C. Zienkiewicz and Y.K . Cheung. *The finite element method in Continuum and structural mechanics*. McGraw-Hill, New York, 1965.

[15] O.C. Zienkiewicz, R. L. Taylor, J. Z. Zhu, and P. Nithiarasu. *The finite element method - The three volume set*. Butterworth-Heinemann, sixth edition, 2005.

[16] O.C. Zienkiewicz and R.L. Taylor. *The finite element method, volume 2: Solid and fluid mechanics. Dynamics and non-linearity*. McGraw-Hill, New York, 1991.

[17] K.K. Gupta and J.L. Meek. A brief history of the beginning of the finite element method. *International Journal for numerical methods in engineering*, **39**:3761–3774, 1996.

[18] T. Oden. Some historic comments on finite elements. *Proceedings of the ACM conference on History of scientific and numeric computation, New York, USA*, 1987.

[19] A. Iserles. *A first course in the numerical analysis of differential equations, cambridge texts in applied mathematics*. Cambridge University Press, Cambridge, 1996.

[20] T. Eibner and J.M. Melenk. An adaptive strategy for hp-FEM based on testing for analyticity. *Comp. Mech.*, **39**:575–595, 2007.

[21] O.C. Zienkiewicz. The background of error estimation and adaptivity in finite element computations. *Computer Methods in Applied Mechanics and Engineering*, **195**:207–213, 2006.

[22] W. Reed and T. Hill. Discontinuous Galerkin method based on non-polynomial approximation spaces. Technical report, LA-UR-73-479, Los Alamos Scientific Laboratory, 1973.

[23] L. Yuan and C.W. Shu. Discontinuous Galerkin method based on non-polynomial approximation spaces. *Journal of Computational Physics*, **218**(1):295–323, 2006.

[24] B. Cockburn, M. Luskin, and C.-W. Shu et al. Enhanced accuracy by post-processing for finite element methods for hyperbolic equations. *Math. Comput.*, **72**(242):577–606, 2003.

[25] R. Hartmann and P. Houston. Adaptive discontinuous Galerkin finite element methods for nonlinear hyperbolic conservation laws. *SIAM J. Sci. Comput.*, **24**(3):979–1004, 2002.

[26] B. Engquist and A. Majda. Absorbing boundary conditions for the numerical simulation of waves. *Mathematics of Computation*, **31**(139):629–651, 1977.

[27] R.L. Higdon. Absorbing boundary conditions for difference approximations to the multidimensional wave equation. *Math. Comput.*, **47**:437–459, 1986.

[28] J. P. Berenger. A perfectly matched layer for the absorption of electromagnetic waves. *Journal of Computational Physics*, **114**:185–200, 1994.

[29] W.C. Chew and W.H. Weedon. A 3D perfectly matched medium from modified Maxwell's equations with stretched coordinates. *Microwave and Optical Technology Letters*, **7**(13), 1994.

[30] P. Bettess, J. Shirron, O. Laghrouche, B. Peseux, R. Sugimoto, and J. Trevelyan. A numerical integration scheme for special finite elements for the Helmholtz equation. *International Journal for Numerical Methods in Engineerin*, **56**(1):531–552, 2003.

[31] W. Desmet. *Wave based prediction technique for coupled vibro-acoustic analysis*. PhD thesis, KULeuven, division PMA, 1998. Also available as `http://people.mech.kuleuven.ac.be/wdesmet/desmet/thesis.pdf`.

[32] E. Trefftz. Ein gegenstück zum ritzschen verfahren. In *Proceedings of the 2nd International Congress on Applied Mechanics*, volume **57**, pages 131–137, Zurich, Switzerland, 1926.

[33] A. P. Zielinski and I. Herrera. Trefftz method: Fitting boundary conditions. *International Journal for Numerical Methods in Engineering*, **24**:871–891, 1987.

[34] C.A. Brebbia and J. Dominguez. *Boundary elements: An introduction course*. Computational Mechanics Publications, McGraw-Hill Book Company, Southampton, 1992.

[35] B. Pluymers. *Wave based modelling methods for steady-state vibro-acoustics*. PhD thesis, KULeuven, division PMA, 2006.

[36] B. Pluymers, W. Desmet, D. Vandepitte, and P. Sas. Application of an efficient wave based prediction technique for the analysis of vibro-acoustic radiation problems. *Journal of Computational and Applied Mathematics (JCAM)*, **168**:353–364, 2004.

[37] B. Pluymers, W. Desmet, D. Vandepitte, and P. Sas. On the use of a wave based prediction technique for steady-state structural-acoustic radiation analysis. *Journal of Computer Modelling in Engineering and Sciences (CMES)*, **7**(2):173–184, 2005.

[38] W. Desmet, B. Pluymers, C. Vanmaele, and D. Vandepitte. A review of the wave based prediction technique for efficient interior acoustic analysis. *Journal of the European Acoustic Association (EAA) - International Journal on Acoustics, Acta Acoustic united with Acustica*, **91**, 2005.

[39] A. Hepberger, B. Pluymers, K. Jalics, H.-H. Priebsch, and W. Desmet. Validation of a wave based technique for the analysis of a multi-domain 3D acoustic cavity with interior damping and loudspeaker excitation. In *Proceedings of the 33rd International Congress and Exposition on Noise Control Engineering*, Prague, Czech Republic, 2004.

[40] G. Green. An essay on the application of mathematical analysis to the theories of electricity and magnetism. Technical report, Printed for the Author by T. Wheelhouse, Nottingham, 1828.

[41] S.G. Mikhlin. *Integral equations*. Pregamon press, Oxford, 1957.

[42] Alexander H. D. Cheng and D. T. Cheng. Heritage and early history of the boundary element method. *Eng. Anal. Bound. Elems.*, **29**:268–302, 2005.

[43] P.K. Banerjee and J. Watson. *Development in boundary element methods.* Elesvier Science Publishing Co., New York, 1986.

[44] P.K. Banerjee. *The boundary element method in engineering.* McGraw-Hill Publications, London, 1994.

[45] C.A. Brebbia, J.C.F. Tells, and L.C. Wrobel. *Boundary element techniques.* Springer-Verlag, Berlin and New York, 1984.

[46] C.A. Brebbia. *Topics in boundary element research, Vol. 1 Basic principles and applications.* Springer-Verlag, Berlin, Heidelberg, New York, Tokyo, 1984.

[47] C.A. Brebbia. *Topics in boundary element research, Vol. 2 Time dependent and vibration problems.* Springer-Verlag, Berlin, Heidelberg, New York, Tokyo, 1985.

[48] C.A. Brebbia. *Topics in boundary element research, Vol. 3 Computational aspects.* Springer-Verlag, Berlin, Heidelberg, New York, Tokyo, 1987.

[49] V. Popov, H. Power, and L. Skerget. *Domain decomposition techniques for boundary elements.* WIT Press, Southampton, 2007.

[50] C.A. Brebbia and S. Walker. *The boundary element techniques in engineering.* Newnas-Butterworths, London, 1979.

[51] M. Bonnet. *Boundary integral equation methods for solids and fluids.* John Wiley, 1995.

[52] R. Kress. *Linear integral equations. Applied mathematical sciences; Vol. 82.* Springer–Verlag, New York Inc., second edition, 1999.

[53] D. Colton and R. Kress. *Integral equation methods in scattering theory.* John Wiley and Sons, New York, 1983.

[54] Kendall E. Atkinson. *The numerical solution of integral equations of the second kind (cambridge monographs on applied and computational mathematics)*. Cambridge University Press, 1997.

[55] Robert Dautray and Jacques-Louis Lions. *Mathematical analysis and numerical methods for science and technology: Volume 4: Integral equations and numerical methods*. Springer-Verlage, 1985.

[56] W. Hackbusch. *Integral equations: Theory and numerical treatment*, volume 120. International Series of Numerical Mathematics (ISNM), 1995.

[57] M.A. Jaswon and G.T. Symm. *Integral equation methods in potential theory and elasticity*. London Academic Press, 1977.

[58] A. A. Becker. *The boundary element method in engineering: A complete Course*. McGraw-Hill Book company Europe, London, 1992.

[59] T.P.A. Mathew. *Domain decomposition methods for the numerical solution of partial differential equations. Lecture notes in computational science and engineering 61*. Springer-Verlage, Berlin, 2008.

[60] A.J. Burton and G.F. Miller. The application of integral equation methods to the numerical solution of some exterior boundary value problems. *Proceeding of the Royal Society of London A*, **323**:201–210, 1971.

[61] W.L. Meyer, W.A. Bell, and B.T. Zinn. Boundary integral solutions of three dimensional acoustic radiation problems. *Journal Sound and Vibration*, **59**(2):245–262, 1978.

[62] T. Terai. On calculation of sound field around three-dimensional objects by integral equation methods. *Journal of Sound and Vibration*, **69**:71–100, 1980.

[63] S.A. Yang. Evaluation of the Helmholtz boundary integral equation and its normal and tangential derivatives in two dimensions. *Journal Sound and Vibration*, **301**(2):864–877, 2007.

[64] R. J. Riddell. Boundary-Distribution of the Helmholtz equation for a region with a corners. *Journal of Computational Physics*, **317**(10):21–41, 1979.

[65] G. Krisnasamy, L.W. Schmerr, T.J. Rudolphi, and F.J. Rizzo. Hypersingular boundary integral equations: Some applications in acoustics and elastic wave scattering. *ASME Journal Applied Mechanics*, **57**:404–414, 1990.

[66] S.K. Bose. Finite part representations of hypersingular equation of acoustic scattering and radiation by open smooth surfaces. *Proc. Indian. Acad. Sci.*, **106**(3):271–280, 1996.

[67] P.A. Martin and F.J. Rizzo. Hypersingular integrals: How smooth must the density be? *International Journal for Numerical Methods in Engineering*, **39**(3):687–704, 1996.

[68] J. Hadamard. *Lectures on Cauchy's problem in linear partial differential equations*. Yale University Press, New Haven, 1923.

[69] V. Sladek and J. Sladek. *Singular integrals in boundary element methods*. Computational Mechanics Publications, Southampton, 1998.

[70] M. Tanaka, V. Sladek, and J. Sladek. Regularization techniques applied to boundary element methods. *Applied Mechanics Reviews*, **47**(10):457–499, 1994.

[71] A.W. Maue. Zur formulierung eines allgemeinen beugungsproblems durch eine integralgleichung. *Zeitschrift für Physik. A*, **126**:601–618, 1949.

[72] K.M. Mitzner. Acoustic scattering from an interface between media of greatly different density. *Journal of Mathematical Physics*, **7**(11):2053–2060, 1966.

[73] H.R. Kutt. The numerical evaluation of principal value integrals by finite part integration. *Numer. Math.*, **24**:205–210, 1975.

[74] D.J. Chappell. *Modelling the transient interaction of an elastic structure with an exterior acoustic field.* PhD thesis, Brighton University, 2007.

[75] K. Hornberger and U. Smilansky. The boundary integral method for magnetic billiards. *J. Phys. A*, **33**:2829–2855, 2000.

[76] H.R. Kutt. Quadrature formula for finite part integrals. Technical report, CSIR Special Report WISK, 178, Pretoria, National Research Institute for Mathematical Sciences, P.O. Box 395, Pretoria 0001, South Africa, 1975.

[77] J.C.F. Telles. A self adaptive coordinate transformation for efficient numerical evaluation of general boundary element integrals. *International journal for numerical methods in engineering*, **24**(4):959–973, 1989.

[78] P.J. Davis and P. Rabinowitz. *Methods of numerical integration.*

[79] K. Hayami. *A projection transformation method for nearly singular surface boundary element integrals.* PhD thesis, Wessex Institute of Technology, Southampton, 1991.

[80] K. Hayami. A new coordinate transformation method for singular and nearly singular integrals over general curved boundary elements. *Boundary elements IX*, **1**:375–399, 1987.

[81] E. Kita and N. Kamiya. Subregion boundary element method. *JSME Int. journal series A*, **37**:72–366, 1994.

[82] X. Lu and W. Wu. A new subregion boundary element technique based on the domain decomposition method. *Engineering Analysis with Boundary Element Method*, **29**:944–952, 2005.

[83] F.C. Araujo and W.J. Mansur. Iterative solvers for BEM systems of equations. In J.J. Connor C.A. Brebbia, editor, *Advances in boundary elements Vol.1. Computations and fundamentals*. Cambridge, USA, Springer-Verlag, Berlin, Heidelberg, 1989.

[84] V. Popov and H. Power. The MRM-MD integral equation method: An efficient approach for the numerical solution of domain dominant problems. *Int. J Num. Math. Eng.*, **44**:327–353, 1999.

[85] R. Sugino, H. Imai, and N. Tosaka. Boundary element scheme with domain decomposition approach for moving interface phenomenon. In *Proceedings 12th international conference on domain decomposition methods*, volume **6**, pages 571–587, 2000.

[86] N. Kamiya, H. Iwase, and E. Kita. Parallel implementation of boundary element method with domain decomposition. *Eng. Anal. Bound. Elems.*, **18**:209–216, 1996.

[87] W. Elliethy and M. Tanaka. Interface relaxation algorithms for BEM-BEM coupling and FEM-BEM coupling. *Computer Methods in Applied Mechanics and Engineering*, **192**:2977–2992, 2003.

[88] D. Chiang and W. Chen. A combined FEM and BEM approach for sound radiation with finite flange. *Journal of vibration and control*, **6**(4):571–587, 2000.

[89] D. Nardini and C.A. Brebbia. A new approach to free vibration analysis using boundary elements. In C.A. Brebbia, editor, *Proceedings 4th International Conference on Boundary Element Methods*. Springer-Verlag, Berlin and New York, 1982.

[90] P.W. Partridge, C.A. Brebbia, and L.C. Wrobel. *The dual reciprocity boundary element method*. Computational Mechanics Publications: Sothampton and Elsevier Applied Science, New York, 1992.

[91] C.A. Brebbia. On two different methods for transforming domain integrals to the boundary. In J.J. Connor C.A. Brebbia, editor, *Advances in boundary elements Vol.1. Computations and fundamentals*. Cambridge, USA, Springer-Verlag, Berlin, Heidelberg, 1989.

[92] M.D. Buhmann. *Radial basis functions: Theory and implementations (Cambridge monographs on applied and computational mathematics)*. Cambridge University Press, 2009.

[93] J. C. F. Telles and J. M. A. Carrer. Static and transient dynamic non-linear stress analysis by the boundary element method with implicit techniques. *Eng. Anal. Bound. Elem.*, **14**:65–74, 1994.

[94] Morcos F. Samaan, Youssef F. Rashed, and Metwally A. Ahmed. The dual reciprocity method applied to free vibrations of 2D structures using compact supported radial basis functions. *Computational Mechanics*, **41**(1):5–105, 2007.

[95] R.H. Lyon and R.G. DeJong. *Theory and application of statistical energy analysis*. Butterworth-Heinemann, Boston, MA, second edition, 1995.

[96] R.S. Langley and V. Cotoni. Response variance prediction in the statistical energy analysis of built-up systems. *Journal of the Acoustical Society of America*, **115**(2):706–718, 2004.

[97] G. Tanner. Dynamical energy analysis-determining wave energy distribution in complex vibro-acoustical structures. *Journal of Sound Vibration*, **320**:1023–1038, 2009.

[98] D.J. Chappell, S. Giani, and G. Tanner. Dynamical Energy Analysis for built-up acoustic systems at high frequency. *J. Acoust. Soc. Am.*, **130**:1420, 2011.

[99] L. Maxit and J.L. Guadyer. Estimation of SEA coupling loss factor using a dual formulation and FEM modal information, part I: Theory. *Journal of Sound and Vibration*, **239**(12-16):1333–1366, 2001.

[100] P.J. Shorter and R. S. Langley. Vibro-acoustic analysis for complex systems. *Journal of Sound Vibration*, **228**(3):669–699, 2005.

[101] D. N. Maksimov and G. Tanner. A hybrid approach for predicting the distribution of vibro-acoustic energy in complex built-up structures. *Integral Methods in Science and Engineering*, pages 233–240, 2011.

[102] R.L. Weaver and O.I. Lobkis. Diffuse field in open systems and the emergence of the Green function. *Journal of acoustic Soc. Am.*, **116**(5):2731–2734, 2004.

[103] K. Vergote, D. Vandepitte, and W. Desmet. On the use of a hybrid wave-based-statistical energy approach for the analysis of vibro-acoustic systems in the mid-frequency range. In *Proceedings of the International Conference on Noise and Vibration ISMA*, pages 2437–2450, Leuven, Belgium, 2010.

[104] F. Haake. *Quantum signature of chaos.* Springer, NewYork, 2001.

[105] M.C. Gutzwiller. *Chaos in classical and quantum mechanics.* Springer, NewYork, 1990.

[106] M. Brack and R.K. Bhaduri. *Semiclassical physics, frontiers in physics series.* Advanced Book Program, Westerview Press, 2003.

[107] H. Stöckmann. *Quantum chaos: An introduction.* Cambridge University Press, 1999.

[108] E. Bogomolny and E. Huges. Semiclassical theory of flexural vibration of plates. *Phys. Rev. A*, **57**(4):5404, 1998.

[109] M.V. Berry and J.P. Keating. A rule for quantizing chaos. *J. Phys. A: Math. Gen.*, **23**:4839, 1990.

[110] J.P. Keating. Periodic orbit resummation and quantization of chaos. *Proceedings of the Royal Society A - Mathematical, Physical and Engineering Sciences*, **436**:99–108, 1992.

[111] E. Doron and U. Smilansky. Semiclassical quantization of chaotic billiards: A scattering theory approach. *Nonlinearity*, **5**:1055–1084, 1992.

[112] T. Prosen. Exact quantum surface of section method. *J. Phys. A:Math. Gen.*, **27**:L709–L714, 1994.

[113] T. Prosen. Quantum surface of section method: Demonstration of semiclassical Berry-Robnik energy level-spacing distribution in a generic two-dimensional Hamiltonian systems. *J. Phys. A: Math. Gen.*, **28**:L349–L356, 1995.

[114] P.A. Boasman. Semiclassical accuracy for billiards. *Nonlinearity*, **7**:485, 1992.

[115] H. Schanz and U. Smilansky. Quantization of Sinai's billiard: A scattering approach. *Chaos, Solutions and Fractals*, **5**(7):1289–1309, 1995.

[116] T. Prosen. General quantum surface-of-section method. *J. Phys. A: Math. Gen.*, **28**:4133–4155, 1995.

[117] R. Blümel, T.M. Antonsen, B. Georgeot, E. Ott, and R.E. Prange. Ray splitting and quantum chaos. *Phys. Rev. E*, **53**(4):3284–3302, 1996.

[118] R.E. Prange, E. Ott, T.M. Antonsen, B. Georgeot, and R. Blümel. Smoothed density of states for problems with ray splitting. *Phys. Rev. E*, **53**(1):201–213, 1996.

[119] R. Blümel, T.M. Antonsen, B. Georgeot, E. Ott, and R.E. Prange. Ray splitting and quantum chaos. *Phys. Rev. Letters*, **76**(14):2476–2479, 1996.

[120] A. Kohler and R. Blümel. Signature of periodic lateral-ray orbits in a rectangular ray-splitting billiard. *Physics Letters A*, **247**:87–92, 1998.

[121] S.C. Creagh. Trace formula for broken symmetry. *Annals of Physics*, **248**:60–94, 1996.

[122] L. Couchman, E. Ott, and T.M. Antonsen. Quantum chaos in systems with ray splitting. *Phys. Rev. A*, **46**(10):6193, 1992.

[123] G. Tanner and N. Søndergaard. Short wave length approximation of a boundary integral operator for homogeneous and isotropic elastic bodies. *Phys. Rev. E: Statistical, Nonlinear and Soft Matter Physics*, **75**(3):036607, 2007.

[124] N. Søndergaard and G. Tanner. Wave chaos in elastic disc. *Physical Review E: Statistical Physics, Plasmas, Fluids, and Related Interdisciplinary Topics*, **66**(6):066211, 2002.

[125] M. Abramowitz and A. Stegun. *Handbook of mathematical functions*. New York: Dover Publications, Inc., ninth edition, 1968.

[126] B. Georgeot and R.E. Prange. Exact and quasiclassical fredholm of quantum billiards. *Phys. Rev. letters*, **74**(15):2851, 1995.

[127] R. Balian and C. Bloch. Distribution of eigenfrequencies for the wave equation in a finite domain. *Ann. Phys.*, **60**:401–447, 1970.

[128] G. Yan and F. Lin. Treatment of corner node problems in boundary element method. In J. J. Connor C. A. Brebbia, editor, *Advances in boundary elements Vol.1. Computations and fundamentals*. Cambridge, USA, Springer-Verlag, Berlin, Heidelberg, 1989.

[129] A.H. Stroud and D. Secrest. *Gaussian quadrature formula*. Prentice-Hall, New York, 1966.

[130] I.S. Gradshteyn, I.M. Ryzhik, and A. Jeffrey. *Table of integrals, series, and products*. Academic Press, fifth edition, 1994.

[131] M. Sieber and F. Steiner. Quantum chaos in the hyperbola billiard. *Phys. Lett. A*, **148**:415, 1990.

[132] G. Tanner, P. Scherer, E.B. Bogomolny, and D. Wintgen B. Eckhardt. Quantum eigenvalues from classical periodic orbits. *Phys. Rev. Lett.*, **67**(18):2410–2413, 1991.

[133] T. Szeredi and D.A. Goodings. Classical and quantum chaos of the wedge billiard. I. Classical mechanics. *Phys. Rev. E*, **48**:3518, 1993.

[134] G. Barton. *Elements of Green function and propagation potential. Diffusion and waves.* Clarendon Press Oxford, 1989.

[135] M. Morse and H. Feshback. *Methods of theoretical physics, part I.* McGraw-Hill Co., Inc, Tokyo, 1953.